

University of Alberta

**Alkyne Migration in Alkylidene Carbene/Carbenoid Species: Synthesis of
Polyynes and Mechanistic Investigations**

by

Sara Eisler ©

A thesis submitted to the Faculty of Graduate Studies and Research in partial
fulfillment of requirements of the degree of Doctor of Philosophy

Department of Chemistry

Edmonton, Alberta

Spring 2004



Library and
Archives Canada

Bibliothèque et
Archives Canada

Published Heritage
Branch

Direction du
Patrimoine de l'édition

395 Wellington Street
Ottawa ON K1A 0N4
Canada

395, rue Wellington
Ottawa ON K1A 0N4
Canada

Your file *Votre référence*

ISBN: 0-612-96260-1

Our file *Notre référence*

ISBN: 0-612-96260-1

The author has granted a non-exclusive license allowing the Library and Archives Canada to reproduce, loan, distribute or sell copies of this thesis in microform, paper or electronic formats.

L'auteur a accordé une licence non exclusive permettant à la Bibliothèque et Archives Canada de reproduire, prêter, distribuer ou vendre des copies de cette thèse sous la forme de microfiche/film, de reproduction sur papier ou sur format électronique.

The author retains ownership of the copyright in this thesis. Neither the thesis nor substantial extracts from it may be printed or otherwise reproduced without the author's permission.

L'auteur conserve la propriété du droit d'auteur qui protège cette thèse. Ni la thèse ni des extraits substantiels de celle-ci ne doivent être imprimés ou autrement reproduits sans son autorisation.

In compliance with the Canadian Privacy Act some supporting forms may have been removed from this thesis.

Conformément à la loi canadienne sur la protection de la vie privée, quelques formulaires secondaires ont été enlevés de cette thèse.

While these forms may be included in the document page count, their removal does not represent any loss of content from the thesis.

Bien que ces formulaires aient inclus dans la pagination, il n'y aura aucun contenu manquant.

Canada

Abstract

Alkyne migration in alkyldiene carbene/carbenoid species has been exploited toward the formation of polyynes. A number of symmetrical and unsymmetrical 1,3-butadiynes, 1,3,5-hexatriynes and 1,3,5,7-octatetraynes have been synthesized in high yields using this rearrangement. The ability to induce multiple rearrangements in a single molecule has greatly facilitated the formation of extended, carbon-rich molecules. Many of the molecules presented in this thesis have been or would be difficult to access via more traditional techniques.

Alkyldiene carbene/carbenoid rearrangements have proven to be useful toward the formation of conjugated polyyne materials. Starting materials are inexpensive and easily available, intermediates are easy to purify, and most reactions involved in the synthetic sequence are uncomplicated. A series of extended conjugated polyynes has been synthesized, including a decayne, only the third to have been fully characterized. The isolation of macroscopic amounts of the polyynes has allowed for a thorough analysis of their physical characteristics. Especially interesting are the nonlinear optical (NLO) properties. Although there have been many theoretical predictions concerning the NLO response of polyynes, the inability to synthesize these carbon-rich structures in macroscopic quantities has prevented their actual measurement. Surprisingly, the NLO response of polyynes is higher than that predicted by theory.

The mechanism of alkyne migration in alkyldiene carbene/carbenoids has been studied. The nature of the intermediate, be it carbene or carbenoid, has been

investigated. For the first time, the migratory ability of alkynes in alkylidene carbene/carbenoid species has been evaluated.

The synthesis of a number of cross-conjugated radialenes has also been accomplished. To better understand the effect of strain on the properties of enyne macrocycles, a series of increasingly strained cycles has also been synthesized and their structural, vibrational and electronic properties studied.

For my parents.

Acknowledgements

I would first like to thank Dr. Frank Hegmann, Aaron Slepko and Dr. Glen Loppnow for the exciting collaborative work, which has greatly enhanced my graduate experience. Dr. Glen Loppnow, thank you especially for giving me my first summer research position eight years ago. Without you I would have done something foolish like go into medical school.

Thank you to my fellow group members for a wonderful five years. In addition to the help I have received when preparing for conferences and my 502, candidacy and defense, coming to the lab has always been fun because of you. To my summer students, Erin Elliott, Erin Chernick, Navjot Chahal, and Eric Hansen, thank you for the wonderful work you did and all the things you taught me. Annabelle Shi Shun, Chad Lewis, Trent Rankin, Colin Vitols, Clement Osei Akoto, Joon Cho, Sorin Ciulei, Mojtaba Gholami, and Thanh Luu thank you for making me laugh and putting up with my messy lab! Katie Campbell and Dr. Yuming Zhao, thank you for your friendship and your support, I cannot even express the many ways in which you have made my graduate studies a great experience.

I am indebted to Drs. Bob MacDonald and Mike Ferguson, for their work on X-ray crystallographic analysis, Randy and Angie in the mass spec lab, Diane, Darlene and Andrea in spectral services, secretaries Diane, Jeanette and Jackie for helping with everything administrative, Ilona, for looking out for me, the computer people, Larry, Shannon, Scott, and the NMR people Glenn, Tom and Gerdy.

Thank you Shannon and Trish, I couldn't hope for better friends. Your encouragement over the past five years has been incredible.

And last, but definitely not least, I would like to thank my boss Rik. I have had not a moments regret since deciding to work with you. Thank you for your constant support and encouragement. You always seem to know exactly what I need, be it either the hard truth, or an ego boosting. I can't imagine a better research director.

Table of Contents

Chapter 1 Introduction	1
1.1 Historical Interest in Conjugated Molecules	1
1.2 Alkylidene Carbenes/Carbenoids and Conjugated Molecules	3
1.2.1 Reactions of Carbenoids/Carbenes	4
<i>1.2.1.1 Formation of Butatrienes</i>	5
<i>1.2.1.2 Hexapentaenes</i>	9
<i>1.2.1.3 Radialenes</i>	10
1.2.2 Alkylidene/Alkyne Rearrangement	14
<i>1.2.2.1 Acetylene to Carbon</i>	14
<i>1.2.2.2 Carbenoid/Carbene to Alkyne</i>	16
1.3 Conclusions	19
1.4 References and Notes	19
Chapter 2 Alkyne Migration in Alkylidene Carbenoid Species: A New Method of Polyne Synthesis	24
2.1 Introduction	24
2.2 Results and Discussion	26
2.2.1 1,2-Migration of Alkynes	26
2.2.2 Formation of Functionalized Triynes	28
2.2.3 Formation of Diynes and Tetrynes	34
2.2.4 Extended Systems	37
2.2.5 Solid State Characterization	41

2.3 Conclusions	45
2.4 References and Notes	45
Chapter 3 Synthesis, Electronic, Nonlinear Optical and Physical Properties of Conjugated Polyynes	49
3.1 Introduction	49
3.2 Results and Discussion	54
3.2.1 Synthesis	54
3.2.2 UV-Vis Spectroscopy	65
3.2.3 Differential Scanning Calorimetry	69
3.2.4 Solid State Structures	71
3.2.5 ¹³ C NMR of Polyynes	78
3.2.6 Nonlinear Optical Properties of Polyynes	81
3.3 Conclusions	85
3.4 References and Notes	85
Chapter 4 Mechanistic Investigations of the 1,2-Migration of an Alkyne in an Alkylidene Carbenoid Rearrangement	91
4.1 Introduction	91
4.2 Carbene or Carbenoid	93
4.3 Migratory Ability of Alkynes in Alkylidene Carbenes/Carbenoids	96
4.3.1 Synthesis of Labeled Dibromoolefins	97
4.3.2 Rearrangement of Labeled Dibromoolefins	98

4.4 Carbenoid Intermediate	105
4.4.1 Trapping of Lithiated Carbenoid Intermediate	106
4.5 Conclusions	111
4.6 References and Notes	112
Chapter 5 Synthesis and Study of Cross-conjugated Macrocycles	114
5.1 Introduction	114
5.2 Expanded Radialenes	116
5.2.1 Synthesis	116
5.2.2 Electronic Properties	120
5.3 Strained Eneyne Macrocycles	125
5.3.1 Synthesis	127
5.3.2 Physical Characteristics and X-ray Structures	129
5.3.3 ¹³ C NMR Spectroscopic Properties	133
5.3.4 Electronic Absorption Characteristics	138
5.3.5 Raman Spectroscopic Properties	142
5.4 Conclusions	147
5.5 References and Notes	148
Chapter 6 Future Outlook	152
Chapter 7 Experimental	157
Appendix A Crystallographic Data	
Appendix B Selected Spectra	

List of Tables

Table 2.1	Summary of synthetic yields for compounds 93-96	30
Table 2.2	Yields for synthesis of diynes 116a-d	36
Table 3.1	UV-Visible characteristics of polyynes 133-138	67
Table 3.2	^{13}C NMR shifts for compounds 132-138 in ppm	81
Table 3.3	Nonlinear optical characteristics of polyynes 132-138	82
Table 5.1	Selected ^{13}C NMR shift data (in ppm) for 233a-d, 227 and 241	134

List of Figures

Figure 1.1	Unsaturated carbenes.	9
Figure 1.2	Radialenes.	10
Figure 2.1	Illustration of crystal packing for compound 121 .	41
Figure 2.2	a) ORTEP drawing for compound 131 . b) View of crystal packing for 131 approximately along the crystal <i>a</i> -axis (<i>n</i> -hexane solvent molecules and hydrogen atoms removed for clarity).	43
Figure 3.1	UV-Visible spectra of polyynes 133-138 in hexanes.	65
Figure 3.2	Power-law plot of E_{\max} versus n , ($E_{\max} = 1/\lambda_{\max} \times 10^7$).	69
Figure 3.3	Differential Scanning Calorimetry traces of polyynes 132-138 .	71
Figure 3.4	(a) Crystal packing diagram of tetrayne 134 , viewed along <i>a</i> -axis. (b) Crystal packing diagram of tetrayne 134 , viewed along the <i>b</i> -axis.	73
Figure 3.5	(a) Crystal packing diagram of pentayne 135 , viewed along the <i>a</i> -axis. (b) Crystal packing diagram of pentayne 135 viewed along the <i>b</i> -axis.	74
Figure 3.6	(a) Crystal packing diagram of hexayne 136 , viewed along the <i>a</i> -axis. (b) Crystal packing diagram of hexayne 136 , viewed along the <i>b</i> -axis.	75
Figure 3.7	(a) ORTEP diagram of octayne 137 . (b) Crystal packing diagram of 137 viewed down the crystallographic <i>a</i> -axis.	77
Figure 3.8	^{13}C NMR spectra of polyynes 132-138 (CD_2Cl_2 , 125 MHz).	79
Figure 3.9	Polyyne molecular second hyperpolarizability (γ) as a function of The number of repeat units (n) in the oligomer chain.	84
Figure 4.1	Labeling studies.	96

Figure 4.2	^{13}C NMR spectrum of labeled diyne 175 .	100
Figure 4.3	^{13}C NMR spectra for 96a , 96b , and 177/178 .	102
Figure 5.1	The π -electron systems of the cross-conjugated framework.	121
Figure 5.2	The <i>cisoid</i> and <i>transoid</i> orientations of the ene-yne-ene conjugated Segment.	121
Figure 5.3	UV-Visible spectra of radialenes 219 , 220 , 225 , and pentamer 217 .	122
Figure 5.4	UV-Visible spectra of model compounds 226 and 227	123
Figure 5.5	a-e) ORTEP drawing of macrocycles 233a-d , 227 . f) ORTEP Drawing of 241 .	130
Figure 5.6	Plot of ^{13}C NMR chemical shifts for a) C(4)/C(12) and b) C(5)/C(13) versus α C(3)-C(4)-C(8)/C(11)-C(12)-C(16).	135
Figure 5.7	UV-Visible spectra of a) macrocycles 233a-c and b) macrocycles 233c-d , 227 , and 241 .	140
Figure 5.8	Raman spectra of cross-conjugated macrocycles 233a-d , 227 , and acyclic 241 in the 900-1700 cm^{-1} spectral region.	143
Figure 5.9	Raman spectra of cross-conjugated macrocycles 233a-d , 227 , and acyclic 241 in the 1450-2300 cm^{-1} spectral region.	144
Figure 5.10	a) Correlation of olefinic Raman frequency with ^{13}C NMR shifts of C(4)/C(12) and b) Correlation of olefinic Raman frequency with ^{13}C NMR shifts	

of C(5)/C(13). c) Correlation of olefinic Raman frequency with bond angle α at C(3)-C(4)-C(8)/C(11)-C(12)-C(16).

147

List of Symbols

\AA	angstrom
δ	chemical shift
ϵ	molar extinction coefficient
λ_{max}	wavelength of maximum absorption
J	coupling constant
γ	molecular second hyperpolarizability

List of Abbreviations

APT	Attached proton test
aq.	aqueous
Bu	butyl
d	doublet
DEA	diethylamine
DMF	<i>N,N</i> -dimethylformamide
DSC	differential scanning calorimetry
ECL	effective conjugation length
EI-MS	electron impact mass spectrometry
ESI	electrospray ionization
Et	ethyl
equiv	equivalent
g	gram
h	hour
HMBC	Heteronuclear multiple bond coherence
HOMO	highest occupied molecular orbital
HRMS	high resolution mass spectrometry
Hz	Hertz
<i>i</i>	iso
IR	infrared
LDA	lithium diisopropylamide
LED	light emitting diode

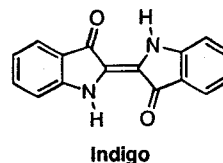
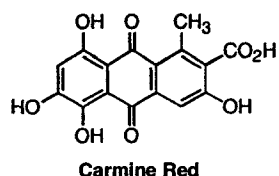
LUMO	lowest unoccupied molecular orbital
m	multiplet
M	molar
Me	methyl
mg	milligram
MHz	megaHertz
mL	milliliter
mmol	millimole
mol	mole
Mp	melting point
MS	mass spectroscopy
<i>m/z</i>	mass-to-charge-ratio
<i>n</i> -BuLi	<i>n</i> -butyl lithium
NLO	nonlinear optical (optics)
nm	nanometer(s)
NMR	nuclear magnetic resonance
NOE	nuclear overhauser effect
ORTEP	oak ridge thermal ellipsoid plot
p	pentet
PCC	pyridinium chlorochromate
Ph	phenyl
ppm	parts per million
Pr	propyl

q	quartet
rt	room temperature
s	singlet
satd.	saturated
t	triplet
<i>t</i>	tertiary
TBAF	tetrabutylammonium fluoride
THF	tetrahydrofuran
THG	third harmonic generation
TIPS	triisopropylsilyl
TLC	thin layer chromatography
TMEDA	<i>N,N,N',N'</i> -tetramethylenediamine
TMS	trimethylsilyl
T-ROESY	transverse rotating frame overhauser effect spectroscopy
UV	ultraviolet
UV-Vis	ultraviolet-visible

Chapter 1 Introduction

1.1 Historical Interest in Conjugated Molecules

Conjugated organic molecules have been prevalent in human culture throughout history¹ and as technology becomes more sophisticated, they play an increasing role in our everyday lives. The historical importance of conjugated organic molecules is clearly demonstrated by the development of dye and pigment technology. Colorants have been an integral part of human culture for thousands of years and modern synthesis of conjugated organic molecules is linked to the millennia-long fascination with colorful molecules. The earliest use of dyes was recorded in China in 2600 B.C. Many organic dyes have since played a critical role in the economy of societies throughout the world.² For example, carmine red and indigo, the structures of which are shown below, are natural products derived from insects and plants native to South and Central America and Asia.³ The colorants were so highly prized in their native countries that decorated blankets and bags of dye were used as tribute to conquering forces. In Roman times, garments colored with Imperial purple, a dye extracted from a mollusk, could cost as much as the cloth's weight in gold. Of course, techniques to extract and utilize these compounds were kept highly secret to ensure a monopoly was maintained. Even so, many entrepreneurs and explorers would risk their lives to smuggle seeds and insect larvae into Europe.



Until 1856, the world's supply of these important organic compounds was dependent on a few sources. William Henry Perkin was an English chemist who discovered Mauveine while attempting to synthesize quinine and was the first person to create a synthetic dye.³ Realizing the financial potential of such a discovery, he immediately patented the dye and established a profitable business. The synthesis of a number of other colored compounds soon followed. The color industry was in this period greatly assisted by the findings of Kekulé who was making his own major discovery, the elucidation of the structure of benzene.^{3,4} His work assisted the color industry dramatically as many organic dyes have an aromatic backbone and the discovery of a synthetic route to azo dyes and the total synthesis of indigo were soon realized. Synthetic dyes and pigments have since become increasingly more facile to synthesize due to advances in organic methodology.

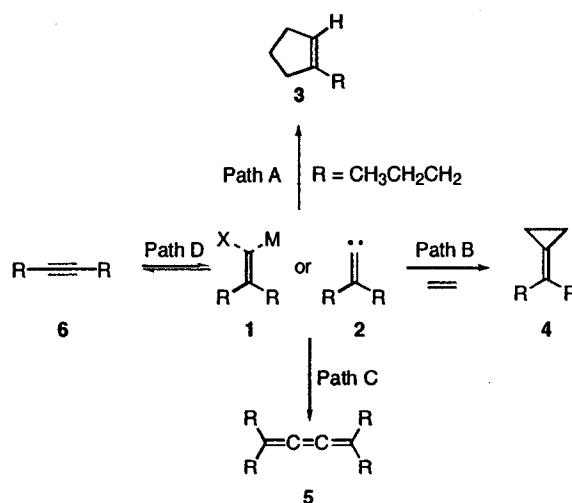
Conjugated materials have continued to provoke interest among scientists, but for many applications other than use as colorants, and the 20th century has seen enormous innovations in the arena of conjugated organic molecules. The invention of lasers (light amplification by stimulated emission of radiation) made possible the exploration of the optical properties of organic molecules. This, in turn, has fostered the incorporation of conjugated molecules into devices for use as light emitting diodes (LEDs), solar cells, optical data storage systems and

photoconductors, to name just a few.⁵⁻⁸ The optical, electronic, optoelectronic, and magnetic properties of conjugated carbon-rich structures have stimulated the development of organic methodology to allow for the facile synthesis of π -conjugated systems. For example, the formation of polyacetylene via Ziegler-Natta catalysis⁹ led to the era of conducting polymers.¹⁰⁻¹² Metal catalyzed coupling reactions have led to the realization of a vast array of novel and interesting structures. Sonogashira,¹³ Castro-Stephens,¹⁴ and Stille,¹⁵ cross-coupling reactions are particularly significant due to their ability to form C-C single bonds between aryl, vinyl and alkynyl moieties. Glaser/Hay,^{16,17} Eglinton/Galbraith¹⁸ and Cadiot-Chodkiewicz¹⁹ protocols are also used extensively to form sp-hybridized systems.

Despite these famous examples, there are still surprisingly few ways to form conjugated systems. One of the most interesting methods, and one of the least well known, is to use alkylidene carbenes/carbenoids.

1.2 Alkylidene Carbenes/Carbenoids and Conjugated Materials

Carbenoid **1** and alkylidene carbene **2** are distinguished by the association of the carbon in **1** with a metal and a halogen (or another leaving group), while the free carbene **2** has no such ties. The two extremes can thus vary greatly in reactivity. Within this range of reactivity, solvent, β -substituent and reaction temperature all affect the reaction outcome.²⁰ For carbenoid intermediates, the metal that is used can also greatly influence a reaction. The manipulation of these parameters leads to a great deal of synthetic variability.



Scheme 1.1

Alkyldiene carbenes/carbenoids are thus a very versatile synthetic tool and are capable of undergoing a diverse range of reactions, some of which are shown in Scheme 1.1. While they are perhaps best known by synthetic chemists as a convenient route to cyclopentene rings,²¹⁻²⁴ pathway A, and cyclopropylidene rings,^{25,26} pathway B, the lesser known pathways C, and D, have been utilized quite effectively to form carbon-rich materials.

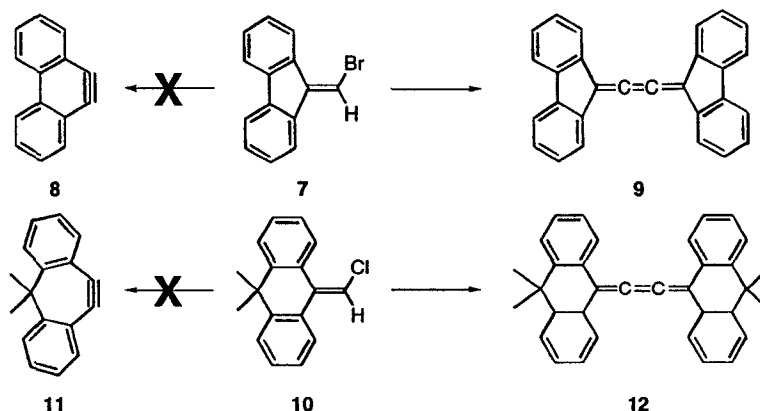
1.2.1 Reactions of Carbenoids/Carbenes

The nature of carbenoid **1** is such that the reactivity of the species is highly dependent on the metal used and the leaving group associated with the unsaturated carbenoid. Changing the metal associated with carbenoid **1** has resulted in a great deal of synthetic variability. Chromium carbenoids have recently been shown to be capable of undergoing a number of reactions including cross-coupling to aryl halides.²⁷ Zirconium carbenoids have also been used to form stereodefined diene, triene and enyne systems.²⁸ Most interesting is the use

of lithium, zinc and copper carbenoid intermediates to form cumulenes and radialenes.

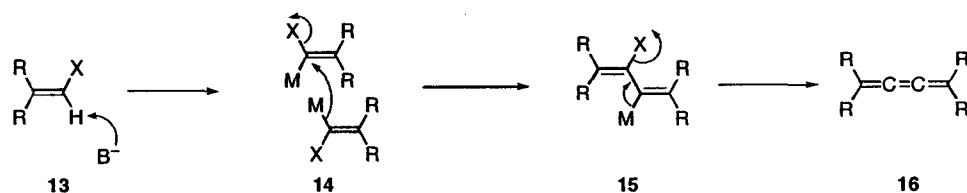
1.2.1.1 Formation of Butatrienes

The first reported formation of butatrienes from alkyldiene carbenoids arose from an attempt to form a strained alkyne system, (Scheme 1.2).²⁹⁻³¹ Elimination to form an acetylene and nucleophilic attack of the carbenoid can often be in competition. Butatrienes have traditionally been realized as products when rearrangement is unfavorable. Such a case is shown in Scheme 1.2, where the resultant alkynes (**8** or **11**) would be highly strained. Thus, treatment of the fluorenyl and anthracenyldienyl systems **7** and **10** with a strong base instead led to formation of butatrienes **9** and **12**. The base used to initiate this transformation greatly affected the product mixture: potassium amide in liquid ammonia led to a 95% yield of butatriene **9**, but the use of phenyl-lithium resulted in formation of numerous by-products and greatly reduced the yield of **9**. The use of phenyl-lithium, while successful, led to the formation of **12** in only 15% yield.



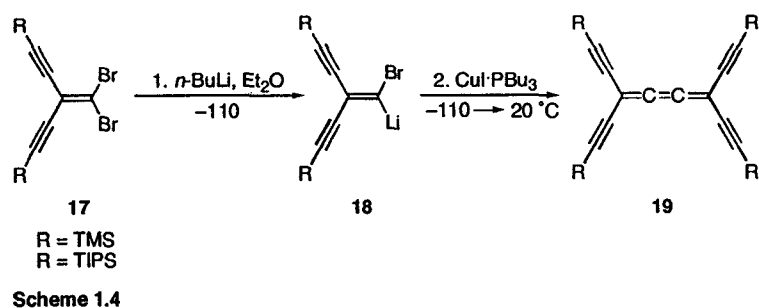
Scheme 1.2

These reactions are believed to proceed via a carbenoid intermediate which is formed by deprotonation of the vinyl proton in **13** as is shown in Scheme 1.3.³²⁻³⁵ Nucleophilic displacement of the vinyl halogen from one carbenoid to another carbenoid results in the conjugated diene **15**. Elimination of a second equivalent of MX then follows, resulting in butatriene **16**.

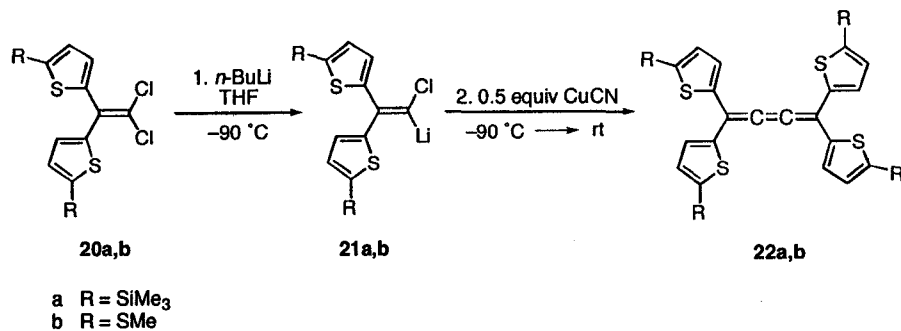


Scheme 1.3

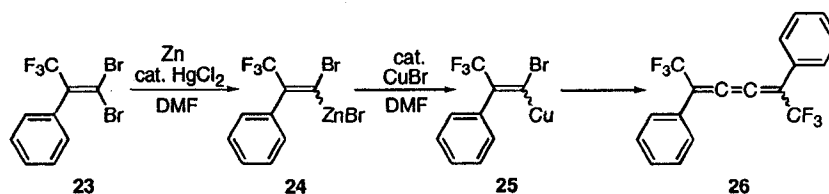
Envisioned as a possible precursor to all-carbon networks, tetraethynylbutatriene **19** was targeted by the Diederich group.³⁶ A carbenoid intermediate was utilized, formed by the reaction of *n*-BuLi with diethynyl-substituted dibromoolefin **17**. In this case, rearrangement of intermediate **18** to an acetylene is suppressed through the combination of low temperature and the ethereal solvent. The method of Iyoda and co-workers³⁷ was then employed and $\text{CuI} \cdot \text{PBU}_3$ was added at -85°C to form a copper complex and promote dimerization. The TMS- and TIPS-capped adducts of **19** were thus obtained in 55% and 42% yield, respectively. While the TMS-capped chromophore displayed limited stability in the solid state, the TIPS adduct resisted decomposition at room temperature.



Copper carbenoids were also employed to form the tetra(2-thienyl)butatrienes as shown in Scheme 1.5.³⁸ Lithiation of 1,1-dichloro-2,2-di(2-thienyl)ethane **20** followed by treatment of the corresponding carbenoid **21** with CuCN afforded the tetrathienyl butatrienes **22a,b** in 50% and 40% yield, respectively.

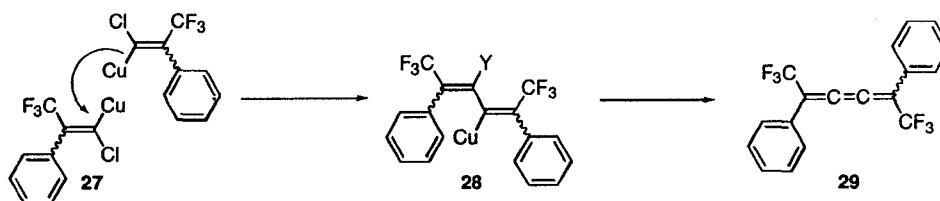


The utility of zinc carbenoids toward the formation of *cis* and *trans* fluorinated butatrienes has recently been explored.³⁹ Zinc carbenoids were chosen because of their thermal stability. Due to the sensitivity of ¹⁹F NMR spectroscopy, insight into the mechanism of this reaction has also been achieved.



Scheme 1.6

The zinc carbenoid was formed by reaction of a dibromoolefin such as **23**, appended in the β -position by a phenyl group and a fluorinated alkane, with acid-washed zinc metal in DMF. Insertion of Zn into the C-Br bond provides intermediate **24**. As the zinc species **24** is stable, the stereochemistry could be determined in some cases. Transmetalation of **24** with a catalytic amount of CuBr was necessary to induce formation of butatriene **26**. A variety of fluorinated structures were formed using this method, with yields between 65-72%. In most cases the *cis* and *trans* isomers were separable by chromatography.



Scheme 1.7

The mechanism of this process, as studied by ^{19}F NMR spectroscopy, gives direct evidence for the nucleophilic attack of one copper carbenoid species onto another to form 1,3-diene **28** (Scheme 1.7). β -Elimination then follows to give the butatriene **29**.

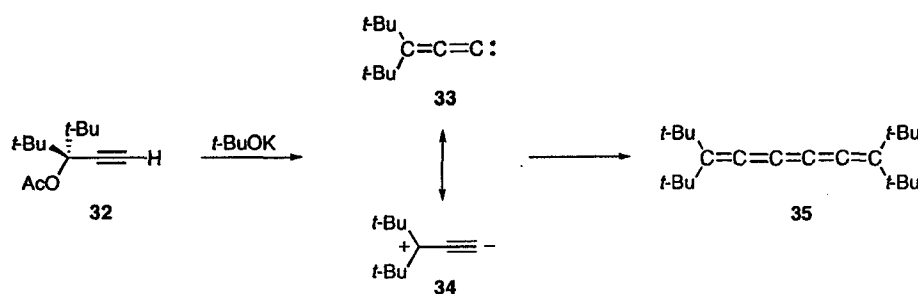
1.2.1.2 Hexapentaenes

Related structurally to the butadienes are the extended cumulenes, such as hexapentaenes. These structures can be derived from unsaturated carbene intermediates such as alkenyldenecarbene **30** and alkatetraenyldenecarbene **31**, Figure 1.1.



Figure 1.1 Unsaturated carbenes.

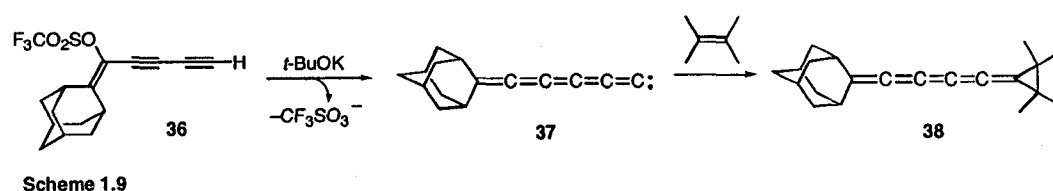
One approach to forming hexapentaenes is shown in Scheme 1.8.⁴⁰ Carbene **33** was formed by the deprotonation of **32** with potassium *t*-butoxide, and subsequent elimination of acetate. Resonance form **34** reacts with another equivalent of **32** to form *t*-butyl capped hexapentaene **35** in 20% yield. A methyl capped hexapentaene has been synthesized using a similar procedure by the Scott group.⁴¹



Scheme 1.8

An alternate procedure was employed by Stang, Scheme 1.9.²⁵ Base-induced elimination of enyne **36** provided the alkatetraenyldenecarbene **37**.

Trapping of the carbene with tetramethylethylene then provides the cumulene **38** in 53% yield.



1.2.1.3 Radialenes

Radialenes are cross conjugated macrocycles and they are represented in Figure 1.2. The realization of the radialenes has a rich history involving a range of synthetic routes and techniques.⁴²⁻⁴⁴ Of primary interest herein is the role that alkylidene carbenoids have played in the evolution of radialene synthesis.

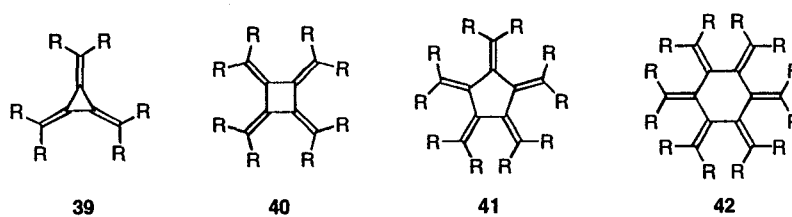
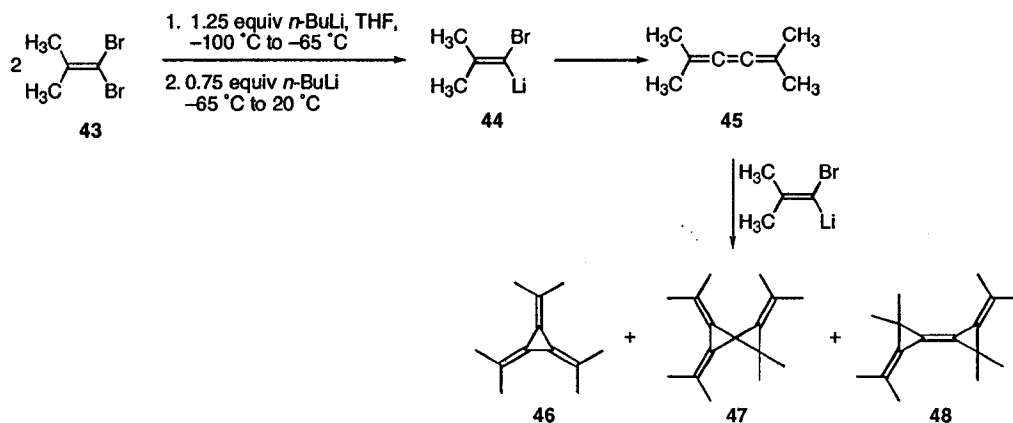


Figure 1.2 Radialenes.

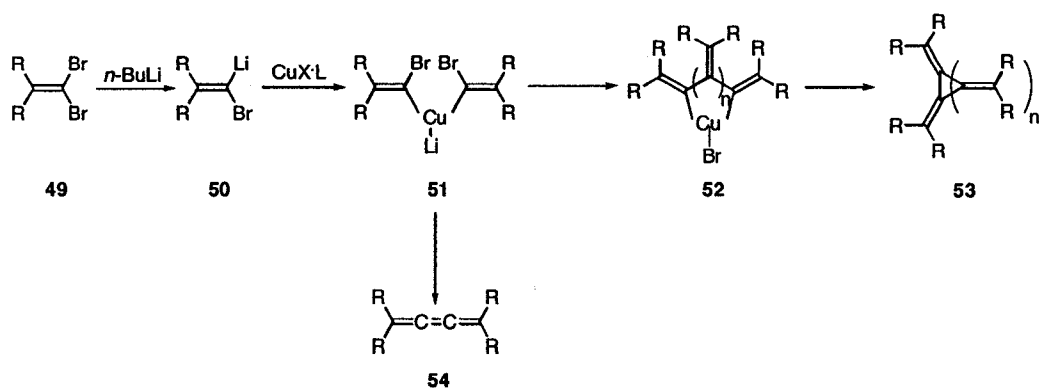
One of the first radialenes, and the first [3]-radialene, was formed using a carbenoid intermediate, and Köbrich's ground-breaking synthesis is shown in Scheme 1.10.³⁴ The requisite carbenoid intermediate **44** is formed by the reaction of dibromoolefin **43** with *n*-BuLi. Due to the bicyclopropylidene by-products that are also isolated from the product mixture, the reaction is believed to proceed via the formation of butatriene **45**, derived from the dimerization of carbenoid **44** as

discussed previously. Addition of another equivalent of **44** to the central bond of the cumulene **45** results in the [3]-radialene **46**. Due to the preferential addition of **44** to the terminal double bond of the cumulene **45** which leads to compounds **47** and **48**, the yield of radialene **46** is rather low (at 17%).



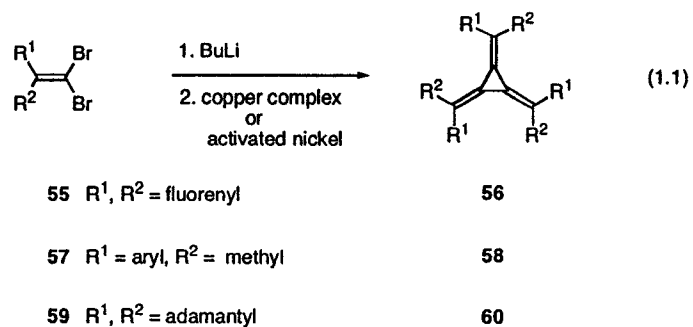
Scheme 1.10

By changing the metal of the carbenoid species to copper, a number of radialenes have been formed by cyclooligomerization. This method led to higher yields, although by-products were formed. The general reaction is shown in Scheme 1.11. As with Köbrich's route, *n*-BuLi was used to form carbenoid **50** from the appropriate dibromoolefins **49**. Transmetalation afforded cuprate **51**. Reductive elimination from intermediate **51** results in formation of butatriene by-products and oligomerization presumably leads to metallacycle **52**. Reductive elimination of metallacyclic intermediate **52** then provides the radialenes.

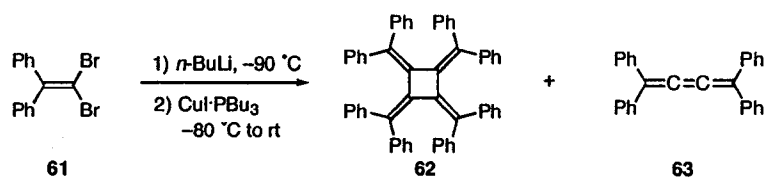


Scheme 1.11

The product ratio of butatriene to radialene could be manipulated by changing the ligand and/or counterion associated with the copper. In the first example, fluorenyl substituted radialene **56a** was synthesized using a copper complex with the corresponding butatriene as a major product (eq 1.1). Out of several salts explored, CuSPh was found to favor the production of radialene **56** over the corresponding butatriene.⁴⁵ Metals other than copper can also be used. For example, activated nickel reacts with dibromides **57** and **59** to form radialenes **58** and **60** in good yields.⁴⁶ Radialene **58** was isolated as a mixture of isomers.



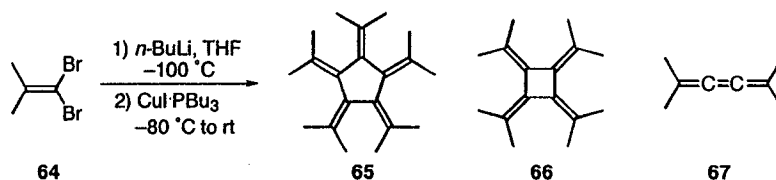
The bulkiness of the pendant R group of the precursor dibromoolefin can have a profound affect on the formation of a radialene. Large groups such as in **55**, **57**, **59**, hinder the formation of longer oligomers, i.e. **52**, Scheme 1.11, that would lead to the [4]-, [5]- and [6]-radialenes. In some cases the formation of even a [3]-radialene can be prohibitive due to steric congestion. Although this can be a limitation, careful selection of the R group can lead to preferential formation of larger radialenes as shown in Scheme 1.12 for the one-pot synthesis of octaphenyl[4]-radialene by Iyoda and co-workers.^{37,47} The optimized conditions involved formation of the lithium carbenoid species, followed by treatment with CuI•PBU₃ at -80 °C and then warming the mixture to room temperature. Radialene **62** was isolated in 48% yield along with 29% formation of butatriene **63**. The [4]-radialene is surprisingly stable, despite the inherent strain in the structure as confirmed by X-ray crystallography.



Scheme 1.12

Unlike the rigid fluorenyl and adamantyl systems that were used to form the [3]-radialenes in equation 1.1, free rotation between the olefin and the phenyl group relieves some of the steric bulk, therefore allowing the [4]-radialene to be formed. The phenyl substituents, however, are too large to allow for formation of a [5]-radialene. Conversely, by using the smaller methyl substituents, [5]-

radialene **65** could be realized.⁴⁸ Exposure of dibromoolefin **64** to the cyclooligomerization conditions resulted in three products, the desired decamethyl[5]radialene **65**, [4]-radialene **66**, and a reactive butatriene **67**. As was determined previously, varying the copper complex resulted in optimized conditions for the formation of the desired radialene. A maximum of 32% of **65** and 23% of **66** was achieved by using CuI•PBU₃. In all attempts, fair amounts of **67** were obtained, but this molecule was too unstable to be isolated during purification.



Scheme 1.13

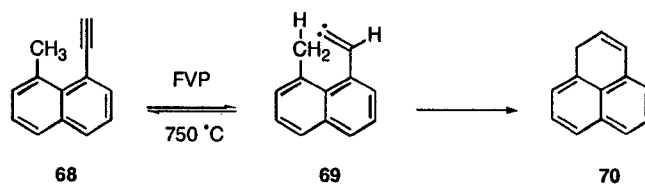
1.2.2 Alkylidene/Alkyne Rearrangement

It is possible for the pendant R group of the carbenoid species **1** to undergo a 1,2-migration to form an alkyne as in **6**. This pathway is known as the Fritsch-Buttenberg-Wiechell (FBW) rearrangement. Alkyne **6** and alkylidene carbene **2** are also known to equilibrate at very high temperatures. Both of these pathways in equation 1.2 have been used to synthesize a number of carbon-rich structures.



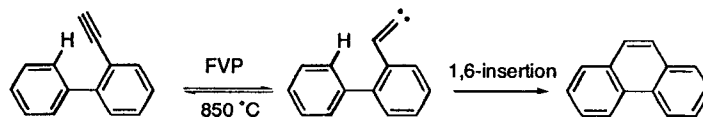
1.2.2.1 Acetylene to Carbene

The benchtop synthesis of molecular carbon allotropes, fullerenes, and fullerene fragments has been an active area of research for many years.⁴⁹⁻⁵¹ Alkylidene carbenes that have been generated via the pathway in equation 1.2, i.e. interconversion of acetylene **6** and carbene **2**, have had an important role in the evolution of fullerene and hydrocarbon chemistry. Equilibration between an alkyne and an alkylidene carbene generally involves subjecting a terminal acetylene, such as **68**, to high temperatures under flash vacuum pyrolysis (FVP) conditions, Scheme 1.14. Cyclization to hydrocarbon **70** then results via C-H bond insertion.



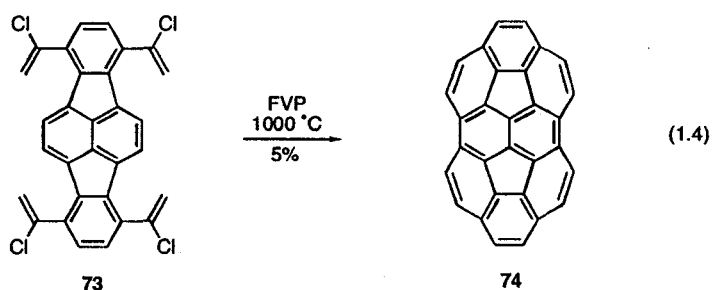
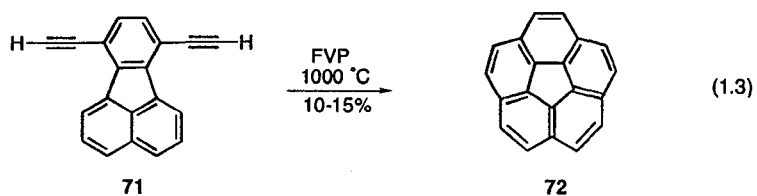
Scheme 1.14

Formative work by R.F.C. Brown outlined the synthetic range of this cyclization with four major scenarios.⁵² One reaction in particular has been critical for the synthesis of fullerene fragments, 1,6-insertions into aromatic C-H bonds, an example of which is shown in Scheme 1.15.^{53,54}



Scheme 1.15

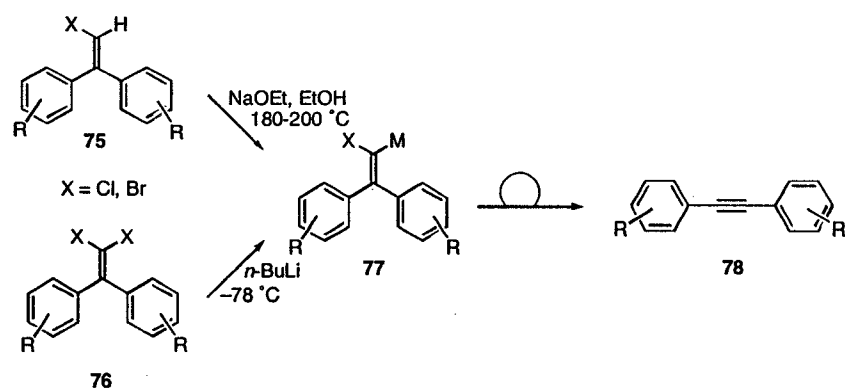
Shown in eq 1.3 is Scott's classic corannulene synthesis, involving a two fold-isomerization of diethynyl **71** to the carbene species.⁵⁵ This is then followed by 1,6-insertion to form the bowl-shaped hydrocarbon **72**. While the corannulene **72** was achieved in 10-15% yield via this route, the Scott group discovered that higher yields could be obtained by forming the ethynyl groups in the gas phase by elimination of HCl. Subsequent isomerization to the carbene, followed by 1,6-insertion ultimately led to higher yields. Rabideau's group utilized this idea to build a larger fragment, semibuckminsterfullerene **74**, Eqn. 1.3.⁵⁶ An analogous loss of HCl from tetrachloride **73** underwent a four-fold isomerization and cyclization gave C₃₀H₁₂ **74** in 5% yield.



1.2.2.2 Carbenoid/Carbene to Alkyne

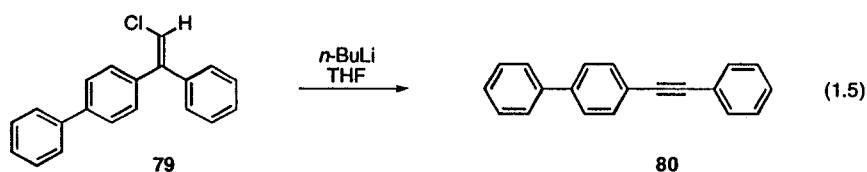
The rearrangement of a carbenoid to an acetylene is commonly known as the Fritsch-Buttenberg-Wiechell (FBW) reaction.^{57,58} Discovered independently by three chemists in 1894, this reaction involves the treatment of a

monohaloolefin such as **75** (Scheme 1.16) with a base to produce the carbenoid intermediate. Subsequent migration of an adjacent phenyl group leads to the tolan **78**. The modern variant of the FBW rearrangement involves treatment of **76** with *n*-BuLi to form intermediate **77**. In many respects, the FBW rearrangement represents one of the earliest synthetic routes towards carbon-rich materials, as acetylenes could now be used as a highly conjugated linker between aromatic systems.

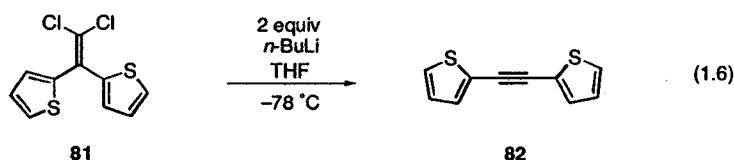


Scheme 1.16

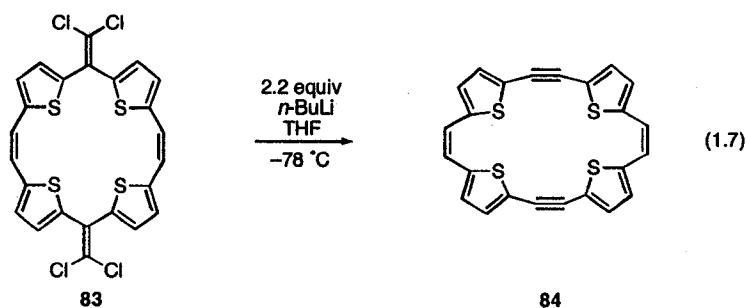
The ability to vary the identity of the migrating aryl group has greatly expanded the scope of the reaction. For example, Köbrich was able to show that chloroolefin **79**, appended in the β position by a phenyl and a biphenyl moiety, rearranges to form the extended system **80** in 63% yield, eq 1.5.⁵⁹



Heteroaryl moieties, such as thiophenes also demonstrate a high migratory potential in the Fritsch-Buttenberg-Wiechell reaction.⁶⁰ The high yielding rearrangement of the bis-thiophene adduct **81** in eq 1.6 set the stage for expansion to larger conjugated systems which incorporate the thiophene moiety.

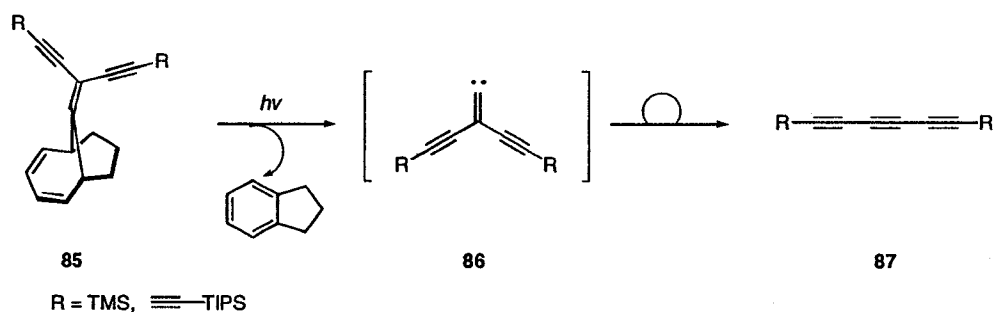


Strained annulene **84** in eq 1.7 was achieved in 30% yield using a double FBW rearrangement. Previous attempts to realize this structure using other methods resulted only in trace formation, the major product consisting of a larger cycle.⁶¹



In a related reaction, Tobe has recently generated alkylidene carbenes with pendant alkynyl moieties as migrating groups to form polyynes.⁶² Carbene species **86** is formed from ene-diyne **85** via photochemical-induced extrusion of

indene. One of the ethynyl or butadienyl moieties then undergoes a 1,2-migration to form the polyynes **87**.



Scheme 1.17

1.2 Conclusions

Alkylidene carbenoids and carbenes have been used to form a number of carbon-rich structures, some of which would have been very difficult to make using other methods of carbon-carbon bond formation. Although not a commonly used technique, there are several instances, such as in the formation of radialenes and fullerene fragments, where alkylidene carbene/carbenoids were a critical part of the synthetic evolution. Unsaturated carbenoids continue to be used for the purpose of forming highly conjugated structures, specifically polyynes containing materials.

1.4 References and Notes

1. Chenciner, R., *Madder Red: A history of luxury and trade*; Curzon Press: Richmond, 2000.

2. Balfour-Paul, J., *Indigo in the Arab World*; Curzon Press: Richmond, 1997.
3. Zollinger, H. *Color Chemistry: Syntheses, Properties, and Applications of Organic Dyes and Pigments*. VCH: Weinheim, 1987.
4. *Kekule Centennial*; Gould, R. F., Ed.; American Chemical Society: Washington, 1966.
5. Wurthner, F., *Angew. Chem. Int. Ed.* **2001**, *40*, 1037.
6. Loufty, R. O.; Hor, A.-M.; Hsiao, C.-K.; Baranyi, G.; Kazmaier, P., *Pure. Appl. Chem.* **1988**, *60*, 1047.
7. Bassler, H., *Adv. Mater.* **1993**, *5*, 662.
8. Nalwa, H. S. *Handbook of Organic Conductive Materials and Polymers*; Wiley: New York, 1997.
9. Natta, G.; Mazzanti, G.; Corradini, P., *Atti Accad. Naz. Lincei Cl. Sci. Fis. Mat. Nat. Rend.* **1958**, *25*, 3.
10. Shirakawa, H., *Angew. Chem. Int. Ed.* **2001**, *40*, 2574.
11. MacDiarmid, A. G., *Angew. Chem. Int. Ed.* **2001**, *40*, 2581.
12. Heeger, A. J., *Angew. Chem. Int. Ed.* **2001**, *40*, 2591.
13. Sonogashira, K.; Tohda, Y.; Hagahira, N., *Tetrahedron Lett.* **1975**, 4467.
14. Castro, C. E.; Stephens, R. D., *J. Org. Chem.* **1963**, *28*, 2163.
15. Stille, J. K., *Angew. Chem., Int. Ed. Engl.* **1986**, *25*, 508.
16. Glaser, C., *Ann. Chem. Pharm.* **1870**, *154*, 137.
17. Hay, A. S., *J. Org. Chem.* **1962**, *27*, 3320.
18. Eglinton, G.; Galbraith, A. R., *Chem. Ind. (London)* **1956**, 737.
19. Chodkiewicz, W., *Ann. Chim. (Paris)* **1957**, *2*, 819.
20. Stang, P. J., *Chem. Rev.* **1978**, *78*, 383.
21. Kirmse, W., *Angew. Chem. Int. Ed. Engl.* **1997**, *36*, 1164.
22. Harada, T.; Fujuwara, T.; Iwazaki, K.; Oku, A., *Org. Lett.* **2000**, *2*, 1855.

23. Schildknecht, K.; Bohnstedt, A. C.; Feldman, K. S.; Sambandam, A., *J. Am. Chem. Soc.* **1995**, *117*, 7544.
24. Fischer, R. H.; Baumann, M.; Köbrich, G., *Tetrahedron Lett.* **1974**, *13*, 1207.
25. Stang, P. J.; Ladika, M., *J. Am. Chem. Soc.* **1981**, *103*, 6437.
26. Bleiholder, R. F.; Shechter, H., *J. Am. Chem. Soc.* **1964**, *86*, 5032.
27. Baati, R.; Barma, D. K.; Falck, J. R.; Mioskowski, C., *J. Am. Chem. Soc.* **2001**, *123*, 9196.
28. Kasatkin, A.; Whitby, R. J., *J. Am. Chem. Soc.* **1999**, *121*, 7039.
29. Hauser, C. R.; Lednicer, D., *J. Org. Chem.* **1957**, *22*, 1248.
30. Curtin, D. Y.; Richardson, W. H., *J. Am. Chem. Soc.* **1959**, *81*, 4719.
31. Köbrich, G., *Angew. Chem., Int. Ed. Engl.* **1965**, *4*, 49.
32. Duraisamy, M.; Walborsky, H. M., *J. Am. Chem. Soc.* **1984**, *106*, 5035.
33. Köbrich, G.; Drischel, W., *Tetrahedron* **1966**, *22*, 2621.
34. Köbrich, G.; Heinemann, H., *Angew. Chem., Int. Ed. Engl.* **1965**, *4*, 594.
35. Tatanabe, M.; Walsh, R. A., *J. Am. Chem. Soc.* **1963**, *85*, 3522.
36. van Loon, J.-D.; Seiler, P.; Diederich, F., *Angew. Chem., Int. Ed. Engl.* **1993**, *32*, 1187.
37. Iyoda, M.; Otani, H.; Oda, M.; Kai, Y.; Baba, Y.; Kasai, N., *J. Am. Chem. Soc.* **1986**, *108*, 5371.
38. Kawase, T.; Muro, S.; Kurata, H.; Oda, M., *J. Chem. Soc., Chem. Comm.* **1992**, 778.
39. Morken, P. A.; Bachand, P. C.; Swenson, D. C.; Burton, D. J., *J. Am. Chem. Soc.* **1993**, *115*, 5430.
40. Hartzler, H. D., *J. Am. Chem. Soc.* **1966**, *88*, 3155.
41. Scott, L.; DeCicco, G. J., *J. Org. Chem.* **1980**, *45*, 4055.
42. Hopfner, T.; Jones, P. G.; Ahrens, B.; Dix, I.; Ernst, L.; Hopf, H., *Eur. J. Org. Chem.* **2003**, 2596.
43. Hopf, H.; Maas, G., *Angew. Chem., Int. Ed. Engl.* **1992**, *31*, 931.

44. Maas, G.; Hopf, H. Synthesis and transformation of radialenes. In *The Chemistry of Dienes and Polyenes*; Rappoport, Z., Eds.; John Wiley and Sons Ltd: Chichester, 1997; pp 927-977.
45. Iyoda, M.; Otani, H.; Oda, M., *Angew. Chem., Int. Ed. Engl.* **1988**, *27*, 1080.
46. Iyoda, M.; Mizusuna, A.; Kurata, H.; Oda, M., *J. Chem. Soc., Chem. Comm.* **1989**, 1690.
47. Iyoda, M.; Nakamura, N.; Todaka, M.; Ohtsu, S.; Hara, K.; Kuwatani, Y.; Yoshida, M.; Matsuyama, H.; Sugita, M.; Tachibana, H.; Inoue, H., *Tetrahedron Lett.* **2000**, *41*, 7059.
48. Iyoda, M.; Otani, H.; Oda, M.; Kai, Y.; Baba, Y.; Kasai, N., *J. Chem. Soc., Chem. Comm.* **1986**, 1794.
49. Mehta, G.; Rao, H. S. P., *Tetrahedron* **1998**, *54*, 13325.
50. Scott, L.; Boorum, M.; McMahon, B. J.; Hagen, S.; Mack, J.; Blank, J.; Wegner, H.; de Meijere, A., *Science* **2002**, *295*, 1500.
51. Hirsch, A. *Fullerenes and Related Structures*; Springer-Verlag: Berlin, 1999.
52. Brown, R. F. C., *Eur. J. Org. Chem.* **1999**, 3211.
53. Brown, R. F. C.; Eastwood, F. W.; Harrington, K. J.; McMullen, G. L., *Aust. J. Chem.* **1974**, *27*, 2393.
54. Brown, R. F. C.; Eastwood, F. W.; Jackman, G. P., *Aust. J. Chem.* **1978**, *31*, 579.
55. Scott, L.; Hashemi, M. M.; Meyer, D. T.; Warren, H. B., *J. Am. Chem. Soc.* **1991**, *113*, 7082.
56. Rabideau, P. W.; Abdourazah, A. H.; Folsom, H. E.; Marcinow, Z.; Sygula, A.; Sygula, R. J., *J. Am. Chem. Soc.* **1994**, *116*, 7891.
57. Fritsch, P., *Liebigs Ann. Chem.* **1894**, *279*, 319.
58. Buttenberg, W. P., *Liebigs Ann. Chem.* **1894**, *279*, 324.
59. Köbrich, G.; Trapp, H.; Hornke, I., *Chem. Ber.* **1967**, *100*, 961.
60. Mouries, V.; Waschbusch, R.; Carran, J.; Savignac, P., *Synthesis* **1998**, 271.
61. Kawase, T.; Darabi, H. R.; Uchimiya, R.; Oda, M., *Chem. Lett.* **1995**, 499.

62. Tobe, Y.; Iwasa, N.; Umeda, R.; Sonoda, M., *Tetrahedron Lett.* **2001**, *42*, 5485.

Chapter 2 Alkyne Migration in Alkylidene Carbenoid Species: A New Method of Polyynes Synthesis

2.1 Introduction

Interest in polyalkynyl containing structures has exploded over the last two decades, and *sp*-hybridized carbon building blocks are targeted for use in a variety of areas.¹⁻³ Many novel nanometer sized molecules incorporate diynes and triynes for structural rigidity in addition to the interesting electronic properties inherent to polyynes.⁴ For example, there is extensive literature on carbon-rich, alkyne containing macrocycles.⁵⁻⁹ Acyclic oligomers containing polyynes segments have also been found to display interesting optical properties.¹⁰

Due to the widespread interest in incorporating the alkynyl moiety into carbon-rich scaffolding, synthetic methods that can accomplish this goal in a facile manner are desirable. The three most commonly used methods to form polyynic structures, oxidative homocoupling techniques, the Cadiot-Chodkiewicz coupling, and Sonogashira coupling, each have their own niche. Oxidative homocoupling procedures such as Glaser,¹¹ Hay,¹² or Eglinton/Galbraith¹³ protocols are used to couple terminal acetylenes to form symmetrical products with an even number of acetylene units, such as diynes and tetraynes. Attempts to use these protocols toward unsymmetrical products or polyynes with an odd number of acetylene units, however, generally result in complex mixtures that are difficult to separate unless a huge excess of one coupling partner is used. A complementary procedure, the Cadiot-Chodkiewicz reaction,¹⁴ can be used to form

unsymmetrical polyynes, with either an even or odd number of acetylene moieties via the coupling of a terminal acetylene and an alkynyl halide. Aryl-alkynyl building blocks can be formed using Sonogashira-Hagihara¹⁵ and related coupling procedures.¹⁶⁻¹⁹ These reactions involve the palladium-catalyzed cross-coupling of an aryl halide or triflate and a terminal alkyne. The common link between the methods is the need for a terminal acetylene as a starting material, molecules which can be unstable and often difficult to work with. The formation of extended polyyne systems can also be problematical as there is a direct correlation between an increase in the number of acetylene units in an unprotected polyyne and a dramatic decrease in stability. Several strategies have been developed to circumvent the need for a sensitive terminal alkyne. Two approaches which avoid a separate deprotection step include the *in situ* desilylation of a protected alkyne and the direct coupling of a trialkylsilyl protected acetylene.²⁰⁻²³ Alternatively, another option is to form the polyyne framework in the final step through either elimination or extrusion of a suitable functional group.^{24,25} While these routes have afforded a number of interesting derivatives, in most cases their generality has yet to be established.²⁶

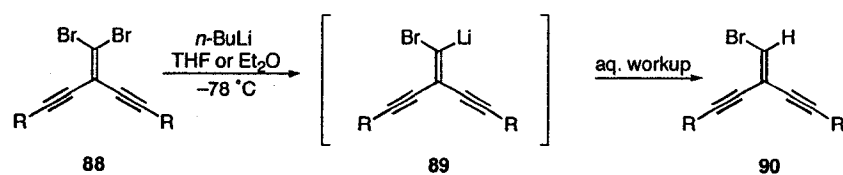
As described earlier, the Fritsch-Buttenberg-Wiechell reaction is an established method of forming acetylenes.²⁷⁻²⁹ Until now, alkynes were not known to migrate in an FBW rearrangement and, in fact, have only been observed to migrate in a few pinacol reactions.^{30,31} We have found that by modifying the FBW rearrangement, it is possible to induce the 1,2-migration of an alkyne in a carbenoid intermediate to form a polyyne.³² Precursors can be strategically functionalized in order to provide polyyne derivatives that would be difficult or impossible to access by other methods. Alkylidene carbenoids are thus an efficient and versatile route to functionalized diyne and triyne building blocks.

Perhaps most remarkable is the ability to perform several simultaneous/consecutive rearrangements in a one-pot approach which has facilitated the formation of extended carbon networks in a few high yielding steps.

2.2 Results and Discussion

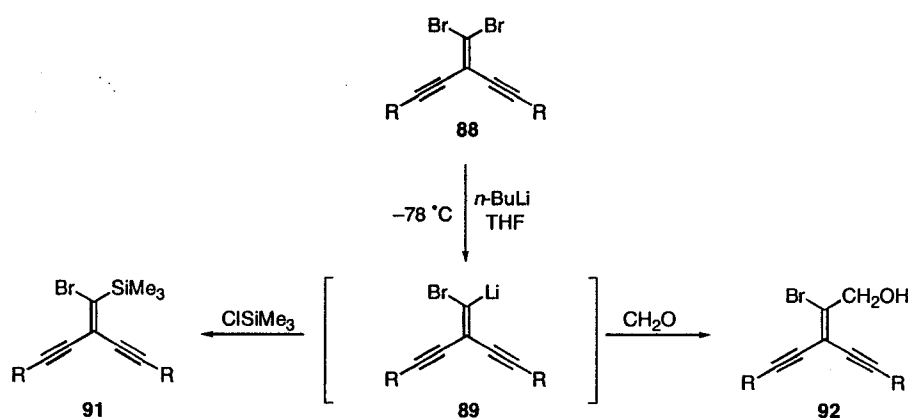
2.2.1 1,2-Migration of Alkynes

Initial attempts to induce rearrangement of a 2,2-dialkynyl-1,1-dibromo-olefin to a triyne involved treating **88** ($R = Si\text{-}i\text{-}Pr_3$) with $n\text{-BuLi}$ in THF at $-78\text{ }^\circ\text{C}$, which are the common FBW rearrangement conditions.³³ Lithium-halogen exchange between $n\text{-BuLi}$ and dibromoolefin **88** presumably resulted in the formation of carbenoid **89**, and the reaction mixture was allowed to warm slowly to various temperatures. These reaction conditions did not, however, afford appreciable amounts of triyne. While mass spectral analysis of the product mixtures did suggest the formation of trace amounts of the desired rearranged product, the protonated species **90** was the major product, presumably resulting from protonation of the lithiated intermediate **89** upon work-up. Likewise, reactions conducted in Et_2O and dioxane were equally unsuccessful.



Scheme 2.1

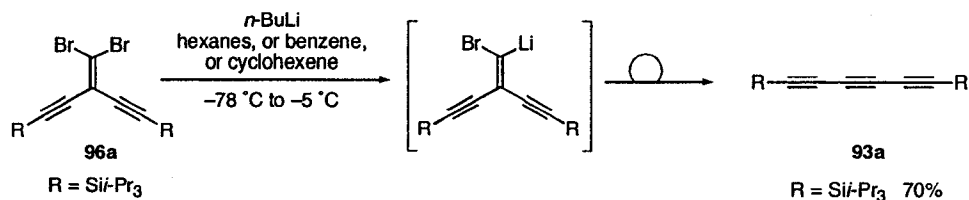
As described earlier, the mode of reactivity of a carbenoid depends on several factors and is very sensitive to reaction conditions. Coordinating solvents, Et₂O and THF are known to stabilize carbenoid **89**, allowing the reactive intermediate to be trapped by an electrophile. There are, in fact, examples in the literature where these conditions have been used to derivatize the dibromoolefin moiety as shown in Scheme 2.2 with the formation of bromide **91** and alcohol **92**, R = Si*i*-Pr₃.³³⁻³⁵



Scheme 2.2

Köbrich's early work determined that solvent polarity can play an important role in the success of a FBW rearrangement.³⁶ Assuming that the solvating ability of Et₂O and THF was a stabilizing factor that prevented or retarded collapse of the vinyl lithium intermediate **89**, the rearrangement was attempted in less polar, noncoordinating solvents, such as hexanes, benzene, and cyclohexene. The reaction was repeated in each of the non-coordinating solvents using otherwise standard conditions (for benzene, *n*-BuLi was added at -15 °C), as shown in Scheme 2.3. TLC analysis indicated loss of starting material and the formation of one product. Upon allowing the reaction to warm the starting material was completely converted to the product, with no production of vinyl

bromide **90** observed after work-up. ^{13}C NMR spectroscopic and mass spectral analysis confirmed the structure as the triyne **93a**. It was found that alkynes not only readily undergo 1,2-shifts in alkylidene carbenoid intermediates, they do so extremely well, as the triyne **93a** was isolated in high yield.



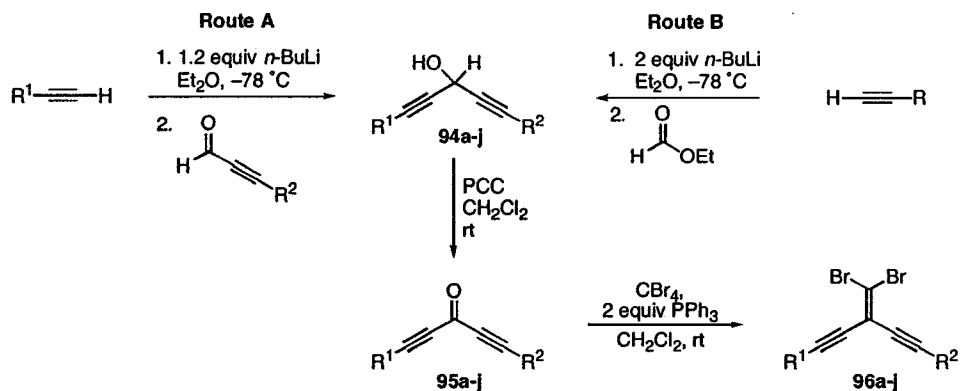
Scheme 2.3

General reaction conditions for triyne formation have been established as follows, 1.2 equiv of *n*-BuLi is slowly added to a $-78\text{ }^\circ\text{C}$ solution of the dibromoolefin in hexanes. The solution is allowed to warm to $-10\text{ }^\circ\text{C}$ over a period of 30 min to 1 hour, then quenched with NH_4Cl . Strictly anhydrous conditions must be maintained prior to quenching to ensure no by-products are formed during the reaction. Formation of protonated products such as **90** greatly complicate purification because they have similar R_f values as the polyynes. If the reaction is kept rigorously free of water, the polyne is the only observed product and can easily be purified by passage through a plug of silica.

2.2.2 Formation of Functionalized Triynes

General use of this rearrangement towards the formation of polyalkynyl systems is highly dependent on the availability of the dibromoolefin precursors. We have therefore exploited several methods where symmetrically and unsymmetrically

functionalized dibromides can be formed in a few simple steps from easily available starting materials.

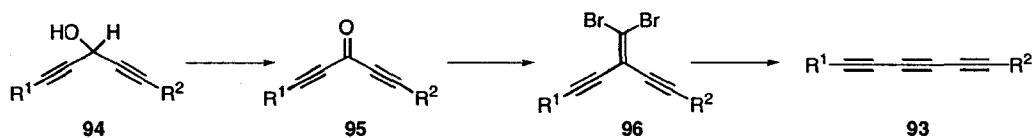


Scheme 2.4

The first method for dibromoolefin formation is shown in Scheme 2.4 and involves formation of the enediyne skeleton from simple acetylenes. There are two routes that can be used: Route A to form an unsymmetrical product involving the addition of the appropriate lithium acetylide to an α,β -ethynyl aldehyde to afford alcohol **94**.³⁷⁻⁴⁰ Route B is used to form symmetrical alcohols via the condensation of 2 equiv of a lithium acetylide into ethyl formate.⁴¹ In both cases, the alcohols can generally be isolated pure after work-up. Oxidation to the ketone **95** can easily be effected in under two hours using PCC. In most cases, the ketones **95** are stable when isolated and can be completely characterized. When the ketone is unstable, or is suspected of being unstable, the PCC reaction is passed through a plug of silica to remove the oxidant and excess CH_2Cl_2 is removed to give a solution of the ketone in ~ 5 mL of CH_2Cl_2 . The crude ketone is then carried directly on to the dibromoolefination reaction. The desired dibromoolefins **96** are then formed via the method of Corey and Fuchs.⁴² Yields for this olefination step are generally excellent, although there are a few cases where the instability of some

derivatives has resulted in lower yields. Dibromides can then be rearranged to triynes using the standard rearrangement conditions described above. Shown in Table 2.1 is a summary of yields for several examples of triynes where the dibromoolefins were formed by the synthetic routes outlined in Scheme 2.4.

Table 2.1 Summary of synthetic yields for compounds 93-94

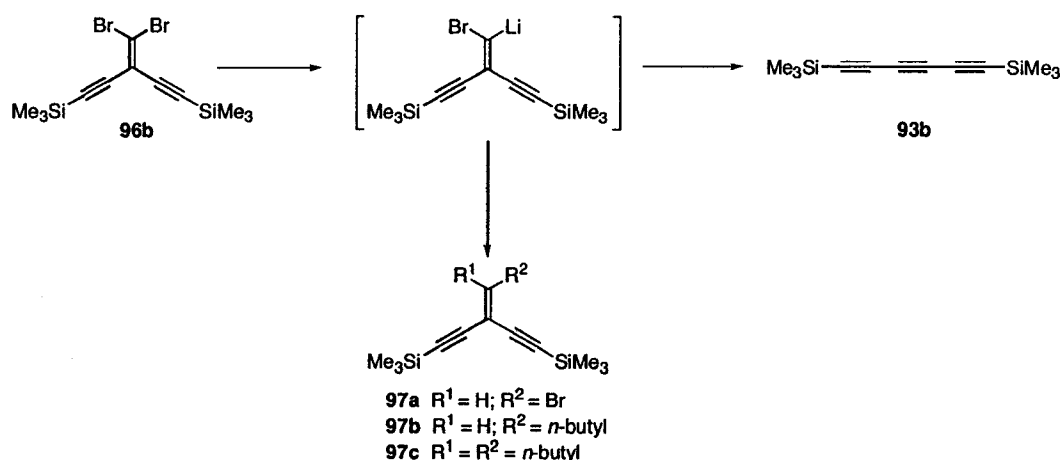


Cmpd	R ¹	R ²	94 [%]	95 [%]	96 [%]	93 [%]
a	<i>i</i> -Pr ₃ Si	<i>i</i> -Pr ₃ Si	[³³]	[³³]	[³³]	70
b	Me ₃ Si	Me ₃ Si	[⁴³]	[⁴³]	[³⁷]	50
c	<i>i</i> -Pr ₃ Si	Me ₃ Si	[³⁷]	[³⁷]	[³⁷]	61
d	1-naphthyl	Me ₃ Si	60	54	54	70
e	1-naphthyl	<i>i</i> -Pr ₃ Si	55	47	82	62
f	<i>n</i> -butyl	<i>n</i> -butyl	92 ⁴⁴	73 ⁴⁵	40	80
g	<i>n</i> -octyl	<i>n</i> -octyl	76 ⁴⁶	87 ⁴⁶	54	66
h	Me ₃ Si	<i>i</i> -Pr ₃ Si-C≡C-C ₆ H ₄ -X	31	-	53 ^[a]	61
i	Me ₃ Si	<i>n</i> -butyl	98	57	60	82
j	2-thienyl	2-thienyl	40	50	47	64

[a] Two-step yield from alcohol.

A variety of substitution patterns are tolerated by the reaction conditions. Symmetrical heteroaryl (96j) and alkyl (96f,g) substituted dibromoolefins easily afford the substituted triynes in good yields.^{22,47} The presence of the trialkylsilyl alkynyl moieties in examples 96a, c-e, and i does not hinder the rearrangement and provides unsymmetrical triynes which can be further derivatized. Formation of the carbon-rich skeleton 93h in a few steps is also noteworthy, with the differential silyl protective

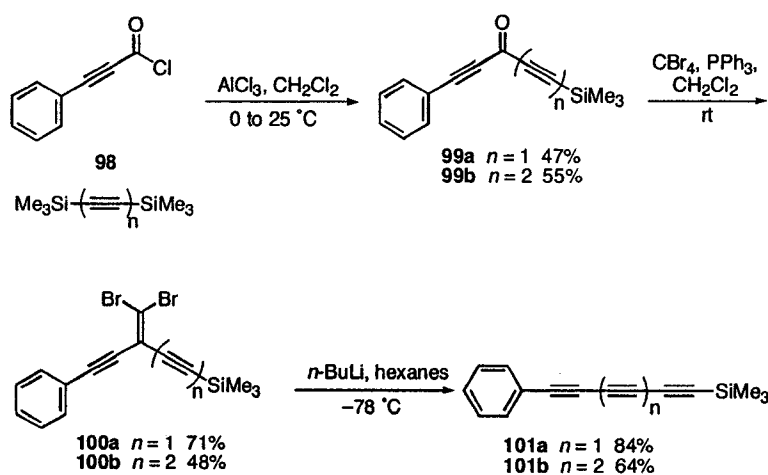
groups allowing for further elaboration. The only dibromoolefin that has consistently failed to rearrange cleanly and in good yield to the triyne is bis-trimethylsilyl protected **96b**. Unlike the other rearrangement examples in Table 2.1, the formation of triyne **93b** was always accompanied by varying amounts of **97a-c**, which were identified by ¹H NMR spectroscopy. As shown in Scheme 2.5, these by-products result from the reaction of the lithiated species with an electrophile, either with a proton upon work-up or with the butyl bromide that is created after lithium-halogen exchange occurs. Although initial attempts to induce the rearrangement of dibromide **96b** to triyne **93b** resulted in extremely low yields of the polyynes and significant amounts of the by-products **97a-c**, it was found that purification of the less stable dibromide **96b** just prior to rearrangement provided the bis-trimethylsilyl triyne **93b** in 50% yield, with a smaller percentage of the unwanted olefins **97a-c** being produced.



Scheme 2.5

The Friedel-Crafts acylation reaction provided an alternate entry into 1,1-dibromoolefins as shown in Scheme 2.6.⁴⁸ Phenylpropynoic acid was easily converted

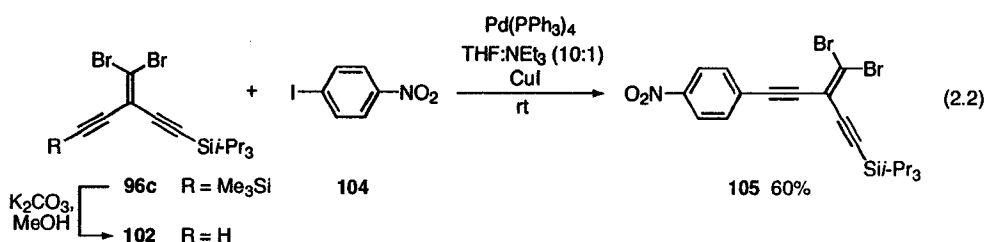
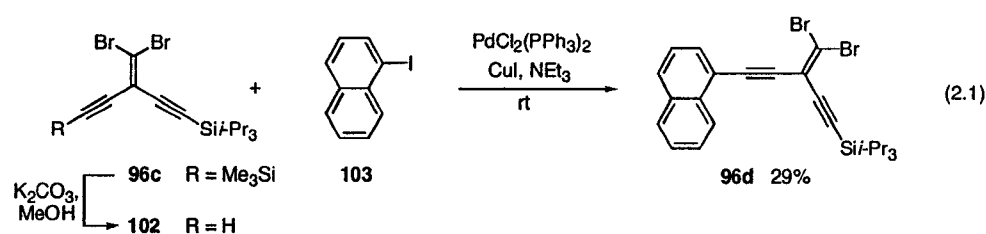
into acid chloride **98** with thionyl chloride and the acylation of acid chloride **98** with bis(trimethylsilyl)acetylene provided ketone **99a** in one step. One of the advantages of using this particular route was that additional acetylene units could be easily incorporated by performing the same acylation reaction of **98** with bis(trimethylsilyl)butadiyne. Ynones **99a,b** were thus isolated in 47% and 55% yields respectively. Dibromo-olefination then afforded **100a,b**, and subsequent rearrangement gave phenyl-capped triyne **101a** and tetrayne **101b** in 84% and 64% yield, respectively. As acetylenic carboxylic acids are readily available via condensation of the appropriate lithium acetylide or Grignard reagent with CO₂,⁴⁹ this pathway nicely broadens the scope of polyyne products that are potentially accessible using this methodology.



Scheme 2.6

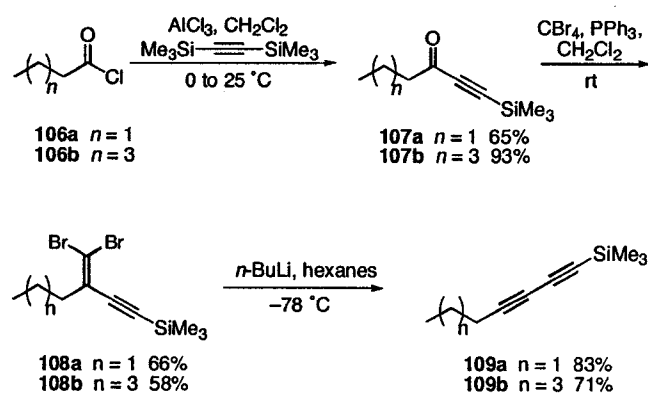
The elaboration of the enyne system via palladium-catalyzed cross-coupling was envisioned as a convenient route into aryl substituted 1,1-dibromoolefins. As shown in equation 2.1, differentially protected enediyne **96c** could be functionalized using the Sonogashira reaction.¹⁵ Protodesilylation produced a stable terminal acetylene **102** but

initial attempts to cross-couple **102** with iodoarene **103** using standard reaction conditions resulted in, at best, 29% yield of the desired product **96d**. Various by-products were also formed, which made purification difficult. The competitive reaction of the terminal acetylene with the vinyl bromide moiety of another equivalent of **96c** was believed to be responsible for the low yield and the formation of by-products. Subsequent experimentation indicated that the reaction is dependant on solvent and catalyst. Preliminary optimization of the procedure has shown that the coupling of dibromide **96c** with the electron deficient arene **104** to give **105**, eq 2.2, can afford increased yields and, more importantly, a decrease in the number of by-products produced.⁵⁰ These results would indicate that the Sonogashira reaction could be a promising route to aryl substituted enediynes.



2.2.3 Formation of Diynes and Tetraynes

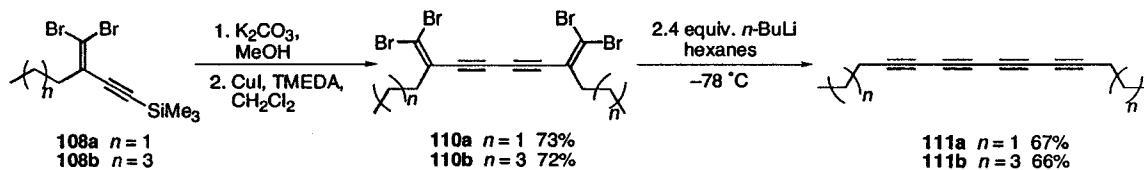
The modified FBW rearrangement may also be used to form diynes by inducing the α -elimination of a "mixed" dibromoolefin. A mixed rearrangement is one in which one of the two possible migrating groups is an alkyne and the other is an aryl, vinyl or alkyl group. Using this approach, a number of substituted 1,3-butadiynes were synthesized in a few steps from commercially available aldehydes or carboxylic acids. The examples below demonstrate the versatility of alkylidene carbenoids when used to form functionalized, acetylenic building blocks.



Scheme 2.7

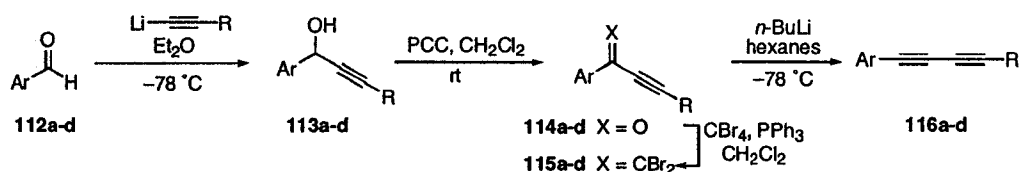
The methods employed to synthesize the dibromoolefins in the triyne examples can also be applied toward the formation of butadiynes. Shown in Scheme 2.7 is the formation of alkyl and trimethylsilyl substituted diynes **109**. Friedel-Crafts acylation of alkyl acid chlorides **106** with bis(trimethylsilyl)acetylene in the presence of AlCl_3 at 0°C easily affords ketones **107a,b** in good to excellent yields.^{51,52} Dibromoolefination of **107** generated **108a,b** in 58-66% yield using standard conditions in CH_2Cl_2 at room temperature. Subjecting dibromides **108a,b** to *n*-Buli at -78°C according to the standard

protocol described above affords diynes **109a** and **109b** as stable oils in good yields of 71-83%, respectively.



Scheme 2.8

The presence of the protective silyl group also allowed for further elaboration toward tetraynes **111** as in Scheme 2.8. The silyl group was removed from the dibromides **108** with K_2CO_3 in MeOH, and the resulting terminal acetylene was carried directly on to an oxidative homocoupling reaction to provide dibromides **110a,b** in good yields. A double rearrangement was induced with 2.4 equiv of *n*-BuLi and cleanly gave alkyl substituted tetraynes **111a,b**.^{22,53}

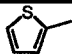
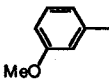
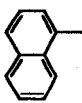
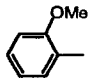


Scheme 2.9

The second synthetic sequence toward unsymmetrical, aryl substituted butadiynes began with the condensation of an aryl aldehyde and a lithium acetylide, as outlined in Scheme 2.9.⁵⁴ The appropriate aryl carboxaldehyde **112** was added to a slight excess of the acetylide, which had been formed previously by the addition of *n*-BuLi to a solution of the terminal acetylene in Et₂O. The resultant alcohol **113** was subsequently oxidized

with PCC and then treated with $\text{CBr}_4/\text{PPh}_3$ to form derivative **115**. The dibromoolefination step is the weakest link in the synthetic sequence and in the two cases where the diyne was terminated by a group other than a trimethylsilyl moiety, the yields from the Corey-Fuchs reaction were dramatically reduced. Although several other reaction conditions have been attempted, this low yielding step remains the predominant limitation of the methodology. Regardless, by employing the usual rearrangement conditions, butadiynes **116a-d** were achieved in excellent yields in most cases. Yields of intermediates and diynes are summarized in Table 2.2. The conversion of *o*-methoxybenzene substituted dibromoolefin **115d** to diyne **116d** proceeded in comparatively low yield. This poor result is believed to be due to coordination of the methoxy group to the lithiated carbenoid intermediate, as has been previously observed by Köbrich.⁵⁵

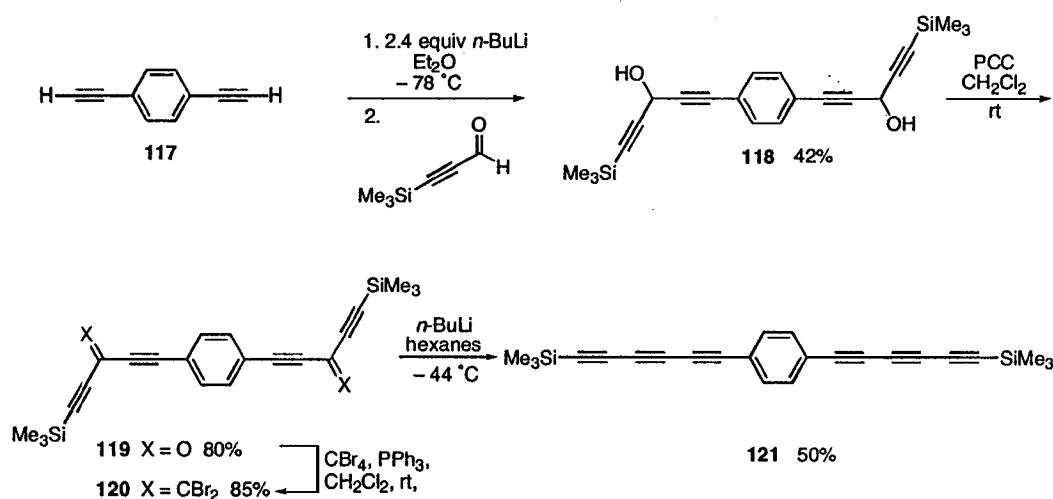
Table 2.2. Yields for Synthesis of Diynes **116a-d** (Scheme 2.9)

Cmpd	Ar	R	113 [%]	114[%]	115[%]	116[%]
a		<i>n</i> -butyl	94	82	16	86
b		<i>n</i> -butyl	88	46	7	92
c		SiMe_3	64	–	44 ^[a]	93
d		SiMe_3	90 ⁵⁶	–	59 ^[a]	43

[a] Two-step yield from alcohol

2.2.4 Extended Systems

One of the primary motivations behind developing methodology to form polyynic building blocks has been the inherent difficulty of forming extended arylyne systems via palladium-catalyzed, cross-coupling protocols. A reaction sequence was thus envisioned where extended systems could be prepared by initiating two or more FBW rearrangements on a single molecule (Scheme 2.10), as had been demonstrated in the formation of tetraynes **111**.



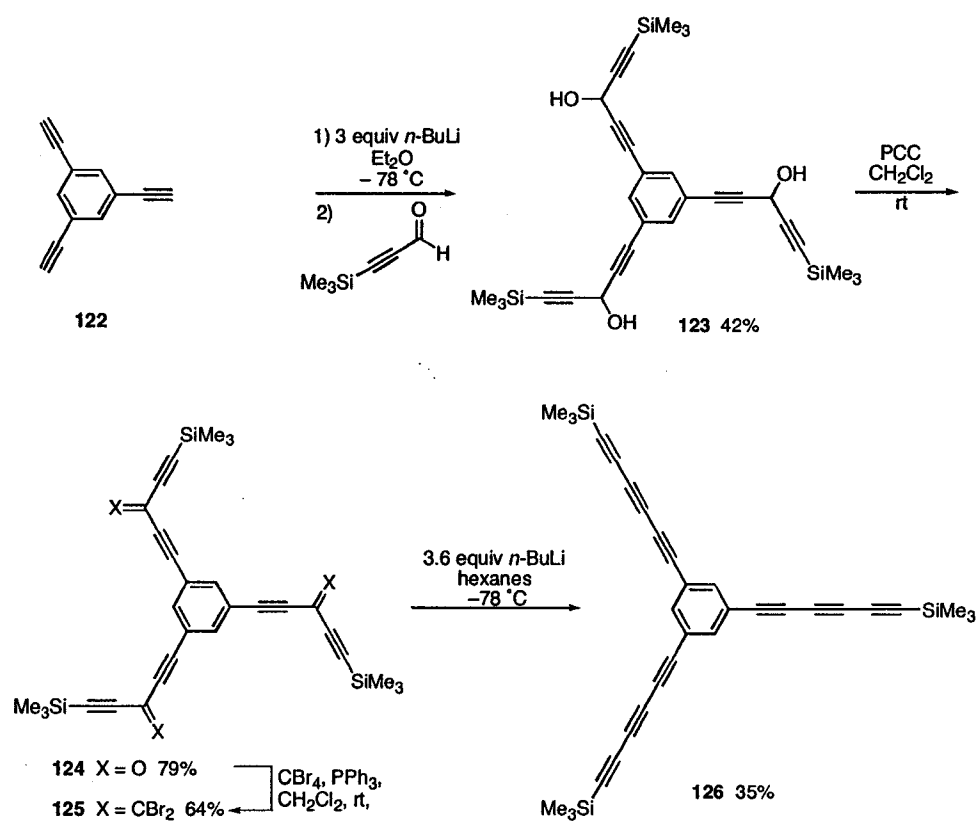
Scheme 2.10

The bis-lithium acetylide of 1,4-diethynyl benzene was formed by the addition of 2 equiv of *n*-BuLi to **117** in Et₂O at -78 °C. Subsequent addition of 2 equiv of 3-trimethylsilylpropynal⁴⁹ provided diol **118**, presumably as a mixture of diastereomers. Oxidation was carried out by PCC, as in the previous examples. The resultant diketone was somewhat unstable and therefore carried directly onto the dibromo-olefination reaction. As the PCC oxidation and the Corey-Fuchs reaction are carried out in the same solvent, it was convenient to simply plug the oxidation reaction mixture through silica

gel, reduce the solvent volume down to ~5 mL then add it to a stirred mixture of CBr₄ and PPh₃. Following this procedure, the tetrabromide **120** was isolated in an excellent yield of 85% over the two steps. The standard conditions used for rearrangement had to be altered, as it was discovered that tetrabromide **120** was insoluble at -78 °C. Warming of the heterogeneous mixture of **120** in hexanes to -44 °C resulted in a homogeneous solution, to which 2.4 equiv of *n*-BuLi was added. By allowing the solution to warm to ~ -5 °C hexayne **121** was isolated in 50% yield. By reducing the volume of a solution of **121** in hexanes, flat, shiny crystals can be formed which are stable for an indefinite period of time under refrigeration.

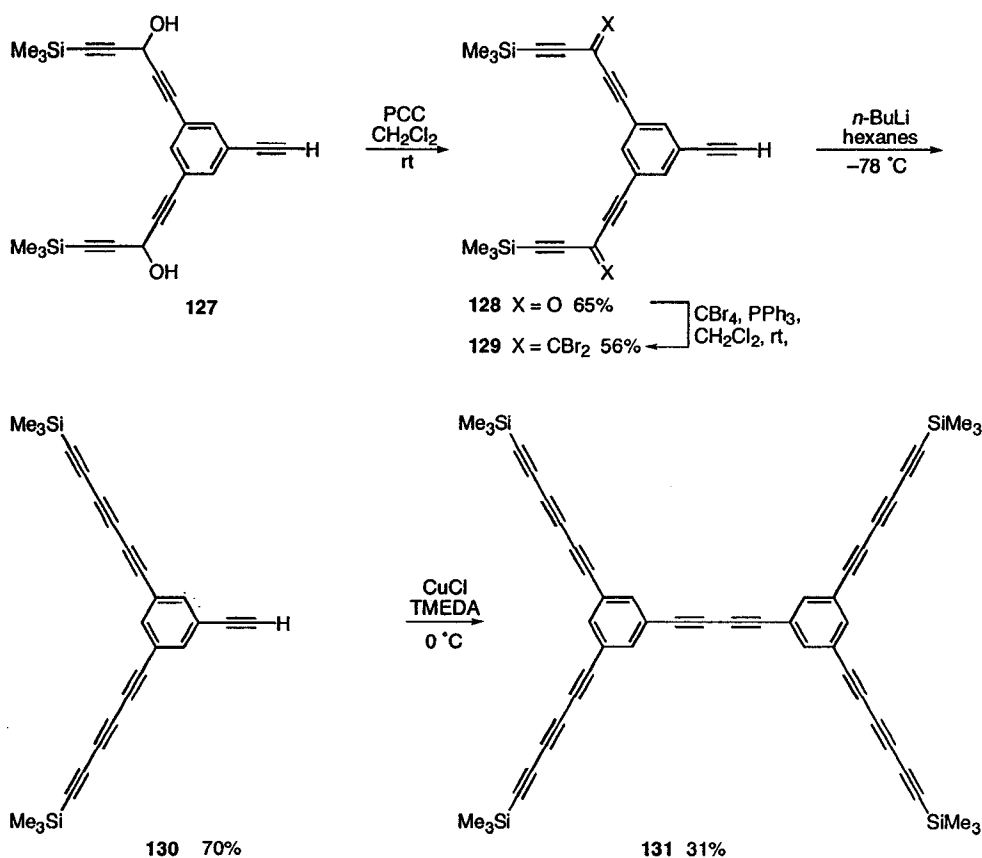
Tris-1,3,5-[1,3,5-hexatriynyl]benzene **126** can be formed in a similar manner as outlined for hexayne **121**. Tris-lithiation of 1,3,5-triethynylbenzene⁵⁷ **122** followed by condensation with trimethylsilyl propargyl aldehyde provided triol **123** in 42% yield. After oxidation with PCC to give trione **124** (a surprisingly stable white solid), three-fold dibromo-olefination gave hexabromide **125** in 64%. Unlike the tetrabromide **120**, **125** is soluble in hexanes at -78 °C and lithium-halogen exchange can be initiated at low temperature. To ensure all three rearrangements are complete, the temperature was allowed to rise to -40 °C before quenching with aqueous NH₄Cl. For the purposes of preventing the formation of possible by-products resulting from unfinished migration of all three dibromo-olefin moieties, the reaction progress must be monitored carefully by TLC. If quenching was initiated at the correct time, no protonated by-products were produced and nonayne **126** could be isolated simply by passing the crude reaction mixture through a short column of silica gel. The overall yield of **126** was 35%, which meant that each individual rearrangement proceeded in an average of 70% yield. Even

though **126** is a white crystalline solid, all attempts to grow crystals have so far proven futile as decomposition occurs when the sample is left neat.



Scheme 2.11

In the examples of polyalkynyl systems presented so far, all terminal acetylenes have been protected by trialkylsilyl moieties. The formation of diol **127**, a by-product that always accompanied the formation of triol **123**, presented an opportunity to investigate the efficiency of the reaction sequence when a terminal acetylene is present.



Scheme 2.12

Beginning with **127**, both the oxidation and dibromoolefination reactions can be performed in reasonable yields to give tetrabromide **129**. Although lithium-halogen exchange is a fast process, it was anticipated that deprotonation of the terminal acetylene would be a competitive reaction, therefore 3.6 equiv of *n*-BuLi were used to initiate α -elimination. Heptyayne **130** was thus formed as an unstable solid in 70% yield. It was expeditiously carried onto an oxidative coupling reaction to give the extended aryl-alkynyl system **131** in 31% yield. In spite of its highly unsaturated, polyyne framework, tetradeayne **131** is surprisingly stable and could be fully characterized spectroscopically.

The ^{13}C NMR spectrum is particularly interesting as all eight unique sp-hybridized carbons are well resolved.

2.2.5 Solid State Characterization

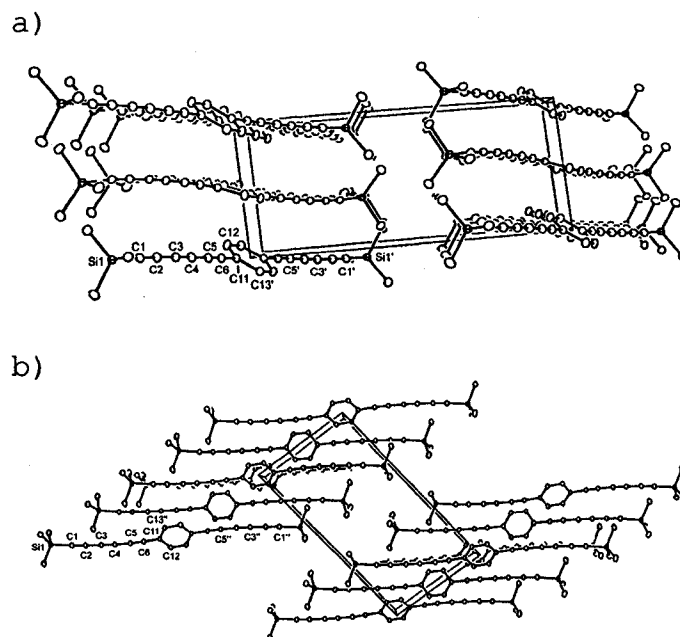


Figure 2.1 Illustration of crystal packing for compound **121** with the unit cell boundaries as indicated: a) view direction parallel to the crystallographic *a*-axis, with atom labels for molecule A, and b) view direction parallel to the crystallographic *b*-axis with atom labels for molecule B. All shown at 20% probability

Single crystallographic X-ray analyses of arylpolyynes **121** and **131** have been performed to reveal the solid state characteristics of these carbon-rich molecules. X-ray quality crystals of hexayne **121** could be obtained from a concentrated hexanes/ CH_2Cl_2 solution via diffusion of MeOH at 4 °C. As described in Figure 2.1, there are two

crystallographically unique molecules present in the unit cell, both of which show gentle curvature through their hexatriynyl arms. This curvature is unremarkable, however, as there are several known examples of polyynes which deviate easily from the usual 180° bond angles.

When recrystallized from hexanes, a presumed polymorph of compound **121** is stable as a solid for an indefinite period of time, crystals formed in the manner described above turn brown upon exposure to ambient conditions. An analysis of packing parameters with respect to topochemical polymerization provides insight into this behaviour. A high degree of alignment is observed along both the *a*- and *b*-axis. When viewed down the *a*-axis (in Figure 2.1a), the molecules are aligned in parallel rows. Within each row the phenyl rings of neighboring molecules are almost coplanar. The closest intermolecular contact, between C1 and C6, is 5.2 Å and is well outside the necessary range of 3.5 – 4 Å required for topochemical polymerization to occur.^{58,59} Other parameters such as the stacking angle ϕ between molecules (34°) and the stacking distance, *d*, (9.1 Å) are also outside the optimal values of $\phi = 27^\circ$ and *d* = 7.5 Å respectively, deeming polymerization in the solid-state along the *a*-axis unfavorable.

When viewed down the *b*-axis, however, as shown in Figure 2.1b, the stacking parameters would indicate that a 1,4-polymerization process is possible.^{58,60} The intermolecular contacts $R_{1,4} = 4.0$ Å and $R_{3,6} = 3.9$ Å are both within the desired range of ≤ 4 Å. The stacking angle and the stacking distance are near optimal for a 1,4-addition, with $\phi = 45$ and *d* = 5.5 Å. It would then seem reasonable to attribute the gradual darkening of the crystal under ambient conditions to competing 1,4- and 3,6-polymerization processes resulting from the parallel alignment of **121** in the solid state.

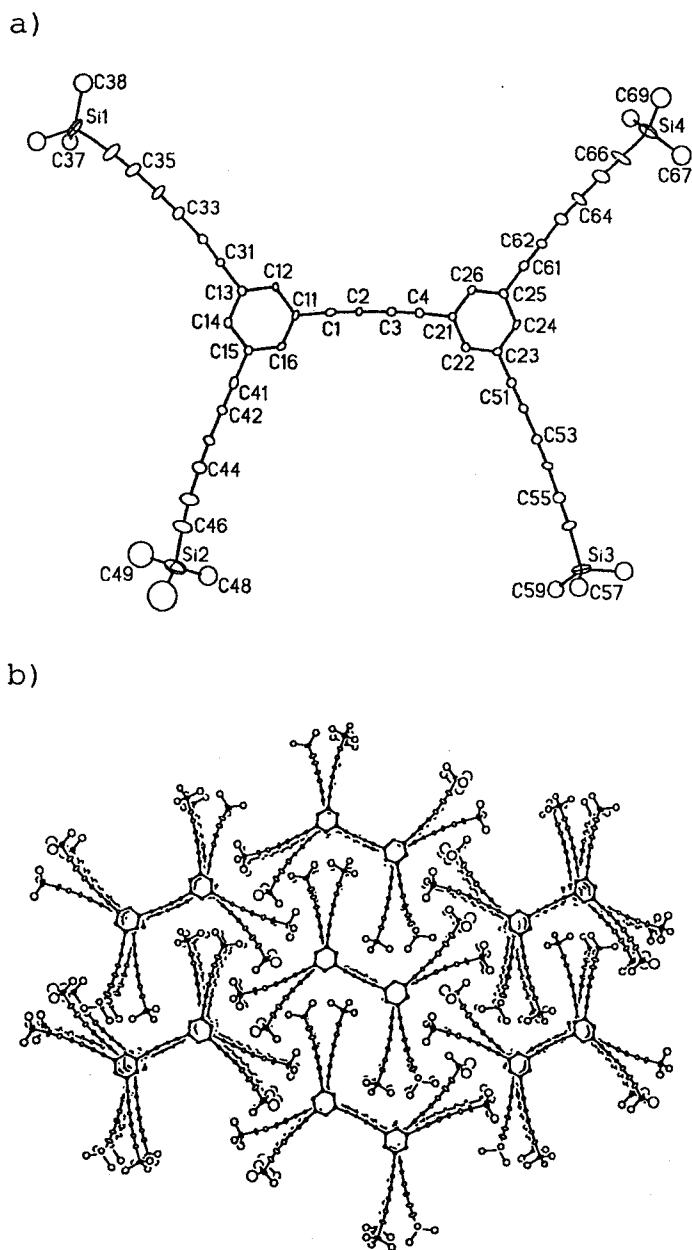


Figure 2.2 a) ORTEP drawing for compound **131**. b) View of crystal packing for **131** approximately along the crystal *a*-axis (*n*-hexane solvent molecules and hydrogen atoms removed for clarity). All shown at 20% probability

Single crystals of **131** suitable for X-ray crystallographic analysis have been grown from diffusion of MeOH into a hexanes/CH₂Cl₂ solution at -10 °C. An ORTEP drawing and a view of the crystal packing diagram are displayed in Figure 2.2. Although positional disorder increases toward the trimethylsilyl substituted termini of the individual triacetylene chains and hampers refinement of this structure, the overall solid state characteristics of this highly unsaturated molecule are still clearly evident. In Figure 2.2a, the slight bend to the butadiynyl moiety, which reduces the symmetry of the molecule, can be seen. This bend causes the bottom two hexatriynyl arms to be closer together than the top two hexatriynyl arms. Figure 2.2b shows the stacking as seen down the crystallographic *a*-axis. The aryl groups, which are nearly coplanar within one molecule, are also nearly coplanar with neighboring molecules and they are offset in a manner expected for face-to-face π -stacking. Each pair of neighboring molecules is related by a center of inversion, so that the butadiynyl segment curves in the opposite direction between pairs of stacked molecules. The alternating packing motif has the effect of causing neighboring hexatriynyl arms to be offset in space, accommodating the trimethylsilyl groups. Crystals of **119** are surprisingly stable under ambient conditions, a property that can be explained by two factors. The offset distance between neighboring triyne groups negates any possibility for polymerization. The butadiynyl moieties, the closest sp-hybridized segments in the structure, are outside the range necessary for a polymerization reaction to occur.⁵⁸⁻⁶⁰ Thus, single crystalline **29** remains reasonably stable at room temperature for periods of up to several days.

2.3 Conclusions

A general route to polyalkynes that allows for the efficient formation of a variety of structures has been developed. This route is based on the previously unreported ability of alkynes to undergo 1,2-migration in an alkylidene carbene/carbenoid species. These carbenoid intermediates are readily formed by lithium halogen exchange between 1,1-dibromo-2-ethynylefins and *n*-BuLi. Symmetrical and unsymmetrical diynes and triynes, functionalized with silyl, aryl, acetylenic and aryl groups, can be realized in a few steps. The dibromo-olefinic precursors are easily accessed via one of several routes, consisting of generally high yielding steps and easily purified intermediates. The ability to perform up to three sequential/consecutive rearrangements within the same molecule allows for the application of alkylidene carbenoid rearrangements towards the formation of extended, carbon-rich molecules that would otherwise be difficult to form using traditional techniques.

2.4 References and Notes

1. de Meijere, A. *Top. Curr. Chem.*; Springer: Berlin, 1999; Vol. 201.
2. Höger, S.; Enkelmann, V.; Bonrad, K.; Tschierske, C., *Angew. Chem., Int. Ed* **2000**, *39*, 2268.
3. Collins, S. K.; Yap, G. P. A.; Fallis, A. G., *Org. Lett.* **2000**, *2*, 3189.
4. Diederich, F.; Rubin, Y., *Angew. Chem., Int. Ed. Engl.* **1992**, *31*, 1101.
5. Tobe, Y.; Furukawa, R.; Sonoda, M.; Wakabayashi, T., *Angew. Chem. Int. Ed* **2001**, *40*, 4072.
6. Campbell, K.; McDonald, R.; Tykwinski, R. R., *J. Org. Chem.* **2002**, *67*, 1133.

7. Nielsen, M. B.; Schreiber, M.; Baek, Y. G.; Seiler, P.; Lecomte, S.; Boudon, C.; Tykwinski, R. R.; Gisselbrecht, J. P.; Gramlich, V.; Skinner, P. J.; Bosshard, C.; Gunter, P.; Gross, M.; Diederich, F., *Chem. Eur. J.* **2001**, *7*, 3263.
8. Marsden, J. A.; Palmer, G. J.; Haley, M. M., *Eur. J. Org. Chem.* **2003**, 2355.
9. Moore, J. S., *Acc. Chem. Res.* **1997**, *30*, 402.
10. Martin, R. E.; Gubler, U.; Cornil, J.; Balakina, M.; Boudon, C.; Bosshard, C.; Gisselbrecht, J. P.; Diederich, F.; Gunter, P.; Gross, M.; Bredas, J.-L., *Chem. Eur. J.* **2000**, *6*, 3611.
11. Glaser, C., *Ann. Chem. Pharm.* **1870**, *154*, 137.
12. Hay, A. S., *J. Org. Chem.* **1962**, *27*, 3320.
13. Eglinton, G.; Galbraith, A. R., *Chem. Ind. (London)* **1956**, 737.
14. Chodkiewicz, W., *Ann. Chim. (Paris)* **1957**, *2*, 819.
15. Sonogashira, K.; Tohda, Y.; Hagahira, N., *Tetrahedron Lett.* **1975**, 4467.
16. King, A. O.; Okahado, N.; Negishi, E., *J. Chem. Soc., Chem. Comm.* **1977**, 683.
17. King, A. O.; Negishi, E.; Villani, F. J.; Silveira Jr, A., *J. Org. Chem.* **1978**, 358.
18. Stille, J. K., *Angew. Chem., Int. Ed. Engl.* **1986**, *25*, 508.
19. *Metal-catalyzed Cross-coupling Reactions*; Diederich, F., Stang, P. J., Eds.; Wiley-VCH: Weinheim, 1998.
20. Nishihara, Y.; Ikegashira, K.; Hirabayashi, K.; Ando, J.; Mori, A.; Hiyama, T., *J. Org. Chem.* **2000**, *65*, 1780.
21. Hatanaka, Y.; Hiyama, T., *Synlett* **1991**, 845.
22. Heuft, M. A.; Collins, S. K.; Yap, G. P. A.; Fallis, A. G., *Org. Lett.* **2001**, *3*, 2883.
23. Bell, M. L.; Chiechi, R. C.; Johnson, C. A.; Kimball, D. B.; Matzger, A. J.; Wan, W. B.; Weakley, T. J. R.; Haley, M. M., *Tetrahedron* **2001**, *57*, 3507.
24. Rubin, Y.; Lin, S. S.; Knobler, C. B.; Anthony, J.; Boldi, A. M.; Diederich, F., *J. Am. Chem. Soc.* **1991**, *113*, 6943.
25. Tobe, Y.; Fujii, T.; Naemura, K., *J. Org. Chem.* **1994**, *59*, 1236.
26. Orita, a.; Yoshioka, N.; Struwe, P.; Braier, A.; Beckmann, A., *Chem. Eur. J.* **1999**, *5*, 1355.

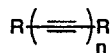
27. Fritsch, P., *Liebigs Ann. Chem.* **1894**, 279, 319.
28. Buttenberg, W. P., *Liebigs Ann. Chem.* **1894**, 279, 324.
29. Wiechell, H., *Liebigs Ann. Chem.* **1894**, 279, 337.
30. Schoenen, F. J.; Porco, J. A.; Schreiber, S. L.; VanDuyne, G. D.; Clardy, J., *Tetrahedron Lett.* **1989**, 30, 3765.
31. Marson, C. M.; Walker, A. J.; Pickering, J.; Hobson, A. D.; Wrigglesworth, R.; Edge, S. J., *J. Org. Chem.* **1993**, 58, 5944.
32. Tobe, Y.; Iwasa, N.; Umeda, R.; Sonoda, M., *Tetrahedron Lett.* **2001**, 42, 5485.
33. Lange, T.; vanLoon, J. D.; Tykwinski, R. R.; Schreiber, M.; Diederich, F., *Synthesis* **1996**, 537.
34. Feldman, K. S.; Weinreb, C. K.; Youngs, W. J.; Bradshaw, J. D., *J. Am. Chem. Soc.* **1994**, 116, 9019.
35. van Loon, J.-D.; Seiler, P.; Diederich, F., *Angew. Chem., Int. Ed. Engl.* **1993**, 32, 1187.
36. Köbrich, G.; Buck, P. In *Chemistry of Acetylenes*; Viehe, H. G., Ed.; Marcel Dekker: New York, 1969.
37. Anthony, J.; Boldi, A. M.; Rubin, Y.; Hobi, M.; Gramlich, V.; Knobler, C. B.; Seiler, P.; Diederich, F., *Helv. Chim. Acta* **1995**, 78, 13.
38. Kulkarni, B. A.; Chattopadhyay, S.; Chattopadhyay, A.; Mamdapur, V. R., *J. Org. Chem.* **1993**, 58, 5964.
39. Wadsworth, D. H.; Geer, S. M.; Detty, M. R., *J. Org. Chem.* **1987**, 52, 3662.
40. van Amsterdam, L. J. P.; Lugtenburg, J., *J. Chem. Soc., Chem. Comm* **1982**, 946.
41. Hauptmann, H.; Mader, M., *Synthesis* **1978**, 307.
42. Corey, E. J.; Fuchs, P. L., *Tetrahedron Lett.* **1972**, 3769.
43. Hauptmann, H., *Tetrahedron* **1976**, 32, 1293.
44. Mahrwald, S.; Quint, S., *Tetrahedron* **2000**, 56, 7463.
45. Metler, T.; Uchida, A.; Miller, S. I., *Tetrahedron* **1968**, 24, 4285.
46. Isele, G. L.; Scheib, K., *Chem. Ber.* **1975**, 108, 2312.
47. Mukai, C.; Miyakoshi, N.; Hanaoka, M., *J. Org. Chem.* **2001**, 66, 5875.

48. Walton, D. R. M.; Waugh, F., *J. Organomet. Chem.* **1972**, *37*, 45.
49. Brandsma, L. *Preparative Acetylenic Chemistry*; Elsevier: Amsterdam, 1988.
50. Work performed by summer student, Eric Hansen, under my supervision.
51. Yogo, T.; Koshina, J.; Suzuki, A., *Synth. Commun.* **1981**, *11*, 769.
52. Heiss, C.; Phillips, R. S., *J. Chem. Soc. Perkin Trans. I* **2000**, 2821.
53. Rossi, R.; Bellina, F.; Catarese, A.; Nannina, L.; Valensin, D., *Tetrahedron* **2000**, *56*, 479.
54. Shun, A. L.K.; Chernick, E. T.; Eisler, S.; Tykwinski, R. R., *J. Org. Chem.* **2002**, *68*, 1339.
55. Köbrich, G.; Trapp, H., *Chem. Ber.* **1966**, *99*, 680.
56. Baldoli, C.; DelButtero, P.; Licandro, E.; Maiorana, S.; Papagni, A.; Torchio, M., *Tetrahedron Lett.* **1993**, *34*, 7943.
57. Uno, M.; Dixneuf, P. H., *Angew. Chem. Int. Ed.* **1998**, *37*, 1714.
58. Baughman, R. H.; Yee, K. C., *J. Polym. Sci. Macromol. Rev.* **1978**, *13*, 219.
59. Enkelmann, V., *Chem. Mater.* **1994**, *6*, 1337.
60. Bassler, H., *Adv. Polym. Sci.* **1984**, *63*, 1.

Chapter 3 Synthesis, Electronic, Non-linear Optical and Physical Properties of Conjugated Polyynes

3.1 Introduction

An sp-hybridized carbon allotrope is notably absent from the list of known carbon allotropes that currently includes diamond, graphite, and the fullerenes.^{1,2} Cyclic allotropes consisting entirely of sp-hybridized carbon have been the object of intense interest for many years.³⁻⁹ Several routes have been designed toward the synthesis of cyclic forms of carbon, and cyclo-C20 and cyclo-C18 have been observed fleetingly via mass spectrometric analysis.^{10,11} Carbyne is the hypothetical linear form of carbon that consists entirely of sp-hybridized carbon.^{12,13} Linear carbyne has so far presented a significant synthetic challenge, and the allure of this elusive allotrope has stimulated a resurgence of interest in end-capped sp-hybridized carbon chains.¹⁴ Polyynes are the oligomeric cousins of carbyne, and it is expected that the properties of carbyne might be predicted by extrapolating trends observed in the spectroscopic data of polyynes.¹⁵ Sp-hybridized carbon oligomers are also interesting in their own right due to their unique electronic, optical and physical properties.



Series 1 R = *t*-Butyl

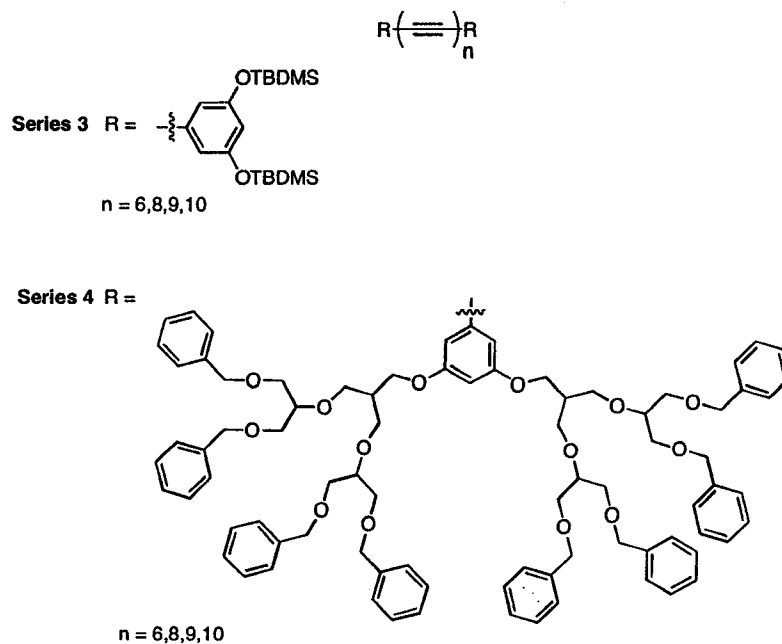
n = 2-8, 10, 12

Series 2 R = SiEt₃

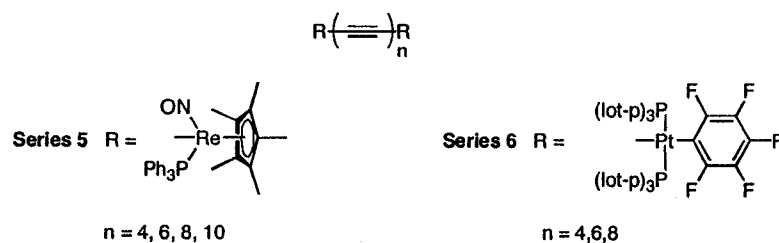
n = 2, 4, 6, 8, 9, 10, 12, 16

The first synthesis of extended polyynes was achieved 53 years ago by the research groups of Bohlmann and Jones, (Series 1).^{16,17} The longest chains were realized using the bulky *t*-butyl end-groups and these studies afforded chain lengths varying from C₈ to as long as C₂₄.¹⁸ Phenyl and methyl moieties were also utilized as end-capping groups in other series of polyynes.¹⁹⁻²¹ The potential of utilizing trialkylsilyl protecting groups for polyyne synthesis was realized by Walton.²² This breakthrough led to the formation of what is still the longest known polyyne, the hexadecayne (n = 16, Series 2). Elemental analysis could be used to confirm the structure of the smaller oligomers in Series 1 and 2 but only qualitative UV-Vis spectroscopy was available to confirm the structure of the majority of the longest polyynes due to the isolation of very small amounts of product.

Modern synthesis of polyynes has focused on three main goals. These goals include (1) experimenting with end-groups to improve stability and manipulate polyyne properties, (2) developing improved synthetic methodology, and (3) using modern methods of analysis to explore fully the properties of polyyne chains. There are a number of research groups who have synthesized small polyyne chains, (< 10 carbons),²³⁻²⁷ but Hirsch and Gladysz are distinguished as leaders in the field of contemporary, extended polyyne synthesis.



Hirsch's group has recently reported the synthesis of two series of polyynes chains, as shown above (Series 3 and 4).^{28,29} Bulky, spherical end groups have been employed for the purpose of providing stability and solubility to the conjugated alkynyl structures. The dendrimeric end-groups function to keep the highly reactive π -systems from interacting and they furnish a stable structure. The dendrimeric decayne is a stable orange solid and was only the second decayne to be isolated and fully characterized (n = 10 in Series 4). It was however, only isolable by HPLC and in very low yield.



Several research groups have experimented extensively with metal end-capping groups on polyynes.³⁰⁻³⁵ Gladysz and co-workers have been successful in synthesizing some of the longest polyynes.³⁶⁻⁴¹ Series 5 and 6 are two examples in which extended carbon chains have been formed and these metal-capped structures constitute a fundamental class of carbon-based molecular wires.⁴² The metal-capped polyynes are highly crystalline, and the solid-state properties of several metal-alkynyl complexes have been elucidated via X-ray crystallographic analysis. The longest polyyne to be studied is the platinum capped octayne.⁴³

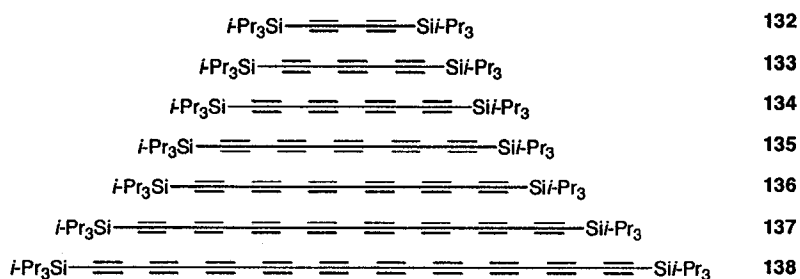
There are surprisingly few ways to make polyyne chains, despite the obvious interest in their formation. In the majority of cases, simple di- and triynes are formed using a combination of oxidative coupling reactions.^{15,44-46} These methods have been effectively applied towards the formation of polyynes as exemplified by the preparation of Series 2 through 6. Synthetic routes that utilize these traditional methods are unfortunately plagued by low yields, unstable intermediates, and for the longer carbon chains, the formation of polyynic by-products which complicate purification.²⁹ One of the greatest problems associated with the study of polyyne molecules is the inability to isolate relatively large quantities of the longest compounds, such as C₁₆ and C₂₀. Isolated yields for several of the polyynes reported above are extremely low and in some cases the yields could not be reported at all. The ability to fully explore the properties of polyynes has thus been greatly restricted.

Our interest in polyynes is motivated both by the synthetic challenge, as well as a desire to explore their fundamental properties. As described previously, the FBW rearrangement has led to a convenient synthesis for diynes, triynes, and 2-dimensional carbon networks (Chapter 2).⁴⁷ Utilizing this reaction toward the realization of extended polyynes is a natural extension to this work and our carbenoid rearrangement offers many synthetic advantages over traditional methods of polyyne synthesis. First, a variety of techniques are available to form the stable dibromoolefinic precursors and provide numerous routes to extend chain length. The facile purification of intermediates is also an important feature of the FBW route, as rigorous manipulation of large, highly conjugated molecules can lead to their decomposition. High yielding steps also provide macroscopic quantities of pure samples. For the current study, a series of triisopropylsilyl-capped (TIPS) polyynes has been targeted. The simple, but bulky, TIPS moiety is incorporated because it provides both solubility and stability. In addition, it does not have a dramatic electronic interaction with the carbon chains, allowing an analysis of an essentially pure sp -hybridized carbon system.

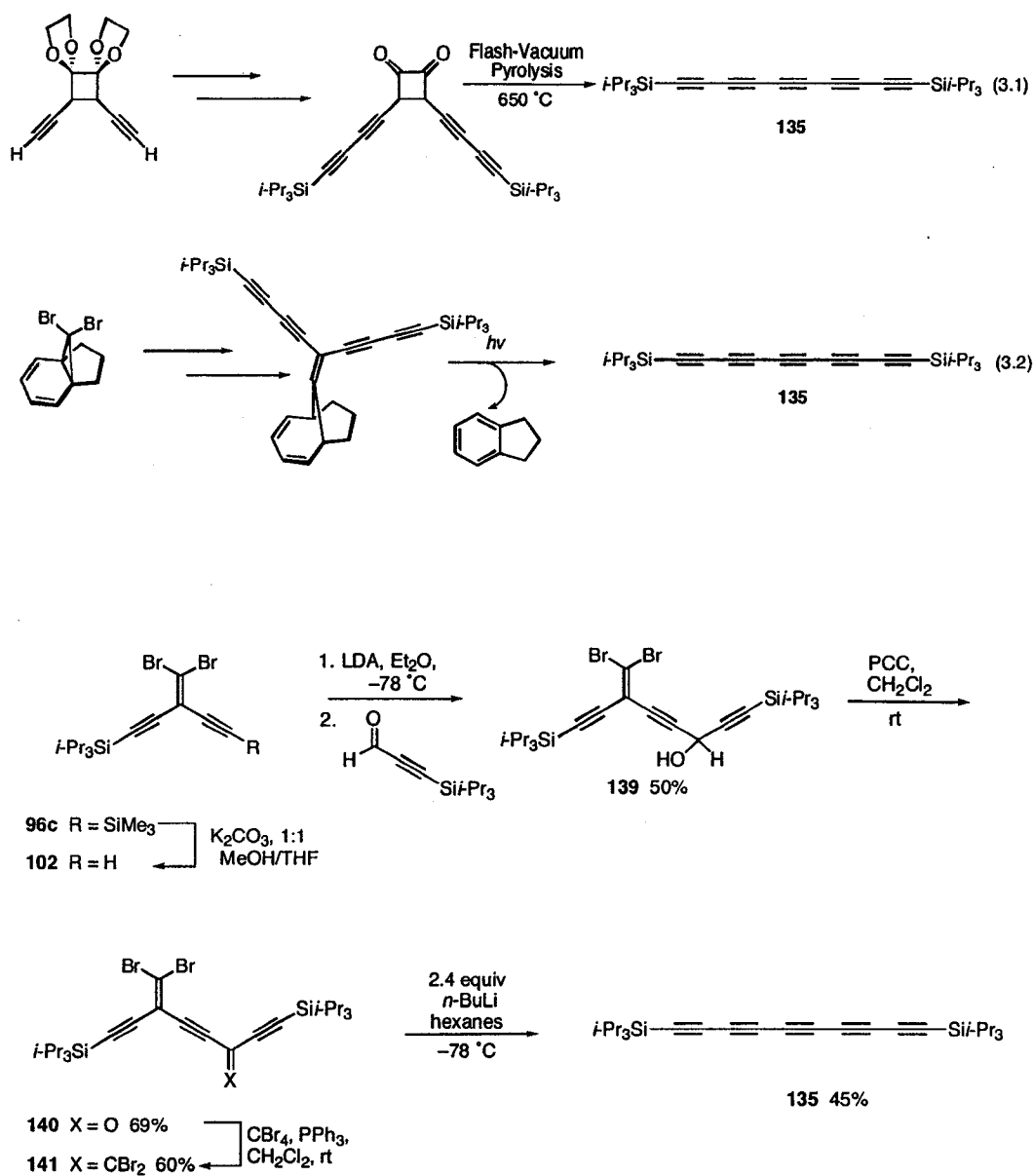
3.2 Results and Discussion

3.2.1 Synthesis

Chart 3.1



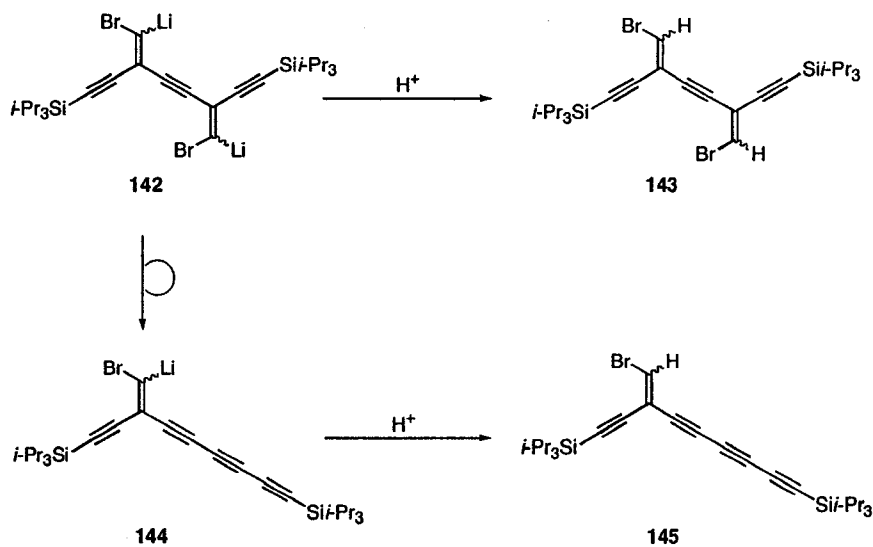
The polyynes synthesized in this study are shown in Chart 3.1. Derivatives **132-133** have been synthesized via either an oxidative coupling procedure (**132, 134**)⁴⁸ or by alkylidene rearrangement (**133**).⁴⁹ While the tri- and tetraynes may be formed fairly easily, the synthesis of longer derivatives such as **135-138** is more complex, and polyynes with an odd number of acetylene units such as pentayne **135** are particularly difficult to form. Shown in equations 3.1 and 3.2 are strategies employed by Diederich and Tobe for the formation of polyynes with an odd number of acetylene units.^{50,51} In these cases, the butadiynyl units are installed using common synthetic techniques, and the final central acetylene unit is formed in the final step using either flash vacuum pyrolysis (3.1) or photochemically-induced extrusion of indene (3.2). These are effective methods, forming the pentaynes in 42% and 59% yield respectively, but their synthetic utility is decreased due to the difficulty of forming the precursors.



Scheme 3.1

Our FBW approach toward the synthesis of pentayne **135** exploited the differentially protected enediyne **96c** (Scheme 3.1). Protodesilylation of **96c** provided terminal acetylene **102**. The subsequent condensation reaction was very sensitive to adventitious water; both the aldehyde and the terminal acetylene had to be rigorously dried. The enediyne **102** was deprotonated to form the lithium

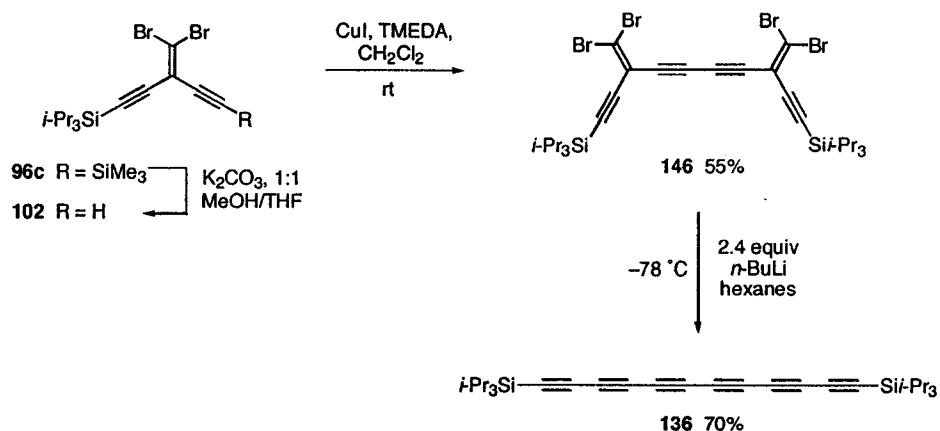
acetylide using LDA in ether at $-78\text{ }^{\circ}\text{C}$. Triisopropylsilylpropargyl aldehyde was slowly added to the acetylide solution and after purification via flash chromatography alcohol **139** was isolated as a stable yellow oil in 50% yield. The alcohol was easily oxidized to ketone **140** in a yield of 69% using PCC, and ketone **140** was then directly carried on to the Corey-Fuchs reaction. Tetrabromide **141** was isolated in 60% yield as a stable yellow oil. The final step, a two-fold rearrangement, proceeded very smoothly using the standard procedure of slow addition of 2.4 equiv of *n*-BuLi to a solution of **141** in hexanes at $-78\text{ }^{\circ}\text{C}$.



Scheme 3.2

The point at which quenching was initiated was essential to the success of the rearrangement. If a proton source was introduced too soon, incomplete migration would produce by-products such as **143** and **145**, resulting from protonation of the lithiated intermediates **142** or **144** respectively (Scheme 3.2). While these products were never isolated pure, their existence was strongly

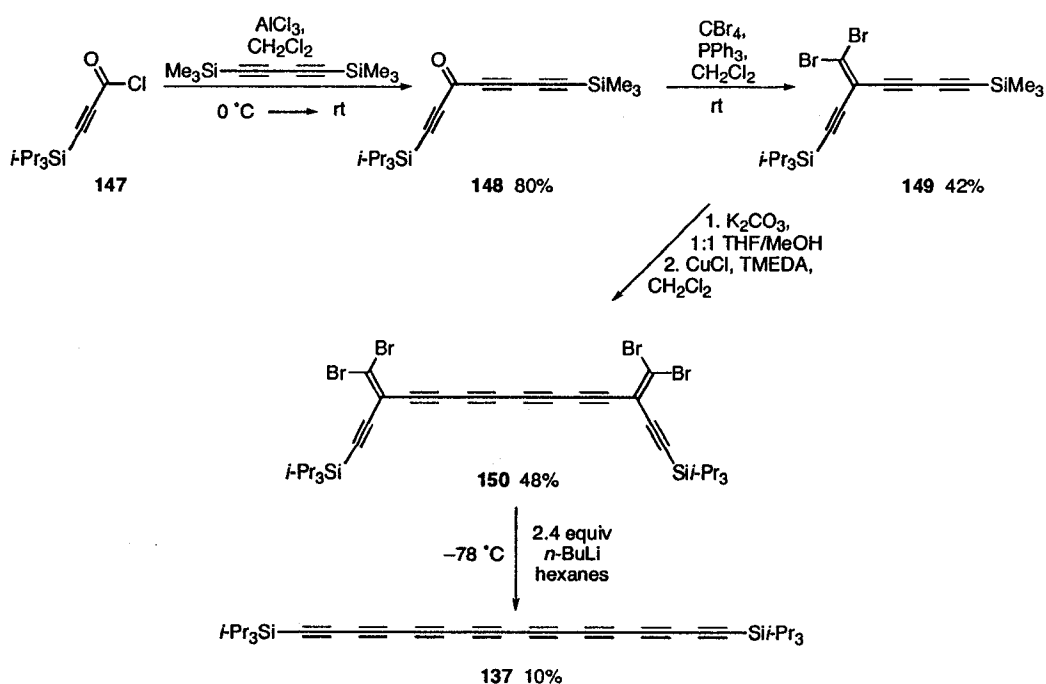
supported by the vinyl signals in the ^1H NMR spectra of crude reaction mixtures. Due to similar retention times of **143**, **144** and the pentayne **135**, the presence of any protonated by-products greatly complicated purification. To monitor the rearrangement, careful TLC analysis was required during the warming stage as the presence of **142** and **144** in the reaction mixture could be detected in this manner. The mixture was therefore allowed to heat up to ~ -5 °C to ensure complete rearrangement, and, after an aqueous work-up and purification on silica, pentayne **135** was isolated as a white solid in 45% yield. The crystalline product **135** is not only thermally stable, with a melting point of 104 °C, but it is stable for an indefinite period of time when kept under refrigeration.



Scheme 3.3

The synthesis of hexayne **136** was more facile than the pentayne due to the symmetry about the central single bond, as this bond may easily be introduced by the Hay/Glaser coupling procedure (Scheme 3.3). The trimethylsilyl group was first selectively removed from **96c** to provide terminal acetylene **102**. The deprotected enediynes were then subjected to the oxidative homocoupling

protocol^{44,52} to provide tetrabromide **146** as the only isolable product in 55% yield. The rather poor yield of this step was due to what is believed to be a competitive cross-coupling reaction between the terminal acetylene and the vinyl bromide in the presence of Cu^{III}.^{53,54} Reaction conditions required to suppress this side reaction have been briefly explored, but remain unoptimized. Regardless, the resulting stable tetrabromide was easily purified, since all by-products were more polar and easily removed by passage of the reaction mixture through a silica plug using hexanes. This dual rearrangement provided the hexayne as a pale yellow solid in 70% yield.

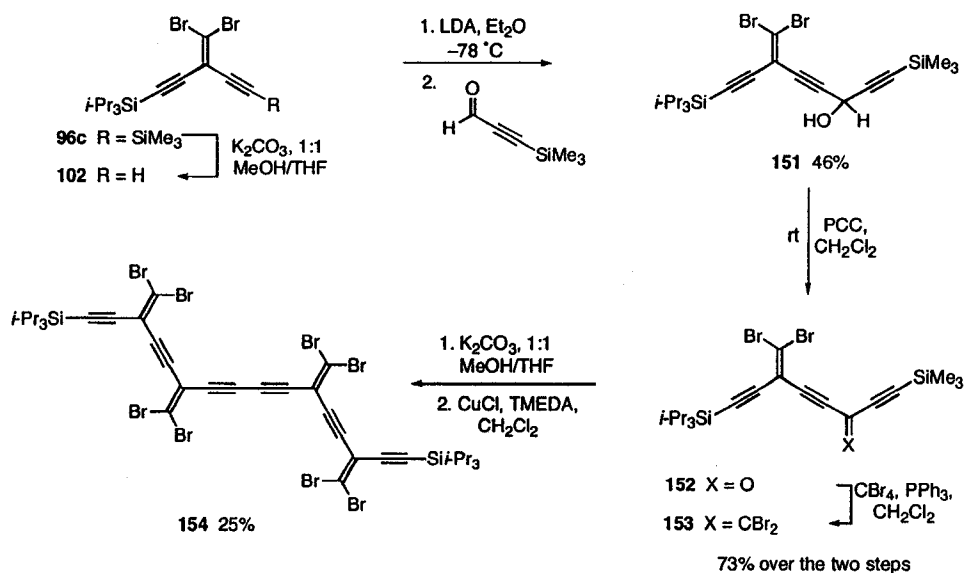


Scheme 3.4

Friedel-Crafts acylation has been a powerful method of directly forming conjugated ketones, as opposed to a sequence of making an alcohol then oxidation

to a carbonyl group as described in the previous chapter. Both an acylation reaction and an oxidative homocoupling reaction were the key steps toward formation of octayne **137** (Scheme 3.4).⁵⁵ The triisopropylsilylpropargyl acid chloride **147** was first realized by reaction of triisopropylsilyl propiolic acid and thionyl chloride. After the excess thionyl chloride was removed under reduced pressure, **147** was treated with 1,4-bis(trimethylsilyl)-1,3-butadiyne in the presence of aluminum chloride in CH₂Cl₂ at 0 °C. The mixture was warmed to rt over 3 hrs, and ketone **148** was isolated as an oil in an excellent yield of 80%. Full spectroscopic characterization was possible, but as the cross-conjugated ynone **148** demonstrated limited stability it was generally carried on directly to the dibromoolefination step to maximize overall yield. The dibromide **149** was formed as a stable yellow oil in 67% using the standard Corey-Fuchs protocol. Containing eight of the necessary sixteen conjugated carbons, **149** was then oxidatively dimerized to form the sixteen-carbon polyynone precursor **150** in 48% yield. It was initially believed that the tetrabromide would be unstable due to the presence of an extended enyne segment. Fortunately, the molecule is quite stable under ambient conditions. Under the general rearrangement conditions, alkyne migration was induced with *n*-BuLi to produce octayne **137** as a stable light orange/yellow solid. The octayne **137** recrystallized easily from hexanes, producing shiny crystals that have been stable indefinitely in the freezer. As was observed in previous examples, the yield of this reaction was very dependent on the temperature when workup is initiated. In the synthesis of pentayne **135**, allowing the carbenoid intermediate to warm to ~ -5 °C ensured reaction

completion and caused a minimal amount of decomposition. The extended π -system of the octayne **137** and of the intermediate resulting from one migration event are apparently more vulnerable under the reaction conditions. Too high a temperature caused decomposition, but quenching at $-78\text{ }^\circ\text{C}$ resulted in a high proportion of by-products resulting from protonation of the carbenoid intermediates. As such, yields of this two-fold reaction were lower than in the cases of the penta- and hexayne. Nonetheless, an overall yield of 10% was obtained, representing a 33% yield for each rearrangement.

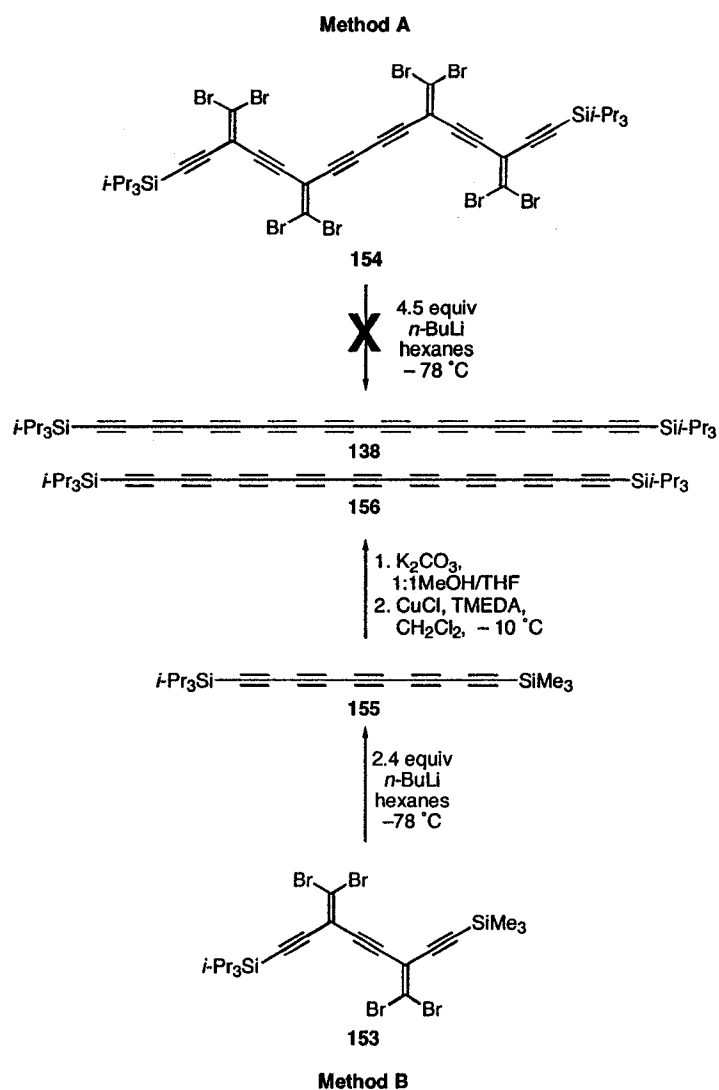


Scheme 3.5

As demonstrated, the polyynes **135-137** are assembled fairly easily, and even the octayne **137** can be constructed in a few days in fairly large quantities. The longer the polyynes, however, the more elaborate the synthesis. This reality is

reflected in the formation of the final compound in the series, **138**, only the third fully characterized decayne known to date (Scheme 3.5).

The initial stages of the synthesis of decayne **138** were very similar to those in the formation of pentayne **135**. The trimethylsilyl protective group was removed from enediyne **96c** using potassium carbonate in MeOH/THF to provide terminal acetylene **102**. LDA was then employed to effect deprotonation of the terminal acetylene and form the lithium acetylide. Trimethylsilylpropargyl aldehyde was added to the acetylide solution at low temperature to ultimately afford alcohol **151** in 46% yield. Unfortunately, a yield better than 46% has never been achieved for this reaction. Nevertheless, the alcohol was formed as a stable yellow oil and was carried onto the oxidation and dibromoolefination steps. For the purpose of effecting a higher yield, the crude product from PCC oxidation was simply passed through silica gel and was carried on directly to the Corey-Fuchs reaction without further purification. Differentially protected tetrabromide **153** was formed as a surprisingly stable solid in 73% yield over the two steps to put into place the 10-carbon section. To form the 20-carbon segment **154**, tetrabromide **153** was selectively deprotected and oxidatively homocoupled. Thus, K_2CO_3 in MeOH/THF effected the removal of the trimethylsilyl group from **153** and the central carbon-carbon bond of **154** was introduced using standard Glaser/Hay conditions. The coupling reaction was complete within 30 minutes and octabromide **154** was isolated in 25% yield as an oil that slowly solidified over time.



Scheme 3.6

Several attempts were then made to perform a quadruple rearrangement on the 20-carbon segment **154** (Scheme 3.6, Method A). As was observed in the case of the octayne, the standard reaction conditions were apparently too harsh for the extended π -system being formed. After addition of the butyllithium to a solution of **154** in hexanes at -78 °C, warming the reaction mixture to -20 °C resulted in incomplete rearrangement and none of the desired product was detected. The reaction conditions were adjusted in hopes of encouraging

complete rearrangement of all alkyldiene centers. The experiment was repeated with warming of the reaction mixture to either 0 °C or room temperature. Unfortunately, both attempts produced an intractable black solid.

An alternative approach was therefore explored as outlined in Scheme 3.6, Method B. The 10-carbon segment **153** was first rearranged to the differentially protected pentayne **155**. Rewardingly, the rearrangement went extremely well, when warmed to -5 °C, and no by-products resulting from incomplete rearrangement were observed by TLC. The less bulky trimethylsilyl group apparently offers much less steric protection of the pentayne core than the TIPS moiety and **155** was found to be much less stable than compound **135**. Furthermore, attempted purification by column chromatography led to partial removal of the trimethylsilyl group. Therefore pentayne **155** was carried on directly to the next step, after first passing through a plug of silica with hexanes to remove baseline material. After protodesilylation of **155**, the very unstable terminal acetylene was carried directly on to the oxidative-coupling reaction toward **138**. Homocoupling of the 10-carbon segment was initially attempted in CH₂Cl₂ at room temperature using an excess of CuCl and TMEDA, the standard Hay conditions. This reaction immediately turned from green/blue to a dark red color as the deprotected polyne was added to the catalyst mixture. TLC analysis indicated the reaction was complete almost immediately. Upon work-up, the crude mixture was passed through a plug of silica and TLC analysis showed the presence of what appeared to be one product. We subsequently discovered,

however, by UV-Vis spectroscopic analysis, the presence of an extremely problematic and unexpected by-product.

Polynes have very distinctive and well-defined UV-Vis absorption bands. It became clear upon analysis of the reaction mixture of **155** → **138** that, in addition to the presence of the decayne **138** as the major product, nonayne **156** was also formed as ~10% of the product mixture. The presence of such a by-product under oxidative homocoupling conditions is not an unknown phenomenon, having been reported previously in the synthesis of Hirsch's dendrimer-capped polyynes.²⁹ These are, however, the only two known examples of this apparent loss of C₂ during a Hay coupling reaction.

As a fairly large amount of very pure sample (≥95%) was desired for characterization, the nonayne had to be either removed via chromatography or its formation prevented by adjusting the reaction conditions. Purification by column chromatography was possible but proved to be a grueling process, as the two polyynes elute with very similar *R_f* values. It subsequently was determined that by lowering the temperature of the homocoupling reaction to -10 °C, the formation of the nonayne was almost completely suppressed, as determined UV-Vis spectroscopic analysis. High field ¹³C NMR spectroscopic analysis also later confirmed that decayne **138** was > 95% pure. Thus, following the oxidative homocoupling reaction of deprotected **155** at -10 °C and work-up, the remaining impurities were removed by column chromatography (silica gel, hexanes), then by passage of a solution of **138** in hexanes through a plug of alumina. The bright orange solid decayne **138** shows limited stability when

exposed to certain conditions such as chromatography (silica gel and alumina) and ambient light and temperatures for extended periods of time. It does, however, demonstrate a fair degree of kinetic stability when kept in the freezer and protected from light. Overall, 51 mg of decayne **138** was isolated from this reaction, representing a yield of 30% over the last two steps.

3.2.2 UV-Vis spectroscopy

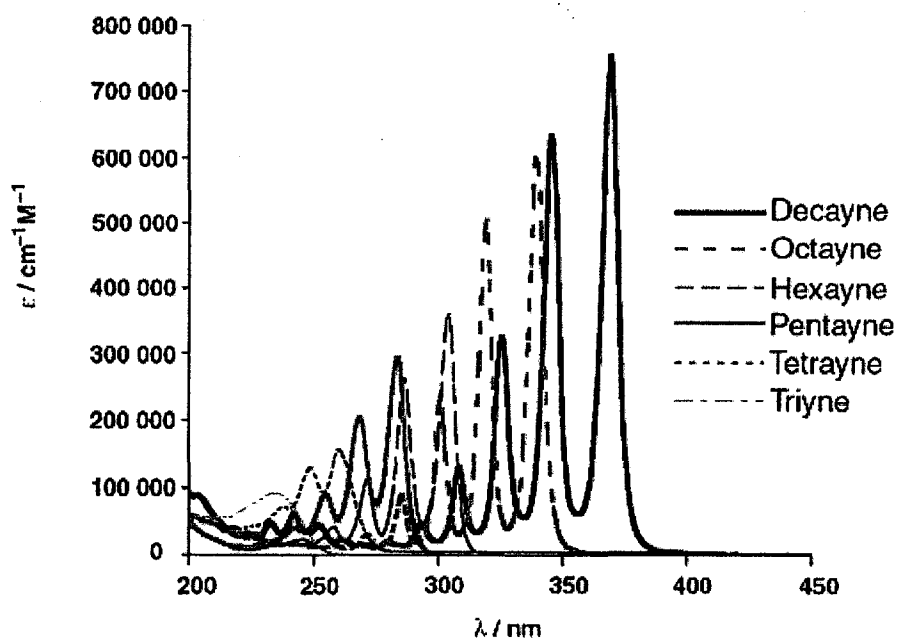


Figure 3.1 UV-Visible spectra of polyynes **133-138** in hexanes.

The linear absorption spectra of polyynes **133-138** are presented in Figure 3.1.⁵⁶ The UV-Visible spectra of conjugated acetylenes are unique in many ways and this type of spectroscopy is one of the most effective ways of identifying polyynes. The high energy region of the spectrum is, for the most part,

transparent for the longer oligomers, with only very weak fine structure for the decayne **138** and octayne **137** apparent between 220 and 270 nm. This interesting feature suggests the possible application of polyynes as optical materials at high-energy wavelengths within this window of transparency. The most interesting part of the spectrum, however, is the lower energy region at ≥ 270 nm, which contains the highest occupied molecular orbital to lowest unoccupied molecular orbital transition (HOMO \rightarrow LUMO) of the conjugated framework. The vibrational fine structure is clearly visible, appearing as a series of narrow absorption peaks with steadily increasing intensity toward the visible region. Interestingly, while the shape of the absorption envelope is fairly symmetrical in the UV-Vis spectra for most organic compounds, for polyynes this is not the case. The lowest energy absorption, λ_{max} , in each polyyne oligomer reflects a transition from the lowest energy vibrational level in the ground state to the lowest energy vibrational level in the excited state, $\nu_{0,0}$.

The fine structure of the UV-Visible spectra allows an analysis of the vibrational energy levels. For pentayne **135**, the average energy difference between vibrational levels is 2036 cm^{-1} . This value steadily decreases as chain length increases until it reaches 1789 cm^{-1} for the decayne. It is difficult to make a rigorous correlation to the bond order of a polyyne in the ground state but it is interesting that there is a significant change in the vibrational levels upon lengthening of the conjugation. This trend may reflect a decrease in triple bond character of the polyynes in solution as chain length is increased, however, this trend has not yet been observed in the solid state.

There is a corresponding increase in the molar absorptivity ϵ as the chain length increases. There are only three known quantitative UV-Visible analyses of a decayne. Gladysz's Re-capped³⁹ and Hirsch's dendrimer capped²⁹ decaynes, have a molar absorptivity of $\epsilon = 200\,000\text{ cm}^{-1}\text{M}^{-1}$ and $\epsilon = 600\,000\text{ cm}^{-1}\text{M}^{-1}$ respectively and the *t*-Bu capped analogs realized by Whiting, Jones and Lee,²⁰ which showed the highest known absorptivity for a polyynes, with $\epsilon = 850\,000\text{ cm}^{-1}\text{M}^{-1}$. The ϵ -values appear to be very dependent on the nature of the endgroup. This tendency is further demonstrated by our simple triisopropylsilyl capped system which shows some of the highest molar absorptivity for polyynes, with octayne **137** at $\epsilon = 600\,000\text{ cm}^{-1}\text{M}^{-1}$, and decayne **138** at $\epsilon = 750\,000\text{ cm}^{-1}\text{M}^{-1}$. Values for λ_{max} and ϵ are summarized in Table 3.1.

Table 3.1. UV-Visible characteristics of polyynes **133-138**

Compound	λ_{max} [nm]	ϵ [$\text{cm}^{-1}\text{M}^{-1}$]
133	234	93 000
134	260	160 000
135	283	290 000
136	304	360 000
137	339	600 000
138	369	750 000

The expected red-shift is observed for λ_{max} as the conjugation length increases, indicating a decrease in the HOMO-LUMO energy gap. This shift is

also reflected in the observed colors of the compounds; the shorter tri-, tetra-, and pentaynes **133**, **134**, **135** are colorless, the hexayne **136** yellow, the octayne **137** yellow-orange, and decayne **138** orange. It is predicted, as it is for any linearly conjugated system, that at a particular chain length, saturation will occur and the energy difference between the HOMO and LUMO will reach a minimum and constant value. Related to the degree of bond-order alternation of the conjugated backbone,⁵⁷ this minimum value would be representative of the theoretical carbon allotrope, carbyne.⁵⁸ A number of theoretical studies have predicted dissimilar degrees of bond-order alternation in sp-hybridized carbon chains, from zero⁵⁹ to fairly sizable values.⁶⁰ The oligomer length at which saturation occurs is commonly known as the effective conjugation length. This value has been estimated theoretically to be near 400 nm for polyynes.⁵⁸ Experimentally based studies have predicted much higher values of 565 nm³⁹ and 569 nm²⁹ for λ_{\max} at saturation. If electron correlation effects are taken into consideration, the empirical power-law $1/\lambda_{\max} = E_{\max} \sim n^{-x}$ best describes the relationship between E_{\max} , λ_{\max} , and n .⁶¹ This relationship is represented in Figure 3.2 and portrays the power-law decrease in E_{\max} as a function of chain length through at least C₂₀. Overall, the TIPS-protected polyyne oligomers yield a fit of $E_{\max} \sim n^{-0.379 \pm 0.002}$ to high precision. This result contrasts that of Gladysz who reported a relationship of $E_{\max} \sim n^{-1}$.³⁹ Our results for the polyynes, however, are close to the well-established relationship of $E_{\max} \sim n^{-0.5}$ observed for many polyenic materials.^{62,63} Saturation of the rate of decrease of the energy difference between the HOMO and the LUMO would cause a leveling of E_{\max} as n is increased. No such change

is observed in Figure 3.2, and a reliable prediction regarding saturation in λ_{max} cannot therefore be made on the basis of these UV-Visible results.

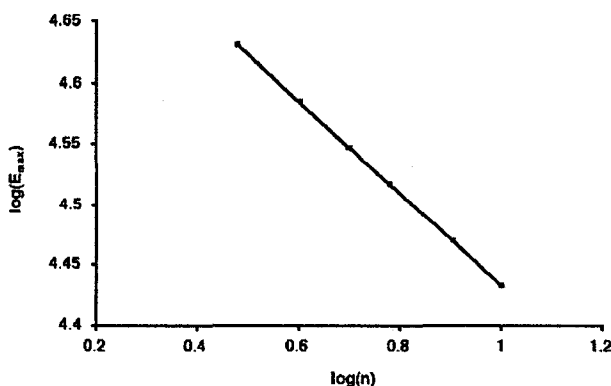


Figure 3.2 Power-law plot of E_{max} versus n , ($E_{max} = 1/\lambda_{max} \times 10^7$).

The solid line represents the line-of-best-fit to the data.

3.2.3 Differential Scanning Calorimetry

The ability to initiate a controlled and specific polymerization reaction between small polyyne chains has been widely studied and is known as topochemical polymerization.^{64,65} Chain cross-linking has also been observed in macrocycles containing diacetylene units where the application of heat can result in the formation of carbon nanotubes.⁶⁶ It is then also reasonable to expect this type of cross-linking in extended polyynes.

Differential scanning calorimetry (DSC) has been performed on the polyynes **132-138** to determine the propensity of the carbon chains to polymerize in a controlled manner, as well as to determine their thermal stability. DSC traces of compounds **132-138** are shown in Figure 3.3. All oligomers show surprising

thermal stability. Polyynes **132-136** all show an endothermic phase transition which corresponds to a reproducible melting point. Diyne **132** has two additional endothermic transitions at 54 °C and 79 °C,⁶⁷ which at present are unexplained. The triyne **133** only has the one endothermic transition but at higher temperatures a large exotherm is observed for **134-138**. An exotherm in the DSC trace would be indicative of either decomposition or an ordered polymerization reaction, for example in a 1,4- or 1,6-manner, between polyynes.^{64,65,68} The broadness of the peaks, ranging from 34 °C to 69 °C between onset and termination of exotherm, would indicate random cross-linking reactions taking place in these three examples, which is reasonable for the presumably liquid state of the sample. This behavior is in contrast to that observed for the octayne, (Figure 3.3). A sharp, symmetrical exotherm is observed, spanning only 14 °C, and is indicative of a sequence-specific polymerization. This result is further supported by X-ray analysis and will be discussed in the following section. Not surprisingly, the decayne **138** has no distinct melting point and shows only a broad exotherm at 123 °C, presumably from decomposition. The possibility of the TIPS-protected decayne undergoing a topochemical polymerization reaction is not to be ruled out. The decayne is a solid when pure but appears to be amorphous. Thermal analysis should be repeated when a crystalline sample can be obtained.

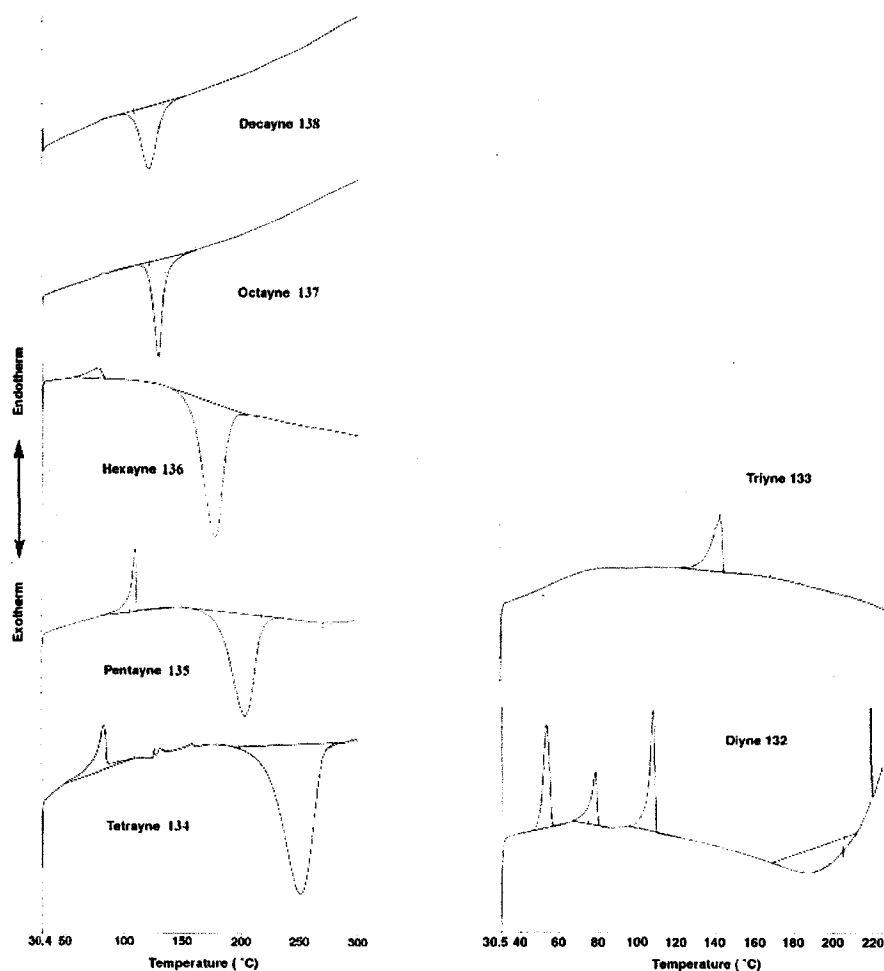
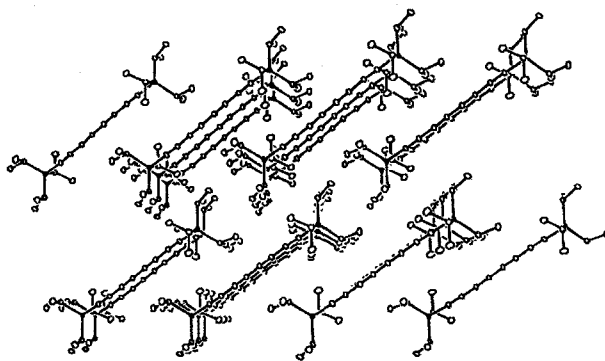


Figure 3.3 Differential Scanning Calorimetry traces of polyynes 132-138.

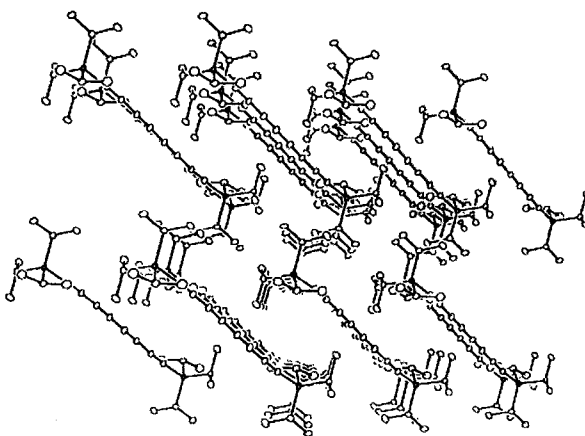
3.2.4 Solid State Structures

As previously mentioned, polyynic molecules can be inherently unstable in the solid state due to intermolecular interactions of the extended π -systems, which facilitates topochemical polymerization. Traditionally, to prevent these intermolecular interactions, bulky end-groups, such as dendrimers, *t*-butyl groups, and metal complexes, have been employed to maintain separation between the

carbon chains. Triisopropylsilyl end-groups have also proven very efficient in providing this separation and is one of the factors that furnishes a stable solid state structure. As topochemical polymerization in di- and triynes is a well studied phenomenon, a set of parameters have been elucidated that describe a system where this reaction is possible.^{64,65,68} These parameters include geometric constraints for neighboring molecules, as well as interatomic distances for reacting centers that are $< 4 \text{ \AA}$. These parameters can be used to explain the stability or instability displayed in the solid state for the TIPS-protected polyynes 134-137.



a)



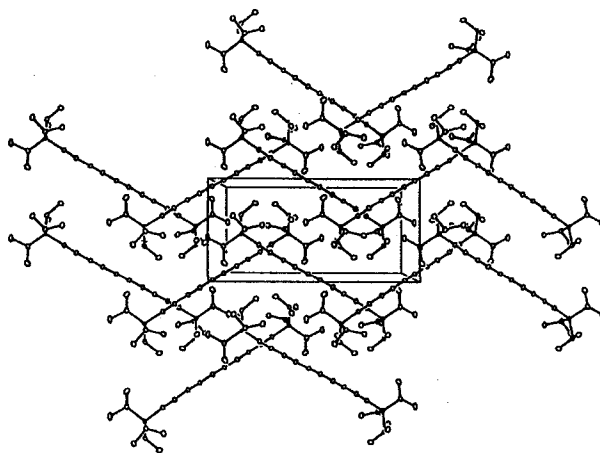
b)

Figure 3.4 a) Crystal packing diagram of tetrayne **134**, viewed along *a*-axis. b) Crystal packing diagram of tetrayne **134**, viewed along the *b*-axis. Shown at 20% probability.

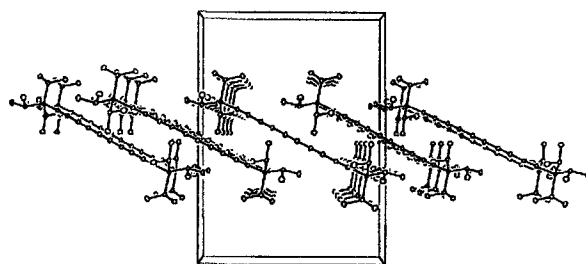
Crystals for compounds **134-136** were grown from slow diffusion of MeOH into a CH₂Cl₂/hexanes solution at 4 °C. All three polyynes have a linear, structure and possess a center of inversion. Shown in Figure 3.4, 3.5 and 3.6 are the crystal packing diagrams of the tetrayne **134**, pentayne **135**, and hexayne **136**. As can be seen from the crystal packing diagram of tetrayne **134** in Figure 3.4, all of the molecules in the unit cell are parallel, as seen looking down both the crystallographic *a*- and *b*-axis. Although molecules are offset in a manner which would deem a 1,6-polymerization reaction possible, interatomic distances are too great in both directions, > 6.0 Å. This renders an inter-chain polymerization reaction unlikely. This structure explains the high degree of thermal stability observed for **134** in the DSC analysis.

The solid state packing of the pentayne **135** and hexayne **136** differ from the tetrayne **134**, in that not all the molecules in the unit cell are aligned parallel to each other. When viewed down the crystallographic *a*-axis, as shown in Figure 3.5a, it can be seen that rows of molecules are oriented ca. 120° with respect to each other in a manner that effectively prevents topochemical polymerization between rows. The alignment within a row can be seen when viewed down the crystallographic *b*-axis in Figure 3.5b. Within each row the molecules are

parallel, although they pack at an interatomic distance of 6.9 Å that is too great for reaction to occur.



a)

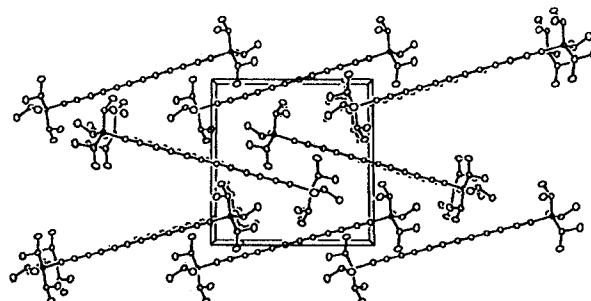


b)

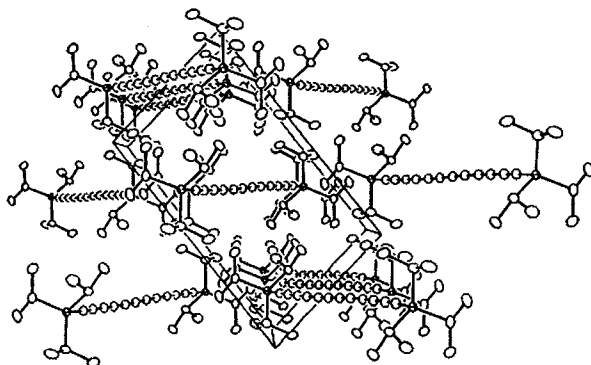
Figure 3.5 a) Crystal packing diagram of pentayne 135, viewed along the *a*-axis. b) Crystal packing diagram of pentayne 135, viewed along the *b*-axis. Shown at 20% probability.

The solid-state structure of hexayne 136 is similar to that for pentayne 135. The molecules are again aligned in rows as viewed down the *a*-axis although there is little overlap between parallel polyynes, Figure 3.6a. Parallel molecules are spaced 5.1 Å apart at their closest contact within a row, still

considered too far apart for a spontaneous reaction. When viewed down the *b*-axis, the closest contact between layers is a non-parallel molecule.



a)

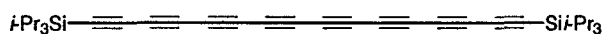


b)

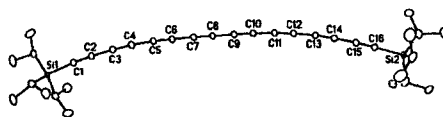
Figure 3.6 a) Crystal packing diagram of hexayne **136**, viewed along the *a*-axis. b) Crystal packing diagram of hexayne **136**, viewed along the *b*-axis. Shown at 20% probability.

For compounds **134-136**, the polyynes are arranged in such a manner as to render topochemical polymerization, in a specific manner, unlikely. The X-ray analysis further supports the DSC results, which would indicate a random polymerization/decomposition reaction is occurring upon heating.

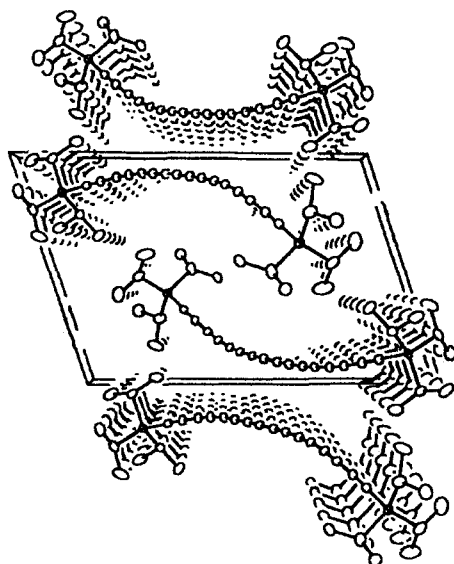
Fortunately, the octayne exhibits sufficient stability as a solid to afford crystals suitable for crystallographic analysis. Of the polyynes discussed so far, the octayne has the most unusual shape. As seen in the ORTEP diagram of **137** in Figure 3.7a, the ends of the polyyne are curved towards each other, the central acetylene units deviate only a few degrees from linearity, while the outer units are bent to nearly 174° . These angles are not particularly exceptional for acetylenes, which can easily support a significant amount of angle strain, but it is interesting that bending is in the same direction. Imagining a tangent at C9, each arm deviates 25° from linearity. Unlike the other TIPS-capped polyynes, there is no element of symmetry within the molecule and all sixteen sp -hybridized carbons are unique in the solid state.



137



a)



b)

Figure 3.7 a) ORTEP diagram of octayne **137**. b) Crystal packing diagram of **137** viewed down the crystallographic *a*-axis. Shown at 20% probability.

The crystal packing diagram for **137** shows that the curvature of the molecule can be seen while viewing down the *a*-axis, Figure 3.7b. Interestingly, the molecules do not pack with the curvature in the same direction, but in an alternating fashion. There is alignment of the gently curving structures down the *a*-axis, however. $R_{1,6}$ is within the range of 3.5 - 4 Å and combined with a translational distance of 7.6 Å, the octayne is well set up for a 1,6-polymerization.^{64,65} While this type of contact can result in an extremely unstable crystal structure, the octayne is stable at room temperature. There seems to be a significant energy barrier that prevents the polymerization reaction from

initiating. The introduction of heat, however, is sufficient to overcome this barrier and initiate a polymerization reaction, as is observed in the DSC trace.

Considering the effect of chain length on bond lengths, very few differences are seen in the solid state between these four structures. There is little change in the average bond lengths of either the single or triple bonds upon moving from the triyne on through to the octayne.

3.2.5 ^{13}C NMR

The distinctive ^{13}C NMR spectra of polyynes **132-138** have proven very useful in confirming the structure of the compounds in this series. Fortunately, each carbon signal is well resolved for all molecules and it is possible to assign each resonance. Shown in Figure 3.8 are the expansions of the region of the carbon NMR spectra for the TIPS-capped polyynes containing the signals of the sp -hybridized carbons. There are two distinct areas of interest. Region 1 contains the two lower field resonances, which are the carbons for the acetylene unit closest to the triisopropylsilyl groups, C1 and C2. Region 2 contains resonances for all of the internal sp -hybridized carbons. The separation of the carbon shifts of the external acetylene unit from the internal resonances is not unexpected, as they are the most chemically distinct of all the carbons in a polyne. What is unexpected, however, is how the resonances change position upon lengthening of the carbon chain. Intuition would suggest that C1 and C2 would be the least affected by an increase in chain length, as the TIPS groups are the only real consistent feature in each molecule. As can be seen in Figure 3.8, however, the

chemical shifts of C1 and C2 converge upon moving from the diyne to the decayne. The resonances for C1 and C2 have been identified based on ^{13}C labeling studies and explanation for this assignment will be discussed in full in Chapter 4. Thus, C2 is assigned to the most downfield resonance, which for the diyne is at 90.4 ppm, and this resonance is shifted slightly upfield for each addition of an alkyne unit until it finally appears at 89.4 for the decayne. C1 is assigned to the next upfield peak at 82.2 ppm. As opposed to C2, the C1 resonance is instead shifted slightly *downfield* for each extension of chain length, and for the decayne it is visible at 88.8 ppm. Following this trend, C1 and C2 can be expected to show overlapping signals in the ^{13}C NMR of longer structures.

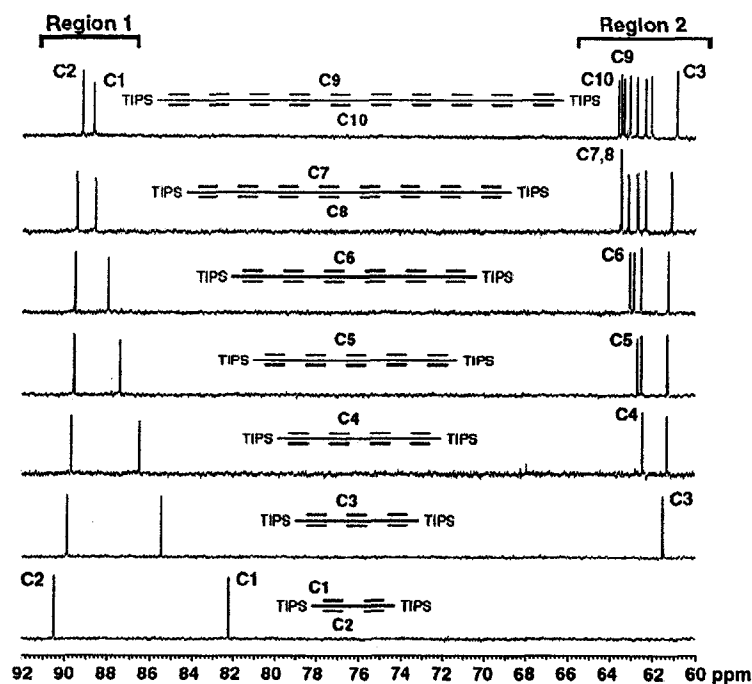


Figure 3.8 ^{13}C NMR spectrum of polyynes 132-138 (CD_2Cl_2 , 125 MHz).

Region 2 of the NMR spectra contains the resonances of the internal carbons, observed between 60 and 64 ppm. At a certain length, saturation should occur and these internal resonances will cease to be resolved but will instead merge into one signal. At C_{20} , however, saturation has yet to be reached, and all internal resonances are resolved at 125 MHz.

For triyne **133**, the signal for C3 is observed at 61.5 ppm. Furthermore, the resonance for C3 appears at nearly the same chemical shift regardless of chain length, for example, it appears at 61.1 ppm in the decayne. In fact, all internal carbons follow this pattern, and chemical shifts change very little from polyynes to polyynes. Thus, an interesting trend is observed upon moving to longer oligomers. There is a continual appearance of the signal for the new central carbon, as one goes to each longer molecule, more downfield than that for the central carbon in the antecedent oligomer. Thus, the signal of C4 in the tetrayne shows at 62.4 ppm, that of C5 in the pentayne is at 62.7 ppm, and the resonance of C6 in the hexayne is found at 63.0 ppm. The assignment becomes more difficult for the 8- and 10-mer as two new carbons are introduced at once, but the preceding trend of the most internal carbons appearing more downfield can be tentatively applied to C7, C8 and C9, C10. These assigned peaks are summarized in Table 3.2. While each additional carbon gives an observable signal, the resonances are appearing closer to each other. It is expected, then, that as chain length approaches C_{∞} , the ^{13}C resonances will converge, reflecting the similarity of all carbons in an infinite chain, with a single signal at 63 ppm. This value is very similar to the one predicted for other polyynes series.^{29,39}

Table 3.2. ^{13}C NMR shifts for compounds 132-138 in ppm

Compound	C1	C2	C3	C4	C5	C6	C7	C8	C9	C10
120	Diyne	82.2	90.4							
121	Triyne	85.5	89.9	61.5						
122	Tetrayne	86.5	89.7	61.3	62.4					
123	Penatyne	87.4	89.6	61.3	62.5	62.7				
124	Hexayne	87.9	89.5	61.2	62.5	62.8	63.0			
125	Octayne	88.5	89.4	61.1	62.3	62.6	63.1	63.4	63.4	
126	Decayne	88.8	89.4	61.1	62.2	62.5	62.9	63.2	63.5	63.6 63.8

3.2.6 Non-linear Optical Properties of Polyynes⁶⁹

The nonlinear optical properties of conjugated oligomers have long intrigued both chemists and physicists alike.⁷⁰ Due to the established relationship between the magnitude of the NLO response and the polarizability of the system being measured, the bi-directional π -electronic system of polyynes generates a great deal of interest. Unfortunately, the synthesis of extended polyyne chains has traditionally been arduous, producing insufficient sample for NLO analysis.

Conversely, there have been many theoretical predictions about the third-order nonlinear optical properties of polyynes.⁷⁰ These studies predict that the molecular second hyperpolarizabilities, γ , for polyynes will increase as a power-law with length, but to a lesser extent than their most structurally related analogues, polyenes and polyenyne.⁷¹⁻⁷⁴

The successful application of the method of alkylidene carbene/carbenoid rearrangements towards the realization of polyynes has allowed for the isolation of reasonable quantities of product. The third order nonlinear optical properties

of the triisopropylsilyl-capped series **132-138** were thus explored,⁷⁵ representing the first study of extended polyynes chains. Surprisingly, the molecular second hyperpolarizabilities, γ , for polyynes increases dramatically as a function of length, surpassing all theoretical expectations. Table 3.3 lists the γ -values for **132-138**. While the γ -values for the shorter polyynes (less than twelve carbons) show only moderate values, those of the longest polyynes, such as **138** ($\gamma = 646 \times 10^{-36}$ esu) are substantial for relatively small molecules.⁷⁶ By way of comparison, β -carotene, with 11 consecutive double bonds, shows a value of $\gamma = 790 \times 10^{-36}$ esu. The similar values for the decayne **138** and β -carotene are surprising, as theoretical studies on oligomers of analogous length predict substantially higher values for polyenes than for polyynes.^{72,77}

Table 3.3 Nonlinear optical characteristics of polyynes **132-138**

Compound	$\gamma \times 10^{-36}$ [esu]
132	2.75 ± 0.28
133	6.99 ± 0.70
134	12.5 ± 2.1
135	35.3 ± 1.2
136	64.3 ± 2.9
137	238 ± 47
138	646 ± 27

Various mathematical approaches have been established to explain the relationship between the γ -values and conjugation length and predict a superlinear increase as a function of oligomer length.⁶¹ For conjugated oligomers shorter than the effective conjugation length (ECL), these theoretical models predict a power-law dependence of $\gamma \sim L^c \sim n^c$, where L is the length of the molecule (in nm) and n is the number of repeat units. Both theoretically and experimentally, the exponent c remains the most commonly used figure of merit for the comparison of different oligomer series.⁶¹ Theoretical studies addressing γ -values for polyene chains predict exponents that range from $c = 1.26$ to 3.3 .^{72,74,78} Notably, studies consistently predict that the power-law increase based on $\gamma \sim n^c$ will be more dramatic for polyenes than for polyynes.

The NLO behavior of polyene samples **132-138** fits well with the relationship $\gamma \sim n^c$ and gives a value of $c = 4.28 \pm 0.13$ (Figure 3.9). This trend shows no saturation of γ through the longest polyene measured, consistent with the linear absorption data. Unlike comparisons of absolute γ -values, comparisons of power-law exponents are less sensitive to the experimental method used. To the best of our knowledge, the exponent $c = 4.28 \pm 0.13$ is the highest nonresonant exponent observed for a series of nonaromatic, conjugated oligomers.⁷⁹ The third-order optical nonlinearities of polyenes have been investigated, with experimental power-law exponents ranging from $c = 2.3$ to 3.6 .^{76,80,81} Polytriacetylenes, the closest structural relative to polyynes, show power-law behavior with a reported exponent of $c = 2.5$, substantially smaller than that reported for polyynes.⁸²

Oligo(1,4-phenyleneethynylene)s show an exponent of $c = 2.5$,⁸³ whereas for polythiophenes values as high as $c = 4.05$ have been reported.⁸⁴

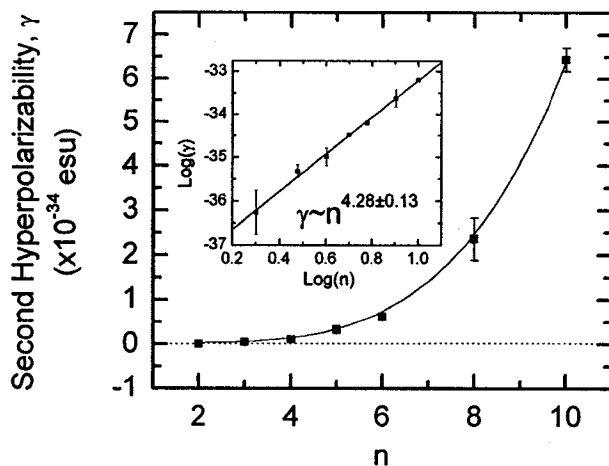


Figure 3.9 Polyne molecular second hyperpolarizability (γ) as a function of the number of repeat units (n) in the oligomer chain. The solid line is a fit of the form $\gamma = a + bn^c$, where a is an offset due to end-group effects, b is a constant, and c is the power-law exponent. The inset shows a log-log plot of the same data with the coefficient a subtracted, yielding a power-law exponent (slope of the solid line) of $c = 4.28 \pm 0.13$ for the polyynes.

The magnitude of the power-laws relationship for polyynes is surprisingly high in comparison to that of other conjugated materials, and several factors may account for this observation. As the major component to molecular hyperpolarizability arises from electron delocalization along the conjugated backbone,^{61,76} a molecule which exhibits minimal conformational distortion in solution would enhance the experimental γ -values. Unlike polyenes, where rotation about the single bonds can occur and therefore interrupt the conjugated system, polyynes provide a more or less cylindrical electronic delocalization

along the conjugated framework. In comparison to an sp^2 -hybridized oligomer, the hyperpolarizability of a polyynes would be less dependent on solution state orientation with respect to the electric field of the incident light source, enhancing γ -values. The power-law exponent for the triisopropylsilyl-capped polyynes, $c = 4.28$, is significantly higher than the predicted values of $c = 1.26$ to 3.3 . This may be due to underestimation of the effects of electron correlation on polyynes hyperpolarizability.⁸⁵

3.3 Conclusions

Alkylidene carbenoid rearrangements have been successfully utilized for the synthesis of a series of triisopropylsilyl-capped polyynes, including a decayne, only the third ever to have been fully characterized spectroscopically. This methodology has facilitated the synthesis of large quantities of highly pure products and the physical, electronic and optical properties have been analyzed. Of particular interest are the third order nonlinear optical characteristics, which have been studied for the first time. These NLO results show a much higher response for polyynes than was generally believed possible by theoreticians, and these responses are, in fact, higher than the NLO response of polyenes, a result that is contrary to the theoretical studies that have been performed to date.

3.4 References and Notes

1. Kroto, H. W., *Angew. Chem. Int., Ed. Engl.* **1992**, *31*, 111.

2. Kraschmer, W.; Lamb, L. D.; Fostiropoulos, K.; Huffman, D. R., *Nature* **1990**, *347*, 354.
3. Faust, R., *Angew. Chem. Int. Ed* **1998**, *37*, 2825.
4. Hunter, J.; Fye, J.; Jarrold, M. F., *Science* **1993**, *260*, 784.
5. Clemmer, D. E.; Jarrold, M. F., *J. Am. Chem. Soc.* **1995**, *117*, 8841.
6. von Helden, G.; Gotts, N. G.; Bowers, M. T., *Nature (London)* **1993**, *363*, 60.
7. Diederich, F.; Rubin, Y.; Chapman, O.; Goroff, N. S., *Helv. Chim. Acta* **1994**, *77*, 1441.
8. McElvany, S. W.; Ross, M. M.; Goroff, N. S.; Diederich, F., *Science* **1993**, *259*, 1594.
9. Goroff, N. S., *Acc. Chem. Res.* **1996**, *29*, 77.
10. Rubin, Y.; Kahr, M.; Knobler, C. B.; Diederich, F.; Wilkins, C. L., *J. Am. Chem. Soc.* **1991**, *113*, 495.
11. Tobe, Y.; Fujii, T.; Matsumoto, H.; Tsumuraya, K.; Noguchi, D.; Nakagawa, N.; Sonoda, M.; Naemura, K.; Achiba, Y.; Wakabayashi, T., *J. Am. Chem. Soc.* **2000**, *122*, 1762.
12. Smith, P. P. K.; Buseck, P. R., *Science* **1982**, *216*, 984.
13. Kudryavtsev, Y. P.; Evsyukov, S.; Guseva, M.; Babaev, V.; Khvostov, V., *Chemistry and Physics of Carbon*. In *Chemistry and Physics of Carbon*; Thrower, P. A., Ed.; Marcel Dekker: New York, 1997; Vol. 25, pp 1-69.
14. Lagow, R. J.; Kampa, J. J.; Wei, H.-C.; Battle, S. L.; Genge, J. W.; Laude, D. A.; Harper, C. J.; Bau, R.; Stevens, R. C.; Haw, J. F.; Munson, E., *Science* **1995**, *267*, 362.
15. Martin, R. E.; Diederich, F., *Angew. Chem. Int. Ed* **1999**, *38*, 1350.
16. Bohlmann, F., *Chem. Ber.* **1953**, *63*, 657.
17. Jones, E. R. H.; Lee, H. H.; Whiting, M. C., *J. Chem. Soc.* **1960**, 3483.
18. Johnson, T. R.; Walton, D. R. M., *Tetrahedron* **1972**, *28*, 5221.
19. Cook, C. L.; Jones, E. R. H.; Whiting, M. C., *J. Chem. Soc.* **1952**, 2883.
20. Armitage, J. B.; Entwistle, N.; Jones, E. R. H.; Whiting, M. C., *J. Chem. Soc.* **1954**, 147.

21. Eastmond, R.; Walton, D. R. M., *Tetrahedron* **1972**, *28*, 4591.
22. Eastmond, R.; Johnson, T. R.; Walton, D. R. M., *Tetrahedron* **1972**, *28*, 4601.
23. Yean, Z.; Stringer, G.; Jobe, I. R.; Kreller, D.; Scott, K.; Koch, L.; Taylor, N.; Marder, T. B., *J. Organomet. Chem.* **1993**, *452*, 115.
24. Bunz, U. H. F., *Angew. Chem., Int. Ed. Engl.* **1996**, *35*, 969.
25. Gao, K.; Goroff, N. S., *J. Am. Chem. Soc.* **2000**, *122*, 9320.
26. Werz, D. B.; Gleiter, R.; Rominger, F., *Organometallics* **2002**, *22*, 843.
27. Hlavaty, J.; Kavan, L.; Kubista, J., *Carbon* **2002**, *40*, 345.
28. Schermann, G.; Grosser, T.; Hampel, F.; Hirsch, A., *Chem. Eur. J.* **1997**, *3*, 1105.
29. Gibtner, T.; Hampel, F.; Gisselbrecht, J. P.; Hirsch, A., *Chem. Eur. J.* **2002**, *8*, 408.
30. Bunz, U. H. F.; Roidl, G.; Altmann, M.; Enkelmann, V.; Shimizu, K., *J. Am. Chem. Soc.* **1999**, *121*, 10719.
31. Bruce, M.; Ke, M.; Low, P. J.; Skelton, B. W.; White, W. H., *Organometallics* **1998**, *17*, 3539.
32. Akita, M.; Chung, M.-C.; Sakurai, A.; Sugimoto, S.; Terada, M., *Organometallics* **1997**, *16*, 4882.
33. Wong, K.-T.; Lehn, J.-M.; Peng, S.-M.; Lee, G.-H., *J. Chem. Soc., Chem. Comm.* **2000**, 2259.
34. Lu, W.; Xiang, H.-F.; Zhu, N.; Che, C.-M., *Organometallics* **2002**, *21*, 2343.
35. Sakurai, A.; Akita, M.; Moro-oka, Y., *Organometallics* **1999**, *18*, 3241.
36. Bartik, T.; Bartik, B.; Brady, M.; Dembinski, R.; Gladysz, J. A., *Angew. Chem., Int. Ed. Engl.* **1996**, *35*, 414.
37. Bartik, B.; Dembinski, R.; Bartik, T.; Arif, A. M.; Gladysz, J. A., *New J. Chem.* **1997**, *21*, 739.
38. Bartik, T.; Weng, W. Q.; Ramsden, J. A.; Szafert, S.; Falloon, S. B.; Arif, A. M.; Gladysz, J. A., *J. Am. Chem. Soc.* **1998**, *120*, 11071.

39. Dembinski, R.; Bartik, T.; Bartik, B.; Jaeger, M.; Gladysz, J. A., *J. Am. Chem. Soc.* **2000**, *122*, 810.
40. Horn, C. R.; Gladysz, J. A., *Eur. J. Inor. Chem.* **2003**, 2211.
41. Stahl, J.; Bohling, J. C.; Bauer, E. B.; Peters, T. B.; Mohr, W.; Martin-Alvarez, J. M.; Hampel, F.; Gladysz, J. A., *Angew. Chem. Int. Ed.* **2002**, *41*, 1872.
42. Mohr, W.; Stahl, J.; Hampel, F.; Gladysz, J. A., *Chem. Eur. J.* **2003**, *9*, 3324.
43. Mohr, W.; Stahl, J.; Hampel, F.; Gladysz, J. A., *Inor. Chem.* **2001**, *40*, 3263.
44. Hay, A. S., *J. Org. Chem.* **1962**, *27*, 3320.
45. Glaser, C., *Ann. Chem. Pharm.* **1870**, *154*, 137.
46. Chodkiewicz, W., *Ann. Chim. (Paris)* **1957**, *2*, 819.
47. Eisler, S.; Tykwinski, R. R., *J. Am. Chem. Soc.* **2000**, *122*, 10736.
48. Bottaro, J. C.; Schmidt, R. J.; Bedford, C. D.; Gilardi, R.; George, C., *J. Org. Chem.* **1990**, *55*, 1916.
49. Eisler, S.; Chahal, N.; McDonald, R.; Tykwinski, R. R., *Chem. Eur. J.* **2003**, *9*, 2542.
50. Rubin, Y.; Lin, S. S.; Knobler, C. B.; Anthony, J.; Boldi, A. M.; Diederich, F., *J. Am. Chem. Soc.* **1991**, *113*, 6943.
51. Tobe, Y.; Iwasa, N.; Umeda, R.; Sonoda, M., *Tetrahedron Lett.* **2001**, *42*, 5485.
52. Siemsen, P.; Livingstone, R. C.; Diederich, F., *Angew. Chem. Int. Ed.* **2000**, *39*, 2633.
53. Stephens, R. D.; Castro, C. E., *J. Org. Chem.* **1963**, *28*, 3313.
54. Kauffmann, T., *Angew. Chem., Int. Ed. Engl.* **1974**, *13*, 291.
55. The synthesis of the octayne **137** was accomplished by summer student, Erin Elliott, under my supervision.
56. This section was written in collaboration with Aaron Slepko, Department of Physics, University of Alberta.
57. Abdurahman, A.; Shukla, A.; Dolg, M., *Phys. Rev. B* **2002**, *65*, 115106.

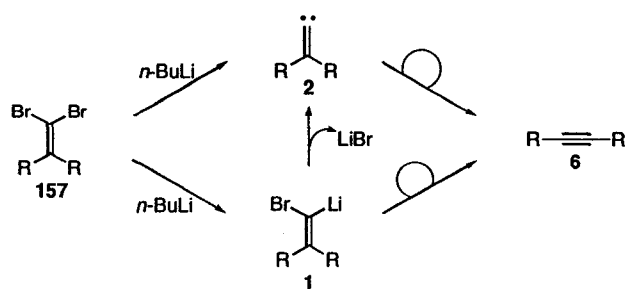
58. Scemama, A.; Chaquin, P.; Gazeau, M.-C.; Benalin, Y., *Chem. Phys. Lett.* **2002**, *361*, 520.
59. Bylaska, E. J.; Weare, J. H.; Kawai, R., *Phys. Rev. B* **1998**, *58*, R7488.
60. Scemama, A.; Chaquin, P.; Gazeau, M.-C.; Benalin, Y., *J. Phys. Chem. A* **2002**, *106*, 3828.
61. Bubeck, C., In *Electronic Materials-The Oligomer Approach*; Müllen, K.; Wegner, G., Eds.; Wiley-VCH: Weinheim, 1998; Chapter 8.
62. Lewis, G. N.; Calvin, M., *Chem. Rev.* **1939**, *39*, 273.
63. Mathy, A., *Phys. Rev. B* **1996**, *53*, 4367.
64. Enkelmann, V., *Chem. Mater.* **1994**, *6*, 1337.
65. Baughman, R. H.; Yee, K. C., *J. Polym. Sci. Macromol. Rev.* **1978**, *13*, 219.
66. Boese, R.; Matzger, A. J.; Vollhardt, K. P. C., *J. Am. Chem. Soc.* **1997**, *119*, 2052.
67. Carre, F.; Devylder, N.; Dutremez, S. G.; Guerin, C.; Henner, B. J. L.; Jolivet, A.; Tomberli, V., *Organometallics* **2003**, *22*, 2014.
68. Bassler, H., *Adv. Polym. Sci.* **1984**, *63*, 1.
69. This section was written in collaboration with Aaron Slepkov, Department of Physics, University of Alberta.
70. Nalwa, H. S., *Handbook of Organic Conductive Materials and Polymers*; Wiley: New York, 1997.
71. Schulz, M.; Tretiak, S.; Chernyak, V.; Mukamel, S., *J. Am. Chem. Soc.* **2000**, *122*, 452.
72. Nalwa, H. S.; Mukai, J.; Kakuta, A., *J. Phys. Chem.* **1995**, *99*, 10766.
73. Albert, I. D. L.; Morley, J. O.; Pugh, D., *J. Phys. Chem. A* **1997**, *101*, 1763.
74. Buma, W. J.; Fanti, M.; Zerbetto, F., *Chem. Phys. Lett.* **1999**, *313*, 426.
75. Slepkov, A. D.; Hegmann, F. A.; Zhao, Y. M.; Tykwinski, R. R.; Kamada, K., *J. of Chem. Phys.* **2002**, *116*, 3834.
76. Nalwa, H. S., In *Nonlinear Optics of Organic Molecules*; Nalwa, H. S.; Miyata, S., Ed.; CRC Press: 1997; Chapters 9 and 11.

77. Perpete, E. A.; Champagne, B.; Andre, J. M.; Kirtman, B., *J. Mol. Struct. (Theochem)* **1998**, *425*, 115.
78. Archibong, E. F.; Thakkar, A. J., *J. Chem. Phys.* **1993**, *98*, 8324.
79. Rumi, M.; Zerbi, G.; Mullen, K.; Muller, G.; Rehahn, M., *J. Chem. Phys.* **1997**, *106*, 24.
80. Samuel, I. D. W., *Science* **1994**, *265*, 1070.
81. Craig, G. S. W., *J. Am. Chem. Soc.* **1993**, *115*, 860.
82. Martin, R. E., *Chem. Eur. J.* **1997**, *3*, 1505.
83. Meier, H.; Ickenroth, d.; Stalmach, U.; Koynov, K.; Bahtiar, A.; Bubeck, C., *Eur. J. Org. Chem.* **2001**, 4431.
84. Zhao, M. T.; Singh, B. P.; Prasad, P. N., *J. Chem. Phys.* **1988**, *89*, 5535.
85. Toto, J. L.; Toto, T. T.; de Melo, C. P., *Chem. Phys. Lett.* **1995**, *245*, 660.

Chapter 4 Mechanistic Investigations of the 1,2-Migration of an Alkyne in an Alkylidene Carbenoid Rearrangement

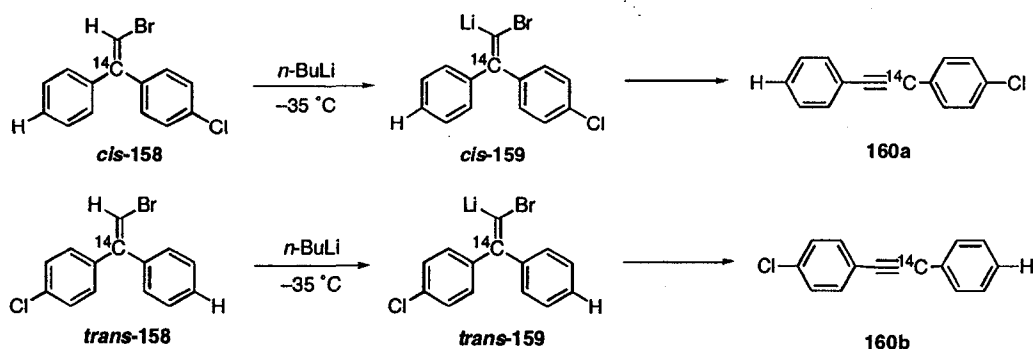
4.1 Introduction

The mechanism of the Fritsch-Buttenberg-Wiechell rearrangement¹⁻³ can be separated into two general steps, the first of which is the formation of an alkylidene intermediate.⁴⁻⁹ This intermediate is the species from which migration is instigated and can take one of two forms. It may be a carbenoid (e.g., **1**, formed from **157** by lithium-halogen exchange, Scheme 4.1) or a free carbene (e.g., **2**, formed by elimination of LiBr from **157**). Whichever of these two species is formed has implications for the second step of the mechanism, the 1,2-migration of a pendant R group. If the carbene **2** is formed, the group with the greatest propensity for migration will do so, whereas if the carbenoid is formed, the stereochemistry of the intermediate may control the identity of the migratory group.



Scheme 4.1

Curtin, Flynn, and Nystrom carried out seminal work on determining the stereochemistry of the reaction and the resultant implications for the nature of a carbenoid intermediate.¹⁰ It was necessary to design an experiment where the site of lithiation could be controlled and the migrating group could be identified. They thus devised an experiment based on the rearrangement of ¹⁴C labeled monobromoolefins **158**, (Scheme 4.2). *Cis*- and *trans*-**158** were synthesized and separated by fractional distillation and chromatography.



Scheme 4.2

Separate treatment of *cis*- and *trans*-**158** with *n*-BuLi resulted in deprotonation of the vinyl proton and the formation of the lithiated intermediates *cis*-**159** and *trans*-**159** respectively. Both intermediate species **159** then rearranged to form tolans **160a** and **160b**. In the case of *cis*-**159**, the major rearranged product was tolan **160a**, which resulted from migration of the phenyl ring. Rearrangement of *trans*-**159** resulted in the formation of labeled tolan **160b**, where the migrating group was instead the *p*-chlorophenyl moiety. In both cases, the migrating group was found almost exclusively to be the moiety *trans* to the bromine in the intermediates *cis*- and *trans*-**159**. The reaction therefore appeared

to proceed stereospecifically, consistent with the presence of a carbenoid intermediate. These results were mirrored in a similar study by Bothner-By, where again migration appeared to be stereospecific with respect to metallation.¹¹

It has been widely propagated since these initial studies that the migrating group in a Fritsch-Buttenberg-Wiechell rearrangement is the one *trans* to the bromine atom. This is not, however, always the case. For example, both Normant¹² and Köbrich^{9,13} have demonstrated that *cis* migration is also a possible pathway. As well, initial results from our group mirror these conclusions.

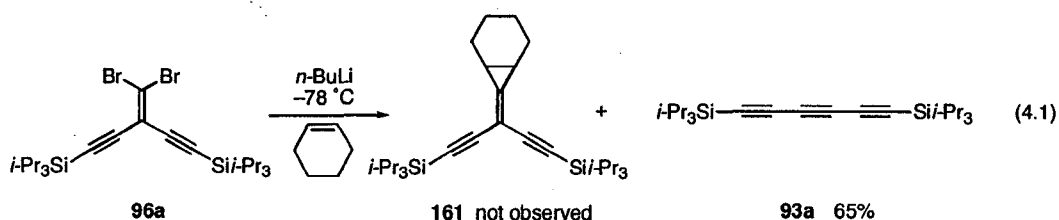
The mechanism of the modified FBW rearrangement has therefore been explored. Three aspects of the rearrangement were investigated, 1) the nature of the intermediate, be it carbene or carbenoid, 2) the migration of the alkynyl moiety in comparison to other functional groups and 3) the regiospecificity of the lithiation step. Our preliminary, albeit incomplete, investigations are presented.

4.2 Carbene or Carbenoid

Carbenes are highly reactive intermediates and their existence can generally only be confirmed by their chemical behavior. Unsaturated carbenes typically undergo insertions into Si-H, O-H, and C-H bonds (the latter only in an intramolecular fashion) and addition into olefins.⁶ The formation of products resulting from these actions indicates that a reaction likely proceeds through a carbene intermediate.

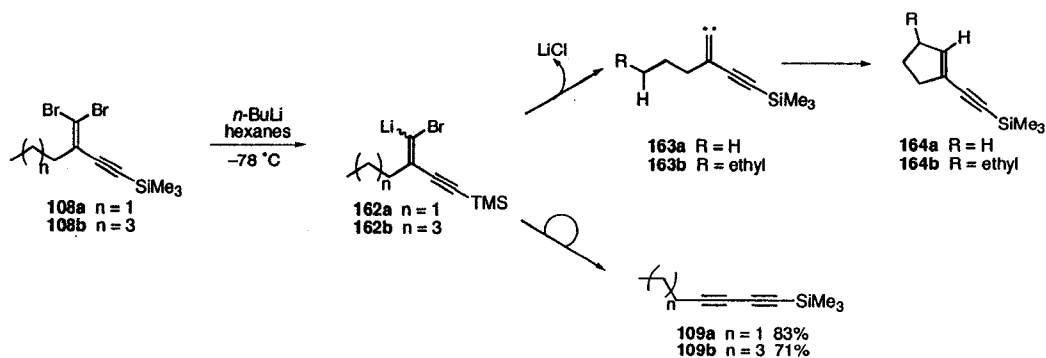
Several attempts were thus made to trap an intermediate in the reaction of **96a** that would be consistent with the behavior expected of a free carbene. An

olefin was used initially to trap the intermediate. Ethynyl substituted dibromoolefin **96a** was rearranged with cyclohexene as solvent, eq 4.1, as isolation of methylenecyclopropane **161** would serve as an indication that a carbene was formed during the reaction. Thus, dibromoolefin **96a** was subjected to slow addition of *n*-BuLi at $-78\text{ }^{\circ}\text{C}$ then warming to ca. $-5\text{ }^{\circ}\text{C}$. Upon work-up and analysis of the crude product, triyne **93a** was found in 65% yield and none of the methylenecyclopropane **161** was detected by ^1H NMR spectroscopic analysis.



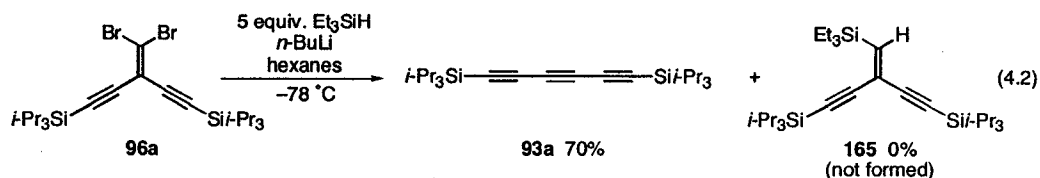
Although carbene derived methylenecyclopropane **161** was not observed, it was possible that a carbene was formed during the course of the reaction but that the subsequent migration of an alkyne was too fast for the intermolecular reaction with the olefin. An attempt was then made to trap the intermediate in an intramolecular fashion. Alkyl substituted dibromoolefins **108a** and **108b** were designed and synthesized with this purpose in mind (Scheme 4.3). Cyclopentenes **164a** and **164b** were the products expected from a 1,5-insertion of an intermediate carbene into a C-H bond, the vinyl proton of which would be easily identifiable in the ^1H NMR spectrum of the product. The usual rearrangement conditions were applied to dibromoolefins **108a** and **108b**. As judged by TLC analysis during the reaction, the starting material went to a single product. The mixture was

quenched with an aqueous solution of NH_4Cl and upon analysis of the crude product mixture, no cyclopentenyl product was detected by ^1H NMR spectroscopic analysis. Dienes **109a** and **109b** were, in fact, isolated in 83% and 71% yield, respectively.



Scheme 4.3

One final attempt was made to probe the intermediacy of an alkylidene carbene. It has been shown that insertion into a Si-H bond can occur much more readily than insertion into a C-H bond, even in an intermolecular manner.⁶ Therefore, enediyne **96a** was rearranged in hexanes in the presence of 5 equivalents of Et_3SiH , according to a literature procedure.⁶ Silane **165** would result from insertion, but compound **165** was not observed upon work-up and ^1H NMR spectroscopic analysis. The triyne **93a** was the sole product, in a yield of 70%.



Making a definitive statement about whether or not a free alkyldiene carbene is formed in our modified FBW rearrangement is difficult, since this species cannot be directly observed. The several attempts toward trapping a carbene intermediate resulted in no formation of carbene derived products, and it is a reasonable assumption that the reaction proceeds via an alkyldiene carbenoid intermediate. This result is in agreement with literature precedent.^{8,14,15}

4.3 Migratory Ability of Alkynes in Alkyldiene Carbenes/Carbenoids

To evaluate the migratory ability of alkynyl groups in an alkyldiene carbenoid species, a ¹³C label was incorporated into the C2 position of the dibromoolefin **166** as shown in Figure 4.1. Several labeling studies were performed by varying the substitution on the 2-position of **166**. The migratory ability of a trialkylsilyl-substituted alkyne was explored relative to an aryl (Study 1), a vinyl (Study 2), an alkyl (Study 3) group and a differentially protected alkynyl moiety (Study 4). Studies 1 and 2 were carried out by Annabelle Shi Shun, Erin Chernick and Paul Bichler. The results of some of their work are presented here for the sake of completion.

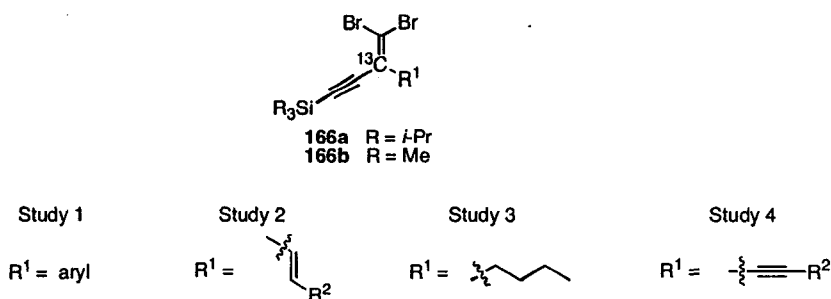
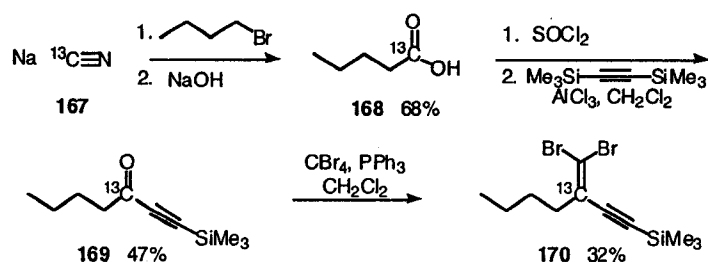


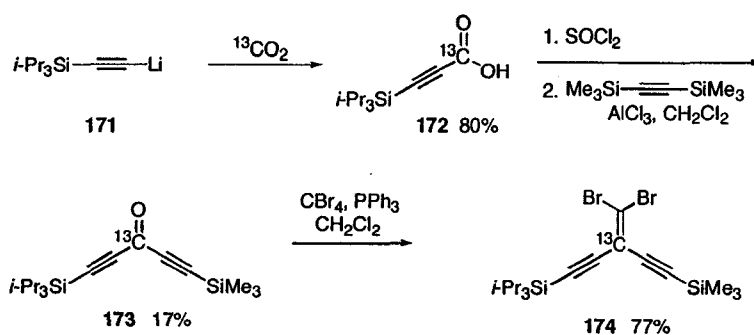
Figure 4.1 Labeling Studies.

4.3.1 Synthesis of Labeled Dibromoolefins



Scheme 4.4

The incorporation of a ^{13}C label into mixed dibromide **170** was accomplished using labeled sodium cyanide **167** (Scheme 4.4).¹⁶ Butyl bromide was added to a solution of Na^{13}CN **167** in water and ethanol and the mixture brought to reflux and left overnight. After work-up, labeled valeric acid **168** was isolated as an oil in 68% yield. Ketone **169** was easily formed in 47% yield utilizing the standard Friedel-Crafts conditions and bis(trimethylsilyl)acetylene.¹⁷ Addition of **169** to a stirred solution of CBr_4 and PPh_3 then provided labeled dibromide **170** in 32% yield.¹⁸ The poor yields of the last two steps were attributed to difficulties in purification. It was very difficult to obtain clean NMR spectra of **169** and **170**, as any impurity that was formed in the reaction was also ^{13}C labeled and resulted in significant signals in the ^{13}C NMR spectra. It was essential that the by-products were removed prior to rearrangement to the diyne, as the presence of extraneous peaks in the ^{13}C NMR spectra could interfere with interpretation.



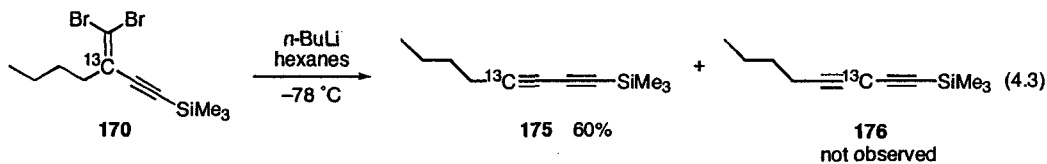
Scheme 4.5

A ^{13}C label was introduced into enediyne **174** using labeled carbon dioxide (Scheme 4.5). A solution of triisopropylsilyl lithium acetylide **171** was added to a condensed solution of $^{13}\text{CO}_2$ to form carboxylic acid **172** in 80% yield. Ketone **173** was formed in 17% yield by the conversion of carboxylic acid **172** to the corresponding acid chloride using thionyl chloride, followed by treatment with AlCl_3 and bis(trimethylsilyl)acetylene in CH_2Cl_2 . Dibromoolefination gave labeled enediyne **174** in 77% yield. As was the case for the alkyl example in Scheme 4.4, the yields tended to be lower in the synthesis leading to **174** than the unlabeled reactions due to more intensive purification.

4.3.2 Rearrangement of Labeled Dibromoolefins

Rearrangement of the labeled dibromides was accomplished using the standard reaction conditions. In the first example, the migratory potential of the trimethylsilylethynyl moiety was evaluated versus an alkyl group (eq 4.3). Alkyl groups have been known to migrate poorly in lithiated alkylidene carbenoids.¹² It was thus predicted that the alkynyl moiety would migrate preferentially to the alkyl group in the modified FBW rearrangement. Confirming this hypothesis,

rearrangement of dibromide **170** yielded only diyne **175** in 60% yield, with no evidence for the formation of the isotopomer **176**.



Isotopomer **175** was identified by an analysis of the coupling patterns observed in the ^{13}C NMR spectrum of this product. The presence of a single intense signal in the ^{13}C NMR spectrum revealed the formation of only one isomer, (Figure 4.2). The signal of the labeled carbon appears at 80.2 ppm. Two doublets are observed at 88.5 and 82.9 ppm with coupling constants of 17 and 15 Hz respectively, consistent with $^2J_{\text{CC}}$ or $^3J_{\text{CC}}$ coupling. The resonance for the fourth sp-hybridized carbon at 65.3 ppm is a doublet with a coupling constant of 189 Hz, corresponding to a $^1J_{\text{CC}}$ value. The presence of only a single resonance $^1J_{\text{CC}}$ coupling between the labeled carbon and an sp-hybridized carbon confirms the formation of **175** as the only product in equation 4.3. Furthermore, coupling between the labeled carbon and the propargylic methylene carbon ($^1J_{\text{CC}} = 66$ Hz) also supports the proposed structure.

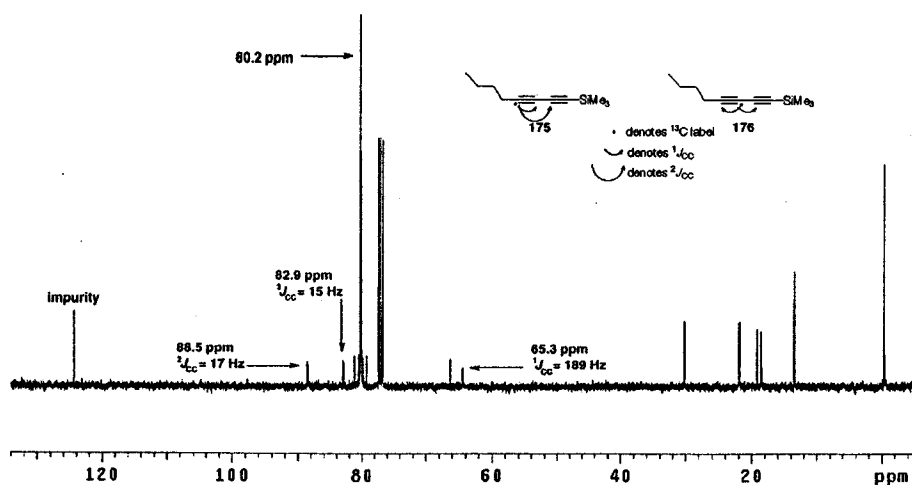
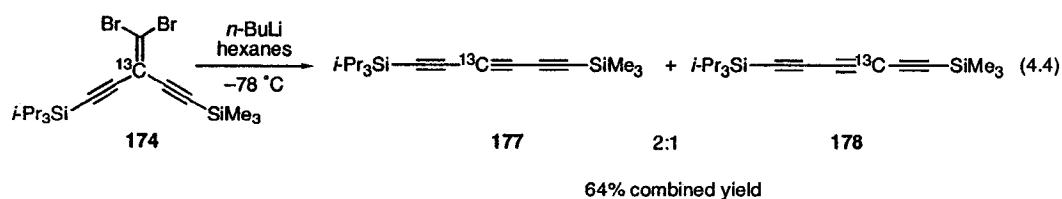


Figure 4.2 ^{13}C NMR spectrum of labeled diyne **175**.

The migratory ability of the trimethylsilylethynyl moiety versus the triisopropylsilylethynyl moiety was investigated (eq 4.4). A priori, it seemed likely that the two alkynyl moieties would compete equally effectively for 1,2-migration, resulting in an approximately 1:1 ratio of isotopomers **177** and **178**, since the methyl and isopropyl groups were several atoms away from the migrating carbon. Surprisingly, migration of the trimethylsilylethynyl moiety clearly dominated the reaction, giving a 2:1 ratio of **177** to **178**, with the reaction proceeding in 64% yield.



The assignment for the carbons in unlabeled triyne **96b** are shown in Figure 4.3 and this assignment is based on the following analysis. The ^{13}C NMR spectrum for triynes **177** and **178** showed the presence of both isomers in a 2:1 ratio based on the integration of two intense signals at 62.4 and 61.0 ppm. These resonances are thus attributed to the carbons of the internal acetylene unit, C3 (e) and C4 (f) of triyne **96b**. In the ^{13}C NMR spectrum of **96a**, resonances a and b correspond closely to resonances a and d in the ^{13}C NMR spectrum of **96b**, and these resonances are assigned to the acetylene unit adjacent to the TIPS moiety. Similarly, in the spectrum of **96c**, resonances a and b correspond to signals b and c of **96b**, and can be assigned to the acetylene unit closet to the TMS group. In the spectrum of labeled triynes **177** and **178** two doublets are observed for resonance a with $^1J_{\text{CC}} = 151$ Hz and $^2J_{\text{CC}} = 19$ Hz. A single doublet is observed for resonance d with $^2J_{\text{CC}} = 13$ Hz. Resonance a must therefore correspond to C2 and resonance d to C1. The same reasoning was applied to the assignment of b and c. For resonance b, two doublets are observed with $^1J_{\text{CC}} = 151$ Hz and $^2J_{\text{CC}} = 19$ Hz. A single doublet is observed for resonance c with $^2J_{\text{CC}} = 15$ Hz. Resonance b must therefore correspond to C5 and resonance c to C6. Given this assignment, the major isomer is determined to be **177** due to the presence of the intense doublet for C2 resulting from $^1J_{\text{CC}}$ to labeled C3. Due to the greater intensity of resonance e, this signal is assigned to C3 and f to C4.

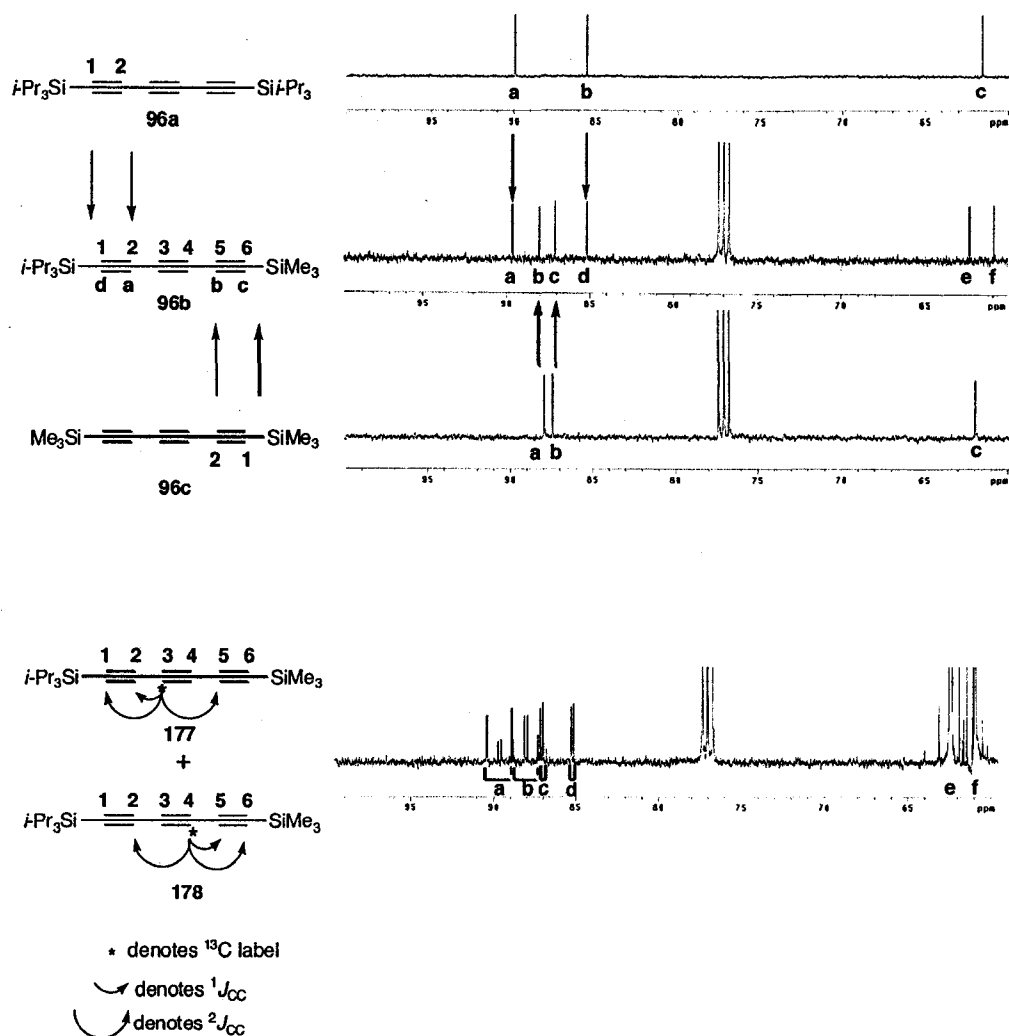
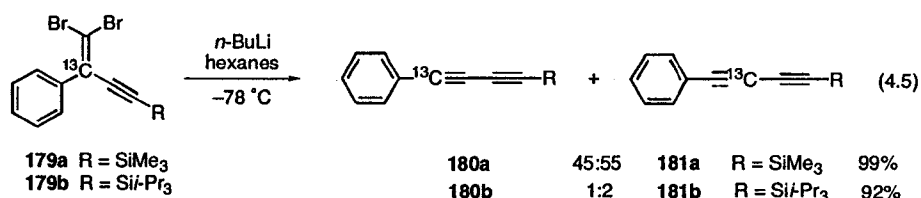


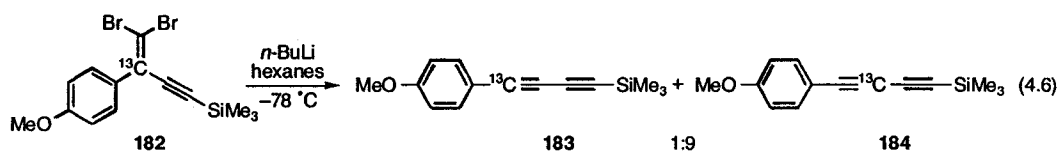
Figure 4.3 ^{13}C NMR spectra for **96a**, **96b**, **96c**, and **177/178**.

The migration of the triisopropylsilyl and trimethylsilyl protected alkynyl moieties was then evaluated relative to a phenyl group, (eq 4.5).¹⁹ When dibromide **179a** was rearranged, close to a 1:1 mixture of isotopomers **180a** and **181a** was formed, with a slight bias towards the product resulting from phenyl migration. The mixture of **180a** and **181a** was isolated in 99% yield.



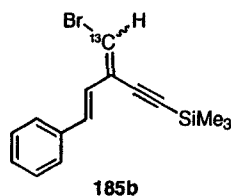
Replacing the trimethylsilyl moiety of **179a** with a triisopropylsilyl group had a significant effect on the ratio of diynes **180b** and **181b** that were formed from the rearrangement of **179b**.²⁰ A higher proportion of the isotopomer resulting from phenyl migration was formed than established in the previous example using **179a**. Diyne **181b** was formed in a two-fold excess in comparison to the diyne formed via alkynyl migration, **180b**. The triisopropylsilylethynyl moiety thus competes less effectively for migration in opposition to the phenyl group, than does the trimethylsilylethynyl moiety. This experiment correlates empirically with the result in the example using compound **174**, that is the likelihood that a trimethylsilyl protected alkyne would migrate preferentially to a triisopropylsilyl protected alkyne.

To explore further how altering the electronics of the dibromide system affects the product distribution, enyne **182** was synthesized with an electron donating methoxy group at the para position of the aryl ring (eq 4.6).²¹ Upon rearrangement, a mixture of two products was obtained. Isotopomer **184**, resulting from aryl migration was the major product of the reaction mixture (>9:1). While the alkynyl moiety is a strong migrating group, the electron donating effect of the methoxy group apparently biases the outcome of the reaction in comparison to the reaction of **179a** and **179b**.



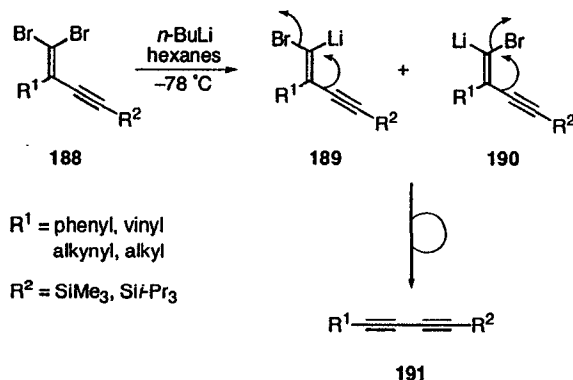
The migration of an alkynyl moiety relative to a styryl group was also explored (eq 4.7, the ^{13}C label in this series was incorporated instead into the external carbon).²² As in the case of the alkynyl vs. phenyl competition, the rearrangement of styryl appended dibromide **185** resulted in an almost 1:1 product mixture of **186**:**187**. Interestingly, different ratios of products **186**:**187** were obtained when the reaction was quenched at different temperatures. At low temperature (-78°C), the product ratio reflected the preferential formation of the isotopomer resulting from alkyne migration. Vinyl bromide **185b**, resulting from protonation of the carbenoid intermediate, was also present in the product mixture when the reaction was quenched at low temperature, suggesting an incomplete reaction. As the temperature was raised prior to quenching, the ratio between **186** and **187** became closer to 1:1 and the amount of protonated by-product **185b** formed was reduced. These results would suggest that overall the alkynyl moiety migrates faster than the vinyl moiety.





4.4 The Carbenoid Intermediate

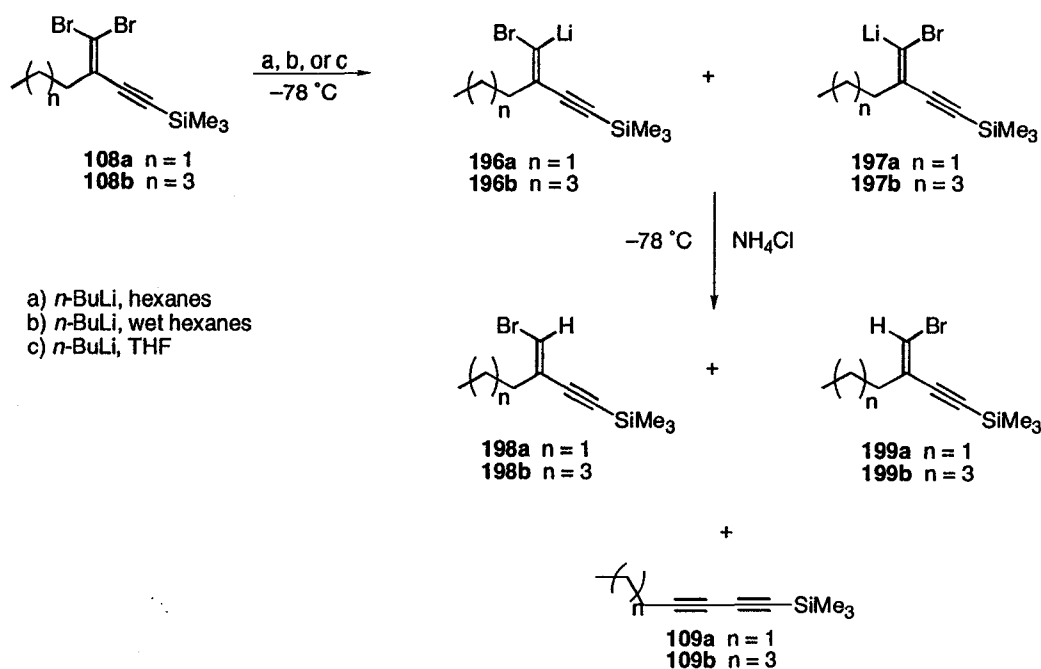
The FBW rearrangement is generally believed to proceed via a carbenoid intermediate.^{4,6,10} Initial mechanistic investigations into the modified alkylidene rearrangement, Section 4.2, also indicate that the 1,2-migration of an alkynyl moiety likely proceeds through a carbenoid intermediate. Migration occurring via a carbenoid species brings to mind three mechanistic questions. First, is the site of lithiation statistical or regioselective? Second, does the 1,2-migration occur *cis* or *trans* to the bromine atom in the carbenoid intermediate, Scheme 4.6, and third, is the migration determined by the comparative migratory ability of the competing migrating groups or is this step influenced by the stereochemistry of the intermediate?



Working toward the answer to these mechanistic questions, the ratio of lithiated species **189** and **190** was determined by trapping with a proton source. Combined with the knowledge of which group had migrated, the stereochemistry of the migration might then be deduced, specifically: does the migration occur *cis* and/or *trans* to the bromide moiety? It is also necessary to consider the possibility of equilibration between lithiated carbenoid intermediates **189** and **190**. It has been established previously that lithiation occurs without loss of stereochemical integrity.⁹

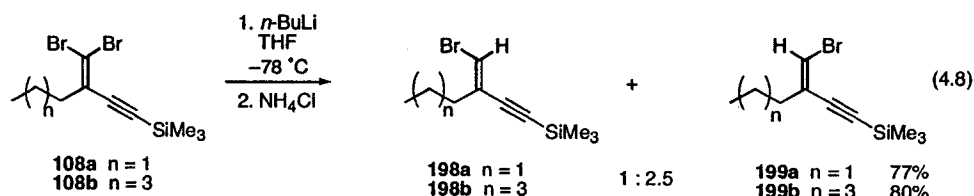
4.4.1 Trapping of Lithiated Carbenoid Intermediate

The trapping of the carbenoid intermediates **192** and **193** generated from **93a** was explored first (Scheme 4.7). In order to form the lithiated species, *n*-BuLi was added to enediyne **93a** at low temperature. To obtain an accurate ratio of intermediates **192** and **193**, the proton source had to be added before migration occurred. As any warming of the reaction would induce rearrangement to the corresponding triyne, quenching of the reaction was initiated at $-78\text{ }^{\circ}\text{C}$. It was determined that lithiation was not at all a random process, and monobromoolefins **194** and **195** were obtained as an inseparable 2:1 mixture in 68% yield. To date, however, we have been unable to identify the stereochemistry of the major and minor isomeric products. It is interesting that the ratio of lithiated intermediates corresponds directly to the ratio of migrating groups that was observed in the labeling studies, i.e. eq 4.4.

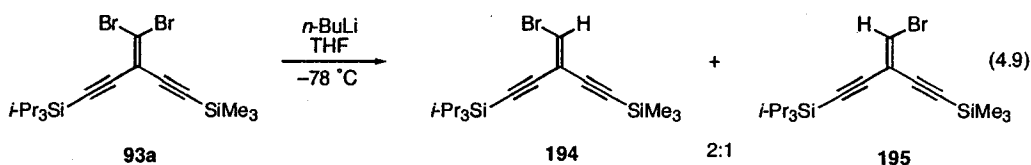


Scheme 4.8

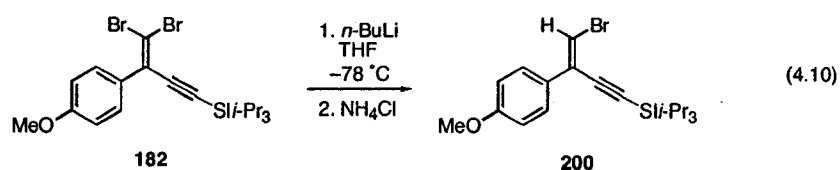
n-BuLi was thus added to dibromide **108a** in THF and the reaction was quenched at low temperature, (eq 4.8). Isomers **198a** and **199a** were obtained in a ratio of 1:2.5, as determined by ¹H NMR spectroscopy, with a combined yield of 77%. Similarly, *n*-BuLi was added to dibromide **108b** in THF and the reaction was quenched at low temperature. Isomers **198b** and **199b** were obtained in a ratio of 1:2.5 with a combined yield of 80%. NOE analysis (TROESY) was used to confirm the stereochemistry of the major product with a strong correlation observed between the vinyl proton and the methylene protons adjacent to the olefin. Monobromoolefins **199a,b** were thus determined to be the major isomers in both cases.



As carbenoid rearrangements are sensitive to subtle changes in the reaction conditions, the lithiation step may proceed in a different manner in THF than in hexanes. In an attempt to determine if changing solvent alters the outcome of the lithiation step, dibromide **93a** was treated with *n*-BuLi and the intermediates trapped via protonation in THF (eq 4.9). Significantly, the lithiation proceeded in the same manner in THF as for hexanes, giving the same apparent ratio of isomers (2:1), in both solvents.

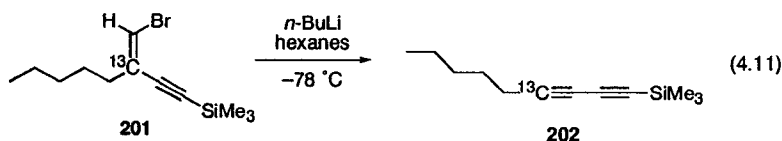


Interestingly, the major lithiated species from the reaction in equation 4.8 was opposite to what was predicted based on the predictions of Curtin and Bothner-By.^{10,11} Our labeling studies have determined that the alkynyl group was the only migrating group, while previous results suggested that 1,2-migration occurs preferentially *trans* to the bromide moiety (*trans*-migration). The predominance of isomer **199a** and **199b** would suggest that in this case migration *cis* to the bromine atom may be the dominant pathway (*cis*-migration). A similar result has been reported by Köbrich.⁹



Cis-migration is not observed in every situation, however, and it appears to be dependent upon both the site of lithiation and the migratory ability of the migrating group. In the *p*-anisyl example (eq 4.10), lithiation in THF gives predominantly isomer **200** (stereochemistry was confirmed by X-ray crystallography). *Trans*-migration seems to be the dominant pathway as the anisyl group was shown to migrate preferentially through labeling studies.

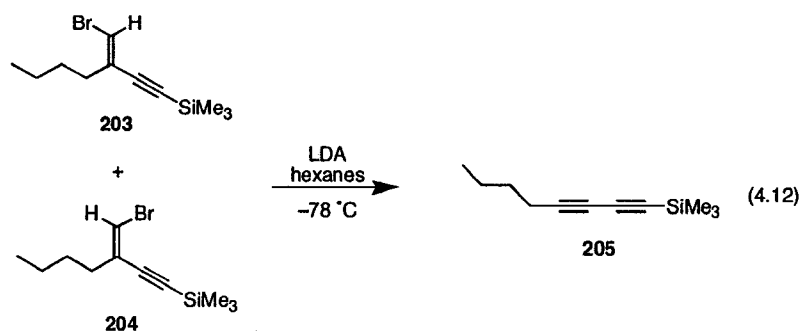
4.4.2 Rearrangement of Monobromoolefins-Future Work



The next step in this mechanistic study is to determine unequivocally if *cis* migration is occurring in hexanes, the following protocol has been devised. The isomers **198b** and **199b** (eq 4.8) are separable by column chromatography, and the rearrangement of each monobromide separately would provide a means to control the stereochemistry of the lithiated intermediate in solution. ^{13}C labeled

monobromoolefin **201** could then be synthesized and rearranged to determine if the alkyne moiety would migrate *cis* to the bromide to give diyne **202** (eq 4.11).

To first test the viability of rearranging labeled monobromoolefin **201**, bromides such as **203** and **204** must first successfully be rearranged. It is predicted that LDA would efficiently effect rearrangement of the monobromoolefins as this base should be strong enough to deprotonate the vinyl proton, but will not initiate lithium-halogen exchange.



4.5 Conclusions

The migratory potential of an alkyne in an alkylidene carbenoid has been determined for the first time in relation to aryl, vinyl and alkyl moieties. Although generally not as efficient as an aryl group, the alkynyl moiety exhibits strong migratory potential. In agreement with literature precedent, alkyne migration in the modified FBW rearrangement appears to proceed through a carbenoid, not a carbene, intermediate. The regiochemistry of lithiation and the stereochemistry of migration have been explored. It has been determined that not only is the lithiation regioselective, migration *cis* to the bromine atom seems to be the dominant pathway in the alkyne versus alkyl case. More information is

necessary to make definitive statements about the stereochemistry of the rearrangement, but the following assessment can reasonably be presented based on literature precedent and the information gathered here. It has been determined that lithiation does not afford a 1:1 mixture of isomers, but rather regioselectivity is influenced by the electronics of the substrate. Both *cis*- and *trans*-migration with respect to the bromine atom are possible pathways available to a migrating group. Which one of these reaction pathways is followed depends upon the relative transition state energies and the comparative migratory abilities of the migrating groups. For example, in a case where the two possible migrating groups possess greatly differing migratory abilities, *cis* migration of the powerful migrating group can be a lower energy pathway than *trans* migration of the poor migrating group. In a case where the two possible migrating groups have similar migratory abilities, *trans* migration appears to be the lower energy pathway and the migrating group(s), is(are) determined by the ratio of lithiated species formed.

4.6 References and Notes

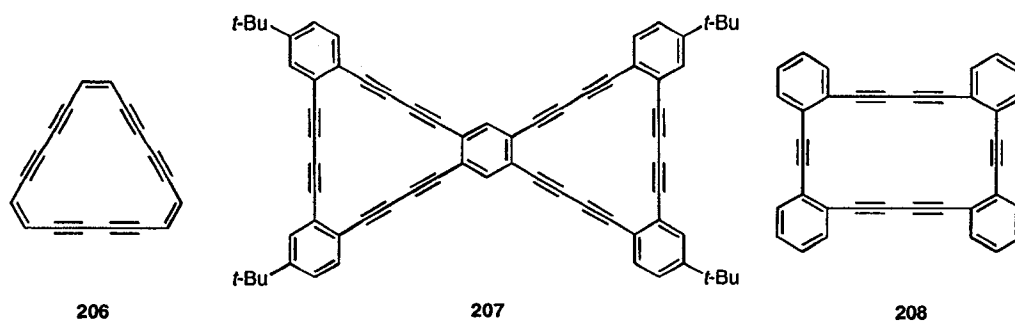
1. Fritsch, P., *Liebigs Ann. Chem.* **1894**, 279, 319.
2. Buttenberg, W. P., *Liebigs Ann. Chem.* **1894**, 279, 324.
3. Wiechell, H., *Liebigs Ann. Chem.* **1894**, 279, 337.
4. Boche, G.; Lohrenz, J. C. W., *Chem. Rev.* **2001**, 101, 697.
5. Kirmse, W., *Angew. Chem., Int. Ed. Engl.* **1997**, 36, 1164.
6. Stang, P. J., *Chem. Rev.* **1978**, 78, 383.

7. Hartzler, H. D. In *Carbenes*; Moss, R. A.; Jones, M., Jr., Eds.; Wiley and Sons: New York, 1983; Vol. 2, pp 43-100.
8. Köbrich, G., *Angew. Chem., Int. Ed. Engl.* **1965**, *4*, 49.
9. Köbrich, G., *Angew. Chem., Int. Ed. Engl.* **1972**, *11*, 473.
10. Curtin, D. Y.; Flynn, E. W.; Nystrom, R. F., *J. Am. Chem. Soc.* **1958**, *80*, 4599.
11. Bothner-By, A. A., *J. Am. Chem. Soc.* **1955**, *77*, 3293.
12. Rezaei, H.; Yamanoi, S.; Chemla, F.; Normant, J. F., *Org. Lett.* **2000**, *2*, 419.
13. Köbrich, G.; Ansari, F., *Chem. Ber.* **1967**, *100*, 2011.
14. Kirmse, W., *Angew. Chem.* **1961**, *73*, 161.
15. Miginiac, P., *Bull. Soc. Chim. France* **1963**, *63*, 235.
16. Ahmad, K.; Strong, F. M., *J. Am. Chem. Soc.* **1948**, *70*, 1699.
17. Walton, D. R. M.; Waugh, F., *J. Organomet. Chem.* **1972**, *37*, 45.
18. Corey, E. J.; Fuchs, P. L., *Tetrahedron Lett.* **1972**, 3769.
19. Work carried out by graduate student Annabelle Shi Shun.
20. Work carried out by summer student Paul Bichler under the supervision of Annabelle Shi Shun.
21. Work carried out by summer student, Erin Chernick, under my supervision.
22. Work carried out by graduate student, Annabelle Shi Shun.

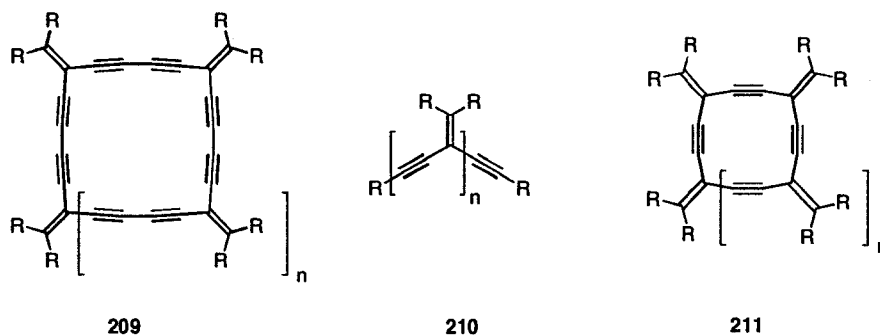
Chapter 5 Synthesis and Study of the Cross-conjugated Macrocycles

5.1 Introduction

Sondheimer's synthesis of **206**¹ in 1972 generated among scientists a great interest in cyclic enyne macrocycles.^{2,3} The determination of the structural, electronic, optical and materials properties of these unique structures has been a motivating factor for their creation, in addition to the desire to form the aesthetically pleasing structures.⁴⁻⁹ A number of novel dehydroannulenes and dehydrobenzoannulenes have since been realized such as the "bowtie" series synthesized by the Haley group.¹⁰ Structure **207** is just one of the many carbon-rich molecules that was formed using the bowtie theme. A diverse range of strained enyne cycles has also been formed.¹¹⁻¹⁵ A number of the strained cycles were envisioned as precursors to fullerenes, for example, **208**, synthesized by the Vollhardt group, reacted violently upon heating to give buckytubes and buckyonions.¹⁶



Although cross-conjugated enyne macrocycles have traditionally received less attention than their linearly conjugated cousins, they have garnered more consideration recently due to their unusual electronic and optical properties.¹⁷⁻²⁵ A number of substituted expanded radialenes **209** have been realized, some of which display large third-order nonlinear optical coefficients.²⁶

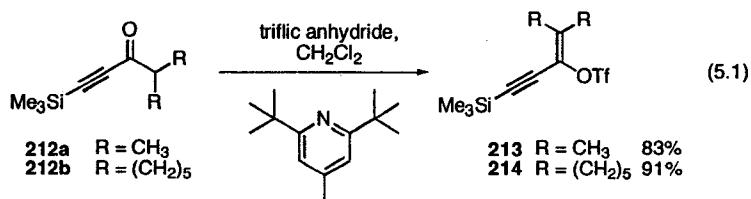


The synthesis of conjugated molecules resulting from the rearrangement of an alkylidene carbenoid species is described in Chapters 2,3 and 4. The incorporation of the enyne, cross-conjugated alkylidenyl unit itself into macrocycles and linear oligomers was also of interest. The electronics of enyne cross-conjugation in oligomeric systems has been investigated by Dr. Yuming Zhao, who first synthesized the *iso*-polydiacetylenes (*iso*-PDAs) **210**.²⁷ In one case, when R = phenyl, an oligomer as long as 15 units was achieved.²⁸ It was suggested through these studies that π -electron communication does exist through the cross-conjugated framework. Formation of the cyclic analogs **211** was also envisioned. The synthesis of **211** would provide an opportunity to explore the electronic properties of cross-conjugated enyne systems without the

conformational disorder that is inherent to the acyclic iso-PDAs. Specifically, information about the contribution of cross- and homoconjugation to the overall electronics was desired. The successful synthesis and electronic properties of three expanded radialenes is thus described.

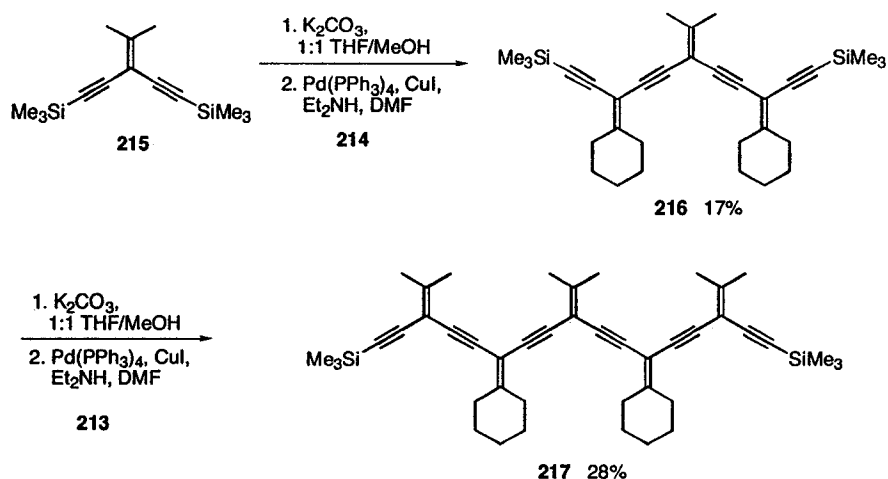
5.2 Expanded Radialenes

5.2.1 Synthesis



A modular approach to expanded radialene **219** (Scheme 5.2) was envisioned based on the availability of vinyl triflates **213** and **214**. These building blocks were synthesized via the method of Stang and Fisk²⁹ (eq 5.1) and their facile synthesis from readily available ketones **212a,b** allowed for the incorporation of different substituents to the radialene framework (Scheme 5.1). As the solubilities of the linear isopropylidene oligomers synthesized by Dr. Zhao were low,³⁰ cyclohexyl groups were incorporated. Thus, the trimethylsilyl protecting groups were removed from enediyne **215**.²⁷ Subsequent palladium catalyzed cross-coupling of the deprotected diyne with vinyl triflate **214** gave the mixed trimer **216** in 17% yield.³¹ Pentamer **217** was formed in an analogous manner: protodesilylation of trimer **216** provided the deprotected diyne and cross-

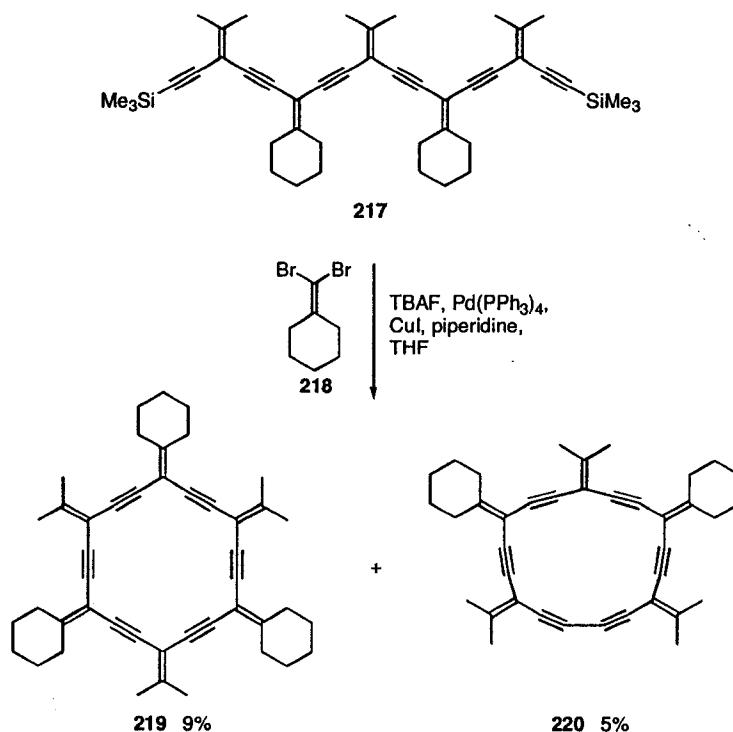
coupling with two equivalents of the isopropylidene vinyl triflate **216** gave the pentamer **217** in a modest yield of 28%.



Scheme 5.1

Ring closure to provide [6]-radialene **219** was envisioned as a double cross-coupling reaction of deprotected pentamer **217** to dibromoolefin **218** (Scheme 5.2). Radialene **220** was an expected by-product resulting from Cu^{II} -catalyzed oxidative homocoupling of deprotected pentamer **217**.³² To prevent the formation of **220**, desilylation of **217** was initiated in situ³³ and the reaction mixture rigorously degassed. Dilute reaction conditions were also employed to favor an intramolecular reaction and prevent the formation of linear oligomers. Thus, tetrabutylammonium fluoride (TBAF) was added to a solution of pentamer **217** and dibromoolefin **218**³⁴ in THF, in the presence of $\text{Pd}(\text{PPh}_3)_4$, CuI and piperidine. By TLC analysis, the sequential formation of the product of deprotected pentamer **217**, then the product resulting from one cross-coupling reaction and finally the cyclization products **219** and **220** were observed. The

transformation of pentamer **217** to the radialenes was complete after a period of seven days at room temperature. Due to the thermal instability observed in the oligomeric macrocycle precursor **217** the cyclization reaction could not be warmed to increase the rate of reaction.



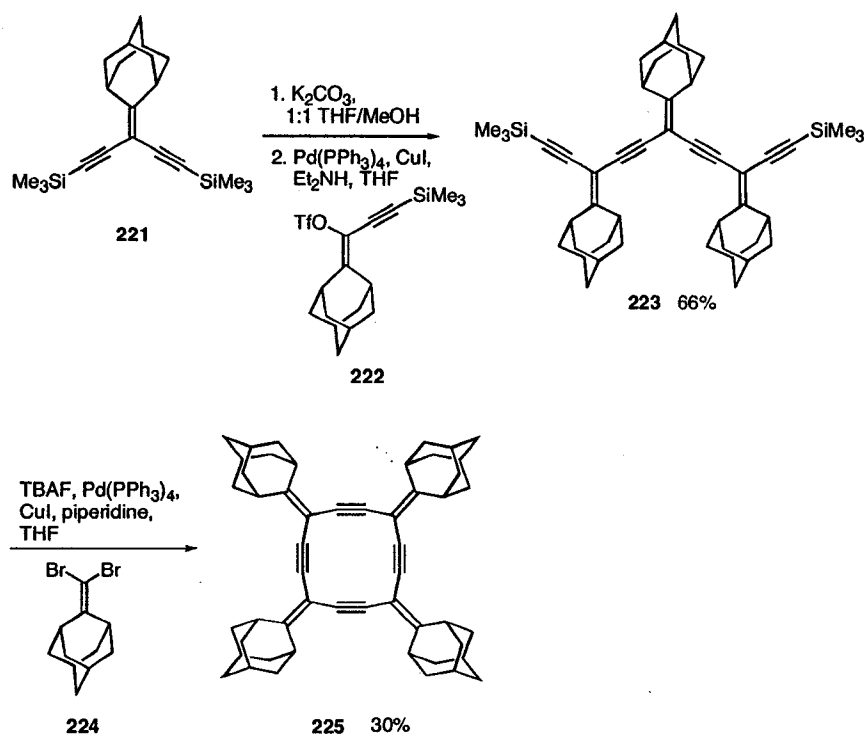
Scheme 5.2

Purification by column chromatography provided the radialenes **219** and **220** as solids that are stable for only short periods of time at room temperature. Although radialene **219** was successfully realized, the low yield was due to the instability of the isopropylidene and cyclohexylvinylidene moieties. The instability was believed to arise from an oxygen ene reaction at the allylic position.^{35,36} Incorporation of the cyclohexyl groups increased the solubility but

decreased the stability of the oligomer as the cyclohexyl allylic protons are held rigidly in the π -plane, facilitating the oxygen ene reaction. Evidence supporting oxygen induced decomposition was the observation that when kept in a degassed solution, radialene **219** was stable for days at room temperature.

Thus, the vinylidene substitution was modified to increase the stability of the radialenes. An adamantyl moiety was chosen, as the allylic protons of the adamantyl would be perpendicular to the vinylidene π -system. Radialene **225** was therefore identified as an initial target (Scheme 5.3). Eneidyne **221**³⁰ was desilylated and cross-coupled to vinyl triflate **222**³⁰ to provide trimer **223**³⁰ in 66% yield. Conditions employed to bring about cyclization to the radialene **225** were similar to those utilized for radialene **219**. Trimer **223** was deprotected in situ with TBAF, then cross-coupled to dibromoolefin **224**. The reaction was complete in eleven days with the formation of very few by-products. Unlike in the case of the [6]-radialene, the by-product resulting from an intramolecular oxidative homocoupling of deprotected **223** was not observed in the reaction mixture. Isolated as a white solid, adamantyl substituted radialene **225** was remarkably more stable than the methyl and cyclohexyl substituted radialene **219** but due to solubility issues, the yield of **225** was only estimated as 30%. Regrettably, **225** was very insoluble and the synthesis of the larger [6]-radialene incorporating the adamantyl functional group was not attempted. The structural assignment of [4]-radialene **225** was supported by the ¹³C NMR spectrum, which shows only 3 signals in the range typical of sp² and sp³ hybridized carbons. Mass spectrometric

analysis, which showed a molecular ion peak at m/z 680.4, is also consistent with the proposed structure.



Scheme 5.3

5.2.2 Electronic Properties

The primary orbitals contributing to the π -electron systems of the cross-conjugated framework are schematically shown in Figure 5.1. There are two separate systems. The out-of-plane system consists of conjugation between the sp -hybridized orbitals of the alkynes and the sp^2 -hybridized orbitals of the olefins, and the in-plane system consists of the isolated, sp orbitals of the alkynes that are orthogonal to the out-of-plane p -orbitals. There is a possibility for overlap between the conjugated segments of the in-plane system as a result of homoconjugation.³⁷



Figure 5.1 The π -electron systems of the cross-conjugated framework.

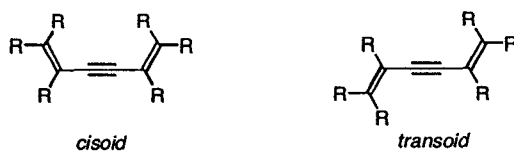


Figure 5.2 The *cisoid* and *transoid* orientations of the ene-yne-ene conjugated segment.

The *cisoid* and *transoid* orientations of the ene-yne-ene conjugated segment is shown in Figure 5.2 and represents the longest linearly conjugated segment of radialenes **219** and **225** and the precursor linear oligomer **217**. In Figure 5.3 is a comparison of the UV/Vis spectrum of radialenes **219**, **220**, **225** and the acyclic pentamer **217**. Acyclic **217** shows two overlapping low-energy absorptions at 283 nm and 305 nm ascribed to the *cisoid* and *transoid* ene-yne-ene orientations. The conformationally restricted radialene **219** shows only a single major low-energy absorption at 286 nm, which should arise from the *cisoid* ene-yne-ene segment, based on restricted rotation in the macrocycle, precluding the *transoid* conformation.

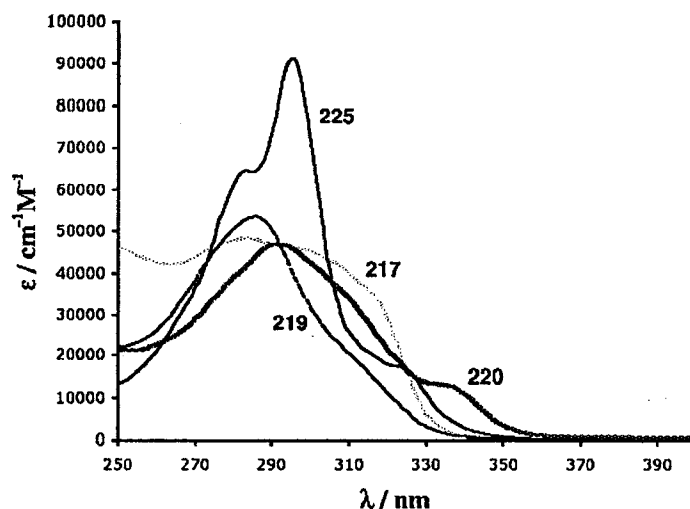


Figure 5.3 UV-Visible spectra of radialenes **219**, **220**, **225** and pentamer **217** in CHCl_3 at rt.

The major electronic absorption for hybrid radialene **220** is slightly bathochromically shifted by 10 nm to 293 nm versus hexamer **219**, presumably due to the increase in planarity, as has been observed for other radialenes.³⁸ Compound **220** also has an additional low-energy band around 336 nm. This electronic transition has been tentatively assigned to the ene-yne-yne-ene conjugated segment. To confirm this assignment, the absorption spectra of model compounds **226**³⁹ and **227**, both of which contain the same ene-yne-yne-ene segment, are shown in Figure 5.4. The lowest energy absorption of acyclic **226** at 328 nm corresponds approximately to that of the 336 nm shoulder in the absorption spectra of radialene **220**, although it is slightly blue-shifted. Individual absorptions are expected for the *cis* and *trans* rotamers of **226** but these are not clearly assignable in the spectrum of **226**. Therefore, cycle **227** was designed and synthesized (see Section 5.3 for synthesis). The length of the alkyl tether was

chosen in order to furnish a structure with similar bond angles and therefore similar strain as hybrid radialene **220**. The conformationally restricted **227** shows major low-energy absorptions similar to its acyclic analog **226** at 290, 309, and 328 nm. By comparison of the two spectra, the bands of the *cis* and *trans* rotamers of **226** appear similar in energy with the *trans* band barely visible as a shoulder at 336 nm on the lowest energy absorption for **226**. This band is absent from the spectrum of **227**. Therefore, the low energy 336 band of **220** can tentatively be assigned to the ene-yne-yne-ene segment.

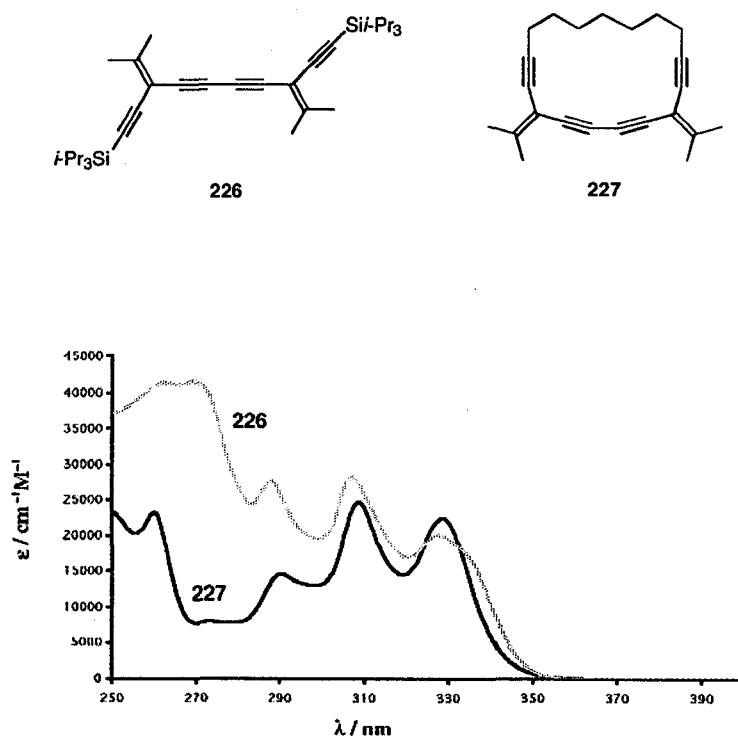
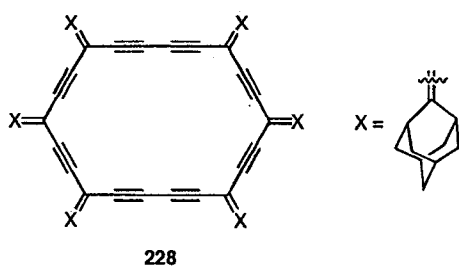


Figure 5.4 UV-Visible spectra of model compounds **226** and **227** in CHCl_3 at rt.

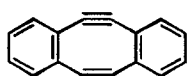
[4]-Radialene **225** shows a major absorption peak at 296 nm which is red-shifted in comparison to the less strained cycles **219** and **220**. Unlike in the UV-Vis spectra of **219** and **220**, however, additional fine structure is observed at 283 nm and presumably results from the more rigid structure of the [4]-radialene over **219** and **220**. Interestingly, the electronic absorption spectrum of **225** also shows a low energy shoulder at 325 nm, similar to the one observed in the UV-Vis spectrum of hybrid radialene **220** at 336 nm. Given the assignment of this peak to the ene-yne-yne-ene segment in **220**, the structure attributed to **225** comes into question. A possible product of the ring closing reaction to the [4]-radialene is unstrained hexamer **228** which contains the ene-yne-yne-ene segment. Even though mass spectrometric analysis and ^{13}C NMR spectroscopy defend the [4]-radialene **225** structural assignment, further supporting evidence is desired to confirm the structure as the strained [4]-radialene over the less strained **228**.

Unfortunately, little is known about the effect of strain on the electronic and physical properties of cross-conjugated systems. For example, a bathochromic shift is observed for the main absorption bands of the radialenes as strain is increased from **219** to **220** to **225**. While it is possible this red-shift could signify an increased contribution from cross- or homoconjugation to the overall electronic communication, it is equally possible that this shift results from increased planarity and/or ring strain. To discover more about the effect of strain on the properties of cross-conjugated enyne systems, we devised a study based on the radialene **227**, using model compounds with increasing amounts of incorporated strain.

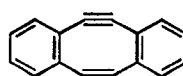


5.3 Strained Eneyne Macrocycles

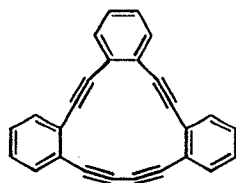
Alkynes are capable of withstanding a fair degree of strain as demonstrated by the formation of, for example, cyclononyne and cyclooctyne.^{40, 41} There are a number of strained enyne macrocycles in the literature which demonstrate significant deviations from the idealized bond angle of 180° for alkyne and butadiene moieties. The acetylene unit(s) in cycles **229**⁴² and **230**,⁴³ for example, possess bond angles of 154.0° and 155.8° respectively. The butadiene containing cycles formed by Vollhardt **231**¹³ and Fallis **232**⁴⁴ are also highly strained, with bond angles as small as 153.4° for **232**.



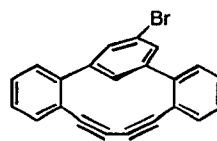
229



230

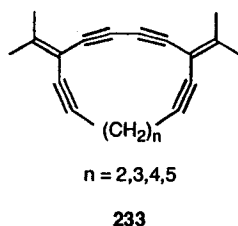


231



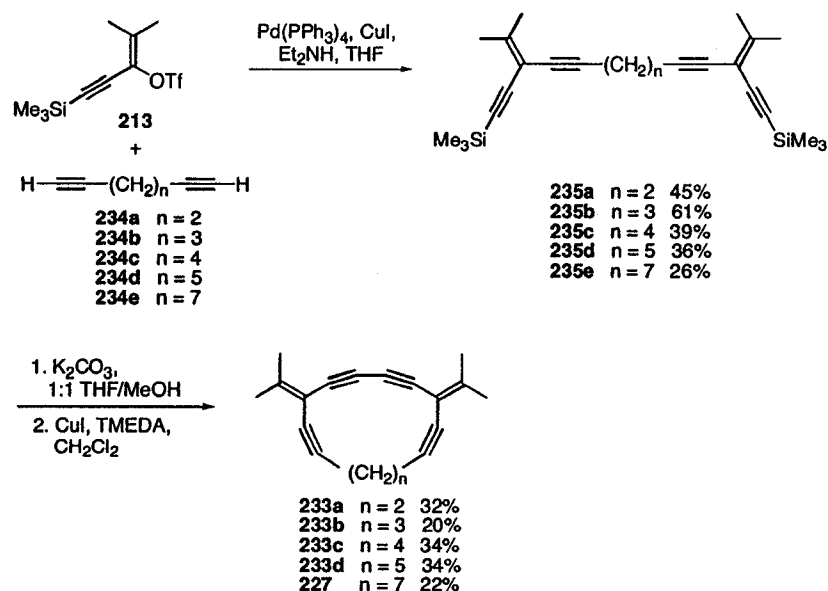
232

In the majority of reports concerning strained cyclic acetylenes, the stability and/or reactivity as a function of ring strain has been examined. For example, the high reactivity of strained cycloalkynes has been exploited toward the formation of fullerenes.^{9,45-49} The electronic properties of strained alkynes have, however, been much less studied.⁵⁰⁻⁵² Homoconjugation in macrocyclic polyacetylenes containing isolated acetylene units has been studied extensively^{53,54} but little has been done to explore the structural and electronic properties of strained cyclic alkynes with extended conjugation. In order to tune and interpret the characteristics of cross-conjugated macrocycles for materials applications, we felt an understanding of the effect of strain on their physical and electronic properties was essential (see Section 5.2). Therefore, a series of cross-conjugated macrocycles was designed. An alkyl tether was used to connect cross-conjugated enediyne moieties, and as the length of the alkyl tether was shortened, the strain of the resulting system was increased. A butadiyne moiety was also incorporated in the macrocycles as the effects of strain on this moiety were particularly interesting due to its prevalence in a variety of carbon-rich macrocycles, including radialene **220**. Thus, expanded dendralenes **233** were synthesized and their physical and electronic properties studied (Scheme 5.4).



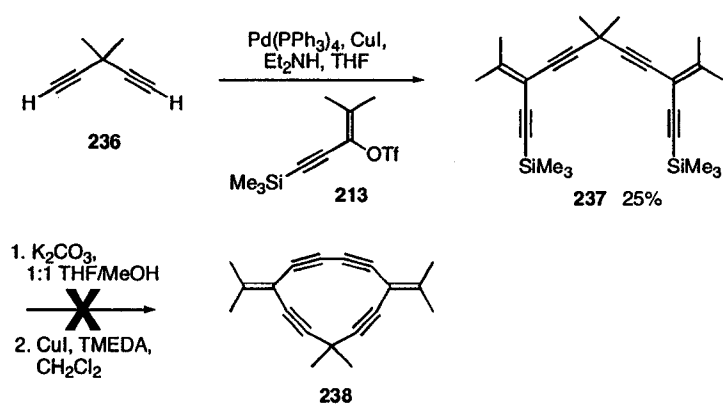
5.3.1 Synthesis

Commercially available diynes **234a-e** were cross-coupled to two equivalents of vinyl triflate **213**²⁹ to form the acyclic **235a-e** (Scheme 5.4). The palladium catalyzed coupling reactions proceeded in moderate yields and the mono-coupled product was always formed along with **235**. Cyclization was achieved via protodesilylation of **235a-e** followed by oxidative homocoupling of the resulting terminal acetylenes under Hay conditions.³² The cyclization reactions were carried out in a dilute solution of CH₂Cl₂ (*ca.* 0.001 M) to encourage an intramolecular reaction and minimize the amount of linear by-products formed via intermolecular reactions. Macrocycles **233a-d** and **227** were isolated as white solids in modest yields by column chromatography. Linear oligomers were always observed by TLC analyses regardless of the conditions employed, contributing to the low yields.



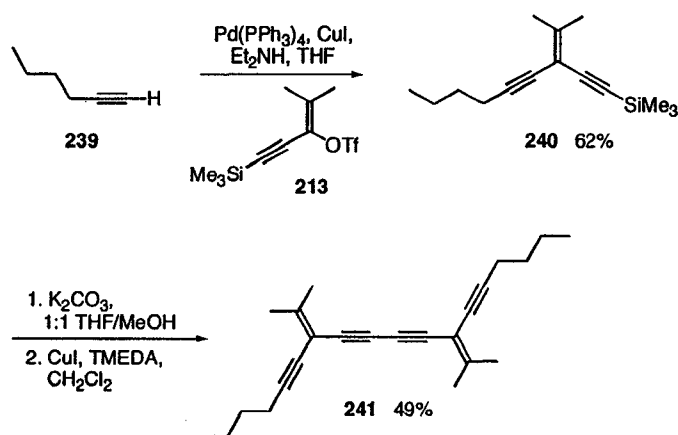
Scheme 5.4

An attempt was made to form what would be the smallest possible expanded dendralene in this series, with $n = 1$ (Scheme 5.5). 3,3-Dimethyl-1,4-pentadiyne **236**⁵⁴ was employed for this purpose as 1,4-pentadiyne is difficult to synthesize and is unstable. Cross-coupling of triflate **213** to diyne **236** resulted in the formation of **237** in 25% yield. The cyclization reaction led only, however, to the formation of linear oligomers with no evidence for the formation of cycle **238**.



Scheme 5.5

An acyclic model compound was also synthesized (Scheme 5.6). 1-Hexyne **239** was coupled to vinyl triflate **213** to afford enediyne **240** in 62% yield. Removal of the trimethylsilyl groups, followed by oxidative coupling gave dimer **241** in 49% yield as a white solid.



Scheme 5.6

5.3.2 Physical Characteristics and X-ray Crystal Structures

Macrocycles **233a-d** and **227** are thermally stable solids with melting or decomposition points all above 100 °C. Only cycles **233c** and **227** show defined melting points of *ca.* 130 and 138 °C, respectively, whereas **233b** shows no melting point and decomposes at just under 110 °C. The most strained cycle, **233a**, shows darkening at 110 °C and then blackening at 146 °C. Heating a single crystalline sample of macrocycle **233d** to 135 °C gave an increasingly orange colored crystal that eventually melted reproducibly at 168 °C. The acyclic tetrayne **241** melts at 71 °C.

The solid-state structures of the macrocycles **233a-d** and **227** and acyclic **241** were confirmed by X-ray crystallographic analysis. X-ray quality crystals of **233a-d**, **227** and **241** were obtained by the diffusion of MeOH into CHCl₃ (or CH₂Cl₂ for **233a**) at 4 °C. ORTEP drawings of all structures are shown in Figure 5.5.

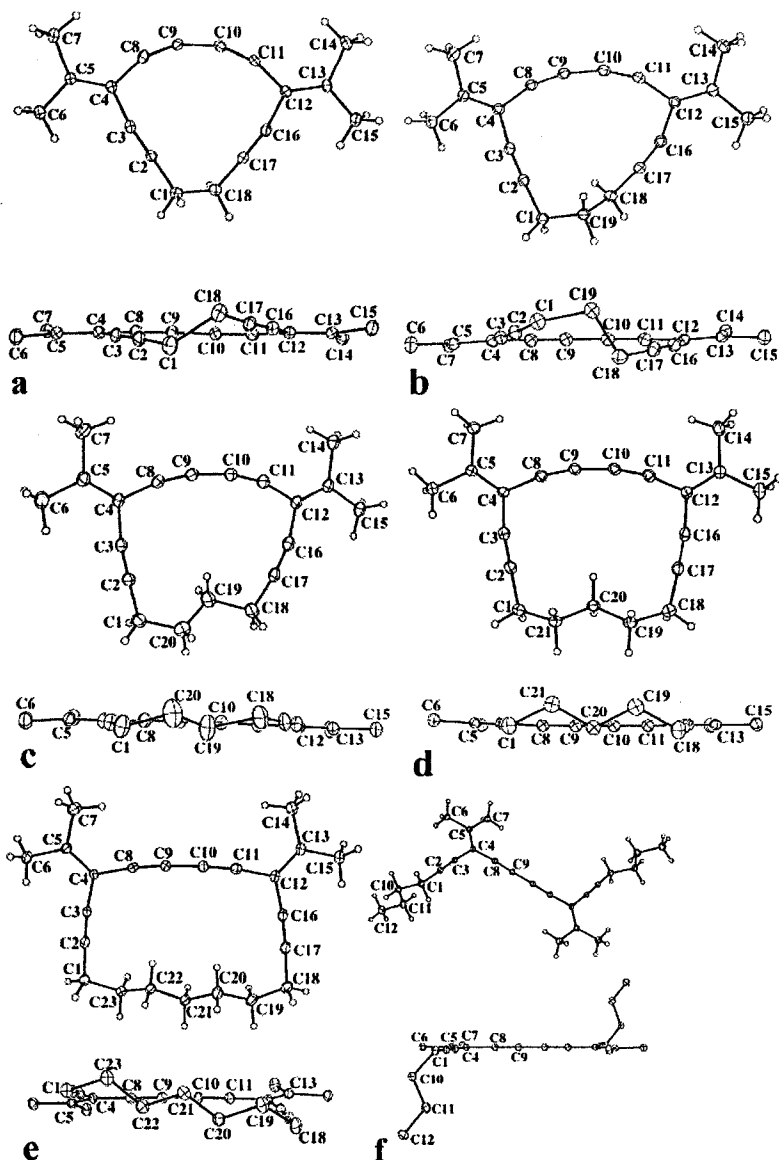


Figure 5.5 a-e) ORTEP drawing of macrocycles **233a-d** and **227**.

f) ORTEP drawing of **241**. All shown @ 20% probability.

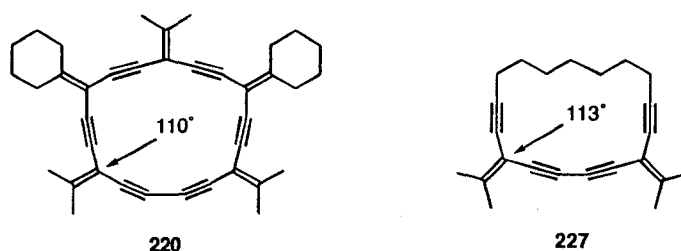
Comparison of these six structures progressing from highly strained **233a** to relatively strain free **227** and acyclic **241** provides insight into how strain is accommodated. Empirically, it is quickly observed that **233a**, **233d** and **227** are approximately symmetrical (C_2 , C_s , and C_2 , respectively), whereas the 13- and 14-

carbon cycles **233b** and **233c** are much less symmetrical. This distortion in **233c** and **233b** results from the inability of the methylene linking groups to orient in a manner that equally disperses the ring strain. The distortion is much greater for **233b** in the solid state than that of **233c**. Raman analyses (vide infra) of both **233b** and **233c** display characteristics consistent with dissymmetric structures in solution.

The planarity of the conjugated portion of the cycles **233a-d**, **227** and acyclic **241** in the solid state varies considerably but there is no direct correlation between decreasing ring size and planarity. The cycles were compared to acyclic model compound **241** which is completely planar, with a twist angle that is necessarily 0° based on solid state symmetry. The twist of the cycles **233a-d**, **227** can be estimated by a dihedral angle between the two "arms" of the conjugated segment linked by the butadiyne moiety. Two arms are defined by the enyne segments C(3)-C(4)-C(5)-C(8) and C(11)-C(12)-C(13)-(16). The twist angle is greatest for **227** at 22.2(2)° and 12.7(3)° for the two crystallographically independent molecules A and B respectively. Not surprisingly, the planarity of **233b** is quite distorted as a result of the dissymmetry of the molecule, with an angle of 8.22(16). The twist is lowest for **233d** and **233c** at 2.82(13)° and 3.36(19)°, respectively. Despite the considerable ring strain of **233a**, the twist angle at 7.0(2)° and 6.2(2)° for the two crystallographic independent molecules A and B, respectively, are greater than that of either **233c** or **233d**. The increased twist and bond strain in the conjugated portion of **233a** is tolerated in order to accommodate the bond angles necessitated by the two methylene groups.

The alkylidene and alkyne bond angles of the most strained expanded dendralene **233a** deviate greatly from the idealized bond angles of 120° and 180° , respectively. The interior alkylidene bond angles for **223a** are reduced to 108° and the alkyne C(10)-C(11)-C(12) is one of the most strained diynes known at 157° . The structure is surprisingly stable despite the strain and can remain in solution under refrigeration for several months without decomposition.

The bond angles for the sp^3 -hybridized carbons of the methylene groups also deviate from the idealized bond angles. The angles about the methylene carbons of the unstrained **241** are on average 113.6° . For the cycles the bond angles span a maximum of 119° to a minimum of 109° .



The realization of the solid state structures of radialenes **233**, **227** allows an evaluation of the assumption made in the previous section (Scheme 5.2), that radialene **227** would serve as a suitable model for hybrid radialene **220**. Molecular modeling studies⁵⁵ predict an interior alkylidene bond angle of 110° for **220**, and this bond angle (e.g., C3/C4/C8) is 113° in **227**, as determined by X-ray crystallographic analysis. While a difference of only 3° between the angles for **220** and the model compound **227** indicate a fairly close approximation, it is

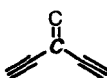
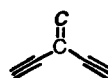
actually dendralene **233c** that possesses the most similar bond angles to **220** with an alkylidene angle of 109.7°.

5.3.3 ¹³C NMR Spectroscopic Properties

Two-dimensional heteronuclear multiple bond coherence (HMBC) experiments for **233a-d**, **227** and **241**, were used to assign all of the resonances for the conjugated carbon skeletons, as summarized in Table 5.1. In all cases, a similar strategy was used for interpretation of each HMBC spectra. The alkylidene methyl protons of C(6)/C(15) and C(7)/C(14) for each molecule showed strong two and three bond (²J_{C-H} and ³J_{C-H}) correlations to the endo- and exocyclic alkylidene carbons C(4)/C(12) and C(5)/C(13), respectively (see X-ray structures in Figure 5.5 for numbering scheme). The exocyclic vinylidene carbons C(5)/C(13) are known to be significantly deshielded, and thus C(4)/C(12) and C(5)/C(13) were assignable.⁵⁶ Weaker four bond correlations were observed between the alkylidene methyl protons and C(3)/C(16) and C(8)/C(11). In some cases, weak five bond couplings to C(9)/C(10) and/or C(2)/C(17) were also observable. The ²J_{C-H} and ³J_{C-H} correlations between the propargylic methylene protons of C(1) and acetylenic carbons C(2) and C(3) identified these carbons. Based on the stronger ⁴J coupling between C(3)/C(16) and the alkylidene methyl protons, C(2)/C(17) and C(3)/C(16) were thus assigned. The assignments of C(2)/C(17) and C(3)/C(16) were corroborated for **233b**, **233d** and **241** by three bond correlations between C(2)/C(17) and the homopropargylic methylene protons of C(19) of **233b**, C(19)/C(21) of **233d**, and C(10) of **241**. The ⁵J_{C-H}

coupling between the C(1) methylene protons and C(8) allowed the assignment of C(8)/C(11); leaving the assignment of C(9)/C(10) to the last ^{13}C NMR resonance.

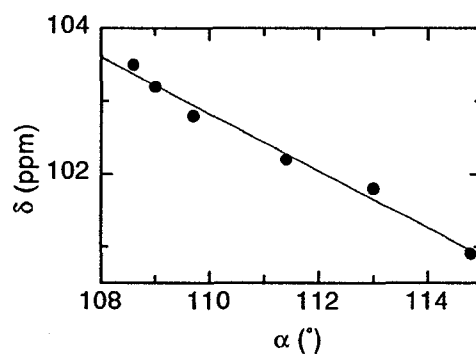
Table 5.1. Selected ^{13}C NMR shift data (in ppm) for **233a-d**, **227** and **241**.^a

	C(2),C(17)	C(3),C(16)	C(4),C(12)	C(5),C(13)	C(8),C(11)	C(9),C(10)
	$\text{CH}_2\text{-C}=\text{C-}$	$\text{CH}_2\text{-C}=\text{C-}$			$\text{-C}=\text{C-C}=\text{C-}$	$\text{-C}=\text{C-C}=\text{C-}$
233a	90.3	81.2	103.5	145.0	105.1	86.5
233b	95.7	81.5	103.2	145.6	98.9	82.5
233c	94.6	80.7	102.8	146.9	90.4	80.0
233d	93.7	79.5	102.2	148.5	88.4	78.2
227	93.8	79.1	101.8	151.3	81.7	75.9
241	93.1	76.4	100.9	156.0	79.5	75.4

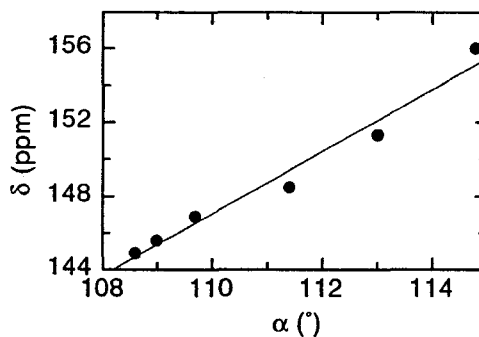
^aAll spectra obtained in CDCl_3 .

The more shielded endocyclic alkyldiene carbon C(4)/C(12) resonances are found over a rather narrow shift range between 100.9-103.5 ppm. For acyclic **241**, these carbons resonate at 100.9 ppm, and they are slightly deshielded to 101.8 ppm for the largest macrocycle **227**. As the ring size is decreased from 17 carbons to 12 carbons upon moving from **227** to **233a**, respectively, a deshielding is observed for these carbons to give values of 102.2 (**233d**), 102.8 (**233c**), 103.2 (**233b**), and 103.5 (**23aa**). These shifts are consistent with the expected rehybridization at C(4)/C(12), as bond angle contraction for C(3)-C(4)-C(8) and C(11)-C(12)-C(16) imparts greater p-character to the σ -bonds of the ring and,

consequently, more s-character to the olefin.^{18,51,57} Conversely, the chemical shifts of the exocyclic vinylidene C(5)/C(13) carbons are shifted significantly upfield as a function of strain, from the value observed for acyclic **241** at δ 156.0 to 151.3 (**227**), 148.5 (**233d**), 146.9 (**233c**), 145.6 (**233b**), and 145.0 (**233a**).



a)



b)

Figure 5.6 Plot of ^{13}C NMR chemical shifts for a) C(4)/C(12) and b) C(5)/C(13) versus α C(3)-C(4)-C(8)/C(11)-C(12)-C(16).

A strong correlation is found between the crystallographic-determined bond angles and ^{13}C NMR shifts of the sp and sp^2 carbons. The angles α were calculated as an average of the X-ray angles at ^{13}C NMR degenerate carbons. As

shown in Figures 5.6a and 5.6b, the relationship between the alkylidene bond angle α at C(3)-C(4)-C(8)/C(12)-C(4)-C(4) and the ^{13}C NMR resonances observed for *both* C(4)/C(12) and C(5)/C(13) is quite linear.

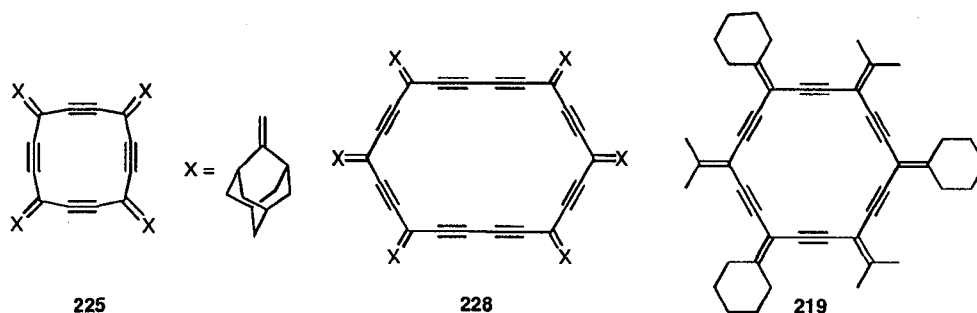
Changes in the relative bond order of the acetylenic moieties C(2)-C(3) and C(8)-C(9) (as well as C(10)-C(11) and C(16)-C(17), respectively) of **233a-d**, **227** and **241** are also easily monitored by their ^{13}C NMR resonances. All acetylenic carbons experience consistent deshielding as ring strain is increased. A similar trend has been reported by Gleiter and coworkers for nonconjugated, cyclic diynes.⁵⁸ In particular, the carbons of the butadiyne carbons C(8)/C(11) and C(9)/C(10) experience significant deshielding as a result of increased ring strain. In the case of C(8)/C(11), the carbons are deshielded by 25 ppm upon going from acyclic **241** (79.5 ppm) to **233a** (105.1 ppm) as bond angles α are decreased from 177 to 156°, respectively. Concurrently, the C(9)/C(10) carbons are deshielded by 11 ppm; from δ 75.4 ppm in **241** to δ 86.5 in **233a** while the corresponding bond angles decrease from 179° in acyclic **241** to 159.6° in **233a**. The relationship between acetylenic bond angles and ^{13}C NMR shifts is nearly linear for all acetylenic carbons with the exception of C(2)/C(17).

The only deviation from the above analysis is the anomalous ^{13}C NMR chemical shift observed for acetylenic carbons C(2)/C(17) of the most strained cycle **233a**. This carbon resonance for **233a** is shielded by 5.4 ppm relative to **233b**, and by 3.5 ppm vs. **227**, which has the most similar bond angle with $\alpha = 175.3^\circ$. The origin of this shielding remains unclear. Based on the work of Gleiter and coworkers,^{58,59} however, two possible influences emerge. The

transannular distance between C(2) and C(17) is 3.08 Å for **233a**. This distance is at the limit of that required for through-space orbital overlap between these carbons and could potentially alter the chemical shift. The transannular distance between C(2) and C(17) for all other cycles is too large for such interactions to occur (e.g., it is already 4.04 Å in **233b**). Alternatively, shielding of C(2)/C(17) acetylenic carbons might result from through-bond interactions between the ethano bridge and the in-plane π -system. Based on photoelectron spectroscopic experiments, similar σ - π electronic interactions have been reported in cycles such as 1,5-cyclooctadiyne, albeit no concurrent change in ^{13}C NMR chemical shift was reported for this molecule.⁵⁸

This chemical shift analysis as a function of ring strain can be applied to the confirmation of the structure of strained [4]-radialene **225** over the unstrained **228**. There are three resonances in the ^{13}C NMR spectrum of the radialene in question, at 160.7, 96.5, and 95.5 ppm. The resonance at 160.7 ppm is assigned to the exocyclic alkylidene carbon. Due to the greater intensity of the peak at 95.5 ppm, this peak can be assigned to the eight degenerate alkynyl carbons. The peak at 96.5 is therefore assigned to the interior alkylidene carbons. The chemical shift of the alkynyl carbons adjacent to an alkylidene moiety has been determined by this study to be very sensitive to strain, and as strain is increased, these acetylenic resonances in all cases appear further downfield (e.g., consider carbons C(8)/C(11) and C(3)/C(16) of **233a-d**, **227**). This analogy can also be extended to **228** and **219**, as the bond angles of **228** are expected to be very similar to those of **219**. The resonances for the alkynyl carbons of **219** appear at 88.3 and 88.2 ppm.

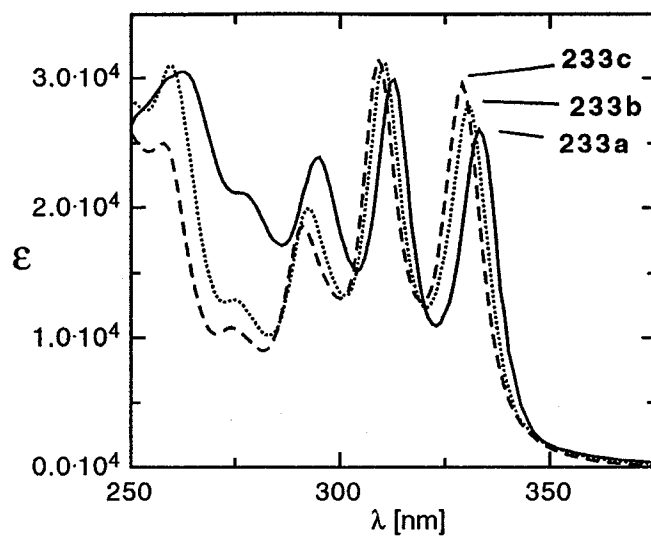
For radialene **225**, however, the resonance for the acetylenic carbon is significantly more downfield at 95.5 ppm, suggesting the presence of a strained alkynyl group. This analysis further supports the structure assignment of the highly strained radialene **225**.



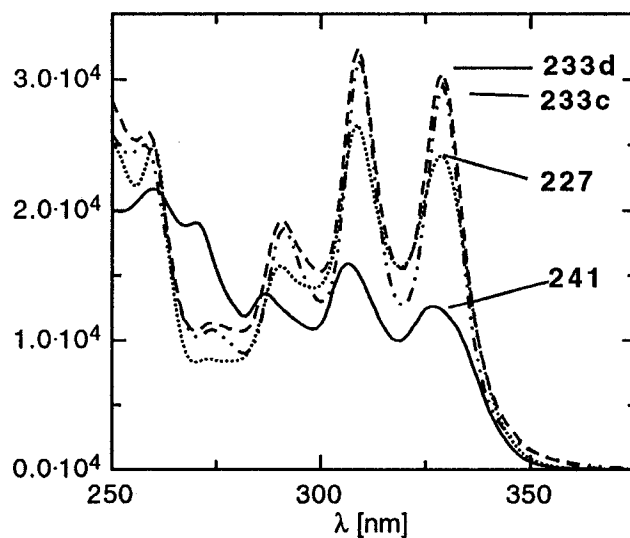
5.3.4 Electronic Absorption Characteristics

As for the expanded radialenes discussed in Section 5.2, two distinct π -electron systems must be considered in the electronic absorption analysis of cyclic dendralenes **234a-d**, **227** and acyclic **241**. One system is composed of the acetylenic π -orbitals directed, more or less, in the molecular plane of each macrocycle. The in-plane system of the butadiyne group is indicative of this system, and its electronic absorption should be observable at approximately 260 nm. Conversely, the out-of-plane π -electron system includes the eight carbons of the linearly conjugated ene-yne-yne-ene segment. Interactions via cross-conjugation²⁷ from the two pendant acetylenic units could influence the electronic absorption(s) of this π -electron system, which are expected in the lower energy region of each electronic absorption spectrum.

The UV absorption spectra for **233a-c** and **234c-d**, **227**, **241** are shown in Figures 5.7a and 5.7b. The similar energies of lower energy absorptions of **241** and those of macrocycles **234c-d**, **227** at *ca.* 290, 309 and 329 nm are apparent and these absorptions arise from the out-of-plane π -electron system of each compound. The major difference in the spectrum of acyclic **241** versus cycles **231c-d**, **227** is the considerable broadening and lower ϵ -values of the low energy absorptions for **241**. The latter is attributed to inhomogeneous broadening as a result of the rotational freedom of the alkylidene units about the butadiyne moiety of **241**. This gives both *cisiod* and *transoid* absorption peaks in which the trans conformer absorbs at a slightly lower energy. Peak broadening and lower ϵ -values are also observed for macrocycle **227** relative to **233d** and **233c**. This is likely due to the more flexible 17 carbon cyclic framework of **227**, which has a lower overall molar absorptivity due to increased deviations from planarity allowed by the long $-(\text{CH}_2)_7-$ tether. Macrocycles **233d** and **233c** show the greatest ϵ -values, and this correlates well with the almost negligible twist angles $2.82(13)^\circ$ and $3.36(19)^\circ$, respectively, observed in the solid state for the conjugated portions of these molecules. Molar absorptivity for the most strained systems **233b** and **233a** is diminished relative to **233c** as twisting increases to accommodate the shorter $-(\text{CH}_2)_3-$ and $-(\text{CH}_2)_2-$ tethers in these conformationally restricted macrocycles.



a)



b)

Figure 5.7 UV-visible spectra of a) macrocycles **233a-c**. b) macrocycles **233c-d**, **227** and acyclic **241**, in CHCl_3 at rt.

The lower energy electronic absorptions for **233c-d**, **227** show little variation in energies as ring strain increases upon going from **233c** to **233b** to

233a, however, a consistent bathochromic shift for all three low energy absorptions is seen. For example, λ_{max} of **233c** at 329 nm shifts to 331 nm in **233b** and to 333 nm in **233a**. As it is the overlap of the eight conjugated out-of-plane carbon sp and sp² π -orbitals of the ene-yne-yne-ene segment that yields these absorption bands, this bathochromic shift evidently derives from increased ring strain rather than homoconjugation (*vide infra*), which would arise from the in-plane π -system. It is not unreasonable to expect that the significant distortion from linearity in **233a** and **233b** slightly diminishes the overlap of the out-of-plane π -orbitals of these molecules. This has the effect of raising the energy of the HOMO to a slightly greater extent than that of the LUMO, resulting in a slightly lower energy transition.⁶⁰

It has been shown for a series of [6]-, [4]-, and [3]radialenes that increased rigidity and enforced planarity as a function of ring contraction gives a decreasing absorption energy in a trend similar to that observed for **233a-d**, **227**.⁶¹ Slight changes in the electronic absorption spectra as a function of ring size have also been reported for expanded radialenes, which contain a similar ene-yne-yne-ene moiety as **233a-d**, **227**.¹⁸ The degree of strain, planarity, and steric interactions in these systems, however, is unknown and makes meaningful comparisons impossible.

The UV spectrum of the smallest dendralene **233a** shows evidence of homoconjugation, which affects the absorption of the in-plane butadiyne π -system at *ca.* 260 nm.^{54,62} Specifically, cycles **233b-d**, **227** and acyclic **241** all display this high energy absorbance at 258-260 nm with increased broadening as the ring

size is contracted. The spectrum of the highly strained cycle **233a** shows a substantially broadened peak at 263 nm, in addition to the shoulder absorption at 259 nm. This bathochromic shift in **233a** relative to **233b-d**, **227** and **241** is most reasonably ascribed to a through-space interaction of the in-plane π -orbital system of **233a** as a result of significantly decreased alkylidene bond angles.⁵⁴

5.3.5 Raman Spectroscopic Properties⁶³

Raman and resonance Raman characterization of electronic structures have been reported for cycloalkynes.^{64,65} None of these studies, however, have addressed the electronic structure of macrocyclic molecules with extended or cross conjugation. Either or both of these attributes should afford significantly different electronic structures relative to less functionalized and linearly conjugated examples. In previous investigations, correlations have been documented between lower resonance frequencies and smaller C-C \equiv C bond angles, and these observations were attributed to rehybridization of the central carbon atom from sp toward sp². The rehybridization results in a lower force constant of the C \equiv C stretch and altered coupling between the C \equiv C and C-C stretches as the C-C \equiv C bond angle varies. These observations are variations of Badger's rule,^{62,66} which empirically relates diatomic stretching frequencies to the electronic nature of the bond. These preceding results all suggest that Raman spectroscopy should be a useful probe of electronic structure in our novel cross-conjugated enyne macrocycles.

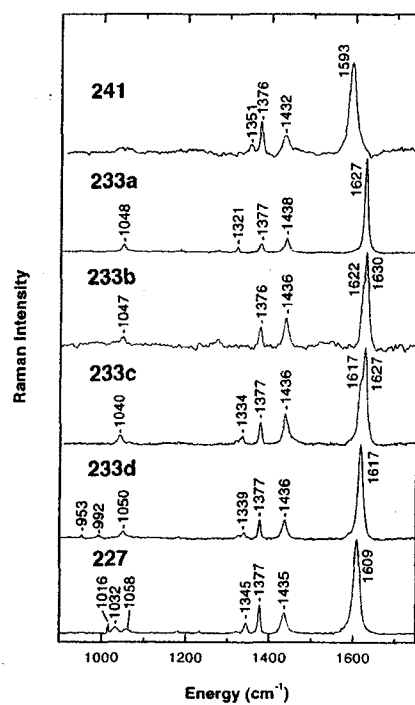


Figure 5.8 Raman spectra of cross-conjugated macrocycles **233a-d**, **227** and acyclic **241** in the 900-1700 cm⁻¹ spectral region taken in CCl₄. Typical accumulation times were 15 minutes.

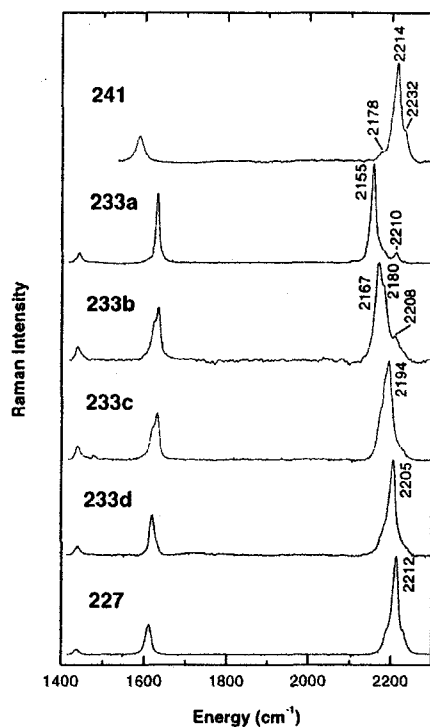


Figure 5.9 Raman spectra of cross-conjugated macrocycles **233a-d**, **227** and acyclic **241** in the 1450-2300 cm^{-1} spectral region taken in CCl_4 . Typical accumulation times were 15 minutes.

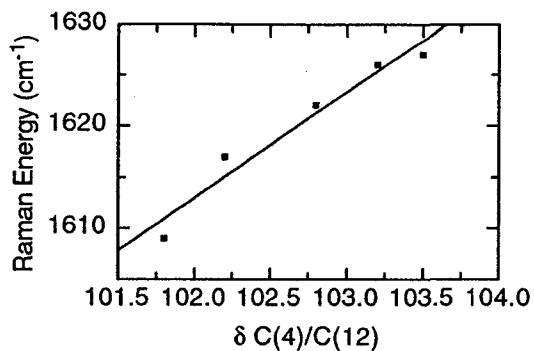
Raman spectra of cross-conjugated enynes **233a-d**, **227** and **241** are shown for the 900-1700 cm^{-1} region in Figure 5.8 and for the 1400-2300 cm^{-1} region in Figure 5.9. The 900-1700 cm^{-1} spectral region contains contributions from C-C and C=C stretches and C-H deformations, whereas the 2100-2300 cm^{-1} spectral region contains contributions only from C \equiv C stretches. The Raman spectra are of good quality, although the spectrum of **233b** exhibits a slightly lower signal-to-noise ratio than the other spectra due to fluorescence in this sample. This fluorescence, however, decayed after several minutes in the laser beam, indicating that it likely originates from the presence of a small amount of fluorescent impurity rather than from the dendralene.

Examination of the spectra in Figures 5.8 and 5.9 reveals some important trends. The spectra all exhibit the greatest intensity in the C \equiv C stretch(es), followed closely by the C=C stretch(es); both the C-C stretches and C-H deformations, probably arising from the methylene groups, are much less intense. These intensities are to be expected, as the double and triple bonds are much more polarizable than the methylene groups.

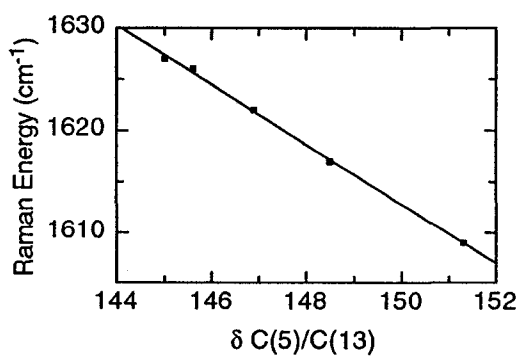
Close inspection of the C=C and C \equiv C stretches, reveals frequency shifts and mode splittings as a function of the increased ring strain upon moving from unstrained **241** to strained **233a**, consistent with the altered electronic structure exhibited in the crystal structure, and both ^{13}C NMR and electronic absorption spectra. In molecules **233b** and **233c**, with 3 and 4 methylene groups

respectively, the C=C and C≡C modes are significantly split, indicating either an inhomogeneity in the sample (*e.g.*, different conformers) or nonequivalence in two or more similar bonds in the molecule. As the X-ray structures of **233b** and **233c** clearly show nonsymmetrical geometry in the solid state for both molecules, it is apparent that in solution there are indeed two nonequivalent sets of sp and sp² bonds.

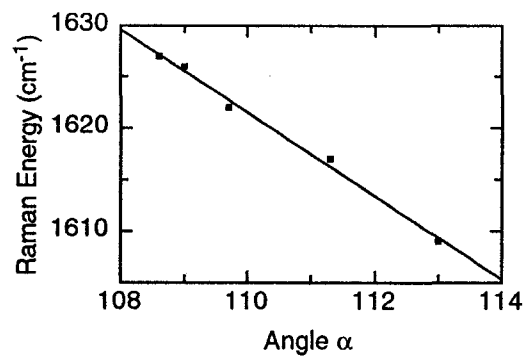
For the C=C stretching frequencies (Figure 5.8), ~1620 cm⁻¹ a clear shift to lower frequency is observed indicating a lower bond order for the alkylidene group as ring strain is decreased. The shift in olefinic stretching frequencies nicely complements the trend observed in the ¹³C NMR shift data, relating the double bond order as a function of ring strain. Indeed, a plot (Figure 10a,b) of the C=C stretching frequencies for **233a-d**, **227** (frequencies averaged for **233b** and **233c**) versus the ¹³C NMR shifts of C(4)/C(12) and C(5)/C(13) affords a linear relationship in both cases, with correlation coefficients of 0.975 and 0.999, respectively. Likewise, a plot of the alkylidene bond angles α for C(3)-C(4)-C(8)/C(11)-C(12)-C(16) versus olefinic stretching frequency, Figure 10c, is also linear with a correlation coefficient of 0.995. Analogous trends in bond order as a function of ring strain have been reported in radialenes⁶¹ and have been well studied for alicyclic ketones and alkylidene cycloalkanes.⁶⁷ In contrast, however, the current study extends the usefulness of Raman analysis for the study of macrocycles with increased conjugation and potential materials applications.



a)



b)



c)

Figure 10 a) Correlation of olefinic Raman Frequency with ^{13}C NMR shifts of C(4)/C(12). b) Correlation of olefinic Raman frequency with ^{13}C NMR shifts of C(5)/C(13). c) Correlation of

olefinic Raman frequency with bond angle α at C(3)-C(4)-C(8)/C(11)-C(12)-C(16).

The C \equiv C stretching frequency(ies) of the strained dendralenes monotonically increase upon going from the **233a** to acyclic **241**, indicating a greater bond order as ring strain is decreased. The trend observed for C \equiv C stretching frequency(ies) mirrors those observed for ^{13}C NMR shifts of the acetylenic carbons and averaged bond angles α , albeit with more substantial deviations from linearity than described above in the analysis of C=C data.^{64,65} Smaller deviations have been observed in cycloalkynes⁶⁴ and are attributed in the present case to altered vibrational mixing, which will change not only the force constant, but also the vibrational character of the normal mode.

5.4 Conclusions

A series of expanded radialenes has successfully been synthesized by utilizing palladium cross-coupling protocols. The modular approach to the synthesis of these cycles allows for the incorporation of functionality to increase stability and solubility. This method also allows for the formation of highly strained macrocycles, for example [4]-radialene **227**. To provide a greater understanding of the structural, vibrational and electronic characteristics of cross-conjugated enyne macrocycles as a function of ring strain, a series of increasingly strained dendralenes were formed. The bond angle deformation is directly correlated to trends in Raman and ^{13}C NMR spectroscopic data and reflects the

variance in the electronic structure as strain is increased. There is, however, only a small influence on the electronic absorption spectra of these compounds.

5.5 References and Notes

1. Okamura, W. H.; Sondheimer, F., *J. Am. Chem. Soc.* **1967**, *89*, 5991.
2. Nomoto, T.; Fukui, K.; Nakagawa, N., *Bull. Chem. Soc. Jpn.* **1976**, *49*, 305.
3. Suzuki, R.; Tsukuda, H.; Watanabe, N.; Kuwatane, Y.; Ueda, I., *Tetrahedron* **1998**, *54*, 2477.
4. Campbell, K.; McDonald, R.; Tykwinski, R. R., *J. Org. Chem.* **2002**, *67*, 1133.
5. Kammermeier, S.; Tykwinski, R. R.; Siemsen, P.; Seiler, P.; Diederich, F., *Chem. Commun.* **1998**, 1285.
6. Mindyuk, O. Y.; Stetzer, M. R.; Heiney, P. A.; Nelson, J.; Moore, J. S., *Adv. Mater.* **1998**, *10*, 1363.
7. Nakamura, N.; Okubo, H.; Yamaguchi, M., *Org. Lett.* **2001**, *3*, 1097.
8. Ohkita, M.; Ando, K.; Yamamoto, K.; Suzuki, T.; Tsuji, T., *Chem. Commun.* **2000**, 83.
9. Bunz, U. H. F.; Rubin, Y.; Tobe, Y., *Chem. Soc. Rev.* **1999**, *28*, 107.
10. Marsden, J. A.; Palmer, G. J.; Haley, M. M., *Eur. J. Org. Chem.* **2003**, 2355.
11. Rubin, Y., *Chem. Eur. J.* **1997**, *3*, 1009.
12. Kawase, T.; Darabi, H. R.; Oda, M., *Angew. Chem., Int. Ed. Engl.* **1996**, *35*, 2664.
13. Baldwin, K. P.; Matzger, A. J.; Scheiman, D. A.; Tessier, C. A.; Vollhardt, K. P. C.; Youngs, W. J., *Synlett* **1995**, 288.
14. Behr, O. M.; Eglington, G.; Galbraith, A. R.; Raphael, R. A., *J. Chem. Soc.* **1960**, 3614.

15. Bunz, U. H. F.; Enkelmann, V., *Chem. Eur. J.* **1999**, *5*, 263.
16. Boese, R.; Matzger, A. J.; Vollhardt, K. P. C., *J. Am. Chem. Soc.* **1997**, *119*, 2052.
17. Boldi, A. M.; Diederich, F., *Angew. Chem., Int. Ed. Engl.* **1994**, *33*, 468.
18. Anthony, J.; Boldi, A. M.; Boudon, C.; Gisselbrecht, J. P.; Gross, M.; Seiler, P.; Knobler, C. B.; Diederich, F., *Helv. Chim. Acta* **1995**, *78*, 797.
19. Schreiber, M.; Tykwinski, R. R.; Diederich, F.; Spreiter, R.; Gubler, U.; Bosshard, C.; Poberaj, I.; Gunter, P.; Boudon, C.; Gisselbrecht, J. P.; Gross, M.; Jonas, U.; Ringsdorf, H., *Adv. Mater.* **1997**, *9*, 339.
20. Sekiguchi, A.; Matsuo, H.; Sakk, *Angew. Chem. Int. Ed.* **1998**, *37*, 1662.
21. Nitschke, J.; Tilley, T. D., *J. Org. Chem.* **1998**, *63*, 3673.
22. Stanger, A.; Ashkenazi, N.; Boese, R.; Blaser, D.; Stellberg, P., *Chem. Eur. J.* **1997**, *3*, 208.
23. Enomoto, T.; Kawase, T.; Kurata, H.; Oda, M., *Tetrahedron Lett.* **1997**, *38*, 2693.
24. Faust, R.; Diederich, F.; Gramlich, V.; Setler, P., *Chem. Eur. J.* **1995**, *1*, 117.
25. Lepetit, C.; Nielsen, M. B.; Diederich, F.; Chauvin, R., *Chem. Eur. J.* **2003**, *9*, 5056.
26. Nielsen, M. B.; Schreiber, M.; Baek, Y. G.; Seiler, P.; Lecomte, S.; Boudon, C.; Tykwinski, R. R.; Gisselbrecht, J. P.; Gramlich, V.; Skinner, P. J.; Bosshard, C.; Gunter, P.; Gross, M.; Diederich, F., *Chem. Eur. J.* **2001**, *7*, 3263.
27. Zhao, Y. M.; Tykwinski, R. R., *J. Am. Chem. Soc.* **1999**, *121*, 458.
28. Zhao, Y., Ph.D Thesis, University of Alberta, Canada, 2002
29. Stang, P. J.; Fisk, T. E., *Synthesis* **1979**, 438.
30. Zhao, Y. M.; Campbell, K.; Tykwinski, R. R., *J. Org. Chem.* **2002**, *67*, 336.
31. Ritter, K., *Synthesis* **1993**, 735.
32. Hay, A. S., *J. Org. Chem.* **1962**, *27*, 3320.
33. Schultz, D. A.; Gwaltney, K. P.; Lee, H., *J. Org. Chem.* **1998**, *63*, 4034.

34. Hassig, R.; Seebach, D.; Siegel, H., *Chem. Ber.* **1984**, *117*, 1877.
35. Orfanopoulos, M.; Stratakis, M.; Elemes, Y., *Tetrahedron* **1989**, *30*, 4875.
36. Orfanopoulos, M.; Stratakis, M.; Elemes, Y., *J. Am. Chem. Soc.* **1990**, *112*, 6417.
37. Brunsveld, L.; Prince, R. B.; Meijier, E. W.; Moore, J. S., *Org. Lett.* **2000**, *2*, 1525.
38. Iyoda, M.; Tanaka, S.; Otani, H.; Nose, M.; Oda, M., *J. Am. Chem. Soc.* **1988**, *110*, 8494.
39. Generously provided by Dr. Yuming Zhao
40. Blomquist, A. T.; Bohrer, J. C., *J. Am. Chem. Soc.* **1952**, *74*, 3643.
41. Blomquist, A. T.; Liu, L. H., *J. Am. Chem. Soc.* **1953**, *75*, 2153.
42. De Graff, R. A. G.; Gorter, S.; Romers, C.; Wong, H. N.; Sondheimer, F., *J. Chem. Soc., Perkin Trans. 2* **1981**, 478.
43. Destro, R.; Pilati, T.; Simonetta, M., *J. Am. Chem. Soc.* **1975**, *97*, 658.
44. Collins, S. K.; Yap, G. P. A.; Fallis, A. G., *Org. Lett.* **2002**, *4*, 11.
45. Faust, R., *Angew. Chem. Int. Ed.* **1998**, *37*, 2825.
46. Kiang, C.-H.; Goddard III, W. A., *Phys. Rev. Lett.* **1996**, *76*, 2515.
47. Rubin, Y.; Parker, T. C.; Pastor, S. J.; Jalisatgi, S.; Boule, C.; Wilkins, C. L., *Angew. Chem. Int. Ed.* **1998**, *37*, 1226.
48. Tobe, Y.; Nakagawa, N.; Naemura, K.; Wakabayashi, T.; Shida, T.; Achiba, Y., *J. Am. Chem. Soc.* **1998**, *120*, 4544.
49. Tykwinski, R. R.; Diederich, F.; Gramlich, V.; Seiler, P., *Helv. Chim. Acta* **1996**, *79*, 634.
50. Meier, H., *Adv. Strain Org. Chem.* **1991**, *1*, 215.
51. Misumi, S.; Kaneda, T. In *The Chemistry of the Carbon-Carbon Triple Bond, Part 2*; Patai, S., Ed.; John Wiley & Sons: Chichester, 1978; p 713.
52. Ando, T.; Nakagawa, M., *Bull. Chem. Soc. Jpn.* **1971**, *44*, 172.
53. Scott, L. T., *Pure. Appl. Chem.* **1986**, *58*, 105.

54. Scott, L.; Cooney, M. J.; Otte, C.; Puls, C.; Haumann, T.; Boese, R.; Carroll, R. J.; Smith III, A. B.; de Meijere, A., *J. Am. Chem. Soc.* **1994**, *116*, 10275.
55. AM1 forcefield, MacSpartan Plus 1.1.9, Wavefunction, Inc., 1998
56. Neidlein, R.; Winter, M., *Synthesis* **1998**, 1362.
57. Wong, H. N.; Sondheimer, F., *Tetrahedron* **1981**, *37*, W99.
58. Gleiter, R.; Kratz, D.; Schafer, W.; Schehlmann, V., *J. Am. Chem. Soc.* **1991**, *113*, 9258.
59. Gleiter, R.; Merger, R.; Irngartinger, H., *J. Am. Chem. Soc.* **1992**, *114*, 8927.
60. Nakagawa, M. In *The Chemistry of the Carbon-Carbon Triple Bond*; Patai, S., Ed.; John Wiley & Sons: Chichester, 1978; p 635.
61. Hopf, H.; Maas, G., *Angew. Chem., Int. Ed. Engl.* **1992**, *31*, 931.
62. Armitage, J. B.; Whiting, M. C., *J. Chem. Soc.* **1952**, 2005.
63. This section was written in collaboration with Dr. Glen Loppnow.
64. Krebs, A.; Wilke, J., *Top. Curr. Chem.* **1983**, *109*, 189.
65. Meier, H.; Hanold, N.; Molz, T.; Bissinger, H. J.; Kolshorn, H.; Zountsas, J., *Tetrahedron* **1986**, *42*, 1711.
66. Badger, R. M., *J. Chem. Phys.* **1934**, *2*, 128.
67. Bellamy, L. J. *Advances in Infrared Group Frequencies*; Methuen: London, 1968.

Chapter 6 Future Outlook

6.1 Introduction

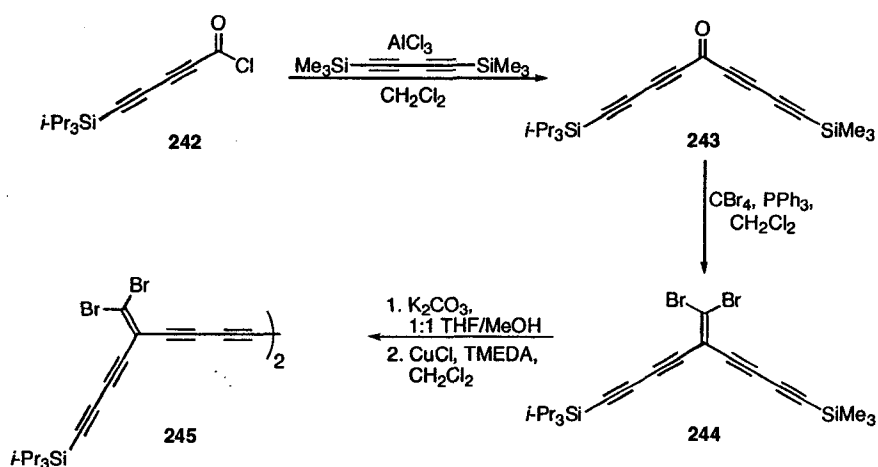
Several projects have been summarized in this thesis, ranging in topic from the development of methodology to the synthesis of carbon-rich molecules. The success of the work described has naturally led to the creation of new projects with novel synthetic targets. Briefly described below are just a few of the directions that this work could be taken.

6.2 Polyynes

There are four general goals for the polyynes chemistry. These are as follows, 1) the development of a synthesis for the decayne that does not involve acetylide chemistry, 2) the formation of longer triisopropylsilyl-capped polyynes chains with subsequent measurement of their NLO responses, 3) the synthesis of polyynes with electron donating and electron withdrawing groups as end caps, and 4) the application of the carbenoid rearrangement toward the formation of cyclic allotropes of carbon.

Although the synthetic route that was used to form the decayne **138** was successful, the inability to form the decayne directly from the octabromide precursor **154** and the low yield of the first step of the synthesis (formation of the alcohol **151** from a lithium acetylide) necessitates the development of an alternative route. One possible sequence involves the use of the Friedel-Crafts reaction with **242** as a key step to form **243**, which after dibromoolefination gives

the 10 carbon segment **244**, Scheme 6.1. Removal of the trimethylsilyl group followed by oxidative coupling would then give the decayne precursor **245**.



Scheme 6.1

One of the advantages to using this sequence is that only two rearrangements would have to be performed on **245** to provide the decayne.

The reactions used to form the polyynes are very easily adapted toward the formation of longer polyyne chains. For example, the route shown in Scheme 6.1 can be modified for this purpose by increasing the number of acetylene units in the acid chloride and/or in the coupling partner in the Friedel-Crafts reaction, Chart 6.1.

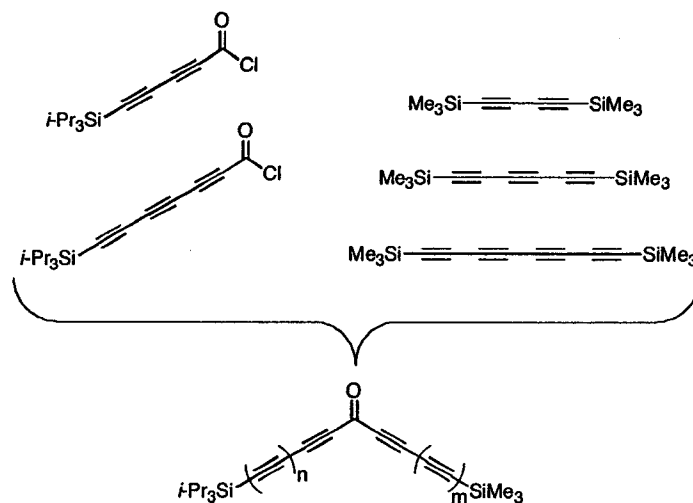
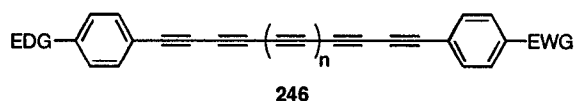
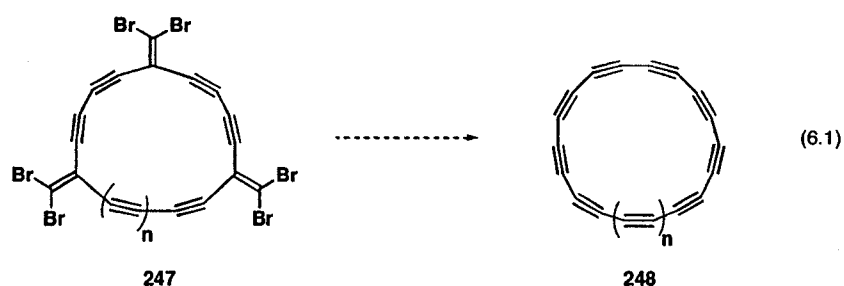


Chart 6.1

Push-pull polyynes such as **246** could also be formed. The exploration of the NLO response of such a series is a primary motivator for synthesizing these unsymmetrical molecules.



A pathway to cyclic allotropes using the alkyldiene carbenoid rearrangement is also envisioned, equation 6.1. Precursors **247** would be formed by oxidative coupling of the acyclic oligomers. Rearrangement of the dibromoolefin moieties could then provide allotropes **248**.



6.3 Mechanism

As described in Chapter 4, the next step in the mechanistic studies of the alkylidene carbenoid rearrangement is to rearrange the labeled monobromoolefins **249** and **250** and determine the geometry of the rearrangement in hexanes, Chart 6.2.

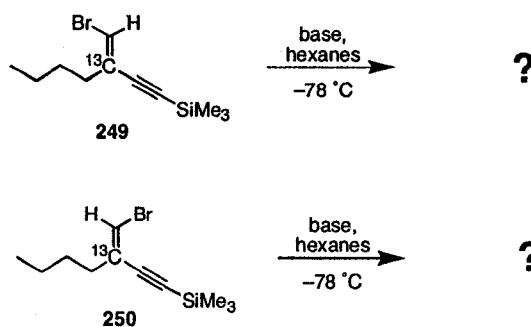
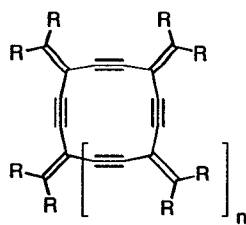


Chart 6.2

There are other aspects of the mechanism which are also interesting and could be explored, such as the geometry of the transition state, the effect of changing the metal of the carbenoid intermediate and determining if there is equilibration between carbenoid intermediates.

6.4 Cross-conjugated Macrocycles

The next step in this project is to vary the functionality on the macrocycles to provide a more soluble and stable series of molecules, **251**. For example, $\text{R}_1 = \text{R}_2 = \text{R}_3 = \text{R}_4 = \text{phenyl}$. A full series of cycles could then be formed where $n = 1, 2, 3$.



251

Other series of radialene cycles could be synthesized where the phenyl ring is substituted. The incorporation of an ester functionality on the phenyl substituent could facilitate the organization of the radialenes into liquid crystals. It would also be interesting to have electron donating and/or electron withdrawing groups on the phenyl substituents, where $R_1 = R_3$ and $R_2 = R_4$.

Chapter 7 Experimental

General Experimental Details. Column chromatography; *silica gel-60* (230-400 mesh) from *Silicycle*. Thin layer chromatography (TLC): plastic sheet coated with *silica gel F₂₅₄* from *Macherey-Nagel*, aluminum sheet coated with aluminium oxide 60; visualization by UV light or KMnO_4 stain. Melting point: Gallenkamp apparatus; uncorrected. UV-visible spectra: *Pharmacia Biotech Ultrospecc 300* or *Varian Cary 400* at ambient temperature; λ in nm (ϵ in $\text{cm}^{-1} \text{M}^{-1}$). IR spectra (cm^{-1}): *Nicolet Magna-IR* (neat). ^1H and ^{13}C NMR: *Varian Gemini-300, -400, or -500* and *Bruker AM-300 or 400* instruments, at ambient temperature in CD_2Cl_2 , CDCl_3 , C_6D_6 ; solvent peaks (7.24, 5.32 and 7.15 ppm, respectively, for ^1H and 53.8, 77.0 and 128.0 ppm, respectively, for ^{13}C) as reference. EI MS (70 eV): *Kratos MS 50* instrument. ESI and MALDI MS: *Micromass Zabspec oaTOF* or *PE Biosystems Mariner TOF* instruments. Elemental analyses were performed by the Microanalytical Service, Department of Chemistry-University of Alberta. Differential scanning calorimetry (DSC); *Perkin Elmer Pyris 1 Differential Scanning Calorimeter*. ^{13}C NMR spectra are broadband decoupled unless otherwise noted in the individual experimental as Attached Proton Test (APT). Coupling constants J are reported as observed.

For IR data, useful functional groups and 3-4 of the strongest absorptions are reported, including but not limited to C-H, C=C and C≡C bond stretches.

For mass spectral analyses, low-resolution data are provided in cases when M^+ is not the base peak; otherwise, only high-resolution data are provided.

3-Trimethylsilylpropynal,¹ 3-triisopropylsilylpropynal,¹ dibromoolefins **96a**,² **96b**,³ and **96c**,³ 1,4-diethynylbenzene **117**,⁴ 1,3,5-triethynylbenzene **122**,⁵ 1,4-bis(triisopropylsilyl)-1,3-butadiyne **132**,⁶ 1-triisopropylsilylethynyl-4-trimethylsilylethynylbenzene,⁷ 1-(trimethylsilylethynyl)-naphthylene,⁸ carboxylic acid **172**,⁹ vinyl triflate **213**,¹⁰ enediyne **215**,¹¹ dibromoolefin **218**,¹² compounds **222**, **223**, and **224**,¹³ and 3,3-dimethyl-1,4-pentadiyne **236**¹⁴ were synthesized as previously reported.

General Methods Reagents were purchased reagent grade from commercial suppliers and used without further purification. All ¹³C labeled starting materials were purchased from Cambridge Isotope Laboratories, Inc. Et₂O, THF and benzene were distilled from sodium/benzophenone ketyl, and hexanes and CH₂Cl₂ were distilled from CaH₂ immediately prior to use. A positive pressure of N₂ was essential to the success of all Pd-catalyzed reactions. Degassing of solvents was accomplished by vigorously bubbling N₂ through the solution for at least 30 min. Anhydrous conditions were essential for the success of alkylidene rearrangement reactions; glassware was flame dried and reactions were performed under an inert atmosphere of either N₂ or Ar. Anhydrous MgSO₄ was used as the drying agent after aqueous workup. Evaporation and concentration *in vacuo* was done at H₂O-aspirator pressure.

Raman Measurements Raman spectra of the cross-conjugated ene-yne were obtained with 1 mL solutions of the sample in carbon tetrachloride. Raman scattering was excited by spherically-focusing the 514.5 nm laser line from an Ar ion laser (Coherent, Santa Clara, CA) onto a spinning 5-mm NMR tube containing the sample solution in a 135° backscattering geometry. The laser power was typically 200 mW. Multi-channel detection of the resonance Raman scattering was obtained with a liquid nitrogen-cooled CCD detector (Princeton Instruments, Trenton, NJ) connected to the first half of a double monochromator (Spex Industries, Metuchen, NJ). Spectral slit widths were 5-7 cm^{-1} . Frequency calibration was performed by measuring Raman scattering of solvents of known frequencies (acetone, acetonitrile, and ethanol) and by measuring atomic emission lines from Kr and Ne lamps. Reported frequencies are accurate to $\pm 2 \text{ cm}^{-1}$. The resonance Raman spectra were analyzed by using a 486DX2-66V computer (Gateway Computers, North Sioux City, SD). A carbon tetrachloride solvent spectrum was subtracted from all solution spectra. The baselines were leveled by subtracting multiple joined line segments from the spectrum.

General Procedure A - Alcohol Formation via Lithium Acetylide. Unless otherwise noted in the individual procedures, a solution of the appropriate terminal acetylene (4.0 mmol) in Et_2O or THF (25 mL) was cooled to $-78 \text{ }^\circ\text{C}$. *n*-BuLi (4.0 mmol) was slowly added over 2 minutes and the mixture allowed to stir for 0.5 hour. The aldehyde (4.0 mmol) or ethyl formate (2.0 mmol) was dissolved in Et_2O (ca. 2 mL), and then added to the lithium acetylide mixture. The reaction

was warmed to 15 °C over a period of 1 h, then quenched with satd. aq. NH₄Cl (20 mL). Et₂O (20 mL) was added, the organic layer separated, washed with satd. aq. NH₄Cl (2 × 20 mL), dried (MgSO₄), and the solvent removed *in vacuo*. The crude reaction was passed through a silica plug to remove baseline material. Column chromatography (silica gel), if necessary, provided the pure alcohols.

General Procedure B - PCC Oxidation of Alcohol to Ketone. Unless otherwise noted in the individual procedures, to a solution of the alcohol (5.00 mmol) in CH₂Cl₂ (50 mL) at rt was added PCC (7.30 mmol), celite (1.5 g), and molecular sieves (4 Å, 1.5 g). TLC analysis was used to monitor the reaction, and oxidation to the ketone was typically complete after 3 h. The reaction mixture was passed through a plug of silica gel (CH₂Cl₂) to remove chromium waste and the solvent removed *in vacuo*. Column chromatography (silica gel), if necessary, provided the pure ketones.

General Procedure C - Friedel-Crafts Acylation.¹⁵ Unless otherwise noted in the individual procedures, thionyl chloride (42 mmol) was added to the carboxylic acid (7.0 mmol) in a dry flask protected from moisture with a drying tube containing CaCl₂, and the mixture allowed to stir overnight at rt. The excess thionyl chloride was then removed *in vacuo* to provide the acid chloride. CH₂Cl₂ (50 mL) was added and the temperature of the solution lowered to 0 °C. Bis(trimethylsilyl)acetylene (7.0 mmol) or bis(trimethylsilyl)butadiyne (7.0 mmol) and AlCl₃ (8.0 mmol) was added and the reaction mixture warmed to rt

over 3 hours. The reaction was carefully quenched by the addition of the reaction to 10% HCl (50 mL) in ice (50 mL). Et₂O (75 mL) was added, the organic layer separated, washed with satd. aq. NaHCO₃ (2 × 20 mL), NaCl (2 × 20 mL), dried (MgSO₄), and the solvent removed *in vacuo*. Column chromatography (silica gel), if necessary, provided the pure ketones.

General Procedure D – Dibromoolefination.¹⁶ Unless otherwise noted in the individual procedures, CBr₄ (4.0 mmol) and PPh₃ (8.0 mmol) were added to CH₂Cl₂ (100 mL) and allowed to stir for 5 minutes at rt until the mixture turned bright orange. The ketone (3.0 mmol) in CH₂Cl₂ (5 mL) was slowly added to the CBr₄/PPh₃ mixture over a period of 1 min. The reaction mixture turned a darker red/orange color upon addition of the ketone. TLC analysis was used to monitor the reaction, indicating that dibromoolefination was typically complete almost immediately. Solvent was reduced to ca. 5 mL, hexanes added (100 mL), the inhomogeneous mixture filtered through silica gel and the solvent removed *in vacuo*. Column chromatography (silica gel), if necessary, provided the pure dibromoolefins.

General Procedure E – Rearrangement of Dibromoolefin to Alkyne. Unless otherwise noted in the individual procedures, a solution of the dibromoolefin (0.40 mmol) in hexanes (12 mL) was cooled to -78 °C. *n*-BuLi (1.2 equiv per dibromoolefin moiety) was slowly added over a period of ca. 2 min. The reaction mixture turned a pale yellow/orange color. TLC analysis indicated that the

reaction was complete soon after addition of base, although warming of the reaction solution in the TLC capillary could influence this analysis. The reaction was warmed to approximately $-5\text{ }^{\circ}\text{C}$ over a period of 0.5 – 1 h then was quenched with satd. aq. NH_4Cl (10 mL). Et_2O (10 mL) was added, the organic layer separated, washed with satd. aq. NH_4Cl (2×20 mL), dried (MgSO_4), and the solvent removed in vacuo. The crude reaction was passed through a plug of silica to remove baseline material. Column chromatography (silica gel), if necessary, gave the desired products.

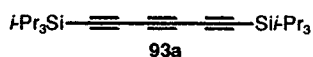
General Procedure F – Palladium-catalyzed cross-coupling. The terminal acetylene (0.20 mmol) was added to a degassed and dry solution of vinyl triflate (1.1 equiv per coupling event) in THF or DMF (5 mL). $\text{Pd}(\text{PPh}_3)_4$ (0.010 mmol), *i*- Pr_2NH or Et_2NH (1 mL), and CuI (0.020 mmol) were sequentially added and the solution stirred at rt until TLC analysis no longer showed the presence of the starting material (ca. 2-4 h). Et_2O (5 mL) and satd. aq. NH_4Cl (5 mL) were added, the organic phase separated, washed with satd. aq. NH_4Cl (2×20 mL), dried (MgSO_4) and the solvent removed *in vacuo*. Column chromatography (silica gel) and/or recrystallization gave the desired enyne.

General Procedure G - Oxidative Coupling. A mixture of the trimethylsilyl-protected alkyne (0.15 mmol) and K_2CO_3 (0.030 mmol) in wet THF/MeOH (30 mL, 1:1 v/v) was stirred for 2 hours. Et_2O (30 mL) and satd. aq. NH_4Cl (30 mL) were added, the organic phases separated, washed with satd. aq. NH_4Cl (2×20

mL), dried (MgSO₄) and the solvent reduced to ca. 2 mL. The terminal acetylene was added to a solution of the Hay catalyst¹⁷ (CuCl or CuI (0.30 mmol) and TMEDA (0.60 mmol) in CH₂Cl₂ (60 mL), previously stirred until homogeneous). This mixture was stirred at rt under air until TLC analysis no longer showed the starting material (ca. 3 h). Et₂O (30 mL) and satd. aq. NH₄Cl (30 mL) were added, the organic phase separated, washed with satd. aq. NH₄Cl (2 × 20 mL), dried (MgSO₄), and the solvent removed *in vacuo*. Column chromatography (silica gel) and/or recrystallization gave the desired product.

General Procedure H – Lithium Diisopropyl Amide Deprotonation. To a mixture of diisopropylamine (3.0 mmol) in Et₂O (10 mL) at –78 °C was added *n*-BuLi (3.0 mmol). The mixture was stirred for 1 h, then transferred via cannula into a round bottom flask containing a solution of the terminal acetylene (3.0 mmol) in Et₂O (100 mL) at –78 °C.

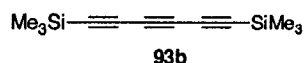
1,6-Bis(triisopropylsilyl)-1,3,5-hexatriyne (93a).



Dibromoolefin **96a** (0.201 g, 0.368 mmol) in hexanes (10 mL) was subjected to rearrangement according to general procedure E using *n*-BuLi (2.17 M in hexanes, 0.17 mL, 0.37 mmol) to afford **93a** (0.0989 g, 70%) as a colorless solid: *R*_f = 0.8 (hexanes); UV-Vis (hexanes) λ_{max} (ε) 234 (93 000) nm; IR (CH₂Cl₂, cast) 2945, 2866, 2154, 1462 cm⁻¹; ¹H NMR (500 MHz, CD₂Cl₂) δ 1.09 (s, 42H); ¹³C NMR (125 MHz, CD₂Cl₂) δ 89.9, 85.5, 61.5, 18.7, 11.6; EI MS *m/z*

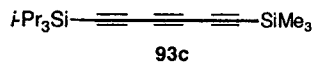
386.3 (M^+ , 34), 343.2 ($[M - i\text{-Pr}]^+$, 100); EI HRMS m/z calcd. for $C_{24}H_{42}Si_2 (M^+)$ 386.2825, found 386.2819. Compound **93a** has been reported previously.¹⁸

1,6-Bis(trimethylsilyl)-1,3,5-hexatriyne (93b).



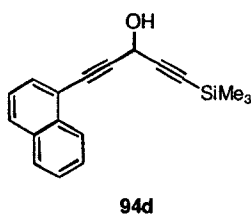
Dibromoolefin **96b** (0.101 g, 0.266 mmol) in hexanes (5 mL) was subjected to rearrangement according to general procedure E using *n*-BuLi (2.5 M in hexanes, 0.13 mL, 0.33 mmol) to afford **93b** (0.029 g, 50%) as a colorless solid: $R_f = 0.7$ (hexanes). Spectral data were consistent with those reported previously.¹⁹

1-Triisopropylsilyl-6-trimethylsilyl-1,3,5-hexatriyne (93c).



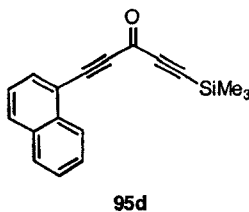
Dibromoolefin **96c** (0.200 g, 0.432 mmol) in hexanes (12 mL) was subjected to rearrangement according to general procedure E using *n*-BuLi (2.2 M in hexanes, 0.20 mL, 0.44 mmol) to afford **93c** (0.0802 g, 61%) as a colorless solid: $R_f = 0.7$ (hexanes). Spectral data were consistent with those reported previously.¹⁸

5-(1-Naphthyl)-1-trimethylsilylpenta-1,4-diyne-3-ol (94d).



To 1-ethynynaphthalene (0.600 g, 3.95 mmol) in THF (25 mL) was added *n*-BuLi (2.5 M in hexane, 1.6 mL, 4.0 mmol) and 3-trimethylsilyl-1-propynal (0.504 g, 4.00 mmol) in Et₂O (5 mL) according to general procedure A to ultimately afford **94d**. Purification by column chromatography (silica gel, CH₂Cl₂) gave **94d** (0.663 g, 60%) as a yellow oil: *R*_f = 0.4 (CH₂Cl₂); IR (CH₂Cl₂ cast) 3347, 3051, 2977, 2228, 2176, 1507 cm⁻¹; ¹H NMR (300 MHz, CDCl₃) δ 8.37 (d, *J* = 8.3 Hz, 1H), 7.90-7.87 (m, 2H), 7.74 (d, *J* = 7.3 Hz, 1H), 7.64-7.53 (m, 2H), 7.46 (dt, *J* = 7.3, 1.2 Hz, 1H), 5.57 (s, 1H), 2.59 (s, 1H), 0.28 (s, 9 H); ¹³C NMR (75.5 MHz, CDCl₃) δ 133.5, 133.1, 130.9, 129.4, 128.3, 127.0, 126.5, 126.1, 125.1, 119.6, 102.0, 90.9, 90.0, 82.8, 53.4, -0.3; EI HRMS *m/z* calcd. for C₁₈H₁₈OSi (M⁺) 278.1127, found 278.1123.

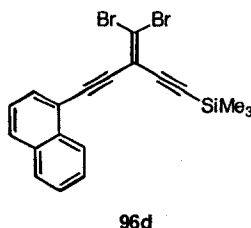
5-(1-Naphthyl)-1-trimethylsilylpenta-1,4-diyn-3-one (95d).



Alcohol **94d** (0.60 g, 2.2 mmol) in CH₂Cl₂ (50 mL) was subjected to oxidation according to general procedure B using celite (0.6 g), molecular sieves (4 Å, 0.6 g), and PCC (0.58 g, 2.7 mmol) to afford **95d** (0.32 g, 54%) as a yellow oil: *R*_f = 0.7 (CH₂Cl₂); IR (CH₂Cl₂ cast) 3059, 2961, 2197, 2176, 2152, 1623 cm⁻¹; ¹H NMR (300 MHz, CDCl₃) δ 8.32 (d, *J* = 8.3 Hz, 1H), 7.98 (d, *J* = 8.3 Hz, 1H), 7.87 (dd, *J* = 7.3, 1.1 Hz, 2H), 7.66-7.53 (m, 2H), 7.46 (dd, *J* = 8.3, 7.2 Hz, 1H), 0.31 (s, 9H); ¹³C NMR (125.3 MHz, CDCl₃) δ 160.5, 134.0, 133.8, 133.1, 132.2,

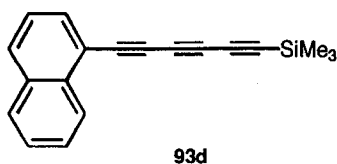
128.6, 127.9, 127.1, 125.7, 125.2, 117.0, 102.9, 99.6, 94.2, 90.6, -0.8; EI HRMS m/z calcd. for $C_{18}H_{16}OSi$ (M^+) 276.0971, found 276.0970.

3-(Dibromomethylidene)-5-(1-naphthyl)-1-trimethylsilylpenta-1,4-diyne (96d).



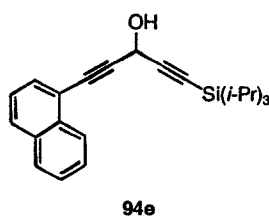
Ketone **95d** (0.276 g, 1.00 mmol) in CH_2Cl_2 (5 mL) was subjected to dibromoolefination according to general procedure D using CBr_4 (0.400 g, 1.21 mmol) and PPh_3 (0.680 g, 2.60 mmol) in CH_2Cl_2 (40 mL). Purification by column chromatography (silica gel, hexanes/ CH_2Cl_2 2:1) afforded **96d** (0.231 g, 54%) as a yellow oil that solidified under refrigeration: Mp 78 °C; R_f = 0.4 (hexanes/ CH_2Cl_2 2:1); IR (CH_2Cl_2) 3058, 2959, 2199, 2153, 798 cm^{-1} ; 1H NMR (300 MHz, $CDCl_3$) δ 8.43 (d, J = 8.4 Hz, 1H), 7.87 (d, J = 7.8 Hz, 1H), 7.86 (d, J = 8.1 Hz, 1H), 7.78 (d, J = 7.2 Hz, 1H), 7.63-7.54 (m, 2H), 7.44 (t, J = 7.8 Hz, 1H), 0.33 (s, 9H); ^{13}C NMR (75.5 MHz, $CDCl_3$) δ 133.2 (2x), 131.0, 129.8, 128.4, 127.2, 126.7, 126.2, 125.2, 119.8, 114.6, 108.9, 102.8, 100.4, 94.4, 90.7, -0.3; EI HRMS m/z calcd. for $C_{19}H_{16}^{79}Br^{81}BrSi$ (M^+) 431.9368, found 431.9380; Anal. Calcd. for $C_{19}H_{16}Br_2Si$ (432.23): C, 52.80; H, 3.73. Found: C, 52.83; H, 3.72.

6-(1-Naphthyl)-1-(trimethylsilyl)-1,3,5-hexatriyne (93d).



Dibromoolefin **96d** (0.0687 g, 0.159 mmol) in hexanes (6 mL) was subjected to rearrangement according to general procedure E using *n*-BuLi (2.5 M in hexanes, 0.080 mL, 0.20 mmol) to afford **93d** (0.0303 g, 70%) as a colorless oil: $R_f = 0.43$ (hexanes); $^1\text{H NMR}$ (300 MHz, CDCl_3) δ 8.26 (d, $J = 8.3$ Hz, 1H), 7.87 (d, $J = 8.2$ Hz, 1H), 7.84 (dd, $J = 7.2, 1.4$ Hz, 1H), 7.77 (dd, $J = 7.2, 1.2$ Hz, 1H), 7.59-7.51 (m, 2H), 7.40 (dd, $J = 8.3, 7.2$ Hz, 1H), 0.22 (s, 9H); $^{13}\text{C NMR}$ (75.5 MHz, CDCl_3 , APT) δ 134.3, 133.1, 133.0, 130.4, 128.6, 127.5, 126.9, 126.0, 125.2, 118.5, 89.8, 88.1, 78.9, 75.4, 68.1, 61.7, -0.5; IR (film) 2959, 2164, 2071, 1505 cm^{-1} ; EI MS m/z 272 (M^+ , 91), 257 ($[\text{M} - \text{CH}_3]^+$, 100); EI HRMS m/z calcd. for $\text{C}_{19}\text{H}_{16}\text{Si}$ (M^+) 272.1021, found 272.1026; Anal. Calcd. for $\text{C}_{19}\text{H}_{16}\text{Si}$ (272.4): C 83.77, H 5.92; found: C 83.65, H 6.06.

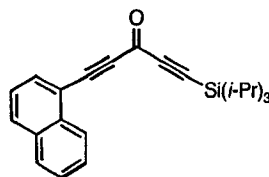
1-Naphthyl-5-triisopropylsilyl-1,4-pentadiyne-3-ol (94e).



To a solution of 1-(1-trimethylsilylethynyl)-naphthalene (0.402 g, 1.79 mmol) in wet MeOH/THF (30 mL, 1:1 v/v) was added K_2CO_3 (0.06 g, 0.4 mmol), and the mixture stirred at rt until TLC showed complete desilylation, ca. 1h. Et_2O (30 mL) and satd. aq. NH_4Cl (30 mL) were added, the organic layer separated, washed with satd. aq. NH_4Cl (2 \times 30 mL), dried over (MgSO_4), and the solvent

reduced *in vacuo* to ca. 5 mL. To the terminal acetylene in dried Et₂O (30 mL) was added *n*-BuLi (2.5 M in hexanes, 0.70 mL, 1.8 mmol) and 3-triisopropylsilylpropynal (0.382 g, 1.82 mmol) according to general procedure A to ultimately afford **94e** (0.359, 55%) as a yellow oil: *R*_f = 0.40 (hexanes/CH₂Cl₂ 1:1); IR (CH₂Cl₂ cast) 3362, 2943, 2865, 2229, 2174, 1462 cm⁻¹; ¹H NMR (400 MHz, CDCl₃) δ 8.33-8.31 (m, 1H), 7.84-7.82 (m, 2H), 7.67 (dd, *J* = 7.1 Hz, 1.1 Hz, 1H), 7.55-7.48 (m, 2H), 7.41 (dd, *J* = 8.3 Hz, 7.2 Hz, 1H), 5.48 (d, *J* = 7.9 Hz, 1H), 2.37 (d, *J* = 7.9 Hz, 1H), 1.12 (s, 21H); ¹³C NMR (100 MHz, CDCl₃, APT) δ 133.5, 133.1, 130.8, 129.3, 128.3, 126.9, 126.5, 126.1, 125.1, 119.6, 104.1, 91.2, 86.4, 82.4, 53.3, 18.6, 11.2; EI MS *m/z* 362 (M⁺, 79), 263 (100); EI HRMS *m/z* calcd. for C₂₄H₃₀OSi (M⁺) 362.2066, found 362.2068.

1-Triisopropyl-5-naphthyl-1,4-pentadiyne-3-one (**95e**).

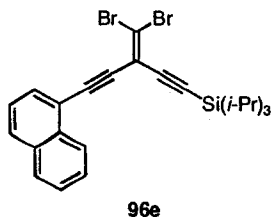


95e

Alcohol **94e** (0.351 g, 0.971 mmol) in CH₂Cl₂ (25 mL) was subjected to oxidation according to general procedure B using celite (0.2 g), molecular sieves (4 Å, 0.2 g) and PCC (0.259 g, 1.20 mmol) to afford **95e** as a yellow oil (0.166 g, 47%): *R*_f = 0.60 (hexanes/CH₂Cl₂ 1:1); IR (CH₂Cl₂ cast) 2944, 2866, 2196, 2174, 2148, 1626 cm⁻¹; ¹H NMR (400 MHz, CDCl₃) δ 8.34 (d, *J* = 8.1 Hz, 1H), 7.98 (d, *J* = 8.3 Hz, 1H), 7.89-7.85 (m, 2H), 7.61-7.54 (m, 2H), 7.48 (dd, *J* = 8.1 Hz, 7.4 Hz, 1H), 1.17 (s, 21 H); ¹³C NMR (100 MHz, CDCl₃, APT) δ 160.2, 134.0, 133.8,

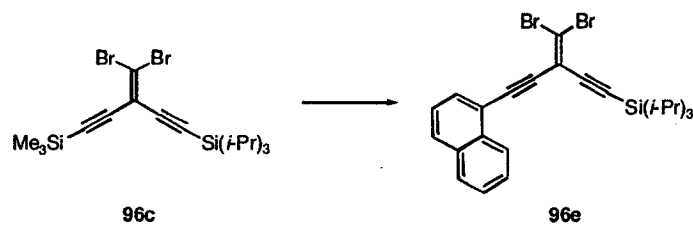
133.1, 132.1, 128.6, 127.8, 127.0, 125.7, 125.2, 117.0, 105.4, 97.6, 94.5, 90.2, 18.5, 11.1; EI HRMS m/z calcd. for $C_{24}H_{28}OSi$ 360.1910 (M^+), found 360.1917.

3-(Dibromomethylidene)-5-(1-naphthyl)-1-triisopropylsilylpenta-1,4-diyne (96e).



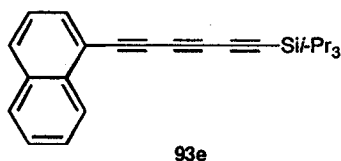
Ketone **95e** (0.166 g, 0.461 mmol) in CH_2Cl_2 (2 mL) was subjected to dibromoolefination according to general procedure D using CBr_4 (0.195 g, 0.589 mmol) and PPh_3 (0.334 g, 1.27 mmol) in CH_2Cl_2 (10 mL) to afford **96e** (0.196 g, 82%) as a yellow oil: $R_f = 0.5$ (hexanes/ CH_2Cl_2 2:1); IR (CH_2Cl_2 cast) 3059, 2942, 2199, 2151, 1585 cm^{-1} ; 1H NMR (300 MHz, $CDCl_3$) δ 8.39-8.36 (m, 1H), 7.88-7.83 (m, 2H), 7.73 (dd, $J = 7.2, 1.2$ Hz, 1H), 7.58-7.49 (m, 2H), 7.42 (dd, $J = 8.1, 7.2$ Hz, 1H), 0.33 (s, 21H); ^{13}C NMR (75.5 MHz, $CDCl_3$) δ 133.3, 133.2, 130.9, 129.8, 128.3, 127.1, 126.7, 126.2, 125.3, 119.9, 114.9, 108.1, 102.3, 99.8, 94.2, 91.1, 18.7, 11.3; EI HRMS m/z calcd. for $C_{25}H_{28}^{79}Br^{81}BrSi$ (M^+) 516.0306, found 516.0305.

3-(Dibromomethylidene)-5-(1-naphthyl)-1-triisopropylsilylpenta-1,4-diyne (96e).



To a solution of **96c** (1.50 g, 3.26 mmol) in wet MeOH (25 mL) was added K_2CO_3 (0.010 g, 0.070 mmol), and the mixture stirred until TLC showed complete desilylation, ca. 2 h. Et_2O (20 mL) and satd. aq. NH_4Cl (20 mL) were added, the organic layer separated, washed with satd. aq. NH_4Cl (2×20 mL), dried ($MgSO_4$), and the solvent reduced *in vacuo* to ca. 5 mL then added to Et_3N (35 mL). This solution was degassed and 1-iodonaphthalene (0.828 g, 3.28 mmol), $PdCl_2(PPh_3)_2$ (0.20 g, 0.28 mmol), and CuI (0.10 g, 0.53 mmol) were added and the solution stirred at rt until TLC analysis no longer showed the presence of the starting material, ca. 5 h. Removal of the Et_3N in *vacuo*, and purification by column chromatography (silica gel, hexanes) afforded **96e** (0.482 g, 29%) as a yellow oil. See above for spectral details.

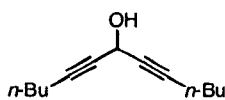
6-(1-Naphthyl)-1-(triisopropylsilyl)-1,3,5-hexatriyne (93e).



Dibromoolefin **96e** (0.205 g, 0.396 mmol) in hexanes (11 mL) was subjected to rearrangement according to general procedure E using *n*-BuLi (2.5 M in hexanes, 0.19 mL, 0.48 mmol) to afford **93e** (0.0878 g, 62%) as an off-white solid: Mp 34-35 °C; $R_f = 0.57$ (hexanes); 1H NMR (300 MHz, $CDCl_3$) δ 8.27 (d, *J*

= 8.1 Hz, 1H), 7.86 (d, $J = 7.9$ Hz, 1H), 7.84 (d, $J = 6.5$ Hz, 1H), 7.76 (d, $J = 7.2$ Hz, 1H), 7.58-7.52 (m, 2H), 7.40 (dd, $J = 8.1, 7.8$ Hz, 1H), 1.10 (s, 21H); ^{13}C NMR (75.5 MHz, CDCl_3 , APT) δ 134.3, 133.1, 132.9, 130.3, 128.6, 127.5, 126.8, 125.9, 125.2, 118.6, 89.8, 87.5, 79.0, 75.0, 68.5, 60.7, 18.6, 11.4; IR (film) 2943, 2182, 2163, 2069, 1462 cm^{-1} ; EI MS m/z 356 (M^+ , 86), 313 ($[\text{M} - i\text{-Pr}]^+$, 100); EI HRMS m/z calcd. for $\text{C}_{25}\text{H}_{28}\text{Si}$ (M^+) 356.1960, found 356.1963.

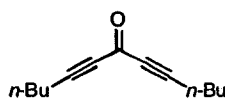
Trideca-5,8-diyn-7-ol (94f).



94f

To 1-hexyne (1.48 g, 18.0 mmol) in Et_2O (50 mL) was added $n\text{-BuLi}$ (2.5 M in hexanes, 7.20 mL, 18.0 mmol) and ethyl formate (0.435 g, 7.50 mmol) in Et_2O (5 mL) according to general procedure A to ultimately afford **94f** (1.33 g, 92%) as a yellow oil: $R_f = 0.2$ (hexanes/ CH_2Cl_2 2:1); IR (CH_2Cl_2) 3381, 2926, 2286, 2226, 1120 cm^{-1} ; ^1H NMR (300 MHz, CDCl_3) δ 5.03 (dp, $J = 7.2$ Hz, 2.1 Hz, 1H), 2.36 (d, $J = 7.2$ Hz, 1H), 2.17 (dt, $J = 7.2$ Hz, 2.1 Hz, 4H), 1.48-1.31 (m, 8H), 0.88-0.83 (m, 6H); ^{13}C NMR (75.5 MHz, CDCl_3 , APT) δ 84.5, 78.1, 52.1, 30.3, 21.7, 18.2, 13.3; EI MS m/z 192.2 (M^+ , 2), 107.5 (100); EI HRMS m/z calcd. for $\text{C}_{13}\text{H}_{20}\text{O}$ (M^+) 192.1514, found 192.1488.

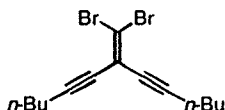
Trideca-5,8-diyn-7-one (95f).



95f

Alcohol **94f** (1.20 g, 6.24 mmol) in CH_2Cl_2 (50 mL) was subjected to oxidation according to the general procedure B using celite (2 g), molecular sieves (4 Å, 2 g), and PCC (2.00 g, 9.28 mmol). Purification by column chromatography (silica gel, hexanes/ CH_2Cl_2 2:1) afforded **95f** (0.874 g, 73%) as a yellow oil: $R_f = 0.4$ (hexanes/ CH_2Cl_2 2:1); IR (film) 2959, 2206, 1628, 1241 cm^{-1} ; ^1H NMR (300 MHz, CDCl_3) δ 2.34 (t, $J = 7.1$ Hz, 4H), 1.55-1.48 (m, 4H), 1.44-1.34 (m, 4H), 0.89-0.85 (m, 6H); ^{13}C NMR (75.5 MHz, CDCl_3 , APT) δ 161.3, 94.5, 82.3, 29.5, 21.9, 18.7, 13.4; EI MS m/z 190.1 (M^+ , 3), 109.1 ($[\text{M} - \text{C}_6\text{H}_9]^+$, 100); EI HRMS m/z calcd. for $\text{C}_{13}\text{H}_{18}\text{O}$ (M^+) 190.1358, found 190.1352.

7-(1,1-Dibromomethylidene)-trideca-5,8-diyne (**96f**).

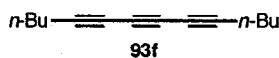


96f

Ketone **95f** (0.800 g, 4.20 mmol) in CH_2Cl_2 (5 mL) was subjected to dibromoolefination according to general procedure D using CBr_4 (1.74 g, 5.26 mmol) and PPh_3 (2.75 g, 10.5 mmol) in CH_2Cl_2 (50 mL). Purification by column chromatography (silica gel, hexane/ CH_2Cl_2 2:1) afforded **96f** (0.585 g, 40%) as a yellow oil that slowly decomposes at rt: $R_f = 0.7$ (hexane/ CH_2Cl_2 2:1); IR (CH_2Cl_2) 2957, 2219, 1331 cm^{-1} ; ^1H NMR (300 MHz, CDCl_3) δ 2.31 (t, $J = 7.0$ Hz, 4H), 1.58-1.38 (m, 8H), 0.92-0.87 (m, 6H); ^{13}C NMR (75.5 MHz, CDCl_3 ,

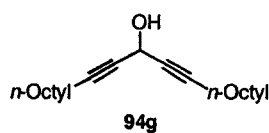
APT) δ 114.7, 105.0, 97.5, 78.1, 30.2, 21.9, 19.4, 13.6; EI HRMS m/z calcd. for $C_{14}H_{18}^{79}Br^{81}Br$ (M^+) 345.9755, found 345.9755.

5,7,9-Tetradecatriyne (93f).



Dibromoolefin **96f** (0.191 g, 0.552 mmol) in hexanes (16 mL) was subjected to rearrangement according to general procedure E using *n*-BuLi (2.5 M in hexane, 0.26 mL, 0.65 mmol) to afford **93f** (0.0821 g, 80%) as light yellow oil: R_f = 0.53 (hexanes); ^1H NMR (300 MHz, CDCl_3) δ 2.26 (t, J = 6.9 Hz, 4H), 1.55-1.33 (m, 8H), 0.84 (t, J = 7.2 Hz, 6H); ^{13}C NMR (75.5 MHz, CDCl_3 , APT) δ 79.3, 65.7, 60.4, 30.2, 22.0, 19.1, 13.5; IR (CH_2Cl_2 cast) 2958, 2216, 1465 cm^{-1} ; EI HRMS m/z calcd. for $C_{14}H_{18}$ (M^+) 187.1487, found 187.1445.

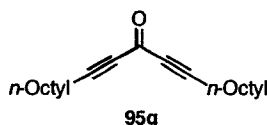
Heneicosa-9,12-diyn-11-ol (94g).



To 1-decyne (2.50 g, 18.1 mmol) in Et_2O (25 mL) at -78 $^\circ\text{C}$ was added *n*-BuLi (2.5 M in hexanes, 7.20 mL, 18.0 mmol) and ethyl formate (0.435 g, 7.50 mmol) in Et_2O (5 mL) according to general procedure A to ultimately afford **94g** (1.74 g, 76%) as a yellow oil: R_f = 0.2 (hexanes/ CH_2Cl_2 2:1); IR (CH_2Cl_2) 3387, 2958, 2285, 2256, 2227, 1118 cm^{-1} ; ^1H NMR (300 MHz, CDCl_3) δ 5.05 (p, J = 2.0 Hz, 1H), 2.38 (bs, 1H), 2.16 (dt, J = 7.1 Hz, 2.0 Hz, 4H), 1.50-1.42 (m, 4H), 1.33-1.23 (m, 20H), 0.86-0.82 (m, 6H); ^{13}C NMR (75.5 MHz, CDCl_3 , APT) δ

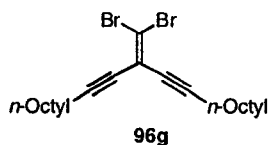
85.1, 78.1, 52.5, 31.8, 29.2, 29.1, 28.9, 28.4, 22.6, 18.7, 14.1; EI MS m/z 304.3 (M^+ , 2), 55 ($[C_4H_7]^+$, 100); EI HRMS m/z calcd. for $C_{21}H_{36}O$ (M^+) 304.2766, found 304.2750.

Heneicosa-9,12-diyn-11-one (95g).



Alcohol **94g** (1.50 g, 4.93 mmol) in CH_2Cl_2 (50 mL) was subjected to oxidation according to general procedure B using celite (1.5 g), molecular sieves (4 Å, 1.5 g), and PCC (1.58 g, 7.33 mmol). Purification by column chromatography (silica gel, hexanes/ CH_2Cl_2 2:1) afforded **95g** (1.30 g, 87%) as a yellow oil: R_f = 0.4 (hexanes/ CH_2Cl_2 2:1); IR (CH_2Cl_2 cast) 2927, 2208, 1629, 1241 cm^{-1} ; 1H NMR (300 MHz, $CDCl_3$) δ 2.33 (t, J = 7.1 Hz, 4H), 1.57-1.52 (m, 4H), 1.36-1.35 (m, 4H), 1.24-1.23 (m, 16H), 0.86-0.81 (m, 6H); ^{13}C NMR (75.5 MHz, $CDCl_3$) δ 161.3, 94.5, 82.3, 31.8, 29.1, 28.9, 28.8, 27.5, 22.6, 19.0, 14.0; EI MS m/z 302.3 (M^+ , 6), 55 ($[C_4H_7]^+$, 100); EI HRMS m/z calcd. for $C_{21}H_{34}O$ (M^+) 302.2610, found 302.2608; Anal. Calcd. for $C_{21}H_{34}O$ (302.49): C, 83.38; H, 11.33. Found: C, 83.17; H, 11.30.

11-(1,1-Dibromomethylidene)-heneicosa-9,12-diyne (96g).



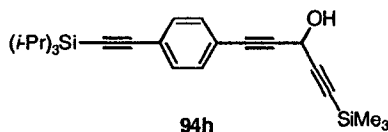
Ketone **95g** (1.15 g, 3.78 mmol) in CH₂Cl₂ (5 mL) was subjected to dibromoolefination according to general procedure D using CBr₄ (1.57 g, 4.74 mmol) and PPh₃ (2.49 g, 9.50 mmol). Purification by column chromatography (silica gel, hexanes/CH₂Cl₂ 2:1) afforded **96g** (0.935 g, 54%) as a yellow oil that slowly decomposes at rt: *R*_f = 0.8 (hexanes/CH₂Cl₂ 2:1); IR (CH₂Cl₂ cast) 2926, 2220 cm⁻¹; ¹H NMR (300 MHz, CDCl₃) δ 2.31 (t, *J* = 7.1 Hz, 4H), 1.58-1.53 (m, 4H), 1.41-1.39 (m, 4H), 1.27-1.21 (m, 16H), 0.88-0.84 (m, 6H); ¹³C NMR (75.5 MHz, CDCl₃, APT) δ 114.8, 105.0, 97.6, 78.2, 31.9, 29.2, 29.1, 28.9, 28.2, 22.7, 19.8, 14.1; EI HRMS *m/z* calcd. for C₂₂H₃₄⁷⁹Br⁸¹Br (M⁺) 458.1007, found 458.1006; Anal. Calcd. for C₂₂H₃₄Br₂ (458.31): C, 57.65; H, 7.48. Found: C, 57.54; H, 7.71.

8,10,12-Eicosatriyne (93g).



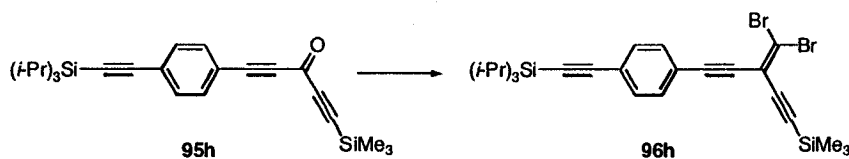
n-BuLi (2.5 M in hexane, 0.20 mL, 0.50 mmol) was added to **96g** (0.194 g, 0.422 mmol) in hexanes (12 mL) according to general procedure E to produce **93g** (0.0835 g, 66%) as a light brown oil. *R*_f = 0.59 (hexanes); ¹H NMR (300 MHz, CDCl₃) δ 2.31 (t, *J* = 7.0 Hz, 4H), 1.60-1.52 (m, 4H), 1.42-1.38 (m, 4H), 1.28-1.21 (m, 16H), 0.88-0.84 (m, 6H); ¹³C NMR (75.5 MHz, CDCl₃, APT) δ 79.4, 65.8, 60.4, 31.9, 29.2, 29.1, 28.9, 28.2, 22.7, 19.4, 14.1; IR (CH₂Cl₂ cast) 2926, 2855, 2216, 1466 cm⁻¹; EI MS *m/z* 298 (M⁺, 36), 131 (100); EI HRMS *m/z* calcd. for C₂₂H₃₄ (M⁺) 298.2661, found 298.2662.

**1-(Trimethylsilyl)-5-((4-triisopropylsilylethynyl)phenyl)-1,4-pentadiyne-3-ol
(94h).**



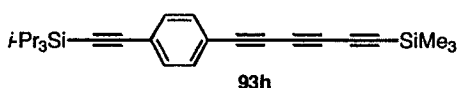
To a solution of 1-triisopropylsilylethynyl-4-trimethylsilylethyl-benzene (0.749 g, 2.11 mmol) in wet MeOH/THF (10 mL, 1:1 v/v) was added K_2CO_3 (0.040 g, 0.29 mmol) and the mixture stirred at rt until TLC analysis showed complete desilylation, ca. 1.5 h. Et_2O (10 mL) and satd. aq. NH_4Cl (10 mL) were added, the organic layer separated, washed with satd. aq. NH_4Cl (2×10 mL), dried ($MgSO_4$), and the solvent reduced *in vacuo* to ca. 2 mL. To the terminal acetylene in Et_2O (10 mL) was added *n*-BuLi (2.5 M in hexanes, 0.85 mL, 2.1 mmol) and 3-trimethylsilylpropynal (0.218 g, 1.72 mmol) according to general procedure A. Purification by column chromatography (silica gel, hexanes/ CH_2Cl_2 1:1) afforded alcohol **94h** (0.267, 31%) as a yellow oil: $R_f = 0.38$ (hexanes/ CH_2Cl_2 , 1:1); IR (CH_2Cl_2 cast) 3322, 2958, 2892, 2234, 2155, 1497 cm^{-1} ; 1H NMR (400 MHz, $CDCl_3$) δ 7.41-7.36 (m, 4H), 5.32 (d, $J = 7.2$ Hz, 1H), 2.30 (d, $J = 7.2$ Hz, 1H), 1.11 (s, 21H), 0.19 (s, 9H); ^{13}C NMR (125 MHz, $CDCl_3$, APT) δ 131.8, 131.6, 124.0, 121.7, 106.4, 101.5, 93.1, 90.0, 87.5, 84.1, 53.2, 18.7, 11.4, -0.2; EI MS m/z 408, (M^+ , 24), 365 ($[M - i-Pr]^+$, 100); EI HRMS m/z calcd. for $C_{25}H_{36}OSi_2$ (M^+) 408.2305, found 408.2307.

1-(Trimethylsilyl)-5((4-triisopropylsilylethynyl)-phenyl)-3-(1,1-dibromomethylidene)-1,4-pentadiyne (96h).



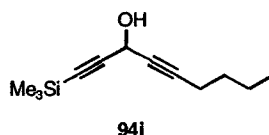
Alcohol **94h** (0.267 g, 0.652 mmol) in CH_2Cl_2 (10 mL) was subjected to oxidation according to general procedure B using celite (0.2 g), molecular sieves (4 Å, 0.2 g) and PCC (0.225 g, 1.05 mmol) to afford **95h**. The solvent was reduced to ca. 2 mL and ketone **95h** was immediately subjected to dibromoolefination according to general procedure D using CBr_4 (0.250 g, 0.754 mmol) and PPh_3 (0.429 g, 1.64 mmol) in CH_2Cl_2 (10 mL). Purification by column chromatography (silica gel, hexanes) afforded **96h** (0.194, 53%) as a yellow solid: Mp 60-61 °C; $R_f = 0.90$ (hexanes/ CH_2Cl_2 1:1); IR (CH_2Cl_2 cast) 2958, 2891, 2203, 2154, 1492 cm^{-1} ; ^1H NMR (500 MHz, CDCl_3) δ 7.437.41- (m, 4H), 1.12 (s, 21H), 0.24 (s, 9H); ^{13}C NMR (125 MHz, CDCl_3 , APT) δ 131.9, 131.3, 124.2, 121.8, 114.1, 109.4, 106.4, 102.7, 100.0, 95.3, 93.5, 87.5, 18.7, 11.4, -0.3; EI MS m/z 562, (M^+ , 25), 518 ($[\text{M} - i\text{-Pr}]^+$, 100); EI HRMS m/z calcd. for $\text{C}_{26}\text{H}_{34}\text{Si}_2^{79}\text{Br}^{81}\text{Br}$ (M^+) 562.0545, found 562.0512. Anal. Calcd. for $\text{C}_{26}\text{H}_{34}\text{Si}_2\text{Br}_2$ (560.10): C, 55.51; H, 6.09. Found: C, 55.73; H, 5.99.

[1-(Trimethylsilyl)-1,3,5-hexatriynyl]-[(4-triisopropylsilylethynyl)benzene] (93h).



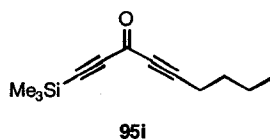
Dibromoolefin **96h** (0.0578 g, 0.103 mmol) in hexanes (5 mL) was subjected to rearrangement according to general procedure E using *n*-BuLi (2.5 M in hexanes, 0.06 mL, 0.15 mmol) to afford **93h** (0.0254 g, 61%) as a yellow oil: $R_f = 0.5$ (hexanes); IR (CH₂Cl₂ cast) 2958, 2891, 2154, 2076, 1506 cm⁻¹; ¹H NMR (500 MHz, CDCl₃) δ 7.43-7.38 (m, 4H), 1.11 (s, 21H), 0.21 (s, 9H); ¹³C NMR (125 MHz, CDCl₃, APT) δ 132.7, 131.9, 124.9, 120.5, 106.2, 94.5, 89.6, 88.0, 76.4, 76.0, 67.8, 61.4, 18.7, 11.4, -0.4; EI MS m/z 402 (M⁺, 57), 359 ([M - *i*-Pr]⁺, 100); EI HRMS m/z calcd. for C₂₆H₃₄Si₂ (M⁺) 402.2199, found 402.2204.

1-Trimethylsilyl-1,4-nonadiyne-3-ol (94i).



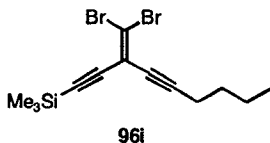
To 1-hexyne (0.389 g, 4.75 mmol) in Et₂O (25 mL) at -78 °C was added *n*-BuLi (2.5 M in hexanes, 1.80 mL, 4.50 mmol) and 3-trimethylsilylpropynal (0.691 g, 5.47 mmol) in ca. 2 mL Et₂O according to general procedure A to ultimately afford **94i** (0.92 g, 98%) as a yellow oil: $R_f = 0.43$ (hexanes/CH₂Cl₂ 1:1); IR (CH₂Cl₂ cast) 3377, 2959, 2293, 2232, 2178, 1466 cm⁻¹; ¹H NMR (400 MHz, CDCl₃) δ 5.07 (bs, 1H), 2.21 (dt, $J = 2.1, 7.1$ Hz, 2H), 2.12 (d, $J = 6.5$ Hz, 1H), 1.53-1.45 (m, 2H), 1.43-1.34 (m, 2H), 0.89 (t, $J = 7.2$ Hz, 3H), 0.12 (s, 9H); ¹³C NMR (100 MHz, CDCl₃, APT) δ 102.6, 88.8, 85.8, 52.8, 30.3, 21.9, 18.4, 13.5, -0.3 (one coincident peak not observed); EI MS m/z 208.1 (M⁺, 0.8), 73.0 ([Me₃Si]⁺, 100); EI HRMS m/z calcd. for C₁₂H₂₀OSi (M⁺) 208.1283, found 208.1272.

1-Trimethylsilyl-1,4-nonadiyne-3-one (95i).



Alcohol **94i** (0.791 g, 3.79 mmol) in CH_2Cl_2 (70 mL) was subjected to oxidation according to general procedure B using celite (1.0 g), molecular sieves (4 Å, 1.0 g), and PCC (1.07 g, 4.98 mmol). Purification by column chromatography (silica gel, hexanes/ CH_2Cl_2 1:1) afforded **95i** (0.448 g, 57%) as a yellow oil: $R_f = 0.62$ (hexanes/ CH_2Cl_2 1:1); IR (CH_2Cl_2 cast) 2961, 2231, 2212, 2148, 1629 cm^{-1} ; ^1H NMR (400 MHz, CDCl_3) δ 2.39 (t, $J = 7.1$ Hz, 2H), 1.61-1.54 (m, 2H), 1.42 (sextet, $J = 7.4$ Hz, 2H), 0.91 (t, $J = 7.3$ Hz, 3H), 0.23 (s, 9H); ^{13}C NMR (100 MHz, CDCl_3 , APT) δ 160.8, 102.8, 97.9, 96.1, 82.2, 29.5, 22.0, 18.9, 13.4, -0.9; EI MS m/z 206, (M^+ , 2), 191 ($[\text{M} - \text{CH}_3]^+$, 82), 163 (100); EI HRMS m/z calcd. for $\text{C}_{12}\text{H}_{18}\text{OSi}$ (M^+) 206.1127, found 206.1129.

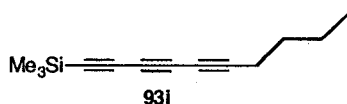
3-Dibromomethylidene-1-trimethylsilyl-1,4-nonadiyne (96i).



Ketone **95i** (0.412 g, 2.00 mmol) in CH_2Cl_2 (5 mL) was subjected to dibromoolefination according to general procedure D using CBr_4 (0.848 g, 2.56 mmol) and PPh_3 (1.28 g, 4.88 mmol) in CH_2Cl_2 (25 mL) to afford **96i** (0.437 g, 60%) as a yellow oil: $R_f = 0.91$ (hexanes/ CH_2Cl_2 1:1); IR (CH_2Cl_2 cast) 2959,

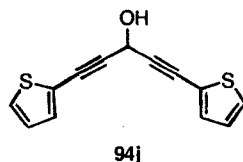
2222, 2147 cm^{-1} ; ^1H NMR (500 MHz, CDCl_3) δ 2.32 (t, $J = 7.0$ Hz, 2H), 1.58-1.52 (m, 2H), 1.48-1.40 (m, 2H), 0.91 (t, $J = 7.3$ Hz, 3H), 0.20 (s, 9H); ^{13}C NMR (100 MHz, CDCl_3 , APT) δ 114.5, 107.7, 101.7, 100.7, 98.4, 77.5, 30.1, 21.9, 19.4, 13.5, -0.4 ; EI HRMS m/z calcd. for $\text{C}_{13}\text{H}_{18}\text{Si}^{79}\text{Br}^{81}\text{Br}$ (M^+) 361.9524, found 361.9525.

1-(Trimethylsilyl)-1,3,5-decatriyne (93i).



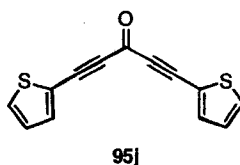
Dibromoolefin **96i** (0.1484 g, 0.4100 mmol) in hexanes (10 mL) was subjected to rearrangement according to general procedure E using *n*-BuLi (2.5 M in hexanes, 0.20 mL, 0.50 mmol) to afford **93i** (0.0677 g, 82%) as a yellow oil: $R_f = 0.54$ (hexanes); ^1H NMR (400 MHz, CDCl_3) δ 2.27 (t, $J = 7.0$ Hz, 2H), 1.54-1.48 (m, 2H), 1.43-1.34 (m, 2H), 0.89 (t, $J = 7.3$ Hz, 3H), 0.16 (s, 9H); ^{13}C NMR (100 MHz, CDCl_3 , APT) δ 88.3, 85.4, 81.0, 65.4, 62.5, 59.9, 30.0, 21.9, 19.1, 13.5, -0.5 ; IR (CH_2Cl_2 cast) 2960, 2874, 2211, 2167, 2079 cm^{-1} ; EI MS m/z 202 (M^+ , 31), 187 ($[\text{M} - \text{CH}_3]^+$, 100); EI HRMS m/z calcd. for $\text{C}_{13}\text{H}_{18}\text{Si}$ (M^+) 202.1178, found 202.1180.

1,5-Bis(2-thienyl)-1,4-pentadiyne-3-ol (94j).



To a solution of 2-Trimethylsilylethynylthiophene (0.878 g, 4.87 mmol) in wet MeOH/THF (20 mL, 1:1 v/v) was added K₂CO₃ (0.14 g, 1.0 mmol) and the mixture stirred at rt until TLC showed complete desilylation, ca. 2 h. Et₂O (20 mL) and satd. aq. NH₄Cl (20 mL) were added, the organic layer separated, washed with satd. aq. NH₄Cl (2 × 20 mL), dried MgSO₄ and the solvent reduced *in vacuo* to ca. 5 mL. To the terminal acetylene in Et₂O (20 mL) was added *n*-BuLi (2.5 M in hexanes, 2.00 mL, 5.00 mmol) and ethyl formate (0.180 g, 2.43 mmol) according to general procedure A. Purification by column chromatography (silica gel, hexanes/CH₂Cl₂ 1:1) afforded **94j** as a light brown oil (0.231 g, 40%): *R*_f = 0.25 (hexanes/CH₂Cl₂ 1:1); IR (CH₂Cl₂ cast) 3335, 3105, 2224, 1517 cm⁻¹; ¹H NMR (400 MHz, CDCl₃) δ 7.28-7.26 (m, 4H), 6.96 (dd, *J* = 3.7, 5.1 Hz, 2H), 5.60 (bs, 1H), 2.79 (s, 1H); ¹³C NMR (100 MHz, CDCl₃, APT) δ 133.1, 133.0, 128.0, 127.9, 127.0, 126.9, 121.6, 89.4, 78.3, 53.3; EI MS *m/z* 244, (*M*⁺, 54), 108 ([C₆H₄S]⁺, 100).

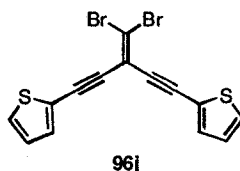
1,5-Bis(2-thienyl)-1,4-pentadiyne-3-one (**95j**).



Alcohol **94j** (0.172 g, 0.705 mmol) in CH₂Cl₂ (10 mL) was subjected to oxidation according to general procedure B using celite (0.2 g), molecular sieves (4Å, 0.2 g), and PCC (0.231 g, 1.07 mmol). Purification by column chromatography (silica gel, hexanes/CH₂Cl₂ 1:1) afforded **95j** (0.0853 g, 50%) as a brown solid: Mp 99–101 °C; *R*_f = 0.33 (hexanes/CH₂Cl₂ 1:1); IR (CH₂Cl₂ cast)

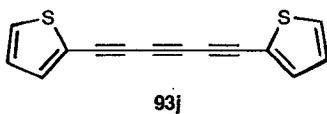
3093, 2170, 1599 cm^{-1} ; ^1H NMR (400 MHz, CDCl_3) δ 7.55 (dd, $J = 1.0, 3.8$ Hz, 2H), 7.53 (dd, $J = 1.1, 5.1$ Hz, 2H), 7.08 (dd, $J = 3.8, 5.1$ Hz, 2H); ^{13}C NMR (100 MHz, CDCl_3 , APT) δ 159.6, 137.5, 132.6, 127.9, 119.3, 93.9, 86.0; EI HRMS m/z calcd. for $\text{C}_{13}\text{H}_6\text{OS}_2$ (M^+) 241.9860, found 241.9847.

3-Dibromomethylidene-1,5-bis(2-thienyl)-1,4-pentadiyne (**96j**).



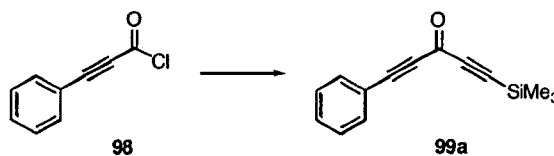
Ketone **95j** (0.0853 g, 0.352 mmol) in CH_2Cl_2 (5 mL) was subjected to dibromoolefination according to general procedure C using CBr_4 (0.154 g, 0.464 mmol) and PPh_3 (0.277 g, 1.06 mmol) in CH_2Cl_2 (10 mL) to afford **96j** (0.066 g, 47%) as a light brown solid: Mp 60-63 $^\circ\text{C}$; $R_f = 0.76$ (hexanes/ CH_2Cl_2 1:1); IR (CH_2Cl_2 cast) 3104, 2023, 2197, 1419 cm^{-1} ; ^1H NMR (500 MHz, CDCl_3) δ 7.35 (dd, $J = 1.1, 5.1$ Hz, 2H), 7.34 (dd, $J = 1.1, 3.7$ Hz, 2H), 7.01 (dd, $J = 3.7, 5.1$ Hz, 2H); ^{13}C NMR (100 MHz, CDCl_3 , APT) δ 133.1, 128.7, 127.2, 121.8, 113.8, 107.6, 89.3, 89.3; EI HRMS m/z calcd. for $\text{C}_{14}\text{H}_6^{79}\text{Br}^{81}\text{BrS}_2$ (M^+) 397.8257, found 397.8250.

1,6-Bis(2-thienyl)-1,3,5-hexatriyne (93j).



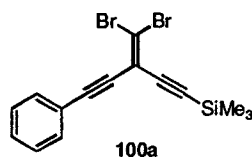
Dibromoolefin **96j** (0.066 g, 0.17 mmol) in hexanes (5 mL) was subjected to rearrangement according to general procedure E using *n*-BuLi (2.5 M in hexanes, 0.08 mL, 0.20 mmol) to afford **93j** (0.0259 g, 64%) as a yellow solid: Mp 58-59 °C; $R_f = 0.42$ (hexanes); IR (CH₂Cl₂ cast) 3114, 2187, 1433 cm⁻¹; ¹H NMR (400 MHz, CDCl₃) δ 7.38 (dd, $J = 1.2, 3.9$ Hz, 2H), 7.32 (dd, $J = 1.2, 5.1$ Hz, 2H), 6.98 (dd, $J = 3.9, 5.1$ Hz, 2H); ¹³C NMR (100 MHz, CDCl₃, APT) δ 135.6, 129.6, 127.3, 121.3, 78.6, 72.7, 68.5; EI HRMS m/z calcd. for C₁₄H₆S₂ (M⁺) 237.9911, found 237.9907.

5-Phenyl-1-trimethylsilyl-1,4-pentadiyne-3-one (99a).



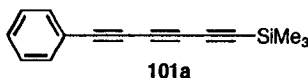
Phenylpropynoic acid (0.999 g, 6.84 mmol) was subjected to Friedel-Crafts acylation according to general procedure C using thionyl chloride (3 mL), bis(trimethylsilyl)acetylene (1.18 g, 6.90 mmol) and AlCl₃ (1.07 g, 8.04 mmol), in CH₂Cl₂ (50 mL). Purification by column chromatography (silica gel, hexanes/CH₂Cl₂ 1:1) afforded **99a** (0.729 g, 47%). Spectral data are consistent with those reported previously.²⁰

5-Phenyl-trimethylsilyl-3-dibromomethylidene-1,4-pentadiyne (100a).



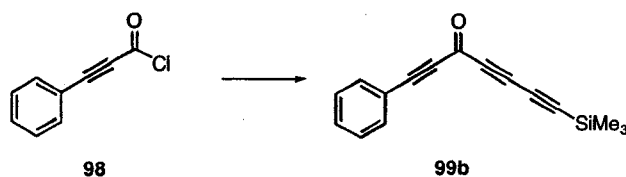
Ketone **99a** (0.669 g, 2.96 mmol) in CH_2Cl_2 (5 mL) was subjected to dibromoolefination according to procedure D using CBr_4 (1.26 g, 3.80 mmol) and PPh_3 (2.14 g, 8.18 mmol) in CH_2Cl_2 (100 mL) to afford **100a** (0.806 g, 71%) as a yellow solid: Mp 76-78 °C; $R_f = 0.74$ (hexanes/ CH_2Cl_2 1:1); IR (CH_2Cl_2 cast) 2960, 2203, 2153, 1597 cm^{-1} ; ^1H NMR (400 MHz, CDCl_3) δ 7.50 (dd, $J = 7.9, 1.7$ Hz, 2H), 7.36-7.30 (m, 3H), 0.24 (s, 9H); ^{13}C NMR (100 MHz, CDCl_3 , APT) δ 131.7, 129.2, 128.4, 122.2, 114.3, 109.1, 102.6, 100.2, 95.8, 85.9, -0.4; EI HRMS m/z calcd. for $\text{C}_{15}\text{H}_{14}\text{Si}^{79}\text{Br}^{81}\text{Br}$ (M^+) 381.9211, found 381.9233.

1-(Trimethylsilyl)-6-phenyl-1,3,5-hexatriyne (101a).



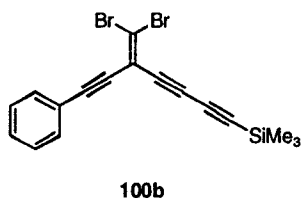
Dibromoolefin **100a** (0.145 g, 0.380 mmol) in hexanes (7 mL) was subjected to rearrangement according to general procedure E using *n*-BuLi (2.5 M in hexanes, 0.15 mL, 0.38 mmol) to afford **101a** (0.0711 g, 84%) as a colorless oil: $R_f = 0.49$ (hexanes); IR (CH_2Cl_2 cast) 2960, 2174, 2076, 1490 cm^{-1} ; ^1H NMR (400 MHz, CDCl_3) δ 7.51-7.49 (m, 2H), 7.36 (d, $J = 7.3$ Hz, 1H), 7.33-7.29 (m, 2H), 0.21 (s, 9H); ^{13}C NMR (100 MHz, CDCl_3 , APT) δ 133.1, 129.8, 128.5, 120.8, 89.0, 88.0, 76.8, 74.3, 66.8, 61.6, -0.5; EI MS m/z 222 (M^+ , 35), 207 ($[\text{M} - \text{CH}_3]^+$, 100); EI HRMS m/z calcd. for $\text{C}_{15}\text{H}_{14}\text{Si}$ (M^+) 222.0865, found 222.0865.

7-Phenyl-1-trimethylsilyl-1,3,6-heptatriyne-5-one (99b).



Phenylpropynoic acid (1.01 g, 6.91 mmol) was subjected to Friedel-Crafts acylation according to general procedure C using thionyl chloride (3 mL), bis-trimethylsilylbutadiyne (1.29 g, 6.62 mmol) and AlCl_3 (0.938 g, 7.04 mmol) in CH_2Cl_2 (50 mL). Purification by column chromatography (silica gel, hexanes/ CH_2Cl_2 1:1) afforded **99b** (0.959 g, 55%) as an unstable light brown oil: $R_f = 0.56$ (hexanes/ CH_2Cl_2 1:1); IR (CH_2Cl_2 cast) 2962, 2196, 2098, 1622 cm^{-1} ; ^1H NMR (500 MHz, CDCl_3) δ 7.60-7.59 (m, 2H), 7.49-7.46 (m, 1H), 7.38 (t, $J = 7.7$, 2H), 0.24 (s, 9H); ^{13}C NMR (125 MHz, CDCl_3 , APT) δ 159.2, 133.3, 131.4, 128.6, 119.0, 99.2, 92.6, 89.1, 85.8, 75.7, 74.1, -0.7; EI MS m/z 250.1 (M^+ , 24), 207.1 ($[\text{C}_{14}\text{H}_{11}\text{Si}]^+$, 100); EI HRMS m/z calcd. for $\text{C}_{16}\text{H}_{14}\text{OSi}$ (M^+) 250.0814, found 250.0808.

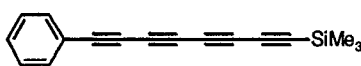
7-Phenyl-1-trimethylsilyl-(5-dibromomethylidene)-1,3,6-heptatriyne (100b).



Ketone **99b** (0.959 g, 4.09 mmol) in CH_2Cl_2 (5 mL) was subjected to dibromoolefination according to general procedure D using CBr_4 (1.69 g, 5.09 mmol) and PPh_3 (2.67 g, 10.2 mmol) in CH_2Cl_2 (100 mL) to afford **100b** (0.804 g,

48%) as a brown solid: Mp 35-37 °C; R_f = 0.69 (hexanes/ CH_2Cl_2 1:1); IR (CH_2Cl_2 cast) 2960, 2222, 2197, 2097, 1487 cm^{-1} ; ^1H NMR (400 MHz, CDCl_3) δ 7.50-7.48 (m, 2H), 7.37-7.30 (m, 3H), 0.22 (s, 9H); ^{13}C NMR (100 MHz, CDCl_3 , APT) δ 131.7, 129.4, 128.4, 121.8, 113.3, 110.9, 96.5, 95.2, 87.2, 85.2, 80.3, 72.2, -0.6; EI HRMS m/z calcd. for $\text{C}_{17}\text{H}_{14}\text{Si}^{79}\text{Br}^{81}\text{Br}$ (M^+) 405.9211, found 405.9219.

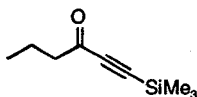
1-(Trimethylsilyl)-8-phenyl-1,3,5,7-octatetrayne (101b).



101b

Dibromoolefin **100b** (0.112 g, 0.275 mmol) in hexanes (7 mL) was subjected to rearrangement according to general procedure E using *n*-BuLi (2.5 M in hexanes, 0.13 mL, 0.33 mmol) to afford **101b** (0.0432 g, 64%) as a colorless oil: R_f = 0.57 (hexanes); IR (CH_2Cl_2 cast) 2961, 2195, 2132, 2059, 1491 cm^{-1} ; ^1H NMR (400 MHz, CDCl_3) δ 7.52-7.50 (m, 2H), 7.41-7.37 (m, 1H), 7.33-7.32 (m, 2H), 0.21 (s, 9H); ^{13}C NMR (100 MHz, CDCl_3 , APT) δ 133.2, 130.0, 128.6, 120.4, 88.8, 87.9, 76.9, 74.4, 67.2, 64.0, 62.2, 61.8, -0.6; EI MS m/z 246 (M^+ , 46), 231 ($[\text{M} - \text{CH}_3]^+$, 100); EI HRMS m/z calcd. for $\text{C}_{17}\text{H}_{14}\text{Si}$ (M^+) 246.0865, found 246.0863.

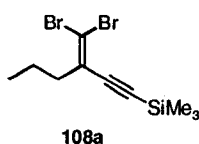
1-(Trimethylsilyl)-1-hexyn-3-one (107a).



107a

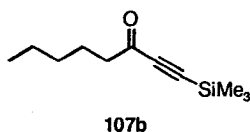
Butyryl chloride (2.00 g, 18.8 mmol) in CH_2Cl_2 (75 mL) was subjected to Friedel-Crafts acylation according to general procedure C using bis(trimethylsilyl)acetylene (3.20 g, 18.8 mmol) and AlCl_3 (2.51 g, 18.8 mmol) to afford **107a** (2.05 g, 65%) as a yellow oil. Spectral data were consistent with those previously reported.²¹

3-(Dibromomethylidene)-1-trimethylsilyl-hexa-1-yne (**108a**).



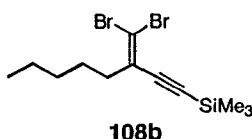
Ketone **107a** (0.790 g, 4.69 mmol) in CH_2Cl_2 (5 mL) was subjected to dibromoolefination according to general procedure D using CBr_4 (1.74 g, 5.35 mmol) and PPh_3 (3.06 g, 11.6 mmol) in CH_2Cl_2 (100 mL). Purification by column chromatography (silica gel, hexanes) to give **108a** (0.99 g, 65%) as a yellow oil: $R_f = 0.63$ (hexanes); IR (CH_2Cl_2 cast) 2962, 2150, 1458 cm^{-1} ; ^1H NMR (300 MHz, CDCl_3) δ 2.29-2.28 (m, 2H), 1.59 (sextet, $J = 7.5$, 2 H), 0.94 (t, $J = 7.4$, 2H), 0.20 (s, 9H); ^{13}C NMR (125 MHz, CDCl_3 , APT) δ 130.9, 103.2, 102.7, 97.6, 38.8, 21.0, 13.6, -0.2; EI MS m/z 323.9 (M^+ , 79), 308.9 ($[\text{M} - \text{CH}_3]^+$, 77), 138.9/136.9 (100); EI HRMS m/z calcd. for $\text{C}_{10}\text{H}_{16}^{79}\text{Br}^{81}\text{BrSi}$ (M^+) 323.9368, found 323.9366.

1-(Trimethylsilyl)-1-nonyne-3-one (**107b**).



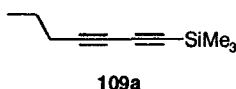
Hexanoyl chloride (2.53 g, 18.8 mmol) in CH_2Cl_2 (75 mL) was subjected to Friedel-Crafts acylation according to general procedure C using bis(trimethylsilyl)acetylene (3.20 g, 18.8 mmol) and AlCl_3 (2.51 g, 18.8 mmol) to afford **107b** (3.43 g, 93%) as a yellow oil. Compound **107b** has been previously reported.²²

3-(Dibromomethylidene)-1-trimethylsilyl-octa-1-yne (**108b**).



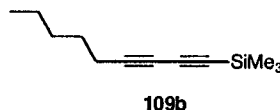
Ketone **107b** (2.10 g, 12.2 mmol) in CH_2Cl_2 (5 mL) was subjected to dibromoolefination according to general procedure D using CBr_4 (4.81 g, 14.5 mmol) and PPh_3 (7.85 g, 30.0 mmol) in CH_2Cl_2 (200 mL). Purification by column chromatography (silica gel, hexanes) to give **108b** (2.46 g, 58%) as a yellow oil: $R_f = 0.86$ (hexanes); IR (CH_2Cl_2 cast) 2958, 2151, 1466 cm^{-1} ; ^1H NMR (400 MHz, CDCl_3) δ 2.31-2.27 (m, 2H), 1.59-1.52 (m, 2H), 1.35-1.27 (m, 4H), 0.89 (t, $J = 7.0$ Hz, 3H), 0.20 (s, 9H); ^{13}C NMR (100 MHz, CDCl_3 , APT) δ 131.1, 103.2, 102.7, 97.5, 36.7, 31.0, 27.1, 22.4, 13.9, -0.3; EI MS m/z 352.0 (M^+ , 48), 73.0 ($[\text{Me}_3\text{Si}]^+$, 100); EI HRMS m/z calcd. for $\text{C}_{12}\text{H}_{20}^{79}\text{Br}^{81}\text{BrSi}$ (M^+) 351.9681, found 351.9692.

1-Trimethylsilyl-hepta-1,3-diyne (**109a**).



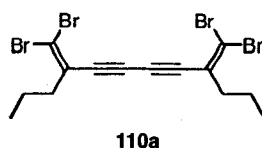
Dibromoolefin **108a** (0.112 g, 0.275 mmol) in hexanes (4 mL) was subjected to rearrangement according to general procedure E using *n*-BuLi (2.5 M in hexanes, 0.088 mL, 0.22 mmol) produce **109a** (0.0375 g, 83%) as a colorless oil: $R_f = 0.48$ (hexanes); IR (CH₂Cl₂ cast) 2964, 2228, 2109 cm⁻¹; ¹H NMR (500 MHz, CDCl₃) δ 2.23 (t, $J = 7.0$ Hz, 2H), 1.53 (sextet, $J = 7.2$ Hz, 2H), 0.97 (t, $J = 7.3$ Hz, 3H), 0.16 (s, 9H); ¹³C NMR (125 MHz, CDCl₃, APT) δ 88.5, 82.9, 80.0, 65.6, 21.7, 21.3, 13.5, -0.2; EI MS m/z 164.1 (M⁺, 7), 149.1 ([M - CH₃]⁺, 52), 70.0 (100); EI HRMS m/z calcd. for C₁₀H₁₆Si (M⁺) 164.1021, found 164.1012.

1-Trimethylsilyl-nona-1,3-diyne (**109b**).



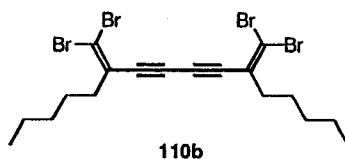
Dibromoolefin **108b** (0.216 g, 0.614 mmol) in hexanes (10 mL) was subjected to rearrangement according to general procedure E using *n*-BuLi (2.5 M in hexanes, 0.27 mL, 0.68 mmol) to afford **109b** (0.084 g, 71%) as a colorless oil: $R_f = 0.73$ (hexanes); IR (CH₂Cl₂ cast) 2959, 2225, 2106 cm⁻¹; ¹H NMR (500 MHz, CDCl₃) δ 2.25 (t, $J = 7.1$ Hz, 2H), 1.54-1.48 (m, 2H), 1.38-1.26 (m, 4H), 0.88 (t, $J = 7.2$ Hz, 3H), 0.16 (s, 9H); ¹³C NMR (125 MHz, CDCl₃, APT) δ 88.5, 83.0, 80.2, 65.4, 31.0, 27.9, 22.2, 19.3, 14.0, -0.20; EI MS m/z 192.1 (M⁺, 11), 177.1 ([M - CH₃]⁺, 100); EI HRMS m/z calcd. for C₁₂H₂₀Si (M⁺) 192.1334, found 192.1323.

4,9-Bis-(dibromomethylidene)-dodeca-5,7-diyne (**110a**).



Tetrabromide **108a** (0.231 g, 0.714mmol) was subjected to desilylation and oxidative homocoupling according to general procedure G using K_2CO_3 (0.022 g, 0.16 mmol) in MeOH/THF (10 mL, 1:1 v/v), CuI (0.0631 g, 0.255 mmol) and TMEDA (1 mL, 6.6 mmol) in CH_2Cl_2 (30 mL). Purification by column chromatography (silica gel, hexanes) afforded **110a** (0.131 g, 73%) as a yellow oil: $R_f = 0.57$ (hexanes); IR (CH_2Cl_2 cast) 2963, 1958, 1771 cm^{-1} ; 1H NMR (500 MHz, $CDCl_3$) δ 2.35-2.31 (m, 4H), 1.60 (sextet, $J = 7.5$, 4H), 0.95 (t, $J = 7.3$ Hz, 6H); ^{13}C NMR (125 MHz, $CDCl_3$, APT) δ 129.9, 100.4, 82.3, 80.5, 38.8, 21.0, 13.5; EI MS m/z 501.8 (M^+ , 78), 152.1 (100); EI HRMS m/z calcd. for $C_{14}H_{14}^{79}Br_2^{81}Br_2$ (M^+) 501.7788, found 501.7788.

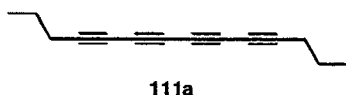
6,11-Bis-(dibromomethylidene)-hexadeca-7,9-diyne (110b).



Tetrabromide **108b** (0.250 g, 0.708 mmol) was subjected to desilylation and oxidative homocoupling according to general procedure G using K_2CO_3 (0.034 g, 0.18 mmol) in MeOH/THF (10 mL, 1:1 v/v), CuI (0.0734 g, 0.385 mmol) and TMEDA (1 mL, 6.6 mmol) in CH_2Cl_2 (30 mL). Purification by column chromatography (silica gel, hexanes) afforded **110b** (0.143 g, 72%) as a yellow oil. $R_f = 0.65$ (hexanes); IR (CH_2Cl_2 cast) 2928, 1543, 1465 cm^{-1} ; 1H NMR (500

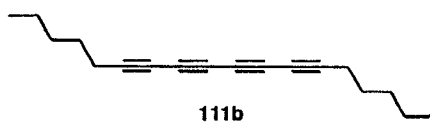
MHz, CDCl₃) δ 2.36-2.32 (m, 4H), 1.61-1.51 (m, 4H), 1.33-1.30 (m, 8H), 0.89 (t, $J = 7.0$ Hz, 6H); ¹³C NMR (125 MHz, CDCl₃, APT) δ 130.2, 100.2, 82.4, 80.6, 36.9, 31.1, 27.3, 22.4, 14.0; EI HRMS m/z calcd. for C₁₈H₂₂⁷⁹Br₂⁸¹Br₂ (M⁺) 557.8414, found 557.8421.

Tetradeca-4,6,8,10-tetrayne (111a).



Dibromoolefin **110a** (0.0935 g, 0.186 mmol) in hexanes (5 mL) was subjected to rearrangement according to general procedure E using *n*-BuLi (2.5 M in hexanes, 0.20 mL, 0.50 mmol) to afford **111a** (0.0229 g, 67%) as a colorless oil: $R_f = 0.56$ (hexanes); IR (CH₂Cl₂ cast) 2966, 2225, 1958 cm⁻¹; ¹H NMR (500 MHz, CDCl₃) δ 2.26 (t, $J = 7.0$ Hz, 4H), 1.55 (sextet, $J = 7.3$ Hz, 4H), 0.97 (t, $J = 7.4$ Hz, 6H); ¹³C NMR (125 MHz, CDCl₃, APT) δ 80.3, 65.9, 61.4, 60.6, 21.6, 21.5, 13.5; EI HRMS m/z calcd. for C₁₄H₁₄ (M⁺) 182.1096, found 182.1103. Compound **111a** has been previously reported.²³

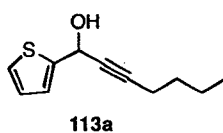
Octadeca-6,8,10,12-tetrayne (111b).



Dibromoolefin **110b** (0.0966 g, 0.173 mmol) in hexanes (5 mL) was subjected to rearrangement according to general procedure E using *n*-BuLi (2.5 M in hexanes, 0.17 mL, 0.43 mmol) to afford **111b** (0.0274 g, 66%) as a colorless

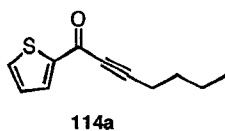
oil: $R_f = 0.59$ (hexanes); IR (CH_2Cl_2 cast) 2931, 2226 cm^{-1} ; ^1H NMR (500 MHz, CDCl_3) δ 2.28 (t, $J = 7.1$ Hz, 4H), 1.53 (p, $J = 7.3$ Hz, 4H), 1.36-1.27 (m, 8H), 0.88 (t, $J = 7.1$ Hz, 6H); ^{13}C NMR (125 MHz, CDCl_3 , APT) δ 80.5, 65.7, 61.5, 60.7, 31.0, 27.7, 22.2, 19.5, 14.0; EI HRMS m/z calcd. for $\text{C}_{18}\text{H}_{22}$ (M^+) 238.1722, found 238.1721. Spectral data are consistent with those reported previously.²⁴

1-(2-Thienyl)hept-2-yn-1-ol (113a).



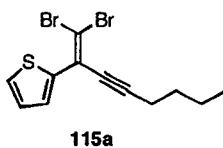
To 1-hexyne (1.46 g, 18.3 mmol) in Et_2O (50 mL) was added $n\text{-BuLi}$ (11.4 mL, 1.6 M in hexanes, 18.2 mmol) and 2-thiophene carboxaldehyde (1.88 g, 16.7 mmol) in Et_2O (5 mL) according to general procedure A to ultimately afford **113a** (3.04 g, 94%) as a yellow oil: $R_f = 0.14$ (hexanes/ CH_2Cl_2 1:1); IR (CH_2Cl_2 cast) 3374, 3105, 2957, 2932, 2871, 2227, 1652, 1538, 1465, 1251 cm^{-1} ; ^1H NMR (400 MHz, CDCl_3) δ 7.26 (dd, $J = 5.1, 1.2$ Hz, 1H), 7.14 (dd, $J = 3.5, 1.2$ Hz, 1H), 6.95 (dd, $J = 5.0, 3.5$ Hz, 1H), 5.62 (s, 1H), 2.37 (bs, 1H), 2.27 (dt, $J = 7.0, 2.0$ Hz, 2H), 1.53 (p, $J = 7.0$ Hz, 2H), 1.43 (sextet, $J = 7.0$ Hz, 2H), 0.91 (t, $J = 7.0$ Hz, 3H); ^{13}C NMR (100 MHz, CDCl_3 , APT) δ 145.5, 126.7, 125.8, 125.3, 87.1, 79.4, 60.4, 30.5, 21.9, 18.4, 13.5; EI HRMS m/z calcd. for $\text{C}_{11}\text{H}_{14}\text{OS}$ (M^+) 194.0765, found 194.0761.

1-(2-Thienyl)hept-2-yn-1-one (114a).



Alcohol **113a** (1.95 g, 10.3 mmol) in CH_2Cl_2 was subjected to oxidation according to general procedure B using celite (2.6 g), molecular sieves (4Å, 2.6 g), and PCC (2.60 g, 12.1 mmol) to afford **114a** (1.62 g, 82%) as a red oil: $R_f = 0.36$ (hexanes/ CH_2Cl_2 1:1); IR (CH_2Cl_2 cast) 3103, 2958, 2229, 2202, 1623, 1515, 1465, 1257 cm^{-1} ; ^1H NMR (400 MHz, CDCl_3) δ 7.87 (dd, $J = 3.8, 1.2$ Hz, 1H), 7.66 (dd, $J = 4.9, 1.2$ Hz, 1H), 7.12 (dd, $J = 4.9, 3.8$ Hz, 1H), 2.46 (t, $J = 7.0$ Hz, 2H), 1.62 (p, $J = 7.0$ Hz, 2H), 1.49 (sextet, $J = 7.2$ Hz, 2H), 0.94 (t, $J = 7.3$ Hz, 3H); ^{13}C NMR (100 MHz, CDCl_3 , APT) δ 170.0, 145.1, 134.77, 134.76, 128.1, 95.3, 79.3, 29.7, 22.0, 18.8, 13.5; EI HRMS m/z calcd. for $\text{C}_{11}\text{H}_{12}\text{OS}$ (M^+) 192.0609, found 192.0610.

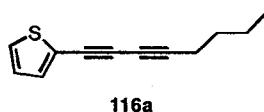
2-(1-Dibromomethylene-2-heptynyl)thiophene (**115a**).



Ketone **114a** (0.043 g, 0.223 mmol) in CH_2Cl_2 (1 mL) was subjected to dibromoolefination according to general procedure D using CBr_4 (0.100 g, 0.325 mmol) and PPh_3 (0.177 g, 0.650 mmol) in CH_2Cl_2 (5 mL). Another equivalent of CBr_4 and PPh_3 was required for completion of the reaction. After work-up as per general procedure D, purification by column chromatography (hexanes/ CH_2Cl_2 1:1) afforded **115a** (0.013 g, 16%) as a yellow oil: $R_f = 0.75$ (hexanes/ CH_2Cl_2 1:1); IR (CH_2Cl_2 cast) 2956, 2223, 1464 cm^{-1} ; ^1H NMR (400 MHz, CDCl_3) δ 7.57

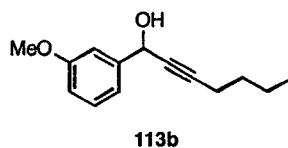
(dd, $J = 3.8, 1.2$ Hz, 1H), 7.35 (dd, $J = 5.1, 1.2$ Hz, 1H), 7.00 (dd, $J = 5.1, 3.8$ Hz, 1H), 2.41 (t, $J = 7.0$ Hz, 2H), 1.63-1.56 (m, 2H), 1.52-1.43 (m, 2H), 0.93 (t, $J = 7.3$ Hz, 3H); ^{13}C NMR (100 MHz, CDCl_3 , APT) δ 139.3, 130.1, 127.3, 126.5, 124.6, 99.3, 95.2, 80.2, 30.3, 22.0, 19.4, 13.6; MS (EI, 70 eV) m/z 347.9 (M^+ , 100); EI HRMS m/z calcd. for $\text{C}_{12}\text{H}_{12}\text{S}^{79}\text{Br}^{81}\text{Br}$ (M^+) 347.9006, found 347.9019.

1-(2-Thienyl)-1,3-octadiyne (116a).



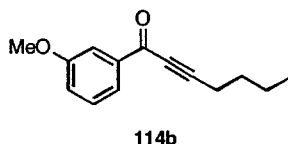
Dibromoolefin **115a** (0.0709 g, 0.204 mmol) in hexanes (12 mL) was subjected to rearrangement according to general procedure E using *n*-BuLi (0.15 mL, 1.6 M in hexanes, 0.24 mmol) to provide diyne **116a** (0.0329 g, 86%) as a yellow oil: $R_f = 0.7$ (hexanes); IR (CH_2Cl_2 cast) 3106, 2957, 2231, 2151, 1465, 1425 cm^{-1} ; ^1H NMR (400 MHz, CDCl_3) δ 7.25 (dd, $J = 3.7, 1.1$ Hz, 1H), 7.23 (dd, $J = 5.1, 1.1$ Hz, 1H), 6.94 (dd, $J = 5.1, 3.7$ Hz, 1H), 2.36 (t, $J = 7.0$ Hz, 2H), 1.59-1.51 (m, 2H), 1.48-1.41 (m, 2H), 0.92 (t, $J = 7.3$ Hz, 3H); ^{13}C NMR (100 MHz, CDCl_3 , APT) δ 133.8, 127.9, 127.0, 122.5, 87.0, 78.5, 67.6, 64.9, 30.2, 21.9, 19.4, 13.5; EI HRMS m/z calcd. for $\text{C}_{12}\text{H}_{12}\text{S}$ (M^+) 188.0660, found 188.0662.

1-(3-Methoxyphenyl)hept-2-yn-1-ol (113b).



To 1-hexyne (1.54 g, 19.3 mmol) in Et₂O (50 mL) was added *n*-BuLi (12.1 mL, 1.6 M in hexanes, 19.4 mmol) and *m*-anisaldehyde (2.37 g, 17.4 mmol) in Et₂O (5 mL) according to general procedure A to ultimately afford **113b** (3.33 g, 88%) as a yellow oil: *R*_f = 0.11 (hexanes/CH₂Cl₂ 1:1); IR (CH₂Cl₂ cast) 3405, 2957, 2872, 2226, 1601, 1587, 1488, 1466, 1259 cm⁻¹; ¹H NMR (400 MHz, CDCl₃) δ 7.29-7.25 (m, 1H), 7.11-7.10 (m, 2H), 6.84 (m, 1H), 5.40 (s, 1H), 3.81 (s, 3H), 2.26 (t, *J* = 7.0, 2.0 Hz, 2H), 2.13 (bs, 1H), 1.53 (p, *J* = 7.0 Hz, 2H), 1.45-1.38 (m, 2H), 0.89 (t, *J* = 7.3 Hz, 3H); ¹³C NMR (100 MHz, CDCl₃, APT) δ 159.8, 142.9, 129.5, 118.9, 113.9, 112.0, 87.6, 79.8, 64.8, 55.2, 30.6, 22.0, 18.5, 13.5; EI HRMS *m/z* calcd. for C₁₄H₁₈O₂ (M⁺) 218.1307, found 218.1301.

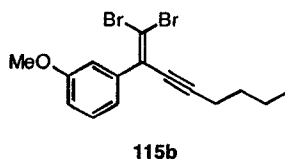
1-(3-Methoxyphenyl)hept-2-yn-1-one (114b).



Alcohol **113b** (2.32 g, 10.6 mmol) in CH₂Cl₂ (125 mL) was subjected to oxidation according to general procedure B using celite (2.7 g), molecular sieves (4Å, 2.7 g), and PCC (2.74 g, 12.8 mmol) to afford **114b** (1.13 g, 49%) as a yellow oil: *R*_f = 0.35 (hexanes/CH₂Cl₂ 1:1); IR (CH₂Cl₂ cast) 2958, 2221, 1645, 1595, 1582, 1484, 1465, 1430 cm⁻¹; ¹H NMR (400 MHz, CDCl₃) δ 7.75 (dd, *J* = 7.3, 1.4 Hz, 1H), 7.63 (dd, *J* = 2.5, 1.4 Hz, 1H), 7.35 (t, *J* = 7.9 Hz, 1H), 7.13 (ddd, *J* = 8.5, 2.5, 1.4 Hz, 1H), 3.83 (s, 3H), 2.47 (t, *J* = 7.1 Hz, 2H), 1.68-1.60 (m, 2H), 1.53-1.44 (m, 2H), 0.94 (t, *J* = 7.3 Hz, 3H); ¹³C NMR (100 MHz, CDCl₃, APT) δ 177.9, 160.0, 138.3, 129.5, 122.7, 120.7, 112.9, 96.6, 79.7, 55.4, 29.8,

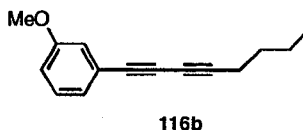
22.0, 18.9, 13.5; EI HRMS m/z calcd. for $C_{14}H_{16}O_2$ (M^+) 216.1150, found 216.1146.

1-(1-Dibromomethylenehept-2-ynyl)-3-methoxybenzene (115b).



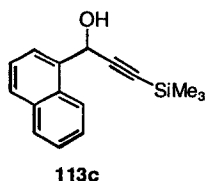
Ketone **114b** (0.880 g, 4.67 mmol) in CH_2Cl_2 (5 mL) was subjected to dibromoolefination according to general procedure D using CBr_4 (1.65 g, 4.99 mmol) and PPh_3 (2.89 g, 10.9 mmol) in CH_2Cl_2 (125 mL). Purification by column chromatography (hexanes/ CH_2Cl_2 1:1) afforded **115b** (0.126 g, 7%) as a yellow/orange oil: $R_f = 0.70$ (hexanes/ CH_2Cl_2 1:1); IR (CH_2Cl_2 cast) 2956, 2215, 1597, 1580 cm^{-1} ; 1H NMR (500 MHz, $CDCl_3$, APT) δ 7.26 (t, $J = 8.0$ Hz, 1H), 6.99 (d, $J = 7.6$ Hz, 1H), 6.94-6.93 (m, 1H), 6.86 (dd, $J = 2.8, 8.0$ Hz, 1H), 3.80 (s, 3H), 2.34 (t, $J = 7.0$ Hz, 2H), 1.54 (tt, $J = 6.8, 7.7$ Hz, 2H), 1.44 (sextet, $J = 7.4$ Hz, 2H), 0.90 (t, $J = 7.3$ Hz, 3H); ^{13}C NMR (125 MHz, $CDCl_3$) δ 159.2, 139.7, 131.1, 129.2, 120.8, 114.0, 113.9, 100.1, 97.4, 80.5, 55.3, 30.4, 22.0, 19.6, 13.6; EI HRMS m/z calcd. for $C_{15}H_{16}O^{79}Br^{81}Br$ (M^+) 371.9547, found 371.9549.

1-(3-Methoxyphenyl)-1,3-octadiyne (116b).



Dibromoolefin **115b** (0.121 g, 0.325 mmol) in hexanes (12 mL) was subjected to rearrangement according to general procedure E using *n*-BuLi (0.23 mL, 1.6 M in hexanes, 0.37 mmol) to afford **116b** (0.0633 g, 92%) as a yellow oil; $R_f = 0.6$ (hexanes/CH₂Cl₂ 2:1); IR (CH₂Cl₂ cast) 3072, 3002, 2958, 2242, 2152, 1601, 1594, 1574, 1489, 1427 cm⁻¹; ¹H NMR (400 MHz, CDCl₃) δ 7.19 (t, $J = 8.0$ Hz, 1H), 7.05 (dd, $J = 1.0, 1.5$ Hz, 1H), 6.98 (dd, $J = 2.6, 1.5$ Hz, 1H), 6.87 (ddd, $J = 8.0, 2.6, 1.0$ Hz, 1H), 3.77 (s, 3H), 2.35 (t, $J = 7.0$ Hz, 2H), 1.58-1.51 (m, 2H), 1.48-1.41 (m, 2H), 0.92 (t, $J = 7.3$ Hz, 3H); ¹³C NMR (100 MHz, CDCl₃, APT) δ 159.2, 129.5, 125.1, 123.1, 117.2, 115.7, 84.9, 74.6, 74.2, 65.0, 55.3, 30.3, 21.9, 19.3, 13.5; EI HRMS m/z calcd. for C₁₅H₁₆O (M⁺) 212.1201, found 212.1200.

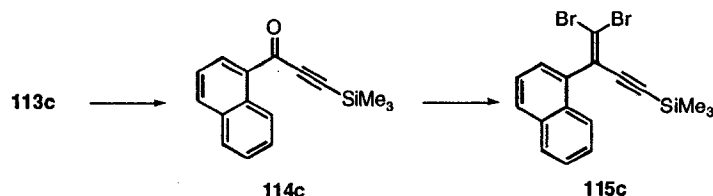
1-(1-Naphthyl)-3-trimethylsilyl-prop-2-yn-1-ol (**113c**).



To (trimethylsilyl)acetylene (0.945 g, 9.62 mmol) in Et₂O (10 mL) was added *n*-BuLi (3.8 mL, 2.5 M in hexanes, 9.5 mmol) and 1-naphthaldehyde (1.5 g, 1.3 mL, 9.6 mmol) according to general procedure A to ultimately afford **113c** (1.54 g, 63%) as a yellow oil: $R_f = 0.25$ (hexanes/CH₂Cl₂ 1:1); IR (CH₂Cl₂ cast) 3364, 3050, 2959, 2173, 1598, 1250 cm⁻¹; ¹H NMR (500 MHz, CDCl₃) δ 8.28 (d, $J = 8.4$ Hz, 1H), 7.87-7.82 (m, 3H), 7.56-7.45 (m, 3H), 6.11 (d, $J = 5.0$ Hz, 1H), 2.24 (d, $J = 5.0$ Hz, 1H), 0.20 (s, 9H); ¹³C NMR (125 MHz, CDCl₃, APT) δ 135.3,

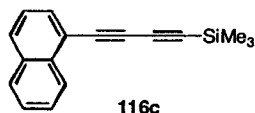
133.9, 130.6, 129.3, 128.6, 126.3, 125.8, 125.2, 124.7, 123.9, 104.7, 92.4, 63.3, -0.1; EI HRMS m/z calcd. for $C_{16}H_{18}OSi$ (M^+) 254.1127, found 254.1126.

[4,4-Dibromo-3-(1-naphthyl)-buten-1-ynyl]trimethylsilane (115c).



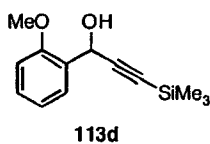
Alcohol **113c** (1.41 g, 5.52 mmol) in CH_2Cl_2 (60 mL) was subjected to oxidation according to general procedure B using celite (2 g), molecular sieves (4 Å, 2 g), and PCC (1.99 g, 9.03 mmol) to afford **114c**. The solvent was reduced to ca. 2 mL and ketone **114c** was immediately subjected to dibromoolefination according to general procedure D using CBr_4 (2.48 g, 7.36 mmol) and PPh_3 (3.87 g, 14.7 mmol) in CH_2Cl_2 (75 mL) to afford **115c** (0.984 g, 44%) as a yellow oil: R_f = 0.83 (CH_2Cl_2); IR (CH_2Cl_2 cast) 3058, 2959, 2141, 1593, 1507 cm^{-1} ; 1H NMR (500 MHz, $CDCl_3$) δ 7.99 (d, J = 8.0 Hz, 1H), 7.90-7.88 (m, 2H), 7.60-7.45 (m, 4H), 0.21 (s, 9H); ^{13}C NMR (125 MHz, $CDCl_3$, APT) δ 135.7, 133.6, 129.9, 129.8, 128.9, 128.3, 126.5, 126.3, 126.1, 125.3, 125.0, 104.8, 102.81, 102.80, -0.2; EI HRMS m/z calcd. for $C_{17}H_{16}Si^{79}Br^{81}Br$ (M^+) 407.9368, found 407.9375.

[4-(1-Naphthyl)-1,3-butadiynyl]trimethylsilane (116c).



Dibromoolefin **115c** (0.757 g, 1.85 mmol) in hexanes (25 mL) was subjected to rearrangement according to general procedure E using *n*-BuLi (1.0 mL, 2.5 M in hexanes, 2.5 mmol) to afford diyne **116c** (0.430 g, 93%) as a yellow oil: $R_f = 0.3$ (hexanes); IR (CH₂Cl₂ cast) 3058, 2959, 2199, 2098, 1585, 1505, 1250 cm⁻¹; ¹H NMR (500 MHz, CDCl₃) δ 8.31 (d, $J = 8.1$ Hz, 1H), 7.86 (d, $J = 7.8$ Hz, 1H), 7.83 (d, $J = 8.1$ Hz, 1H), 7.73 (dd, $J = 7.2, 1.1$ Hz, 1H), 7.57 (ddd, $J = 8.3, 6.8, 1.4$ Hz, 1H), 7.51 (ddd, $J = 8.1, 6.8, 1.4$ Hz, 1H), 7.40 (dd, $J = 8.3, 7.2$ Hz, 1H), 0.27 (s, 9H); ¹³C NMR (125 MHz, CDCl₃, APT) δ 134.0, 133.0, 132.2, 129.7, 128.3, 127.1, 126.6, 126.0, 125.1, 119.0, 91.7, 88.0, 78.8, 75.1, -0.2; EI HRMS m/z calcd. for C₁₇H₁₆Si (M⁺) 248.1021, found 248.1019.

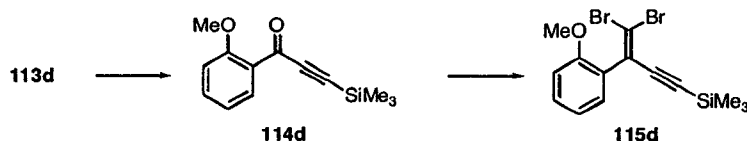
1-(2-Methoxyphenyl)-3-trimethylsilylprop-2-yn-1-ol (**113d**).



To (trimethylsilyl)acetylene (1.10 g, 11.2 mmol) in Et₂O (50 mL) was added *n*-BuLi (4.4 mL, 2.5 M in hexanes, 11.0 mmol) and 2-methoxybenzaldehyde (1.50 g, 11.0 mmol) in Et₂O (5 mL). Due to the insolubility of the aldehyde, the reaction mixture was allowed to warm to room temperature and stirred overnight. Work-up as per general procedure A afforded **113d** (2.33 g, 90%) as a pale yellow oil: $R_f = 0.2$ (hexanes/CH₂Cl₂ 1:1); IR (CH₂Cl₂ cast) 3426, 2959, 2172, 1601, 1590, 1491, 1464 cm⁻¹; ¹H NMR (500 MHz, CDCl₃) δ 7.58-7.56 (m, 1H), 7.29 (m, 1H), 6.97 (m, 1H), 6.89 (d, $J = 8.3$ Hz, 1H), 5.69 (d, $J = 6.0$ Hz, 1H), 3.87 (s, 3H), 2.90 (d, $J = 6.0$ Hz, 1H), 0.19 (s, 9H); ¹³C NMR (125 MHz, CDCl₃, APT) δ

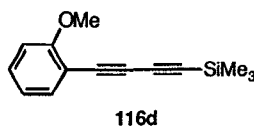
156.8, 129.6, 128.5, 127.9, 120.8, 110.8, 104.5, 90.9, 61.4, 55.6, -0.03; EI MS m/z 234.1 (M^+ , 62); EI HRMS m/z calcd. for $C_{13}H_{18}O_2Si$ (M^+) 234.1076, found 234.1070. Anal. Calcd. for $C_{13}H_{18}O_2Si$: C, 66.62; H, 7.74. Found C, 66.53; H, 7.86. Compound **113d** has been previously reported.²⁵

[4,4-Dibromo-3-(2-methoxyphenyl)-buten-1-ynyl]trimethylsilane (115d).



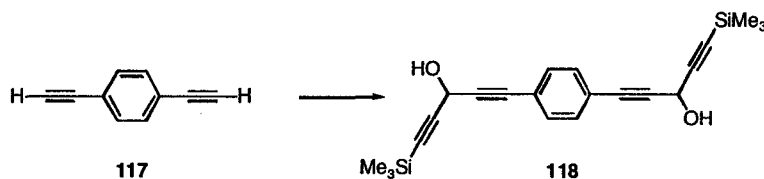
Alcohol **113d** (1.93 g, 8.25 mmol) in CH_2Cl_2 (80 mL) was subjected to oxidation according to general procedure B using celite (3 g), molecular sieves (4Å, 3 g), and PCC (2.77 g, 12.7 mmol) to afford **114d**. The solvent was reduced to ca. 2 mL and ketone **114d** was immediately subjected to dibromoolefination according to general procedure D using CBr_4 (3.53 g, 10.7 mmol) and PPh_3 (5.56 g, 21.3 mmol) in CH_2Cl_2 (100 mL) to afford **115d** (1.91 g, 59%) as a yellow oil: $R_f = 0.85$ (CH_2Cl_2); IR (CH_2Cl_2 cast) 3003, 2959, 2898, 2835, 2149, 1597, 1582, 1542, 1489, 1462 cm^{-1} ; 1H NMR (500 MHz, $CDCl_3$) δ 7.34-7.31 (m, 1H), 7.19 (dd, $J = 5.7, 1.7$ Hz, 1H), 6.93 (dt, $J = 7.4, 1.1$ Hz, 1H), 6.90 (d, $J = 7.4$ Hz, 1H), 3.84 (s, 3H), 0.18 (s, 9H); ^{13}C NMR (125 MHz, $CDCl_3$, APT) δ 155.9, 130.0, 129.7, 127.9, 127.1, 120.5, 111.6, 102.9, 102.8, 102.2, 55.7, -0.2; EI HRMS m/z calcd. for $C_{14}H_{16}OSi^{79}Br^{81}Br$ (M^+) 387.9317, found 387.9325.

[4-(2-Methoxyphenyl)-1,3-butadiynyl]trimethylsilane (116d).



Dibromoolefin **115d** (0.0820 g, 0.211 mmol) in hexanes (12 mL) was subjected to rearrangement according to general procedure E using *n*-BuLi (0.10 mL, 2.5 M in hexanes, 0.25 mmol) to afford **116d** (0.0206 g, 43%) as a yellow oil: $R_f = 0.7$ (hexanes/ CH_2Cl_2 1:1); IR (CH_2Cl_2 cast) 2959, 2836, 2204, 2103, 1594, 1273 cm^{-1} ; ^1H NMR (500 MHz, CDCl_3) δ 7.43-7.42 (m, 1H), 7.30 (m, 1H), 6.89-6.84 (m, 2H), 3.86 (s, 3H), 0.21 (s, 9H); ^{13}C NMR (125 MHz, CDCl_3 , APT) δ 161.6, 134.5, 130.7, 120.4, 110.6, 91.0, 88.1, 77.9, 73.3, 55.8, -0.2 (one coincident peak not observed); EI HRMS m/z calcd. for $\text{C}_{14}\text{H}_{16}\text{OSi}$ (M^+) 228.0971, found 228.0967.

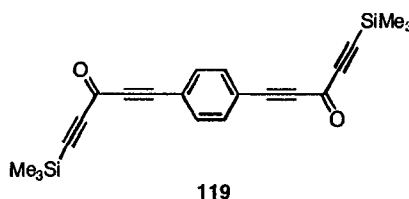
Compound (118).



To 1,4-diethynylbenzene **117** (0.949 g, 7.53 mmol) in THF (25 mL) was added *n*-BuLi (2.5 M in hexanes, 6.00 mL, 15.0 mmol) and 3-trimethylsilyl-1-propynal (2.00 g, 15.8 mmol) in Et_2O (5 mL) according to general procedure A. Purification by crystallization from hexanes at -4 °C afforded **118** (1.19 g, 42%) as a colorless solid, presumably as a mixture of stereoisomers: Mp 99 °C; $R_f = 0.2$ (CH_2Cl_2); IR (μscope) 3314, 2959, 2237, 2177, 1500 cm^{-1} ; ^1H NMR (300 MHz, CDCl_3) δ 7.42 (s, 4H), 5.34 (d, $J = 6$ Hz, 2H), 2.41 (d, $J = 6$ Hz, 2H), 0.21 (s,

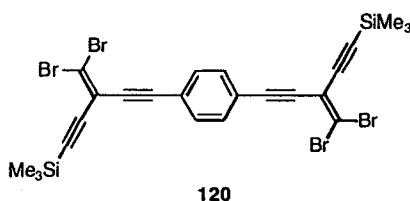
18H); ^{13}C NMR (75.5 MHz, CDCl_3) δ 131.7, 122.4, 101.6, 90.0, 87.8, 83.8, 53.0, -0.3; EI MS m/z 378.1 (M^+ , 72), 73.0 ($[\text{Me}_3\text{Si}]^+$, 100); EI HRMS m/z calcd. for $\text{C}_{22}\text{H}_{26}\text{O}_2\text{Si}_2$ (M^+) 378.1471, found 378.1468. Anal. Calcd. for $\text{C}_{22}\text{H}_{26}\text{O}_2\text{Si}_2$ (378.61): C, 69.79; H, 6.92. Found: C, 69.61; H, 7.02.

1,4-Bis-(5-trimethylsilyl-3-one-penta-1,4-diyne)-benzene (119).



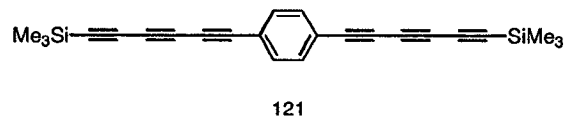
Alcohol **118** (1.0 g, 2.6 mmol) in CH_2Cl_2 (100 mL) was subjected to oxidation according to general procedure B using celite (1.5 g), molecular sieves (4 Å, 1.5 g), and PCC (1.43 g, 6.63 mmol). Purification by crystallization from hexanes at -4 °C afforded **119** (0.78 g, 80%) as a yellow solid: Mp 101 °C; R_f = 0.3 (CH_2Cl_2); IR (μscope) 3090, 2961, 2208, 2151, 1613, 1143 cm^{-1} ; ^1H NMR (300 MHz, CDCl_3) δ 7.65 (s, 4H), 0.28 (s, 18H); ^{13}C NMR (75.5 MHz, CDCl_3) δ 160.1, 133.3, 122.2, 102.5, 100.3, 91.1, 89.3, -0.9; EI HRMS m/z calcd. for $\text{C}_{22}\text{H}_{22}\text{O}_2\text{Si}_2$ (M^+) 374.1158, found 374.1150. Anal. Calcd. for $\text{C}_{22}\text{H}_{22}\text{O}_2\text{Si}_2$ (374.58): C, 70.54; H, 5.92. Found: C, 70.32; H, 5.94.

Compound (120).



Dione **119** (0.681 g, 1.82 mmol) in CH₂Cl₂ (5 mL) was subjected to dibromoolefination according to general procedure D using CBr₄ (1.51 g, 4.56 mmol) and PPh₃ (2.40 g, 9.16 mmol) in CH₂Cl₂ (80 mL). Purification by column chromatography (silica gel, hexanes) afforded **120** (1.05 g, 85%) as a yellow solid: Mp 68-69 °C; *R*_f = 0.3 (hexanes); IR (μscope) 3044, 2898, 2207, 2157, 1515, 1249 cm⁻¹; ¹H NMR (300 MHz, CDCl₃) δ 7.49 (s, 4H), 0.25 (s, 18H); ¹³C NMR (75.5 MHz, CDCl₃) δ 131.7, 122.9, 114.1, 109.8, 103.0, 100.0, 95.1, 88.1, -0.4; EI HRMS *m/z* calcd. for C₂₄H₂₂⁷⁹Br₂⁸¹Br₂Si₂ (M⁺) 685.7953, found 685.7945; Anal. Calcd. for (686.23): C₂₄H₂₂Br₄Si₂ C, 42.01; H, 3.23. Found: C, 42.12; H, 3.37.

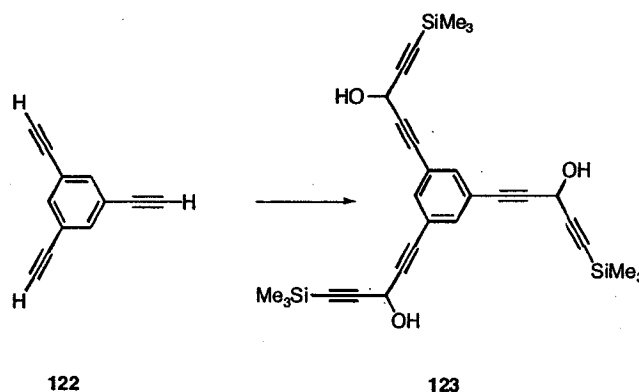
Bis-1,4-[6-(trimethylsilyl)-1,3,5-hexatriynyl]benzene (121).



Dibromoolefin **120** (0.173 g, 0.252 mmol) in hexanes (15 mL) was subjected to rearrangement according to general procedure E using *n*-BuLi (2.5 M in hexane, 0.24 mL, 0.60 mmol). Due to the insolubility of **120**, *n*-BuLi was added at -44 °C instead of -78 °C. Purification by column chromatography (silica gel, hexanes) provided **121** (0.0463 g, 50%) as a pale yellow solid: Mp 180 °C (decomp.); *R*_f = 0.42 (hexanes); IR (μscope) 2956, 2167, 2075, cm⁻¹; ¹H NMR (300 MHz, CDCl₃) δ 7.44 (s, 4H), 0.20 (s, 18H); ¹³C NMR (75 MHz, CDCl₃) δ 133.0, 122.2, 90.2, 87.9, 77.2, 75.9, 68.4, 61.2, -0.5; EI MS *m/z* 366 (M⁺, 98), 351

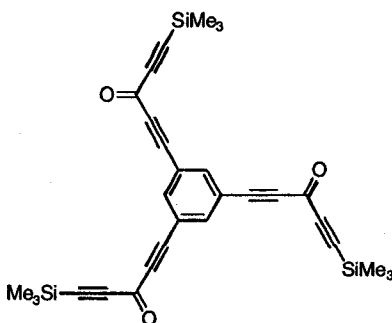
($[M - CH_3]^+$, 100); EI HRMS m/z calcd. for $C_{24}H_{22}Si_2$ 366.1260 (M^+), found 366.1265.

Compound (123).



To 1,3,5-triethynylbenzene **122** (1.49 g, 4.06 mmol) in Et_2O (50 mL) was added n -BuLi (2.5 M in hexane, 4.90 mL, 12.2 mmol) and 3-trimethylsilyl-1-propynal (1.90 g, 15.1 mmol) in Et_2O (5 mL) according to general procedure A. Column chromatography (hexanes/ Et_2O 7:3) afforded **123** (0.891 g, 42%) as a viscous light yellow oil, presumably a mixture of stereoisomers, that solidified under refrigeration. **123**: Mp 59 °C; R_f = 0.3 (hexanes/ Et_2O 95:5); IR (CH_2Cl_2 cast) 3313, 2959, 2225, 2179 cm^{-1} ; 1H NMR (300 MHz, $CDCl_3$) δ 7.51 (s, 3H), 5.35 (d, J = 7.3 Hz, 3H), 2.62 (d, J = 7.3 Hz, 3H), 0.25 (s, 27H); ^{13}C NMR (75.5 MHz, $CDCl_3$) δ 135.0, 122.7, 101.3, 90.2, 87.3, 82.3, 52.9, -0.4; EI MS m/z 528.2 (M^+ , 5), 73.0 ($[Me_3Si]^+$, 100); EI HRMS m/z calcd. for $C_{30}H_{36}O_3Si_3$ (M^+) 528.1972, found 528.1959.

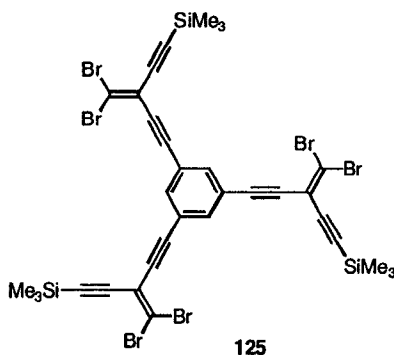
Compound (124).



124

Triol **123** (0.851 g, 1.61 mmol) in CH_2Cl_2 (150 mL) was subjected to oxidation according to general procedure B using celite (1.2 g), molecular sieves (4 Å, 1.2 g), and PCC (2.19 g, 10.2 mmol). Purification by column chromatography (silica gel, CH_2Cl_2) afforded **124** (0.665 g, 79%) as a light yellow oil: $R_f = 0.2$ (hexanes/ CH_2Cl_2 2:1); IR (CH_2Cl_2 cast) 2962, 2200, 2154, 1632, 1583 cm^{-1} ; ^1H NMR (300 MHz, CDCl_3) δ 7.83 (s, 3H), 0.26 (s, 27H); ^{13}C NMR (75.5 MHz, CDCl_3) δ 159.5, 138.6, 121.5, 102.2, 100.8, 90.0, 86.2, -0.6; EI MS m/z 522.2 (M^+ , 56), 73.0 ($[\text{Me}_3\text{Si}]^+$, 100); EI HRMS m/z calcd. for $\text{C}_{30}\text{H}_{30}\text{O}_3\text{Si}_3$ (M^+) 522.1503, found 522.1499.

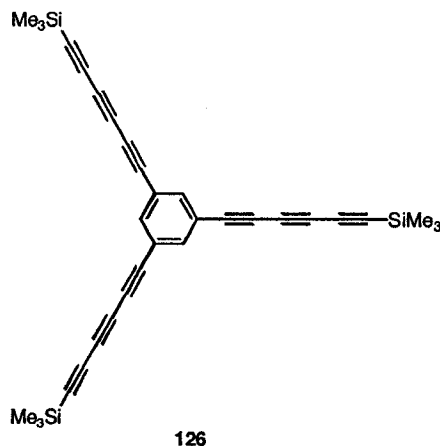
Compound (125).



125

Trione **124** (0.665 g, 1.27 mmol) in CH_2Cl_2 (5 mL) was subjected to dibromoolefination according to general procedure D using CBr_4 (1.62 g, 4.89 mmol) and PPh_3 (2.57 g, 9.82 mmol) in CH_2Cl_2 (150 mL). Purification by column chromatography (silica gel, hexanes/ CH_2Cl_2 2:1) to afford **125** (0.806 g, 64%) as a yellow oil: $R_f = 0.7$ (hexane/ CH_2Cl_2 2:1); IR (CH_2Cl_2 cast) 2960, 2216, 2153, 1582, 1250 cm^{-1} ; ^1H NMR (300 MHz, CDCl_3) δ 7.61 (s, 3H), 0.24 (s, 27H); ^{13}C NMR (50 MHz, CDCl_3) δ 134.6, 123.2, 113.8, 110.4, 103.2, 99.8, 93.2, 87.3, -0.5; ESI MS (CH_2Cl_2 , with AgOTf added) m/z 1098.6 ($[\text{M} + \text{Ag}^+]$, 100); HRMS calcd. for $\text{C}_{33}\text{H}_{30}^{79}\text{Br}_3^{81}\text{Br}_3\text{Si}_3^{109}\text{Ag}$ ($[\text{M} + \text{Ag}^+]$) 1098.5742, found 1098.5750.

Tris-1,3,5-[6-(trimethylsilyl)-1,3,5-hexatriynyl]benzene (126).

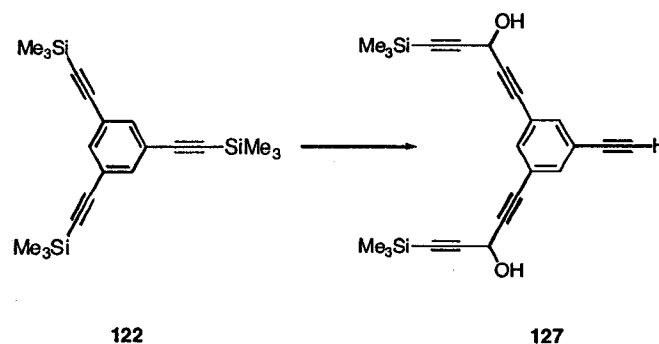


Dibromoolefin **125** (0.174 g, 0.176 mmol) in hexanes (20 mL) was subjected to rearrangement according to general procedure E using *n*-BuLi (2.5 M in hexane, 0.25 mL, 0.63 mmol) to afford **126** (0.0317 g, 35%) as a creme colored solid: Mp 160 °C; $R_f = 0.5$ (hexanes); IR (CH_2Cl_2 cast) 2960, 2168, 2074, 1575 cm^{-1} ; ^1H NMR (300 MHz, CDCl_3) δ 7.65 (s, 3H), 0.23 (s, 27H); ^{13}C NMR (75

MHz, CDCl₃, APT) δ 138.1, 122.8, 90.9, 87.6, 76.3, 74.1, 68.2, 60.9, -0.6; EI

HRMS m/z calcd. for C₃₃H₃₀Si₃ 510.1655 (M⁺), found 510.1648.

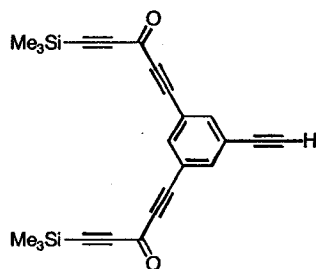
Compound (127).



1,3,5-Tris-(1-trimethylsilylethynyl)benzene **122** (1.56 g, 4.25 mmol) and K₂CO₃ (0.4 g, 2 mmol) were added to wet THF/MeOH (50 mL, 1:1 v/v) and stirred until TLC analysis showed complete desilylation, 2h. Et₂O was added, the solution washed with saturated satd. aq. NH₄Cl, and dried over MgSO₄. The solvent was reduced to ca. 10 mL and added to dried Et₂O (250 mL). *n*-BuLi (2.5 M in hexanes, 5.1 mL, 13 mmol) was subsequently added at -78 °C and allowed to stir for an hour. 3-Trimethylsilylpropynal (1.67 g, 13.2 mmol) was added and general procedure A was followed. Column chromatography (silica gel, hexanes/CH₂Cl₂ 8:2), gave **127** (0.623 g, 36%) as an orange oil. R_f = 0.13 (hexanes/CH₂Cl₂ 4:1); IR (CH₂Cl₂ cast) 3291(OH and \equiv C-H), 2960, 2235, 2179, 1584 cm⁻¹; ¹H NMR (400 MHz, CDCl₃) δ 7.50-7.48 (m, 3H), 5.30 (s, 2H), 3.08 (s, 2H), 2.51 (s, 1H), 0.19 (s, 18H); ¹³C NMR (100 MHz, CDCl₃) δ 135.3, 135.0, 122.9, 122.8, 101.3, 90.2, 87.3, 82.3, 81.6, 78.8, 52.9, -0.4; EI MS m/z 402.1 (M⁺,

9), 73.0 ($[\text{Me}_3\text{Si}]^+$, 100); EI HRMS m/z calcd. for $\text{C}_{24}\text{H}_{26}\text{O}_2\text{Si}_2$ (M^+) 402.1471, found 402.1459.

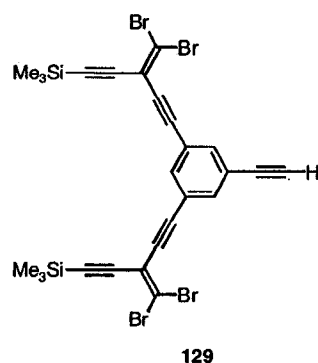
Compound (128).



128

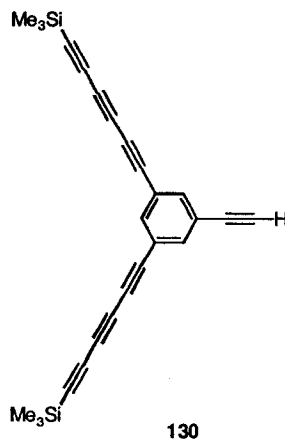
Alcohol **127** (0.0220 g, 0.0546 mmol) in CH_2Cl_2 (20 mL) was subjected to oxidation according to general procedure B using celite (0.1 g), molecular sieves (4 Å, 0.1 g), and PCC (0.037 g, 0.17 mmol) to afford **128** (0.0142 g, 65%) as a white solid: Mp 72-74 °C; R_f = 0.71 (hexanes/ Et_2O 7:3); IR (CH_2Cl_2 cast) 3289, 2962, 2210, 2153, 2103, 1631 cm^{-1} ; ^1H NMR (400 MHz, CDCl_3) δ 7.80-7.78 (m, 1H), 7.77-7.76 (m, 2H), 3.18 (s, 1H), 0.27 (s, 18H); ^{13}C NMR (100 MHz, CDCl_3 , APT) δ 159.8, 138.2, 137.0, 124.1, 121.0, 102.3, 100.6, 89.7, 87.3, 80.4, -0.9 (one coincident signal not observed); EI HRMS m/z calcd. for $\text{C}_{24}\text{H}_{22}\text{O}_2\text{Si}_2$ (M^+) 398.1158, found 398.1160.

Compound (129).



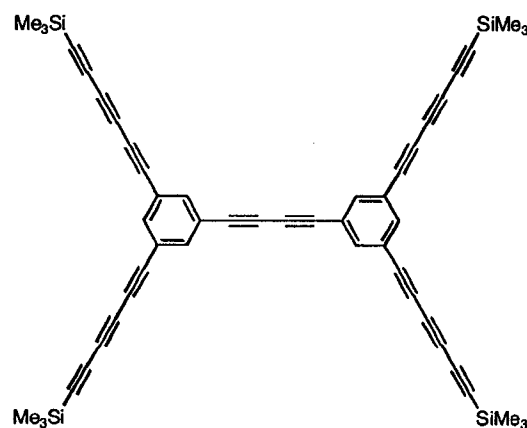
Ketone **128** (0.156 g, 0.392 mmol) in CH_2Cl_2 (3 mL) was subjected to dibromoolefination according to general procedure D using CBr_4 (0.316 g, 0.954 mmol) and PPh_3 (0.514 g, 1.96 mmol) in CH_2Cl_2 (50 mL) to afford **129** (0.151 g, 56%) as a white solid: Mp 118-120 °C; $R_f = 0.78$ (hexanes/ CH_2Cl_2 1:1); IR (CH_2Cl_2 cast) 3298, 2959, 2211, 2153, 1581 cm^{-1} ; ^1H NMR (400 MHz, CDCl_3) δ 7.61-7.59 (m, 3H), 3.10 (s, 1H), 0.24 (s, 18H); ^{13}C NMR (100 MHz, CDCl_3 , APT) δ 135.3, 134.4, 123.2, 123.1, 113.8, 110.3, 103.2, 102.5, 99.8, 93.3, 87.2, 79.0, -0.5; EI MS m/z 402.1 (M^+ , 40), 73.0 ($[\text{Me}_3\text{Si}]^+$, 100); EI HRMS m/z calcd. for $\text{C}_{26}\text{H}_{22}^{79}\text{Br}_2^{81}\text{Br}_2\text{Si}_2$ (M^+) 709.7953, found 709.7975.

1-Ethynyl-3,5-bis[6-(trimethylsilyl)-1,3,5-hexatriynyl]benzene (130).



Dibromoolefin **129** (0.151 g, 0.213 mmol) in hexanes (25 mL) was subjected to rearrangement according to general procedure E using *n*-BuLi (2.5 in hexanes, 0.25 mL, 0.63 mmol). Due to the insolubility of **129**, *n*-BuLi was added at $-44\text{ }^{\circ}\text{C}$ instead of $-78\text{ }^{\circ}\text{C}$. Following work-up, the reaction mixture was passed through a short column (silica gel, hexanes) to give the crude product **130** (0.06 g, ca. 70%) as a relatively unstable compound if taken to dryness, but of sufficient purity (>95%) to be taken on directly to the next step. $R_f = 0.38$ (hexanes); IR (CDCl₃, cast) 3299, 2960, 2169, 2075, 1578 cm⁻¹; ¹H NMR (400 MHz, CDCl₃) δ 7.58 (s, 3H), 3.12 (s, 1H), 0.22 (s, 18H); ¹³C NMR (125 MHz, CDCl₃, APT) δ 136.9, 123.5, 122.1, 89.9, 87.7, 80.9, 79.5, 75.9, 74.1, 67.8, 60.9, 53.4, -0.5 ; EI MS m/z 390.1 (M⁺, 39), 73.0 ([Me₃Si]⁺, 100); EI HRMS m/z calcd. for C₂₆H₂₂Si₂ (M⁺) 390.1260, found 390.1258.

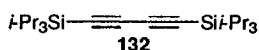
1,4-[Bis-1-[3,5-bis[6-(trimethylsilyl)-1,3,5-hexatriynyl]phenyl]butadiyne
(**131**).



131

Compound **130** (0.0295 g, 0.0755 mmol) was subjected to oxidative homocoupling by addition of **130** to a solution of CuI (0.026 g, 0.14 mmol) and TMEDA (1 mL) in CH₂Cl₂ (35 mL) at rt, previously stirred until homogeneous. TLC analysis indicated reaction was complete after 0.5 h. Purification by column chromatography (silica gel, hexanes) afforded **131** (0.0092 g, 31%) as a white solid: *R_f* = 0.31 (hexanes); IR (CH₂Cl₂ cast) 2959, 2168, 2074, 1574 cm⁻¹; ¹H NMR (400 MHz, CD₂Cl₂, 25 °C) δ 7.65-7.64 (m, 6H), 0.23 (s, 36H); ¹³C NMR (100 MHz, CD₂Cl₂, APT) δ 137.9, 137.7, 123.2, 122.7, 90.8, 87.6, 80.0, 76.2, 75.4, 74.2, 68.1, 60.8, -0.6; ESI MS (nitromethane, with AgOTf added) *m/z* 887 [M + Ag⁺, 100]

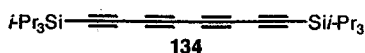
1,4-Bis(triisopropylsilyl)-1,3-tetradiyne (132).



Mp 98-100 °C. *R_f* = 0.84 (hexanes). UV-Vis (hexanes) λ_{max} (ε) 208 (48 000)nm; IR (CH₂Cl₂, cast) 2945, 2866, 2061, 1463 cm⁻¹; ¹H NMR (500 MHz, CD₂Cl₂) δ 1.09 (s, 42H) ; ¹³C NMR (125 MHz, CD₂Cl₂) δ 90.4, 82.2, 18.8, 11.8. EI MS *m/z* 362.3 (M⁺, 38), 319.2 ([M - *i*-Pr]⁺, 100); EI HRMS *m/z* calcd. for C₂₂H₄₂Si₂ (M⁺) 362.2825, found 362.2818. Spectral data are consistent with those reported previously.⁶

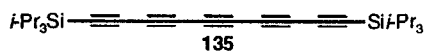
For triyne **133**, see **96a**.

1,8-Bis(triisopropylsilyl)-1,3,5,7-octatetrayne (134).



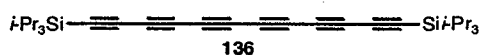
Mp 72-75 °C. $R_f = 0.87$ (hexanes). UV-vis (hexanes) λ_{max} (ϵ) 260 (157 000), 248 (130 000), 239 (84 000) nm; IR (CH_2Cl_2 , cast) 2944, 2866, 2042, 1462 cm^{-1} ; ^1H NMR (500 MHz, CD_2Cl_2) δ 1.09 (s, 42H); ^{13}C NMR (125 MHz, CD_2Cl_2) δ 89.7, 86.5, 62.4, 61.3, 18.7, 11.7. EI MS m/z 362.3 (M^+ , 38), 319.2 ($[\text{M} - i\text{-Pr}]^+$, 100); EI HRMS m/z calcd. for $\text{C}_{26}\text{H}_{42}\text{Si}_2$ (M^+) 410.2825, found 410.2825.

1,10-Bis(triisopropylsilyl)-1,3,5,7,9-decapentayne (135).



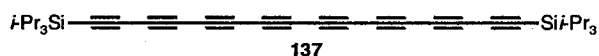
Dibromoolefin **141** (0.270, 0.357 mmol) in hexanes (25 mL) was subjected to rearrangement according to general procedure E using *n*-BuLi (2.5 M in hexanes, 0.34 mL, 0.857 mmol). Purification by column chromatography (silica gel, hexanes) afforded **135** (0.0697 g, 45%) as a white solid: Mp 104-105 °C; $R_f = 0.79$ (hexanes); UV-vis (hexanes) λ_{max} (ϵ) 284 (293 500), 268 (205 300), 255 (89 800), 242 (42 000) nm; IR (CH_2Cl_2 , cast) 2943, 2178, 2030, 1461 cm^{-1} ; ^1H NMR (500 MHz, CD_2Cl_2) δ 1.09 (s, 42 H); ^{13}C NMR (125 MHz, CD_2Cl_2) δ 89.5, 87.4, 62.7, 62.5, 61.3, 18.7, 11.7. EI MS m/z 434.3 (M^+ , 37), 391.2 ($[\text{M} - i\text{-Pr}]^+$, 100); EI HRMS m/z calcd. for $\text{C}_{28}\text{H}_{42}\text{Si}_2$ (M^+) 434.2825, found 434.2822. Compound **135** has been reported previously.^{10,11}

1,12-Bis(triisopropylsilyl)-1,3,5,7,9,11-dodecahexayne (136).



Dibromoolefin **146** (0.198 g, 0.254 mmol) in hexanes (16 mL) was subjected to rearrangement according to general procedure E using *n*-BuLi (2.5 M in hexanes, 0.22 mL, 0.55 mmol). Purification by column chromatography (silica gel, hexanes) provided **136** (0.0816 g, 70%) as a yellow solid: Mp 78-80 °C; $R_f = 0.87$ (hexanes); UV-vis (hexanes) $\lambda_{\max} (\epsilon)$ 304 (359 200), 286 (262 000), 271 (111 900), 258 (43 100), 245 (24 200) nm; IR (CH_2Cl_2 , cast) 2866, 2158, 2030, 1462 cm^{-1} ; ^1H NMR (500 MHz, CD_2Cl_2) δ 1.09 (s, 42 H); ^{13}C NMR (125 MHz, CD_2Cl_2) δ 89.5, 87.9, 63.0, 62.8, 62.5, 61.2, 18.7, 11.8. EI MS m/z 458.3 (M^+ , 42), 415.2 ($[\text{M} - i\text{-Pr}]^+$, 100); EI HRMS m/z calcd. for $\text{C}_{30}\text{H}_{42}\text{Si}_2$ (M^+) 458.2825, found 458.2834.

1,16-Bis(triisopropylsilyl)-1,3,5,7,9,11,13,15-hexadecaoctayne (137).



Dibromoolefin **150** (0.394 g, 0.476 mmol) in hexanes (50 mL) was subjected to rearrangement according to general procedure E using *n*-BuLi (2.5 M in hexanes, 0.45 mL, 1.13 mmol). The solution was allowed to warm up to -20 °C, then quenched with satd. aq. NH_4Cl (20 mL). Et_2O was added (20 mL), the organic layer was separated, dried (MgSO_4) and solvent removed in vacuo. Purification by column chromatography (silica gel, hexanes), followed by recrystallization (hexanes/ CH_2Cl_2 1:1) afforded **137** (0.0241 g, 10%) as a light brown solid: Mp 93-95 °C; $R_f = 0.95$ (hexanes); UV-vis (hexanes) $\lambda_{\max} (\epsilon)$ 339 (603 000), 319 (505 400), 301 (237 100), 285 (89 200), 271 (31 700) nm; IR (CH_2Cl_2 , cast) 2943, 2119, 2021, 1958, 1461 cm^{-1} ; ^1H NMR (500 MHz, CD_2Cl_2) δ

1.08 (s, 42 H); ^{13}C NMR (125 MHz, CD_2Cl_2) δ 89.4, 88.5, 63.4, 63.4, 63.1, 62.6, 62.3, 61.1, 18.7, 11.7. ESI MS (nitromethane, AgOTf added) m/z 674 ($[\text{M} + \text{Ag}^+ + \text{solvent}]$, 30), 1121 ($[\text{2M} + \text{Ag}]^+$, 100).

First attempted synthesis of decayne 138 from octabromide 154

Dibromoolefin **154** (0.103 g, 0.0864 mmol) in hexanes (50 mL) at $-78\text{ }^\circ\text{C}$ was subjected to rearrangement by the slow addition of *n*-BuLi (2.5 M in hexanes, 0.17 mL, 0.43 mmol) over a period of five minutes. The solution was allowed to warm up to $-20\text{ }^\circ\text{C}$ over a period of 2 h, then quenched with satd. aq. NH_4Cl (50 mL). Et_2O (50 mL) was added, the organic layer separated, washed with satd. aq. NH_4Cl ($2 \times 50\text{ mL}$) and the solvent removed *in vacuo*. No decayne was observed in the black, carbonaceous product mixture, only products presumably resulting from incomplete rearrangement of the four dibromoolefin moieties.

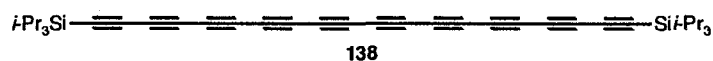
Second attempted synthesis of decayne 138 from octabromide 154.

Dibromoolefin **154** (0.137 g, 0.115 mmol) in hexanes (50 mL) at $-78\text{ }^\circ\text{C}$ was subjected to rearrangement by the slow addition of *n*-BuLi (2.5 M in hexanes, 0.21 mL, 0.53 mmol) over a period of five minutes. The solution was allowed to warm up to $0\text{ }^\circ\text{C}$ over a period of 2 h, then quenched with satd. aq. NH_4Cl (50 mL). Et_2O (50 mL) was added, the organic layer separated, washed with satd. aq. NH_4Cl ($2 \times 50\text{ mL}$) and the solvent removed *in vacuo*. No decayne was observed in the black, carbonaceous product mixture, only products presumably resulting from incomplete rearrangement of the four dibromoolefin moieties.

Third attempted synthesis of decayne 138 from octabromide 154.

Dibromoolefin **154** (0.153 g, 0.128 mmol) in hexanes (75 mL) at $-78\text{ }^{\circ}\text{C}$ was subjected to rearrangement by the slow addition of *n*-BuLi (2.5 M in hexanes, 0.23 mL, 0.58 mmol) over a period of five minutes. The solution was allowed to warm up to rt over a period of 2 h, then quenched with satd. aq. NH_4Cl (50 mL). Et_2O (50 mL) was added, the organic layer separated, washed with satd. aq. NH_4Cl ($2 \times 50\text{ mL}$) and the solvent removed *in vacuo*. Neither decayne, nor products resulting from incomplete rearrangement, were observed in the black, carbonaceous product mixture.

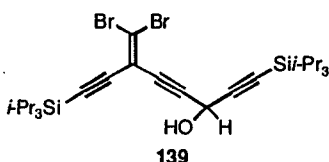
1,20-Bis(triisopropylsilyl)-1,3,5,7,9,11,13,15,17,19-einacosadecayne (138).



Dibromoolefin **153** (0.407 g, 0.607 mmol) in hexanes (30 mL) at $-78\text{ }^{\circ}\text{C}$ was subjected to rearrangement by the addition of *n*-BuLi (2.5 M in hexanes, 0.58 mL, 1.46 mmol) over a period of two minutes. The solution was allowed to warm up to $-5\text{ }^{\circ}\text{C}$ over an hour and a half, then quenched with satd. aq. NH_4Cl (10 mL). Hexanes (20 mL) was added, the organic layer separated, and the crude reaction mixture passed through a plug of silica (hexanes) and the solvent removed *in vacuo* to produce a ca. 10 mL solution of **155**. To this solution was added MeOH/THF (100 mL, 1:1 v/v) and K_2CO_3 (0.1 g, 0.7 mmol) and the mixture was stirred at rt until TLC showed complete desilylation, ca. 0.25 hr. Et_2O (50 mL) and satd. aq. NH_4Cl (50 mL) were added, the organic layer

separated, dried (MgSO₄), and reduced to ca. 60 mL, then added to a – 10 °C solution of CuCl (0.121 g, 1.23 mmol) and TMEDA (0.75 mL) in CH₂Cl₂ (175 mL), the solution having been previously oxygenated by passing O₂ through for 0.5 h. Upon addition of **155**, the solution turned reddish-brown. The reaction was monitored by TLC and within 15 minutes was quenched with satd. aq. NH₄Cl (100 mL). Et₂O (100 mL) was added (20 mL), the organic layer was separated, dried (MgSO₄) and solvent removed *in vacuo*. Purification by column chromatography (silica, hexanes, then alumina, hexanes) afforded **138** (0.051 g, 30%) as an orange solid: Mp 105-113 °C (decomp.); *R_f* = 0.88 (hexanes); UV-vis (hexanes) λ_{max} (ε) 369 (753 400), 345 (633 400), 325 (326 000), 308 (130 800), 293 (47 300) nm; IR (CH₂Cl₂, cast) 2923, 2072 (doublet), 1462 cm⁻¹; ¹H NMR (500 MHz, CD₂Cl₂) δ 1.08 (s, 42 H); ¹³C NMR (125 MHz, CD₂Cl₂) δ 89.3, 88.8, 63.8, 63.6, 63.5, 63.2, 62.9, 62.5, 62.2, 61.0, 18.7, 11.7. MS (MALDI, retinoic acid matrix) 555.3 (MH⁺).

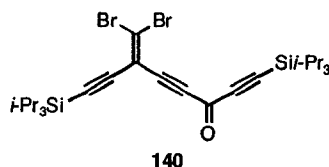
1,8-Bis(triisopropylsilyl)-3(dibromomethylidene)-6-hydroxy-octa-1,4,7-triynes (139).



Enediyne **96c** (1.18 g, 2.55 mmol) and K₂CO₃ (0.11 g, 0.77 mmol) were added to wet MeOH/THF (50 mL, 1:1 v/v) and stirred at rt until TLC analysis showed complete desilylation, ca. 1 h. Hexanes (50 mL) and satd. aq. NH₄Cl (50 mL) were added, the organic layer separated, washed with satd. aq. NH₄Cl (6 × 50

mL), dried (MgSO₄), passed through a plug of alumina, and the solvent removed. To the terminal acetylene **102** in Et₂O (100 mL) at -78 °C was added LDA (0.60 M, 4.4 mL, 2.6 mmol), which was formed according to general procedure H. After stirring for 1 hr, triisopropylsilylpropargylaldehyde (0.499 g, 2.37 mmol) was added in one portion and the solution warmed to rt. Et₂O (100 mL) and satd. aq. NH₄Cl (100 mL) were added, the organic phase separated, dried (MgSO₄), and the solvent reduced to give an orange oil. Purification by column chromatography (silica gel, hexanes/CH₂Cl₂ 1:1) afforded **139** (0.760 g, 50%) as a yellow oil: *R*_f = 0.38 (hexanes/CH₂Cl₂ 1:1); IR (CH₂Cl₂, cast) 3385, 2943, 2151, 1660 cm⁻¹; ¹H NMR (400 MHz, CDCl₃) δ 5.23 (d, *J* = 8.1, 1H), 2.32 (d, *J* = 8.3, 1H), 1.08 (s, 21 H), 1.06 (s, 21 H); ¹³C NMR (100 MHz, CDCl₃, APT) δ 113.6, 110.4, 102.7, 101.5, 100.2, 92.1, 86.9, 80.4, 53.1, 18.5 (2×), 11.1 (2×). EI MS *m/z* 600.1 (M⁺, 20), 75.0 (100); EI HRMS *m/z* calcd. for C₂₇H₄₄OSi₂⁷⁹Br⁸¹Br (M⁺) 600.1277, found 600.1285.

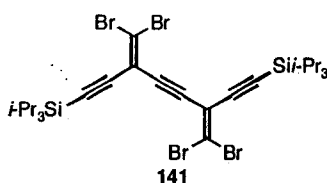
1,8-Bis(triisopropylsilyl)-3-(dibromomethylidene)-octa-1,4,7-triyne-6-one
(**140**).



Alcohol **139** (0.151 g, 0.250 mmol) in CH₂Cl₂ (25 mL) was subjected to oxidation according to general procedure B using celite (0.1 g), molecular sieves (4 Å, 0.1 g), and PCC (0.0881 g, 0.409 mmol). Purification by column chromatography silica gel, hexanes/CH₂Cl₂ 2:1) afforded **140** (0.103 g, 69%) as a

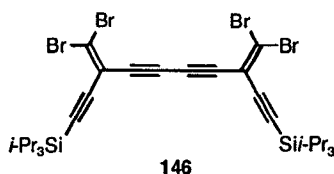
yellow oil: $R_f = 0.70$ (hexanes/ CH_2Cl_2 1:1); IR (CH_2Cl_2 , cast) 2944, 2235, 2190, 2149, 1633 cm^{-1} ; ^1H NMR (500 MHz, CDCl_3) δ 1.09 (s, 42 H); ^{13}C NMR (125 MHz, CDCl_3 , APT) δ 159.4, 116.2, 112.7, 104.6, 102.3, 100.2, 99.1, 92.6, 85.6, 18.6, 18.5, 11.2, 11.1; EI MS m/z 598.1 (M^+ , 2), 555 ($[\text{M} - i\text{-Pr}]^+$, 100); EI HRMS m/z calcd. for $\text{C}_{27}\text{H}_{42}\text{Si}_2\text{O}^{79}\text{Br}^{81}\text{Br}$ (M^+) 598.1121, found 598.1150.

1,8-Bis(triisopropylsilyl)-3,6-bis(dibromomethylidene)-1,4,7-octatriyne (141).



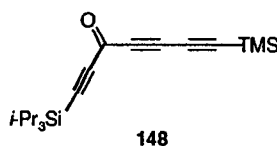
Ketone **140** (0.0991 g, 0.166 mmol) in CH_2Cl_2 (2 mL) was subjected to dibromoolefination according to general procedure D using CBr_4 (0.0922 g, 0.278 mmol) and PPh_3 (0.145 g, 0.553 mmol) in CH_2Cl_2 (5 mL). Purification by column chromatography (silica gel, hexanes) afforded **141** (0.0745 g, 60%) as a colorless solid: Mp 65-67 $^\circ\text{C}$; $R_f = 0.78$ (hexanes/ CH_2Cl_2 1:1); IR (CH_2Cl_2 , cast) 2942, 2151, 1462 cm^{-1} ; ^1H NMR (500 MHz, CD_2Cl_2) δ 1.08 (s, 42 H); ^{13}C NMR (125 MHz, CDCl_3 , APT) δ 114.1, 110.2, 101.2, 100.4, 91.5, 18.7, 11.2. EI MS m/z 754.0 (M^+ , 65), 157 ($[i\text{-Pr}_3\text{Si}]^+$, 100); EI HRMS m/z calcd. for $\text{C}_{28}\text{H}_{42}\text{Si}_2^{79}\text{Br}_2^{81}\text{Br}_2$ (M^+) 753.9518, found 753.9519. Anal. Calcd. for $\text{C}_{28}\text{H}_{42}\text{Si}_2^{79}\text{Br}_2^{81}\text{Br}_2$: C, 44.58; H, 5.61. Found: C, 44.38; H, 5.43.

1,10-Bis(triisopropylsilyl)-3,8-bis(dibromomethylidene)-deca-1,4,6,9-tetrayne (146).



Enediyne **96c** (0.190 g, 0.411 mmol) was subjected to desilylation and oxidative homocoupling according to general procedure G using K_2CO_3 (0.030 g, 0.217 mmol) in MeOH/THF (20 mL, 1:1 v/v) and CuI (0.0485 g, 0.25 mmol) and TMEDA (1 mL, 6.6 mmol) in CH_2Cl_2 (20 mL). Purification by column chromatography (silica gel, hexanes) afforded **146** (0.0873 g, 55%) as an off-white solid. Mp 64-65 °C. $R_f = 0.71$ (hexanes). IR (CH_2Cl_2 , cast) 2943, 2152, 1462 cm^{-1} ; 1H NMR (360 MHz, CD_2Cl_2) δ 1.20 (s, 42H); ^{13}C NMR (75 MHz, CD_2Cl_2 , APT) δ 113.9, 113.3, 102.0, 101.0, 80.9, 79.3, 18.7, 11.5. EI HRMS m/z calcd. for $C_{30}H_{42}Si_2^{79}Br_2^{81}Br_2$ (M^+) 777.9518, found 777.9527. Anal. Calcd. for $C_{30}H_{42}Si_2Br_4$: C, 46.29; H, 5.44. Found: C, 46.67; H, 5.55.

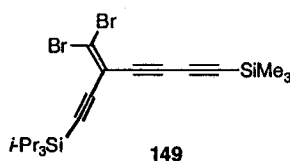
1-Triisopropylsilyl-7-trimethylsilylhepta-1,4,6-tri-ene-3-one (148).



Propynoic acid (5.05 g, 22.0 mmol) was subjected to Friedel-Crafts acylation according to general procedure C using thionyl chloride (7.89 g, 66.4 mmol), bis(trimethylsilyl)butadiyne (4.54 g, 23.4 mmol) and $AlCl_3$ (3.57 g, 26.8 mmol) in CH_2Cl_2 (250 ml). Purification by passage of the crude reaction mixture through a silica plug (hexanes/ CH_2Cl_2 1:1) afforded **148** (5.81, 80%) as an orange-yellow oil: $R_f = 0.70$ (hexanes/ CH_2Cl_2 1:1); IR (CH_2Cl_2 cast) 2946, 2196,

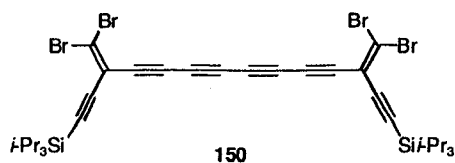
2149, 2030, 1628 cm^{-1} ; ^1H NMR (400 MHz, CDCl_3) δ 1.09 (s, 21H), 0.18 (s, 9H); ^{13}C NMR (75 MHz, CDCl_3 , APT) δ 159.0, 104.6, 99.1, 98.8, 85.8, 75.4, 74.2, 18.5, 11.1, -0.8. EI MS m/z 330.2 (M^+ , 42), 287.1 ($[\text{M} - i\text{-Pr}]^+$, 100); EI HRMS calcd. for $\text{C}_{19}\text{H}_{30}\text{OSi}_2$ (M^+) 330.1835, found 330.1828.

1-Triisopropylsilyl-7-trimethylsilyl-3-(dibromomethylidene)hepta-1,4,6-triyne (149).



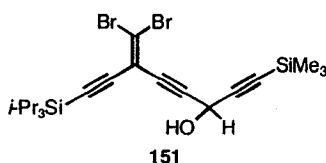
Ketone **148** (5.13 g, 15.5 mmol) in CH_2Cl_2 (5 mL) was subjected to dibromoolefination according to general procedure D using CBr_4 (6.23 g, 18.8 mmol) and PPh_3 (10.5 g, 40.1 mmol) in CH_2Cl_2 (400 mL). Purification by column chromatography (silica gel, hexanes) afforded **149** (3.15 g, 42%) as a yellow oil: R_f = 0.88 (hexanes/ CH_2Cl_2 1:1); IR (CH_2Cl_2 cast) 2944, 2106, 1463 cm^{-1} ; ^1H NMR (400 MHz, CDCl_3) δ 1.09 (s, 21H), 0.21 (s, 9H); ^{13}C NMR (75 MHz, CDCl_3 , APT) δ 113.6, 112.3, 101.0, 100.8, 94.9, 87.3, 80.1, 72.4, 18.6, 11.2, -0.5; EI MS m/z 486.0 (M^+ , 30), 73.0 ($[\text{Me}_3\text{Si}]^+$, 100); EI HRMS m/z calcd. for $\text{C}_{20}\text{H}_{30}\text{Si}_2^{79}\text{Br}^{81}\text{Br}$ (M^+) 486.0232, found 486.0229. Anal. Calcd. for $\text{C}_{20}\text{H}_{30}\text{Si}_2^{79}\text{Br}^{81}\text{Br}$: C, 49.38; H, 6.22. Found: C, 49.63; H, 6.17.

1,14-Bis(triisopropylsilyl)-3,12-bis(dibromomethylidene)tetradeca-1,4,6,8,10,13-hexayne (150).



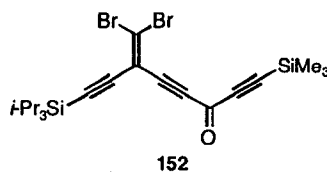
A mixture of **149** (1.95 g, 4.01 mmol) and K_2CO_3 (0.0120 g, 0.086 mmol) in MeOH/THF (100 mL, 1:1 v/v) was stirred at rt until TLC showed complete desilylation, ca. 0.25 h. Et_2O (100 mL) and satd. aq. NH_4Cl (100 mL) were added, the organic layer extracted, dried over $MgSO_4$, and the solvent reduced to ca. 5 mL. The deprotected vinyl bromide was then added to a 0 °C solution of $CuCl$ (0.403 g, 4.07 mmol) and TMEDA (1 mL) in CH_2Cl_2 (400 mL), the solution having been previously oxygenated by passing O_2 through for 0.5 h. The reaction was monitored by TLC and after 0.5 h was quenched with satd. aq. NH_4Cl (200 mL), extracted, dried ($MgSO_4$) and reduced to give a red-brown oil. Purification by column chromatography (silica gel, hexanes) afforded **150** (0.807 g, 48%) as a bright yellow solid: Mp 65-67 °C; $R_f = 0.64$ (hexanes); IR (CH_2Cl_2 cast) 2943, 2198, 2149, 2124, 2075, 1462 cm^{-1} ; 1H NMR (400 MHz, $CDCl_3$) δ 1.09 (s, 42H); ^{13}C NMR (75 MHz, $CDCl_3$, APT) δ 114.5, 113.2, 102.0, 100.4, 80.0, 74.1, 70.4, 64.8, 18.6, 11.2; ES MS m/z 996 ($[M + Ag^+ + CH_3NO_2]^+$, 100). Anal. Calcd. for $C_{34}H_{42}Si_2^{79}Br_2^{81}Br_2$: C, 49.41; H, 5.12. Found: C, 49.10; H, 5.04.

3-(Bromomethylidene)-6-hydroxy-1-triisopropylsilyl-8-trimethylsilyl-octa-1,4,7-triynyl (151).



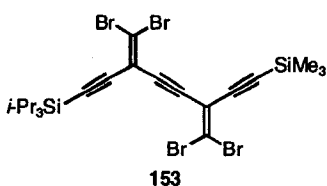
Enediyne **96c** (2.89 g, 6.25 mmol) and K_2CO_3 (0.25 g, 1.8 mmol) were added to wet MeOH/THF (100 mL, 1:1 v/v) and stirred at rt until TLC analysis showed complete desilylation, ca. 1 h. Hexanes (100 mL) and satd. aq. NH_4Cl (100 mL) were added, the organic layer separated, washed with satd. aq. NH_4Cl (6 \times 100 mL), dried ($MgSO_4$), passed through a plug of alumina, and the solvent removed. To the terminal acetylene **102** in Et_2O (250 mL) at $-78^\circ C$ was added LDA (1.2 M, 5.4 mL, 6.5 mmol), which was formed according to general procedure H. After stirring for 1 hr, trimethylsilylpropargylaldehyde (1.90 g, 15.0 mmol) was added in one portion and the solution warmed to rt. Et_2O (100 mL) and satd. aq. NH_4Cl (100 mL) were added, the organic phase separated, dried ($MgSO_4$), and the solvent reduced to give an orange oil. Purification by column chromatography (silica gel, hexanes/ CH_2Cl_2 1:1) afforded **151** (1.49 g, 46%) as a yellow oil: $R_f = 0.32$ (hexanes); IR (CH_2Cl_2 , cast) 3361, 2944, 2180, 2153, 1463 cm^{-1} ; 1H NMR (400 MHz, $CDCl_3$) δ 5.21 (d, $J = 6.4$, 1H), 2.25 (d, $J = 7.6$, 1H), 1.09 (s, 21H), 0.17 (s, 9H); ^{13}C NMR (100 MHz, $CDCl_3$, APT) δ 113.6, 110.4, 101.5, 100.6, 100.3, 91.9, 90.5, 80.8, 53.1, 18.6, 11.1, -0.4 ; EI MS m/z 516 (M^+ , 16), 473 ($[M - i-Pr]^+$, 50), 73 ($[Me_3Si]^+$, 100); EI HRMS m/z calcd. for $C_{21}H_{32}OSi_2^{79}Br^{81}Br$ (M^+) 516.0338, found 516.0334.

3-(Dibromomethylidene)-1-triisopropylsilyl-8-trimethylsilyl-octa-1,4,7-triyne-6-one (152).



Alcohol **151** (3.40 g, 6.59 mmol) in CH_2Cl_2 (100 mL) was subjected to oxidating according to general procedure B using celite (1.5 g), molecular sieves (4 Å, 1.5 g), and PCC (1.75 g, 8.14 mmol). The crude solution was filtered through a plug (silica gel, CH_2Cl_2), solvent reduced to give a yellow oil and the product was carried directly to dibromoolefination reaction: $R_f = 0.38$ (hexanes/ CH_2Cl_2 2:1); IR (CH_2Cl_2 , cast) 2944, 2236, 2190, 2153, 2102, 1633 cm^{-1} ; ^1H NMR (400 MHz, CDCl_3) δ 1.09 (s, 21H), 0.24 (s, 9H); ^{13}C NMR (100 MHz, CDCl_3 , APT) δ 159.7, 116.1, 112.7, 102.4, 102.2, 101.1, 100.3, 92.4, 86.1, 18.5, 11.1, -1.0; EI MS m/z 514 (M^+ , 1), 471 ($[\text{M} - i\text{-Pr}]^+$, 100); EI HRMS m/z calcd. for $\text{C}_{21}\text{H}_{30}\text{OSi}_2^{79}\text{Br}^{81}\text{Br}$ (M^+) 514.0181, found 514.0178.

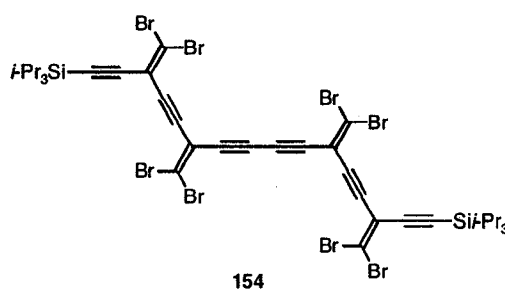
3,6-Bis-(dibromomethylidene)-1-triisopropylsilyl-8-trimethylsilyl-octa-1,4,7-triyne (153).



Crude ketone **152** in CH_2Cl_2 (5 mL) was subjected to dibromoolefination according to general procedure D using CBr_4 (2.76 g, 8.32 mmol) and PPh_3 (4.34 g, 16.5 mmol) in CH_2Cl_2 (100 mL). Purification by column chromatography (silica gel, hexanes/ CH_2Cl_2 1:1) afforded **153** (3.22 g, 73%) as a light yellow oil: $R_f = 0.81$ (hexanes/ CH_2Cl_2 2/1); IR (CH_2Cl_2 , cast) 2943, 2153, 1462 cm^{-1} ; ^1H

NMR (500 MHz, CDCl₃) δ 1.09 (s, 21H), 0.20 (s, 9H); ¹³C NMR (100 MHz, CDCl₃, APT) δ 114.1, 113.9, 110.5, 110.2, 103.3, 101.2, 100.5, 99.3, 91.7, 91.3, 18.6, 11.2, -0.5; EI MS *m/z* 669.9 (M⁺, 13), 73.0 ([C₃H₉Si]⁺, 100); EI HRMS *m/z* calcd. for C₂₂H₃₀Si₂⁷⁹Br₂⁸¹Br₂ (M⁺) 669.8579, found 669.8567.

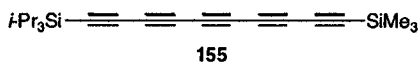
3,6,11,14-Tetra(dibromomethylidene)-1,16-di(triisopropylsilyl)-hexadeca-1,4,7,9,12,16-hexayne (154).



A mixture of **153** (1.11 g, 1.66 mmol) and K₂CO₃ (0.0796 g, 0.577 mmol) in MeOH/THF (100 mL, 1:1 v/v) was stirred at rt until TLC showed complete desilylation, ca. 0.5 h. Et₂O (100 mL) and satd. aq. NH₄Cl (100 mL) were added, the organic layer extracted, dried (MgSO₄), and the solvent reduced to ca. 5 mL. The deprotected vinyl bromide was then added to a solution of CuCl (0.202 g, 2.10 mmol) and TMEDA (2 mL) in CH₂Cl₂ (200 mL) at 0 °C, the solution having been previously oxygenated by passing O₂ through for 0.5 h. The reaction was monitored by TLC and after 0.3 h was quenched with satd. aq. NH₄Cl (200 mL), extracted, dried (MgSO₄) and reduced to give a red-brown oil. Purification by column chromatography (silica gel, hexanes) afforded **154** (0.241 g, 25%) as a yellow solid: *R_f* = 0.48 (hexanes); ¹H NMR (500 MHz, CDCl₃) δ 1.13 (s, 42H);

^{13}C NMR (100 MHz, CD_2Cl_2 , APT) δ 114.4, 114.2, 113.2, 111.4, 101.6, 101.3, 93.0, 90.3, 80.2, 79.9, 18.8, 11.5.

1-Triisopropylsilyl-10-trimethylsilyl-1,3,5,7,9-decapentayne (155).



Dibromoolefin **153** (0.203, 0.303 mmol) in hexanes (25 mL) was subjected to rearrangement according to general procedure E using *n*-BuLi (2.5 M in hexanes, 0.29 mL, 0.73 mmol) to provide **155** (0.0733, 69%) as a yellow oil: R_f = 0.71 (hexanes); IR (CH_2Cl_2 , cast) 2945, 2158, 2101, 1462 cm^{-1} ; ^1H NMR (500 MHz, CD_2Cl_2) δ 1.09 (s, 21H), 0.22 (s, 9H); ^{13}C NMR (125 MHz, CD_2Cl_2) δ 89.5, 89.4, 87.5, 87.5, 62.9, 62.8, 62.4, 62.3, 62.1, 61.2, 18.7, 11.7, -0.5.

Rearrangement of 96a in cyclohexene.

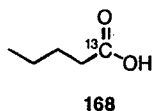
To enediyne **96a** (0.121 g, 0.221 mmol) in cyclohexene (15 mL) at -78 °C was added *n*-BuLi (2.5 M in hexanes, 0.11 mL, 0.27 mmol). The reaction was warmed to -5 °C, then quenched with satd. aq. NH_4Cl (10 mL). Et_2O (10 mL) was added, the organic layer separated, washed with satd. aq. NH_4Cl (2×10 mL), dried (MgSO_4), and the solvent removed *in vacuo* to afford triyne **93a** (0.0553 g, 65%). No evidence of **161** was observed by ^1H NMR analysis.

Rearrangement of 96a in the presence of Et_3SiH

To enediyne **96a** (0.107, 0.187 mmol) in hexanes (5 mL) at -78 °C was added *n*-BuLi (2.5 M in hexanes, 0.090 mL, 0.23 mmol). The reaction was

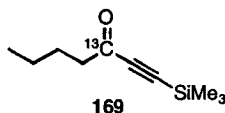
warmed to $-5\text{ }^{\circ}\text{C}$, then quenched with satd. aq. NH_4Cl (5 mL). Et_2O (5 mL) was added, the organic layer separated, washed with satd. aq. NH_4Cl ($2 \times 10\text{ mL}$), dried (MgSO_4), and the solvent removed *in vacuo* to afford triyne **93a** (0.0509 g, 70%). No evidence of **165** was observed by ^1H NMR analysis.

1- ^{13}C -pentanoic acid (**168**).



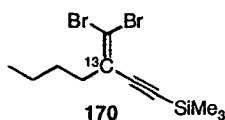
To $\text{Na } ^{13}\text{C}\equiv\text{N}$ **167** (0.982 g, 20.0 mmol) in ethanol (3 mL) and water (1 mL) was added butyl bromide (2.24 g, 16.3 mmol) and the reaction brought to reflux. After stirring overnight, the solution was cooled and filtered into NaOH (0.966 g, 24.1 mmol) in water (2 mL) and the reaction was again brought to reflux and stirred overnight. The ethanol was then allowed to evaporate, 50% sulfuric acid (2 mL) was added and the solution extracted with Et_2O ($2 \times 10\text{ mL}$). The solvent was removed to provide **168** (1.14 g, 68%) as a light yellow oil: IR (CHCl_3 , cast) 3500-2500 (broad carboxylic $-\text{OH}$ peak), 2931, 1668 cm^{-1} ; ^1H NMR (400 MHz, CDCl_3) δ 2.33 (dt, $J = 7.3, 7.4$, 2H), 1.60 (dp, $J = 4.4, 7.4$, 2H), 1.35 (sextet, $J = 7.5$, 2H), 0.90 (t, $J = 7.4$, 3H); ^{13}C NMR (100 MHz, CDCl_3 , APT) δ 180.6, 33.8 (d, $J = 55\text{ Hz}$), 26.7 (d, $J = 2\text{ Hz}$), 22.1 (d, $J = 4\text{ Hz}$), 13.6.

3- ^{13}C -1-trimethylsilyl-1-heptyn-3-one (**169**)



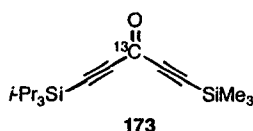
Carboxylic acid **168** (0.947 g, 9.27 mmol) was subjected to Friedel-Crafts acylation according to general procedure C using thionyl chloride (3 mL), bis(trimethylsilyl)acetylene (1.636 g, 9.60 mmol) and AlCl₃ (1.249 g, 9.30 mmol) in CH₂Cl₂ (25 mL). Purification by column chromatography (silica gel, hexanes/CH₂Cl₂ 1:1) afforded **169** (0.799 g, 47%) as a light brown oil: *R*_f = 0.45 (hexanes/CH₂Cl₂ 1:1); IR (CH₂Cl₂ cast) 2961, 2150, 1639 cm⁻¹; ¹H NMR (400 MHz, CDCl₃) δ 2.52 (dt, *J* = 7.1, 2H), 1.62 (dp, *J* = 4.5, 7.4, 2H), 1.32 (sextet, *J* = 7.6, 2H), 0.89 (t, *J* = 7.4, 3H), 0.21 (s, 9H); ¹³C NMR (100 MHz, CDCl₃, APT) δ 188.2, 102.0 (d, *J* = 79 Hz), 97.4 (d, *J* = 9 Hz), 45.0 (d, *J* = 45 Hz), 26 (d, *J* = 2 Hz), 22.0 (d, 4 Hz), 13.7, -0.8; EI MS *m/z* 183.1 (M⁺, 1), 126.0 ([M - C₄H₉]⁺, 100); EI HRMS *m/z* calcd. for C₉H₁₈SiO¹³C (M⁺) 183.1160, found 183.1148.

3-¹³C-3-(Dibromomethylidene)-1-trimethylsilylhepta-1-yne (170).



Ketone **169** (0.645 g, 3.53 mmol) in CH₂Cl₂ (5 mL) was subjected to dibromoolefination according to general procedure D using CBr₄ (1.43 g, 4.31 mmol) and PPh₃ (2.32 g, 8.85 mmol) in CH₂Cl₂ (50 mL). Purification by column chromatography (silica gel, hexanes) afforded **170** (0.384 g, 32%) as a yellow oil: *R*_f = 0.89 (hexanes/CH₂Cl₂ 1:1); IR (CH₂Cl₂ cast) 2959, 2149, 1465 cm⁻¹; ¹H NMR (400 MHz, CDCl₃) δ 2.33-2.27 (m, 2H), 1.58-1.49 (m, 2H), 1.34 (sextet, *J* = 7.5, 2H), 0.91 (t, *J* = 7.3, 2H), (s, 9H); ¹³C NMR (100 MHz, CDCl₃) δ 131.0, 103.1, 102.7 (d, *J* = 77 Hz), 97.4 (d, *J* = 89 Hz), 36.54 (d, 43 Hz), 29.5 (d, *J* = 2 Hz), 22.1 (d, 4 Hz), 13.9, -0.3; EI MS *m/z* 339.0 (M⁺, 73), 138.9/136.9 (100); EI HRMS *m/z* calcd. for C₁₀H₁₈¹³CSi⁷⁹Br⁸¹Br (M⁺) 338.9558, found 338.9551.

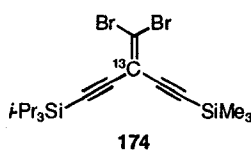
3-¹³C-1,4-Diyne-triisopropylsilyl-5-trimethylsilyl-penta-3-none (173)



Carboxylic acid **172** (1.21 g, 5.33 mmol) was subjected to Friedel-Crafts acylation according to general procedure C using thionyl chloride (4 mL) and bis(trimethylsilyl)acetylene (0.883 g, 518 mmol) and AlCl₃ (0.697 g, 5.22 mmol) in CH₂Cl₂ (25 mL). Purification by column chromatography (silica gel, hexanes/CH₂Cl₂ 2:1) afforded **173** (0.283 g, 17%) as a light yellow oil: *R*_f = 0.60 (hexanes/CH₂Cl₂ 2:1); IR (CH₂Cl₂ cast) 2946, 2155, 2097, 1599 cm⁻¹; ¹H NMR

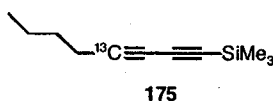
(400 MHz, CDCl₃) δ 1.07 (s, 21H), 0.21 (s, 9H); ¹³C NMR (100 MHz, CDCl₃) δ 159.8, 105.0 (d, *J* = 95 Hz), 103 (d, *J* = 94 Hz), 99.1 (d, *J* = 12 Hz), 97.8 (d, *J* = 12 Hz), 18.3, 11.0, -1.1; EI MS *m/z* 307.2 (M⁺, 22), 264.1 ([M - C₃H₇]⁺, 100); EI HRMS *m/z* calcd. for C₁₆H₃₀¹³CSi₂O (M⁺) 307.1869, found 307.1866.

3-¹³C-3-(Dibromomethylidene)-1-triisopropylsilyl-5-trimethylsilyl-penta-1,4-diyne (174).



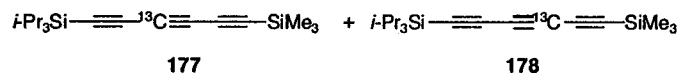
Ketone **173** (0.246 g, 0.803 mmol) in CH₂Cl₂ (1 mL) was subjected to dibromoolefination according to general procedure D using CBr₄ (0.356 g, 1.07 mmol) and PPh₃ (0.538 g, 2.05 mmol) in CH₂Cl₂ (10 mL). Purification by column chromatography (silica gel, hexanes) afforded **174** (0.286 g, 77%) as a yellow oil: *R_f* = 0.68 (hexanes); IR (CH₂Cl₂ cast) 2944, 2156, 2113, 1463 cm⁻¹; ¹H NMR (400 MHz, CDCl₃) δ 1.09 (s, 21 H), 0.21 (s, 9H); ¹³C NMR (100 MHz, CDCl₃) δ 114.7, 109.4 (d, *J* = 93 Hz), 102.4 (d, *J* = 9 Hz), 102.0 (d, *J* = 93), 100.4 (d, 93 Hz), 99.7 (d, 9 Hz), 18.6, 11.2, -0.5; EI MS *m/z* 463.0 (M⁺, 42), 420.0 ([M - C₃H₇]⁺, 80), 73.0 ([Me₃Si]⁺, 100); EI HRMS *m/z* calcd. for C₁₇H₃₀¹³CSi₂⁷⁹Br⁸¹Br (M⁺) 463.0266, found 463.0287.

4-¹³C-1-Trimethylsilyl-octa-1,3-diyne (175).



Dibromoolefin **170** (0.119 g, 0.351 mmol) in hexanes (5 mL) was subjected to rearrangement according to general procedure E using *n*-BuLi (2.5 M in hexanes, 0.17 mL, 0.43 mmol) to afford **175** (0.0369 g, 60%) as a colorless oil. $R_f = 0.55$ (hexanes); IR (CH₂Cl₂ cast) 2959, 2200, 2091 cm⁻¹; ¹H NMR (400 MHz, CDCl₃) δ 2.25 (dt, $J = 6.9, 11$ Hz, 2H), 1.53-1.35 (m, 4H), 0.88 (t, $J = 7.3$ Hz, 3H), 0.16 (s, 9H); ¹³C NMR (100 MHz, CDCl₃, APT) δ 88.5 (d, $J = 17$ Hz), 82.9 (d, $J = 15$ Hz), 80.2, 65.3 (d, $J = 189$ Hz), 30.1 (d, $J = 4$ Hz), 21.9 (d, $J = 4$ Hz), 18.9 (d, $J = 66$ Hz), 13.5, -0.3; EI MS m/z 179.1 (M⁺, 21), 164.1 ([M - CH₃]⁺, 100); EI HRMS m/z calcd. for C₁₀H₁₈Si¹³C (M⁺) 179.1211, found 179.1209.

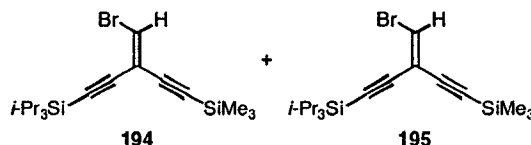
3-¹³C-1-Triisopropylsilyl-6-trimethylsilyl-hexa-1,3,6-triynes (177) and 4-¹³C-1-triisopropylsilyl-6-trimethylsilyl-hexa-1,3,6-triynes (178).



Dibromoolefin **174** (0.130 g, 0.280 mmol) in hexanes (10 mL) was subjected to rearrangement according to general procedure E using *n*-BuLi (2.5 M in hexanes, 0.13 mL, 0.33 mmol) to afford an inseparable 2:1 mixture of triynes **177** and **178** (0.054, 64%) as a clear yellow oil: $R_f = 0.71$ (hexanes); IR (CH₂Cl₂ cast) 2945, 2158, 1463 cm⁻¹; ¹H NMR (400 MHz, CDCl₃) δ 1.06 (s, 21H), 0.18 (s, 9H); ¹³C NMR (100 MHz, CDCl₃) **177**: δ 89.6 (d, $J = 151$ Hz), 89.1 (d, $J = 19$ Hz), 87.1 (d, $J = 15$ Hz), 85.2 (d, $J = 13$ Hz), 62.4, 61.0, 18.5, 11.2, -0.6; **178** 89.6 (d, $J = 19$ Hz), 88.1 (d, $J = 151$ Hz), 87.1 (d, $J = 15$ Hz), 85.2 (d, $J = 13$ Hz), 62.4,

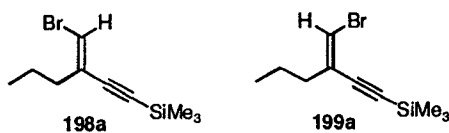
61.0, 18.5, 11.2, -0.6; EI MS m/z 303.2 (M^+ , 29), 260.1 ($[M - C_3H_7]^+$, 100); EI HRMS m/z calcd. for $C_{17}H_{30}Si_2^{13}C$ (M^+) 303.1920, found 303.1921.

(E- and Z-)3-(Monobromomethylidene)-1-triisopropylsilyl-5-trimethylsilylpenta-1,4-diyne (194 and 195)



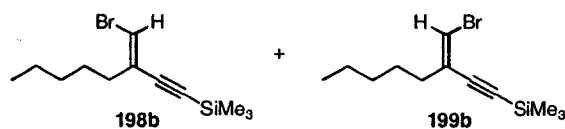
n-BuLi (1.6 M in hexanes, 0.20 mL, 0.32 mmol) was added to **93c** (0.125 g, 0.270 mmol) in wet hexanes (10 mL) (two drops of water were added to the hexanes and allowed to stir overnight). Satd. aq. NH_4Cl (10 mL) and Et_2O (10 mL) were added, the organic layer separated, washed with satd. aq. NH_4Cl (2 \times 10 mL) and the solvent removed *in vacuo* to afford an inseparable mixture (2:1 ratio, stereochemistry unknown) of vinyl bromides **194** and **195** (0.0705 g, 68%) as a yellow oil. R_f = 0.83 (hexanes); IR (CH_2Cl_2 cast) 2944, 2155, 1463 cm^{-1} ; 1H NMR (400 MHz, $CDCl_3$) δ major: 6.92 (s, 1H), 1.09 (s, 42 H), 0.18 (s, 9H) and minor: 6.92 (s, 1H), 1.06 (s, 42H), 0.19 (s, 9H); EI MS m/z 384.1 (M^+ , 12), 341.0 ($[M - C_3H_7]^+$, 69), 73.0 ($[Me_3Si]^+$, 100) ; EI HRMS m/z calcd. for $C_{18}H_{31}BrSi_2$ (M^+) 384.1127, found 384.1124.

(E- and Z-)3-(Monobromomethylidene)-1-trimethylsilyl-hexa-1-yne (198a and 199a)



n-BuLi (1.6 M in hexanes, 0.18 mL, 0.29 mmol) was added to **108a** (0.078 g, 0.241 mmol) in THF (5 mL) at $-78\text{ }^{\circ}\text{C}$, then quenched at the same temperature within 0.3 h with satd. aq. NH_4Cl (5 mL). Extraction with Et_2O (10 mL) and removal of the solvent afforded a potentially separable mixture (1:2.5) of vinyl bromides **198a** and **199a** (0.0457 g, 77%) as a yellow oil: $R_f = 0.46, 0.64$ (hexanes); IR (CH_2Cl_2 cast) 3072, 2960, 2147, 1585, 1458 cm^{-1} ; ^1H NMR (400 MHz, CDCl_3) δ 6.57 (s, 1H) (minor), 6.31 (t, $J = 1.3$, 2H) (major), 2.25 (dt, $J = 7.3, 0.7$, 2H) (minor), 2.14 (dt, $J = 7.4, 1.3$, 2H) (major), 1.59-1.51 (m, 4H) (mixed), 0.94 (t, $J = 7.3$, 3H) (minor), 0.89 (t, $J = 7.3$, 3H) (major), 0.21 (s, 9H) (major), 0.17 (s, 9H) (minor); ^{13}C NMR (100 MHz, CDCl_3) δ 130.2, 111.1, 102.4, 102.2, 38.9, 35.1, 21.3, 20.5, 13.5, 13.3, $-0.1, -0.2$; T-ROESY (400 MHz, CDCl_3) δ 6.31 \leftrightarrow 2.14; EI MS m/z 246.0/244.0 (M^+ , 60/59), 73.0 ($[\text{Me}_3\text{Si}]^+$, 100); EI HRMS m/z calcd. for $\text{C}_{10}\text{H}_{17}^{81}\text{BrSi}$ / $\text{C}_{10}\text{H}_{17}^{79}\text{BrSi}$ (M^+) 246.0263/244.0282, found 246.02661/244.0279.

(*E*- and *Z*-)3-(Monobromomethylidene)-1-trimethylsilyl-nona-1-yne (**198b** and **199b**)



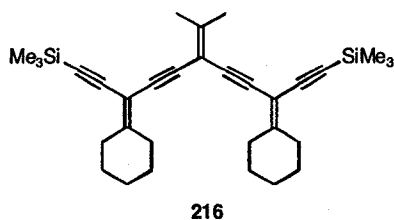
n-BuLi (2.5 M in hexanes, 0.15 mL, 0.38 mmol) was added to **108b** (0.111 g, 0.316 mmol) in THF (3 mL) at $-78\text{ }^{\circ}\text{C}$, then quenched at the same

temperature within 0.3 h with satd. aq. NH_4Cl (5 mL). Extraction with Et_2O (10 mL) and removal of the solvent afforded a potentially separable mixture (1:2.5) of vinyl bromides **198b** and **199b** (0.0685 g, 80%) as a yellow oil: $R_f = 0.45, 0.63$ (hexanes); IR (CH_2Cl_2 cast) 3072, 2958, 2146, 1584, 1466 cm^{-1} ; ^1H NMR (400 MHz, CDCl_3) δ 6.56 (s, 1H) (minor), 6.31 (s, 2H) (major), 2.27 (t, $J = 7.3$, 2H) (minor), 2.18-2.14 (m, 2H) (major), 1.54-1.50 (m, 4H) (mixed), 1.33-1.24 (m, 8H) (mixed), 0.91-0.86 (m, 6H) (mixed), 0.21 (s, 9H) (major), 0.17 (s, 9H) (minor); ^{13}C NMR (100 MHz, CDCl_3) δ 130.4, 129.4, 114.9, 110.9, 103.3, 102.4, 102.2, 95.8, 36.9, 33.1, 31.1, 30.9, 27.7, 27.6, 26.8, 22.4, 22.3, 13.9, 13.9, -0.14, -0.18; T-ROESY (400 MHz, CDCl_3) δ 6.31 \leftrightarrow 2.16; EI MS m/z 274.1/272.1 (M^+ , 9/9), 73.0 ($[\text{Me}_3\text{Si}]^+$, 100); EI HRMS m/z calcd. for $\text{C}_{12}\text{H}_{21}^{81}\text{BrSi}/\text{C}_{12}\text{H}_{21}^{79}\text{BrSi}$ (M^+) 274.0576/272.0596, found 274.0571/272.0593.

Trapping via protonation of lithiated intermediate derived from **93c**.

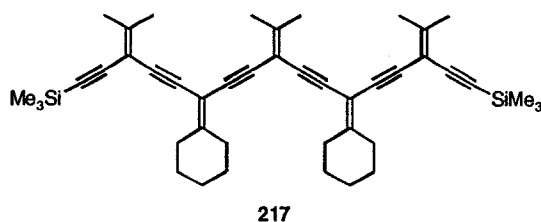
n-BuLi (1.6 M in hexanes, 0.13 mL, 0.21 mmol) was added to **93c** (0.0935 g, 0.202 mmol) in THF (5 mL) at -78 $^\circ\text{C}$, then quenched at the same temperature within 0.3 h with H_2O (5 mL). The reaction was warmed to rt, satd. aq. NH_4Cl (5 mL) and Et_2O (5 mL) were added, the organic layer separated, washed with satd. aq. NH_4Cl (2×5 mL) and the solvent removed *in vacuo* afford an inseparable mixture (2:1 ratio, stereochemistry unknown) of vinyl bromides **194** and **195**.

Compound (216)



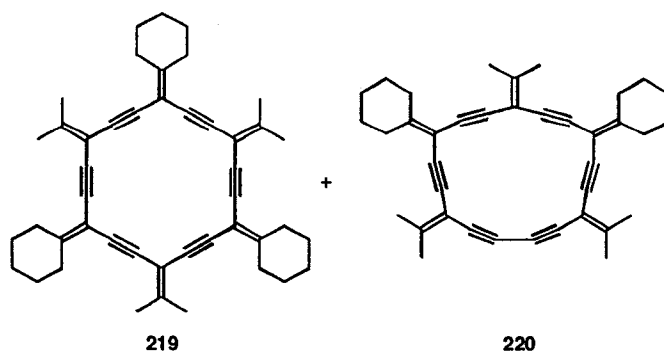
Enediyne **215** (1.51 g, 6.06 mmol) and K_2CO_3 (0.115 g, 0.832 mmol) were added to wet THF/MeOH (60 mL, 1:1 v/v) and the mixture stirred at rt until TLC analysis showed complete desilylation, ca. 2 h. Et_2O (60 mL) and satd. aq. NH_4Cl (60 mL) were added, the organic phase separated, washed with satd. aq. NH_4Cl (2 \times 60 mL), dried ($MgSO_4$), and the solvent reduced to ca. 2 mL. The deprotected monomer was subjected to cross-coupling according to general procedure F using cyclohexane triflate **214** (4.52 g, 13.3 mmol), $Pd(PPh_3)_4$ (0.279 g, 0.241 mmol), and CuI (0.1 g, 0.5 mmol) in DMF (200 mL) and DEA (10 mL). Purification by column chromatography (silica gel, hexanes/ CH_2Cl_2 1:1) gave **216** (0.489 g, 17%) as a colorless solid: Mp 97-99 $^\circ C$; $R_f = 0.27$ (hexanes/ CH_2Cl_2 10:1); IR (CH_2Cl_2 cast) 2938, 2146, 1601, 1579 cm^{-1} ; 1H NMR (300 MHz, $CDCl_3$) δ 2.50-2.00 (m, 8H), 2.02 (s, 6H), 1.57-1.51 (m, 12H), 0.17 (s, 18H); ^{13}C NMR (75 MHz, $CDCl_3$) δ 161.4, 153.0, 101.8, 101.6, 98.5, 95.8, 88.6, 87.7, 32.8, 27.6, 26.2, 22.7, 0.6; EI HRMS m/z calcd. for $C_{27}H_{50}Si_4$ (M^+) 486.29895; found 486.29916.

Compound (217)



Trimer **216** (0.468g, 0.965mmol) and K_2CO_3 (0.018 g, 0.13 mmol) were added to wet MeOH/THF (10 mL, 1:1 v/v) and stirred at rt until TLC analysis showed complete desilylation, ca. 2 h. Et_2O (10 mL) and satd. aq. NH_4Cl (10 mL) were added, the organic phase separated, washed with satd. aq. NH_4Cl (2×10 mL), dried ($MgSO_4$), and the solvent reduced to ca. 2 mL. The deprotected trimer was subjected to cross-coupling according to general procedure F using methyl triflate **213** (0.682 g, 2.27 mmol), $Pd(PPh_3)_4$ (0.081 g, 0.070 mmol), and CuI (0.032 g, 0.17 mmol) in DMF (30 mL) and DEA (30 mL). Purification by column chromatography, (silica gel, hexanes/ CH_2Cl_2 10:1) and recrystallization ($Et_2O/MeOH$) gave **217** (0.173 g, 28%) as a colorless solid: Mp 125-126 °C; $R_f = 0.15$ (hexane/ CH_2Cl_2 10:1); UV-vis ($CHCl_3$) λ_{max} 283 (48 000), 305 (46 000) nm; IR (CH_2Cl_2 cast) 2953, 2147, 1602 cm^{-1} ; 1H NMR (300 MHz, $CDCl_3$) δ 2.54-2.58 (m, 8H), 2.02 (s, 6H), 2.01 (s, 6H), 1.99 (s, 6H), 1.62-1.54 (m, 12H), 0.17 (s, 18); ^{13}C NMR (75 MHz, $CDCl_3$) δ 159.6, 154.5, 152.6, 101.9, 101.9, 101.8, 98.4, 95.8, 88.5, 88.3, 88.0, 87.9, 32.8, 27.7, 26.3, 22.8, 22.7 (2 \times), 0.6. EI HRMS m/z calcd. for $C_{44}H_{56}Si_2$ (M^+) 640.39203; found 640.39028.

Compounds (219 and 220)



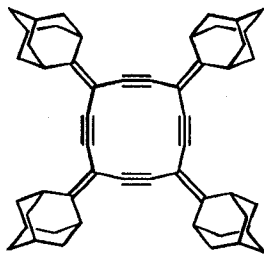
A mixture of pentamer **217** (0.139 g, 0.217 mmol), Pd(PPh₃)₄ (0.047 g, 0.041 mmol), piperidine (0.45 mL), dried THF (35 mL), and dibromide (0.046 g, 0.18 mmol), was put under a N₂ atmosphere and degassed using approximately 20 freeze/pump/thaw cycles. TBAF (1 M in THF, 0.3 mL, 0.3 mmol) was added and the mixture was stirred for 7 days. By TLC (hexanes/CH₂Cl₂ 4.5:1) analysis, spots for the desired product and one for the oxidatively coupled product were observed soon after the deprotected starting material was formed. Five spots were observed for four days, starting material **217** (*R_f* = 0.41), monodeprotected (*R_f* = 0.37), bisdeprotected (*R_f* = 0.32) and the two macrocycles, **219** (*R_f* = 0.24), **220** (*R_f* = 0.26). Deprotected starting material never completely disappeared and after seven days the reaction was quenched with satd. aq. NH₄Cl (30 mL) and Et₂O (30 mL), the organic phase separated, washed with satd. aq. NH₄Cl (2 × 30 mL), dried (MgSO₄) and the solvent removed *in vacuo*. Purification by column chromatography (silica gel, hexanes/CH₂Cl₂ 4.5:1) gave hexamer **219** (0.012 g, 9%) and pentamer **220** (0.006 g, 5%).

(**219**) Colorless solid: Mp 150 °C (dec.); UV-vis (CHCl₃) λ_{max} (ε) 286 (53600) nm; IR (solid) 2927, 2198, 1577 cm⁻¹; ¹H NMR (300 MHz, CD₂Cl₂) δ 2.80 (m, 12 H), 2.12 (s, 18 H), 1.70 (m, 18 H); ¹³C NMR (125 MHz, CD₂Cl₂) δ 160.7, 153.3, 102.1, 98.6, 88.3, 88.2, 33.4, 28.1, 26.5, 23.0. EI HRMS *m/z* calcd. for C₄₅H₄₈ (M⁺) 588.3756, found 588.3750.

(**220**) Colorless solid: Mp 140 °C (dec.); UV-vis (CHCl₃) λ_{max} (ε) 336 (13 200), 293 (47 000) nm; IR (solid) 2928, 2201, 2134, 1577 cm⁻¹; ¹H NMR (300 MHz, CD₂Cl₂) δ 2.65-2.57 (m, 8H), 2.14 (s, 6H), 2.08 (s, 6H), 2.07 (s, 6H), 1.68-1.52

(m, 12H); ^{13}C NMR (125 MHz, CD_2Cl_2) δ 160.7, 154.7, 153.1, 102.3, 102.1, 98.8, 89.4, 89.0, 88.6, 88.4, 83.0, 77.2, 33.6, 33.4, 28.1, 28.1, 26.6, 23.3, 23.2, 22.9; EI HRMS m/z calcd. for $\text{C}_{38}\text{H}_{38}$ (M^+) 494.2974; found 494.2967.

Compound (225)

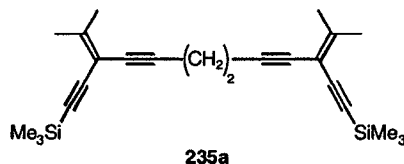


225

A mixture of trimer **223** (0.140 g, 0.206 mmol), $\text{Pd}(\text{PPh}_3)_4$ (0.0235 g, 0.0203 mmol), CuI (0.0069 g, 0.0362 mmol), piperidine (0.5 mL), dibromide **222** (0.0629 g, 0.206 mmol) in THF (20 mL) was put under an inert atmosphere of N_2 and degassed using approximately 10 freeze/pump/thaw cycles. TBAF (1 M in THF, 0.2 mL, 0.2 mmol) was added and the mixture stirred for 11 days. The reaction was allowed to stir for 11 days when starting material was no longer observed by TLC (silica gel, hexanes/ CH_2Cl_2 5:1) analysis. The reaction was quenched with satd. aq. NH_4Cl (20 mL) and Et_2O (20 mL), the organic phase separated, washed with satd. aq. NH_4Cl (2×20 mL), dried (MgSO_4) and the solvent removed *in vacuo*. Purification by column chromatography (silica gel, hexanes/ CH_2Cl_2 5:1) provided the [4]-radialene **225** (0.04 g, 30%) as an off-white solid: Mp 220 °C (decomp); $R_f = 0.49$ (hexanes/ CH_2Cl_2 2:1); IR (C_6D_6 cast) 2916, 2279, 1724, 1616 cm^{-1} ; ^1H NMR (C_6D_6 , 300 MHz) δ 3.38 (bs, 8H), 1.72-1.62 (m, 48H); ^{13}C NMR (C_6D_6 , 125 MHz) δ 160.6, 96.5, 95.5, 39.3, 37.2, 36.9, 28.3; UV-

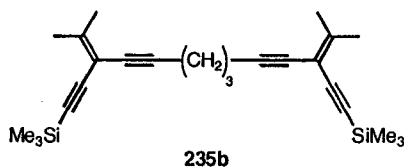
vis (CHCl₃) λ_{max} (ϵ) 283 (64 500), 296 (91 000), 290 (16 500) nm; EI HRMS m/z calcd. for C₅₂H₅₆ (M⁺) 680.4382, found 680.4378.

3,10-Bis(trimethylsilylethynyl)-2,11-dimethyldodeca-2,10-diene-4,8-diyne (235a).



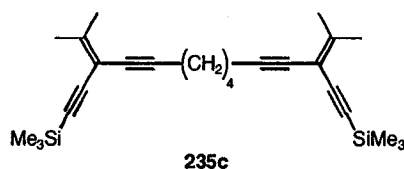
1,5-Hexadiyne (0.050 mL of 4M soln. in pentane, 0.20 mmol) was subjected to cross-coupling according to general procedure F using vinyl triflate **213** (0.13 g, 0.43 mmol), Pd(PPh₃)₄ (0.012 g, 0.010 mmol), Et₂NH (1 mL), and CuI (0.004 g, 0.02 mmol) in THF (5 mL). Purification by column chromatography (silica gel, hexanes/CH₂Cl₂ 10/1) afforded **235a** (0.034 g, 45%) as a colorless solid: Mp 80-82 °C. R_f = 0.45 (hexanes/CH₂Cl₂ 10:1). IR (solid) 2956, 2149, 1601, 1438 cm⁻¹; ¹H NMR (CDCl₃, 300 MHz) δ 2.64 (s, 4H), 2.03 (s, 6H), 2.02 (s, 6H), 0.23 (s, 18H). ¹³C NMR (CDCl₃, 75.5 MHz) δ 154.7, 102.2, 101.4, 95.6, 90.5, 78.1, 22.6 (2 \times), 20.0, 0.1; EI HRMS m/z calcd. for C₂₄H₃₄Si₂ (M⁺) 378.2199, found 378.2205.

3,11-Bis(trimethylsilylethynyl)-2,12-dimethyltrideca-2,11-diene-4,9-diyne (235b).



1,6-Heptadiyne (0.024 g, 0.246 mmol) was subjected to cross-coupling according to general procedure F using vinyl triflate **213** (0.147 g, 0.488 mmol), Pd(PPh₃)₄ (0.017 g, 0.015 mmol), Et₂NH (0.5 mL), and CuI (0.007 g, 0.04 mmol) in THF (6 mL). Purification by column chromatography (silica gel, hexanes/CH₂Cl₂ 10/1) afforded **235b** (0.059 g, 61%) as a colorless solid: Mp 67-69 °C; *R*_f = 0.15 (hexanes/CH₂Cl₂ 10:1); IR (CHCl₃ cast) 2935, 2145, 1595, 1428 cm⁻¹; ¹H NMR (CDCl₃, 300 MHz) δ 2.53 (t, *J* = 7.1 Hz, 4H), 2.03 (s, 6H), 2.01 (s, 6H), 1.83 (p, *J* = 7.1, 2H), 0.23 (s, 18H); ¹³C NMR (CDCl₃, 75.5 MHz) δ 154.1, 102.4, 101.5, 95.5, 91.3, 77.8, 28.0, 22.6 (2×), 18.8, 0.1; EI HRMS *m/z* calcd. for C₂₅H₃₆Si₂ (M⁺) 392.2356, found 392.2357.

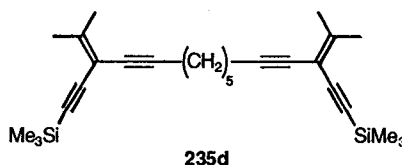
3,12-Bis(trimethylsilylethynyl)-2,13-dimethyltetradeca-2,12-diene-4,10-diyne (235c).



1,7-Octadiyne (0.090 g, 0.85 mmol) was subjected to cross-coupling according to general procedure F using vinyl triflate **213** (0.600 g, 2.00 mmol), Pd(PPh₃)₄ (0.049 g, 0.042 mmol), Et₂NH (2 mL), and CuI (0.025 g, 0.13 mmol) in DMF (25 mL). Purification by column chromatography (silica gel, hexanes/CH₂Cl₂ 10/1) afforded **235c** (0.135 g, 39%) as a colorless solid: Mp 78-79 °C; *R*_f = 0.45 (hexanes/CH₂Cl₂ 4:1); IR (solid) 2958, 2229, 2150, 1459 cm⁻¹; ¹H NMR (CDCl₃, 300 MHz) δ 2.36 (t, *J* = 6.0, 4H), 1.97 (s, 6H), 1.95 (s, 6H),

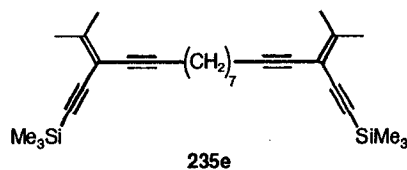
1.69-1.64 (m, 4H), 0.17 (s, 18H); ^{13}C NMR (CDCl_3 , 125 MHz) δ 153.9, 102.4, 101.6, 95.4, 91.9, 76.8, 27.9, 22.6 (2 \times), 19.1, 0.1; EI HRMS m/z calcd. for $\text{C}_{26}\text{H}_{38}\text{Si}_2$ (M^+) 406.2512, found 406.2505.

3,13-Bis(trimethylsilylethynyl)-2,14-dimethyl-pentadeca-2,13-diene-4,11-diyne (235d).



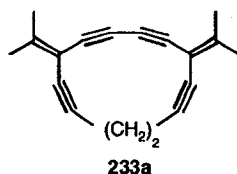
1,8-Nonadiyne (0.108 g, 0.900 mmol) was subjected to cross-coupling according to general procedure F using vinyl triflate **213** (0.600 g, 2.00 mmol), $\text{Pd}(\text{PPh}_3)_4$ (0.150 g, 0.130 mmol), Et_2NH (2 mL), and CuI (0.050 g, 0.26 mmol) in DMF (30 mL). Purification by column chromatography (silica gel, hexanes/ CH_2Cl_2 10/1) afforded **235d** (0.137 g, 36%) as a light yellow oil. $R_f = 0.2$ (hexanes/ CH_2Cl_2 18:1). IR (CHCl_3 cast) 2959, 2148, 1433 cm^{-1} ; ^1H NMR (CDCl_3 , 300 MHz) δ 2.36-2.31 (m, 4H), 1.97 (s, 6H), 1.95 (s, 6H), 1.59-1.53 (m, 6H), 0.17 (s, 18H); ^{13}C NMR (CDCl_3 , 125 MHz) δ 153.9, 102.5, 101.6, 95.4, 92.2, 76.8, 28.3, 28.2, 22.6, 22.5, 19.5, 0.1; EI HRMS m/z calcd. for $\text{C}_{27}\text{H}_{40}\text{Si}_2$ (M^+) 420.2669, found 420.2668.

3,15-Bis(trimethylsilylethynyl)-2,16-dimethyl-heptadeca-2,15-diene-4,13-diyne (235e).



1,10-Undecadiyne (0.200 g, 1.35 mmol) was subjected to cross-coupling according to general procedure F using vinyl triflate **213** (0.900 g, 3.00 mmol), Pd(PPh₃)₄ (0.050 g, 0.043 mmol), Et₂NH (3 mL), and CuI (0.025 g, 0.13 mmol) in DMF (30 mL). Purification by column chromatography (silica gel, hexanes/CH₂Cl₂ 10/1) afforded **235e** (0.158 g, 26%) as a light yellow oil. $R_f = 0.45$ (hexanes/CH₂Cl₂ 4:1). IR (CHCl₃ cast) 2933, 2149, 1433 cm⁻¹; ¹H NMR (CDCl₃, 300 MHz) δ 2.32 (t, $J = 6.9$, 4H), 1.98 (s, 6H), 1.96 (s, 6H), 1.58-1.48 (m, 4H), 1.44-1.34 (m, 6H), 0.17 (s, 18H); ¹³C NMR (CDCl₃, 75.5 MHz) δ 153.6, 102.5, 101.7, 93.5, 92.4, 76.6, 28.8, 28.7, 28.6, 22.5 (2x), 19.5, 0.1; EI HRMS m/z calcd. for C₂₉H₄₄Si₂ (M⁺) 448.2982, found 448.2972.

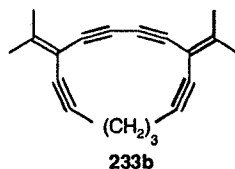
5,12-Diisopropylidene-cyclododeca-1,3,6,10-tetrayne (**233a**).



Compound **235a** (0.0622 g, 0.164 mmol) was subjected to desilylation and oxidative homocoupling according to general procedure G using CuI (0.060 g, 0.32 mmol), and TMEDA (0.1 mL) in CH₂Cl₂ (60 mL). Purification by column chromatography (silica gel, hexanes/CH₂Cl₂ 2/1) afforded **233a** (0.0122 g, 32%) as a colorless solid. Sample discolors at 110 °C, decomposes at 146 °C. $R_f = 0.55$ (hexanes/CH₂Cl₂ 2:1). UV-vis (CHCl₃) λ_{\max} (ϵ) 333 (26 000), 313 (29 900), 295

(13 900), 276 (21 100), 263 (30 500), 259 (30 000) nm; IR (CH₂Cl₂ cast) 2907, 2149, 1622, 1340 cm⁻¹; ¹H NMR (CDCl₃, 300 MHz) δ 2.65 (s, 4H), 1.98 (s, 6H), 1.90 (s, 6H); ¹³C NMR (CDCl₃, 125 MHz) δ 145.0, 105.1, 103.5, 90.3, 86.5, 81.2, 23.4, 22.1, 19.8; ¹³C – ¹H HMBC (500 MHz, CDCl₃) δ 145.0 ↔ 1.90, 1.98; δ 105.1 ↔ 1.90, 1.98, 2.65; δ 103.5 ↔ 1.90, 1.98, 2.65; δ 90.3 ↔ 2.65; δ 86.5 ↔ 1.98; δ 81.2 ↔ 1.90, 1.98, 2.65; δ 23.4 ↔ 1.98; δ 22.1 ↔ 1.90; δ 19.8 ↔ 2.65. EI HRMS *m/z* calcd. for C₁₈H₁₆ (M⁺) 232.1252, found 232.1253.

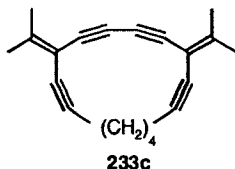
5,13-Diisopropylidene-cyclotrideca-1,3,6,11-tetrayne (233b).



Compound **235b** (0.0593 g 0.151 mmol) was subjected to desilylation and oxidative homocoupling according to general procedure G using CuI (0.062 g, 0.32 mmol), and TMEDA (0.1 mL) in CH₂Cl₂ (60 mL). Purification by column chromatography (silica gel, hexanes/CH₂Cl₂ 4/1) afforded **233b** (0.0074 g, 20%) as a colorless solid. Sample discolors at 100 °C, decomposes at 109-111 °C; *R_f* = 0.34 (hexanes/CH₂Cl₂ 5:1); UV-vis (CHCl₃) λ (ε) 331 (27 800), 311 (31 100), 292 (19 900), 275 (12 900), 259 (30 900) nm; IR (CHCl₃ cast) 2904, 2145, 1617, cm⁻¹; ¹H NMR (CDCl₃, 300 MHz) δ 2.45 (t, *J* = 6.2, 4H), 2.00 (p, *J* = 6.2, 2H), 1.90 (s, 6H), 1.85 (s, 6H); ¹³C NMR (CDCl₃, 125 MHz) δ 145.6, 103.2, 98.9, 95.7, 82.5, 81.5, 28.0, 23.1, 22.2, 19.8; ¹³C – ¹H HMBC (500 MHz, CDCl₃) δ 145.6 ↔ 1.85, 1.90; δ 103.2 ↔ 1.85, 1.90, 2.45; δ 98.9 ↔ 1.85, 1.90, 2.45;

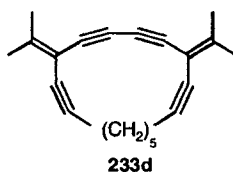
δ 95.7 \leftrightarrow 1.85, 1.90, 2.00, 2.45; δ 82.5 \leftrightarrow 1.85, 1.90; δ 81.5 \leftrightarrow 1.85, 1.90, 2.45;
 δ 28.0 \leftrightarrow 2.45; δ 23.1 \leftrightarrow 1.90; δ 22.2 \leftrightarrow 1.85; δ 19.8 \leftrightarrow 2.00, 2.45; EI HRMS
 m/z calcd. for $C_{19}H_{18}$ (M^+) 246.1409, found 246.1408.

5,14-Diisopropylidene-cyclotetradeca-1,3,6,12-tetrayne (233c).



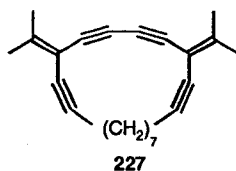
Compound **235c** (0.0285 g, 0.0701 mmol) was subjected to desilylation and oxidative homocoupling according to general procedure G using CuI (0.028 g, 0.15 mmol), and TMEDA (0.5 mL) in CH_2Cl_2 (30 mL). Purification by column chromatography (silica gel, hexanes/ CH_2Cl_2 4/1) afforded **233c** (0.0062 g, 34%) as a colorless solid: Mp 129-130 °C; R_f = 0.34 (hexanes/ CH_2Cl_2 5:1); UV-vis ($CHCl_3$) λ_{max} (ϵ) 329 (29 500), 309 (31 500), 290 (18 600), 275 (10 700), 258 (25 000) nm; IR (solid) 2905, 2214, 2192, 2118, 1618, 1334 cm^{-1} ; 1H NMR ($CDCl_3$, 300 MHz) δ 2.38-2.32 (m, 4H), 1.91 (s, 6H), 1.89 (s, 6H), 1.74 (AA'BB', 4H); ^{13}C NMR ($CDCl_3$, 125 MHz) δ 146.9, 102.8, 94.6, 90.4, 80.7, 80.0, 29.2, 22.9, 22.2, 19.9; $^{13}C - ^1H$ HMBC (500 MHz, $CDCl_3$) δ 146.9 \leftrightarrow 1.89, 1.91; δ 102.8 \leftrightarrow 1.89, 1.91; δ 90.4 \leftrightarrow 1.89, 1.91; δ 80.7 \leftrightarrow 1.89, 1.90; δ 80.0 \leftrightarrow 1.89, 1.90, 2.35; δ 29.2 \leftrightarrow 1.74; δ 22.9 \leftrightarrow 1.89; δ 22.2 \leftrightarrow 1.91; δ 19.9 \leftrightarrow 2.35. EI HRMS m/z calcd for $C_{20}H_{20}$ (M^+) 260.1565, found 260.1564.

5,15-Diisopropylidene-cyclopentadeca-1,3,6,13-tetrayne (233d).



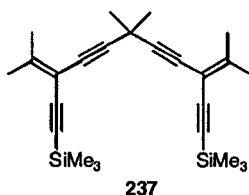
Compound **235d** (0.110 g, 0.260 mmol) was subjected to desilylation and oxidative homocoupling according to general procedure G using CuI (0.090 g, 0.47 mmol), and TMEDA (0.15 mL) in CH₂Cl₂ (60 mL). Purification by column chromatography (silica gel, hexanes/CH₂Cl₂ 9/1) afforded **233d** (0.024 g, 34%) as a colorless solid. Solid turns orange at 135 °C and then melts 168 °C. $R_f = 0.25$ (hexanes/CH₂Cl₂ 9:1); UV-vis (CHCl₃) $\lambda_{max}(\epsilon)$ 329 (30 500), 309 (32 400), 291 (19 300), 275 (11 300), 259 (26 000) nm; IR (solid) 2905, 2215, 2130, 1617, 1349 cm⁻¹; ¹H NMR (CDCl₃, 300 MHz) δ 2.42 (t, $J = 5.6$ Hz, 4H), 1.92 (s, 6H), 1.89 (s, 6H), 1.76-1.64 (m, 2H), 1.59-1.48 (m, 4H); ¹³C NMR (CDCl₃, 125 MHz) δ 148.5, 102.2, 93.7, 88.4, 79.5, 78.2, 29.8, 28.9, 22.9, 22.2, 19.9; ¹³C – ¹H HMBC (500 MHz, CDCl₃) δ 148.5 \leftrightarrow 1.89, 1.92, 2.42; δ 102.2 \leftrightarrow 1.89, 1.92, 2.42; δ 93.7 \leftrightarrow 1.54, 2.42; δ 88.4 \leftrightarrow 1.89, 1.92, 2.42; δ 79.5 \leftrightarrow 1.89, 1.92, 2.42; δ 78.2 \leftrightarrow 1.89, 1.92; δ 29.8 \leftrightarrow 2.42; δ 28.9 \leftrightarrow 1.70, 2.42; δ 22.9 \leftrightarrow 1.92; δ 22.2 \leftrightarrow 1.89; δ 19.9 \leftrightarrow 1.54, 1.70. EI HRMS m/z calcd. for C₂₁H₂₂ (M⁺) 274.1722, found 274.1726.

5,17-Diisopropylidene-cycloheptadeca-1,3,6,15-tetrayne (227).



Compound **235e** (0.040 g, 0.089 mmol) was subjected to desilylation and oxidative homocoupling according to general procedure G using CuI (0.030 g, 0.16 mmol), and TMEDA (0.1 mL) in CH₂Cl₂ (30 mL) (0.006 g, 22%). Purification by column chromatography (silica gel, hexanes/CH₂Cl₂ 9/1) afforded **227** as a colorless solid: Mp 136-138 °C; *R_f* = 0.4 (hexanes/CH₂Cl₂ 4:1); UV-vis (CHCl₃) λ_{max} (ε) 328 (24 500), 309 (26 500), 290 (15 700), 276 (8 400), 260 (29 000) nm; IR (solid) 2931, 2227, 2133, 1604 cm⁻¹; ¹H NMR (CDCl₃, 300 MHz) δ 2.36-2.33 (m, 4H), 1.96 (s, 6H), 1.95 (s, 6H), 1.62-1.49 (m, 8H), 1.34-1.23 (m, 2H); ¹³C NMR (CDCl₃, 125 MHz,) δ 151.3, 101.8, 93.8, 81.7, 79.1, 75.9, 30.3, 29.6, 28.9, 22.6, 22.5, 19.6; ¹³C – ¹H HMBC (500 MHz, CDCl₃) δ 151.3 ↔ 1.95, 1.96; δ 101.8 ↔ 1.95, 1.96; δ 93.8 ↔ 1.95, 1.96, 2.35; δ 81.7 ↔ 1.95, 1.96; δ 79.1 ↔ 1.95, 1.96, 2.35; δ 75.9 ↔ 1.95, 1.96. EI HRMS *m/z* calcd. for C₂₃H₂₆ (M⁺) 302.2035, found 302.2035.

3,9-Bis(trimethylsilylethynyl)-2,6,6,10-Tetramethyl-undeca-2,9-diene-4,7-diyne (237).



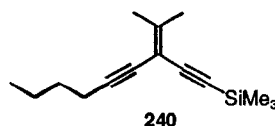
The volatile dimethyl pentadiyne **236** (0.215 g, 0.907 mmol) was subjected to cross-coupling according to general procedure F using vinyl triflate **213** (0.509 g, 1.69 mmol), Pd(PPh₃)₄ (0.052 g, 0.045 mmol), Et₂NH (1.0 mL), and CuI (0.015 g, 0.078 mmol) in THF (10 mL). Purification by column

chromatography (silica gel, hexanes/CH₂Cl₂ 5/1) afforded **237** (0.090 g, 25%) as a colorless solid. Mp 104-106 °C. *R_f* = 0.40 (hexanes/CH₂Cl₂ 5:1). IR (CH₂Cl₂ cast) 2960, 2249, 2153, 1439 cm⁻¹; ¹H NMR (CDCl₃, 300 MHz) δ 1.98 (s, 6H), 1.96 (s, 6H), 1.56 (s, 6H), 0.18 (s, 18H); ¹³C NMR (CDCl₃, 75.5 MHz) δ 155.1, 102.1, 101.3, 95.7, 95.4, 76.4, 31.3, 27.2, 22.7, 22.6, 0.1; EI HRMS *m/z* calcd. for C₂₅H₃₆Si₂(M⁺) 392.2356, found 392.2354.

Attempted cyclization of **237**.

Compound **237** (0.040 g 0.10 mmol) was subjected to desilylation and oxidative homocoupling according to general procedure G using CuI (0.030 g, 0.16 mmol), and TMEDA (1 mL) in CH₂Cl₂ (100 mL). No product was observed in the reaction mixture after work-up, only what is presumed to be linear oligomers and starting material.

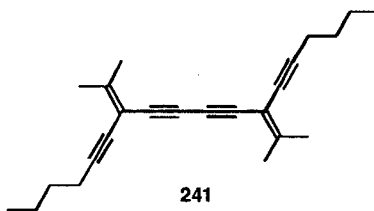
3-Trimethylsilylethynyl-2-methyl-non-2-en-4-yne (**240**).



1-Hexyne (0.302 g, 3.67 mmol) was subjected to cross-coupling according to general procedure F using vinyl triflate **213** (0.214 g, 0.714 mmol), Pd(PPh₃)₄ (0.024 g, 0.021 mmol), Et₂NH (1.0 mL), and CuI (0.011 g, 0.058 mmol) in THF (5.0 mL). Purification by column chromatography (silica gel, hexanes/CH₂Cl₂ 5/1) afforded **240** (0.103 g, 62%) as a light yellow oil. *R_f* = 0.59 (hexanes/CH₂Cl₂ 5:1); IR (CH₂Cl₂ cast) 2932, 2149, 1432 cm⁻¹; ¹H NMR

(CDCl₃, 300 MHz) δ 2.32 (t, J = 6.9 Hz, 2H), 1.98 (s, 3H), 1.96 (s, 3H), 1.52-1.38 (m, 4H), 0.90 (t, J = 7.2 Hz, 3H), 0.17 (s, 9H); ¹³C NMR (C₆D₆, 75.5 MHz) δ 152.6, 103.4, 102.8, 95.2, 92.6, 77.9, 30.8, 22.2, 22.1, 22.0, 19.2, 13.4, 0.1; EI HRMS m/z calcd. for C₁₅H₂₄Si (M⁺) 232.1647, found 232.1638.

7,11-Diisopropylidene-octadeca-5,8,10,13-tetrayne (241).



Compound **240** (0.103 g, 0.444 mmol) was subjected to desilylation and oxidative homocoupling according to general procedure G using CuI (0.042 g, 0.22 mmol), and TMEDA (1 mL) in CH₂Cl₂ (30 mL). Purification by column chromatography (silica gel, hexanes/CH₂Cl₂ 10/1) afforded **241** (0.0346 g, 49%) as a colorless solid. Mp 71-72 °C. R_f = 0.32 (hexanes/CH₂Cl₂ 10:1). UV-vis (CHCl₃) λ_{max} (ϵ) 327 (12 500), 307 (15 800), 286 (13 900), 271 (19 100), 260 (21 700) nm; IR (CH₂Cl₂ cast) 2932, 2221, 2136, 1590, 1361 cm⁻¹; ¹H NMR (CDCl₃, 300 MHz) δ 2.33 (t, J = 6.9, 4H), 2.01 (s, 6H), 1.99 (s, 6H), 1.54-1.40 (m, 8H), 0.90 (t, J = 7.2, 6H); ¹³C NMR (CDCl₃, 125 MHz) δ 156.0, 100.9, 93.1, 79.5, 76.4, 75.4, 30.8, 22.7, 22.0, 21.1, 19.1, 13.6; ¹³C – ¹H HMBC (500 MHz, CDCl₃) δ 156.0 \leftrightarrow 1.99, 2.01, 2.33; δ 100.9 \leftrightarrow 1.99, 2.01, 2.33; δ 93.0 \leftrightarrow 1.47, 2.33; δ 79.5 \leftrightarrow 1.99, 2.01, 2.33; δ 76.4 \leftrightarrow 1.99, 2.01, 2.33; δ 75.3 \leftrightarrow 1.99, 2.01; δ 30.8 \leftrightarrow 0.90, 1.47, 2.33; δ 22.7 \leftrightarrow 0.90, 1.47, 1.99, 2.01, 2.33; δ 22.0 \leftrightarrow 0.90, 1.47, 1.99,

2.01, 2.33; δ 19.1 \leftrightarrow 1.47; δ 13.6 \leftrightarrow 1.47. EI HRMS m/z calcd. for $C_{24}H_{30}$ (M^+)
318.2347, found 318.2349.

1. Brandsma, L. *Preparative Acetylenic Chemistry*; Elsevier; Amsterdam, 1988.
2. Lange, T.; van Loon, J.-D.; Tykwinski, R.R.; Schreiber, M.; Diederich, F. *Synthesis* **1996**, 537.
3. Anthony, J.; Boldi, A.M.; Rubin, Y.; Hobi, M.; Gramlich, V.; Knobler, C.B.; Seiler, P.; Diederich, F. *Helv. Chim. Acta.* **1995**, 78, 13.
4. Tour, J. M.; Rawlett, A. M.; Kozaki, M. Yao, Y.; Jagessar, R. C.; Dirk, S. M.; Price, D.; Reed, M. A.; Zhou, C.-W.; Chen, J.; Wang, W.; Campbell, I. *Chem. Eur. J.* **2001**, 7, 5118.
5. Uno, M.; Dixneuf, P. H., *Angew. Chem. Int. Ed.* **1998**, 37, 1714.
6. Bottaro, J. C.; Schmidt, R. J.; Bedford, C. D.; Gilardi, R.; George, C., *J. Org. Chem.* **1990**, 55, 1916.
7. Lavastre, O.; Plass, J.; Bachmann, P.; Guesmi, S.; Moinet, C. Dixneuf, P.H. *Organometallics*, **1997**, 16, 184.
8. Butler, I. R.; Soucy-Breau, C., *Can. J. Chem.* **1991**, 69, 1117.
9. Synthesized by Erin Chernick.
10. Stang, P. J.; Fisk, T. E., *Synthesis* **1979**, 438.
11. Zhao, Y. M.; Tykwinski, R. R., *J. Am. Chem. Soc.* **1999**, 121, 458.
12. Hassig, R.; Seebach, D.; Siegel, H., *Chem. Ber.* **1984**, 117, 1877.
13. Zhao, Y.M.; Campbell, K.; Tykwinski, R.R., *J. Org. Chem.* **2002**, 67,
14. Scott, L.; Cooney, M. J.; Otte, C.; Puls, C.; Haumann, T.; Boese, R.; Carroll, R. J.; Smith III, A. B.; de Meijere, A., *J. Am. Chem. Soc.* **1994**, 116, 10275.
15. Walton, D. R. M., Waugh, F. *J. Organomet. Chem.* **1972**, 37, 45.
16. Corey, E. J.; Fuchs, P. L. *Tetrahedron Lett.* **1972**, 3769.
17. Hay, A. S. *J. Org. Chem.* **1962**, 27, 3320.
18. Rubin, Y.; Lin, S. S.; Knobler, C. B.; Anthony, J.; Boldi, A. M.; Diederich, F., *J. Amer. Chem. Soc.* **1991**, 113, 6943.

19. Tobe, Y.; Iwasa, N.; Umeda, R.; Sonoda, M., *Tetrahedron Lett.* **2001**, *42*, 5485.
20. Wadsworth, D. H.; Geer, S. M.; Detty, M. R., *J. Org. Chem.* **1987**, *52*, 3662.
21. Heiss, C.; Phillips, R. S., *J. Chem. Soc. Perkin Trans I* **2000**, 2821.
22. Yogo, T., Koshins, J.; Suzuki, A. *Synth. Commun.* **1981**, *11*, 769.
23. Rossi, R.; Bellina, F.; Catarese, A.; Nannina, L.; Valensin, D., *Tetrahedron*, **2000**, *56*, 479.
24. Heuft, M. A.; Collins, S. K.; Yap, G. P.; Fallis, A. G., *Org. Lett.* **2001**, *3*, 2883.
25. Baldoli, C.; DelButtero, P.; Licandro, E.; Maiorana, S.; Papagni, A.; Torchio, M., *Tetrahedron Lett.* **1993**, *34*, 7943.

Appendix A - Crystallographic Data

University of Alberta Department of Chemistry
X-Ray Crystallography Laboratory
Structure Report for Compound 121

XCL Code: RRT0133

Date: 25 September 2001

Compound: 1,4-Bis(1-trimethylsilylhexa-1,3,5-triynyl)benzene

Formula: C₂₄H₂₂Si₂

Supervisor: R. R. Tykwinski **Crystallographer:** R. McDonald

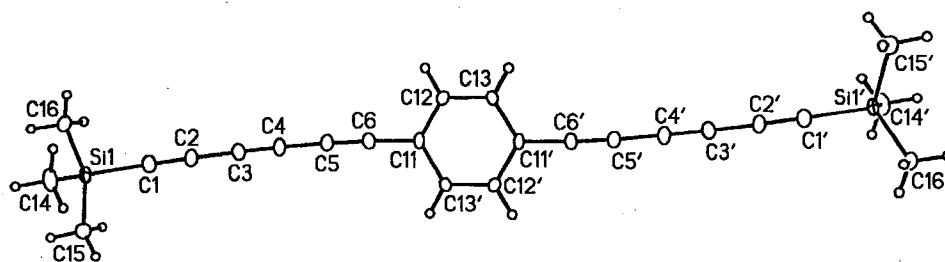


Figure A1. Perspective view of one of the two crystallographically-independent molecules of 1,4-bis(1-trimethylsilylhexa-1,3,5-triynyl)benzene (molecule A) showing the atom labelling scheme. Non-hydrogen atoms are represented by Gaussian ellipsoids at the 20% probability level. Hydrogen atoms are shown with arbitrarily small thermal parameters. Primed atoms are related to unprimed ones via the crystallographic inversion center (0, 0, 0) at the center of the benzene ring.

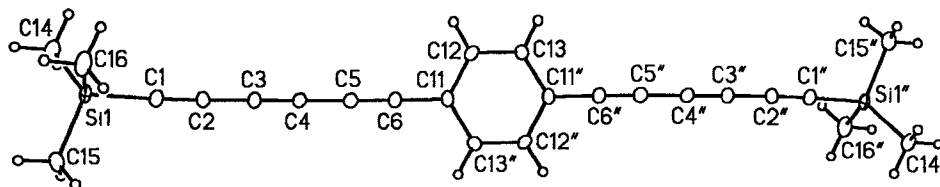


Figure A2. View of the second crystallographically-independent molecule of 1,4-bis(1-trimethylsilylhexa-1,3,5-triynyl)benzene (molecule B). Double-primed atoms are related to unprimed ones via the crystallographic inversion center ($1/2, 1/2, 0$) at the center of the benzene ring.

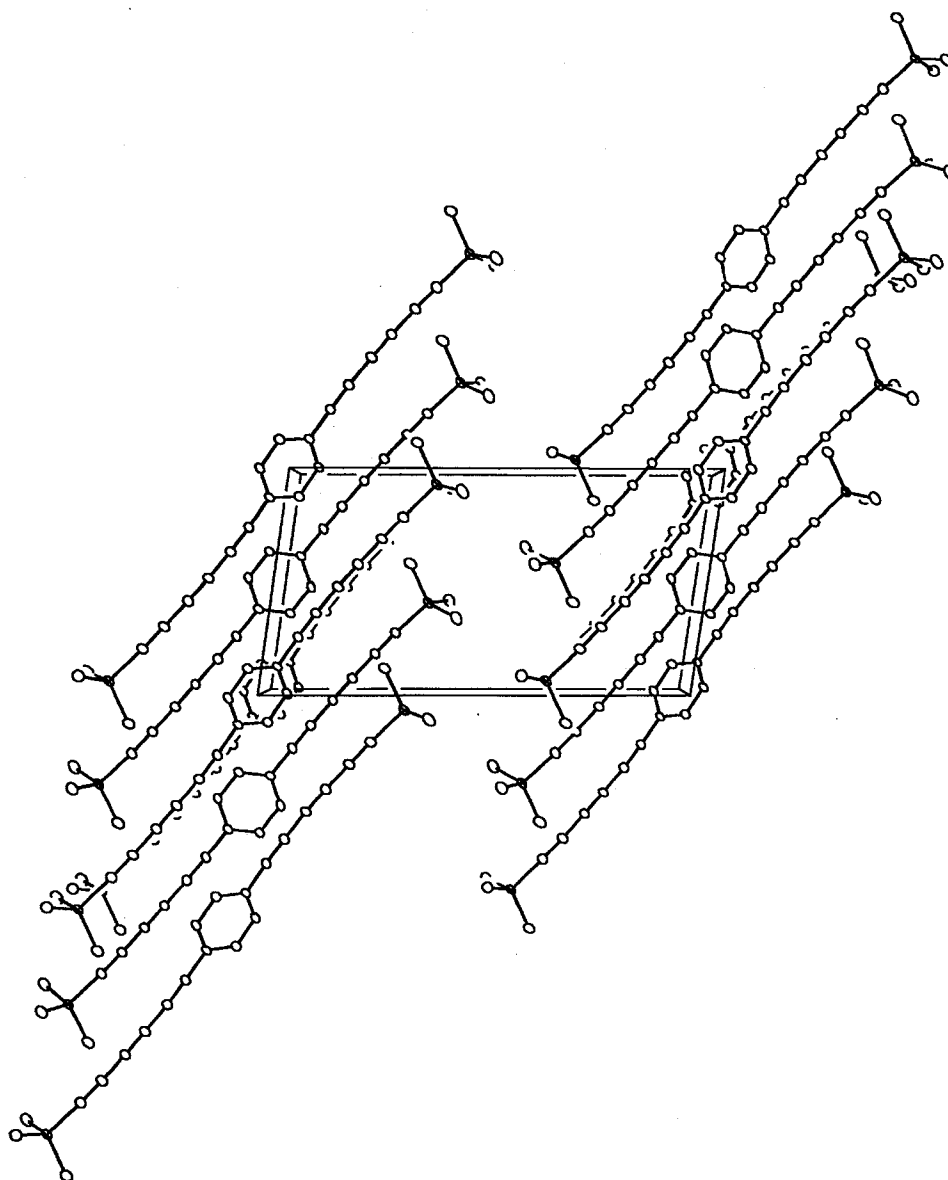


Figure A3. Illustration of crystal packing, with the unit cell boundaries as indicated. The view direction is parallel to the crystallographic *a* axis. Hydrogen atoms have been omitted.

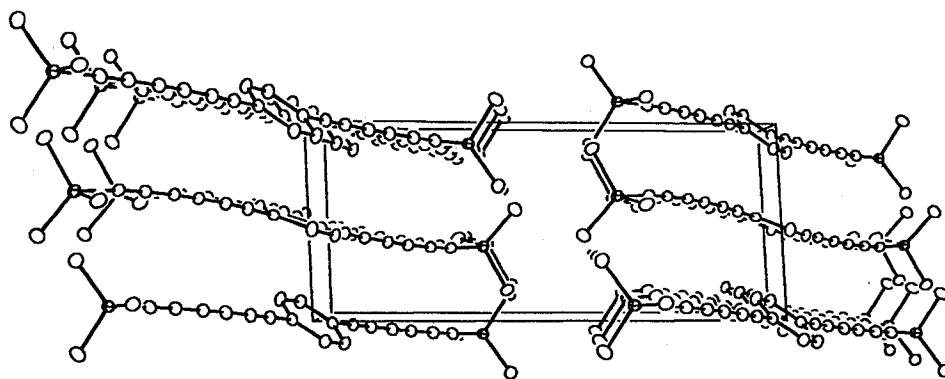


Figure A4. Crystal packing diagram, with the view direction parallel to the crystallographic *b* axis.

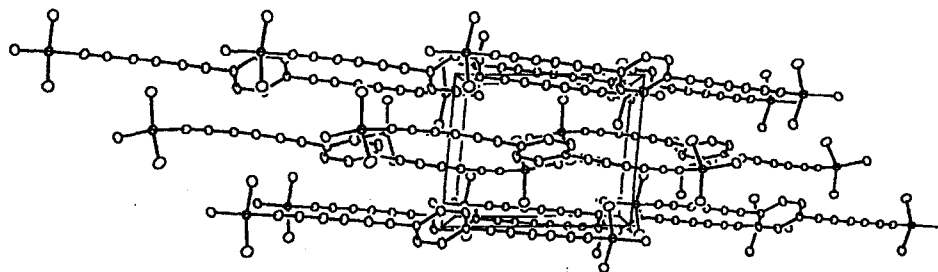


Figure A5. Crystal packing diagram, with the view direction parallel to the crystallographic *c* axis.

Table A1. Crystallographic Experimental Details**A. Crystal Data**

formula	C ₂₄ H ₂₂ Si ₂
formula weight	366.60
crystal dimensions (mm)	0.38 × 0.31 × 0.04
crystal system	triclinic
space group	PI (No. 2)
unit cell parameters ^a	
<i>a</i> (Å)	7.1643 (15)
<i>b</i> (Å)	9.1375 (19)
<i>c</i> (Å)	17.305 (4)
α (deg)	98.116 (4)
β (deg)	92.197 (4)
γ (deg)	95.230 (5)
<i>V</i> (Å ³)	1115.3 (4)
<i>Z</i>	2
ρ _{calcd} (g cm ⁻³)	1.092
μ (mm ⁻¹)	0.163

B. Data Collection and Refinement Conditions

diffractometer	Bruker PLATFORM/SMART 1000
CCD ^b	
radiation (λ [Å]) (0.71073)	graphite-monochromated Mo Kα
temperature (°C)	-80
scan type	ω scans (0.2°) (25 s exposures)
data collection 2θ limit (deg)	52.84
total data collected ≤ 21)	4891 (-6 ≤ <i>h</i> ≤ 8, -11 ≤ <i>k</i> ≤ 8, -21 ≤ <i>l</i>
independent reflections	4153 (<i>R</i> _{int} = 0.0499)
number of observed reflections (<i>NO</i>)	2084 [<i>F</i> _o ² ≥ 2σ(<i>F</i> _o ²)]
structure solution method	direct methods (<i>SHELXS-86</i> ^c)
refinement method (<i>SHELXL-93</i> ^d)	full-matrix least-squares on <i>F</i> ²
absorption correction method	Gaussian integration (face-indexed)
range of transmission factors	0.9938–0.9402
data/restraints/parameters	4153 [<i>F</i> _o ² ≥ -3σ(<i>F</i> _o ²)] / 0 / 235
goodness-of-fit (<i>S</i>) ^e	0.954 [<i>F</i> _o ² ≥ -3σ(<i>F</i> _o ²)]
final <i>R</i> indices ^f	
<i>R</i> ₁ [<i>F</i> _o ² ≥ 2σ(<i>F</i> _o ²)]	0.0699
<i>wR</i> ₂ [<i>F</i> _o ² ≥ -3σ(<i>F</i> _o ²)]	0.1546
largest difference peak and hole	0.311 and -0.228 e Å ⁻³

^aObtained from least-squares refinement of 1693 centered reflections.

(continued)

Table A1. Crystallographic Experimental Details (continued)

^bPrograms for diffractometer operation, data collection, data reduction and absorption correction were those supplied by Bruker.

^cSheldrick, G. M. *Acta Crystallogr.* **1990**, A46, 467–473.

^dSheldrick, G. M. *SHELXL-93*. Program for crystal structure determination. University of Göttingen, Germany, 1993. Refinement on F_o^2 for all reflections (all of these having $F_o^2 \geq -3\sigma(F_o^2)$). Weighted R -factors wR_2 and all goodnesses of fit S are based on F_o^2 ; conventional R -factors R_1 are based on F_o , with F_o set to zero for negative F_o^2 . The observed criterion of $F_o^2 > 2\sigma(F_o^2)$ is used only for calculating R_1 , and is not relevant to the choice of reflections for refinement. R -factors based on F_o^2 are statistically about twice as large as those based on F_o , and R -factors based on ALL data will be even larger.

^e $S = [\sum w(F_o^2 - F_c^2)^2 / (n - p)]^{1/2}$ (n = number of data; p = number of parameters varied; $w = [\sigma^2(F_o^2) + (0.0590P)^2]^{-1}$ where $P = [\text{Max}(F_o^2, 0) + 2F_c^2]/3$).

^f $R_1 = \sum ||F_o| - |F_c|| / \sum |F_o|$; $wR_2 = [\sum w(F_o^2 - F_c^2)^2 / \sum w(F_o^4)]^{1/2}$.

Table A2. Selected Interatomic Distances (Å)

<i>(a) Molecule A</i>			<i>(b) Molecule B</i>		
Atom1	Atom2	Distance	Atom1	Atom2	Distance
Si1	C1	1.849(4)	Si1	C1	1.850(4)
Si1	C14	1.852(4)	Si1	C14	1.854(4)
Si1	C15	1.860(4)	Si1	C15	1.853(4)
Si1	C16	1.847(4)	Si1	C16	1.862(4)
C1	C2	1.211(5)	C1	C2	1.208(5)
C2	C3	1.376(5)	C2	C3	1.370(5)
C3	C4	1.197(5)	C3	C4	1.209(5)
C4	C5	1.372(5)	C4	C5	1.371(5)
C5	C6	1.197(5)	C5	C6	1.196(5)
C6	C11	1.434(5)	C6	C11	1.442(5)
C11	C12	1.392(5)	C11	C12	1.391(5)
C11	C13'	1.404(5)	C11	C13''	1.395(5)
C12	C13	1.385(5)	C12	C13	1.386(5)

Table A3. Selected Interatomic Angles (deg)

<i>(a) Molecule A</i>			
Atom1	Atom2	Atom3	Angle
C1	Si1	C14	107.12(18)
C1	Si1	C15	106.83(19)
C1	Si1	C16	108.60(19)
C14	Si1	C15	110.8(2)
C14	Si1	C16	110.8(2)
C15	Si1	C16	112.42(19)
Si1	C1	C2	177.7(4)
C1	C2	C3	178.1(5)
C2	C3	C4	178.6(5)
C3	C4	C5	178.2(5)
C4	C5	C6	177.4(5)
C5	C6	C11	177.9(4)
C6	C11	C12	121.0(4)
C6	C11	C13'	119.5(4)
C12	C11	C13'	119.5(4)
C11	C12	C13	120.7(4)
C11'	C13	C12	119.8(4)

(b) Molecule B

Atom1	Atom2	Atom3	Angle
C1	Si1	C14	107.94(18)
C1	Si1	C15	108.06(19)
C1	Si1	C16	106.83(18)
C14	Si1	C15	112.1(2)
C14	Si1	C16	110.8(2)
C15	Si1	C16	110.9(2)
Si1	C1	C2	175.4(4)
C1	C2	C3	177.8(4)
C2	C3	C4	177.6(4)
C3	C4	C5	178.9(4)
C4	C5	C6	178.0(4)
C5	C6	C11	179.4(5)
C6	C11	C12	119.9(4)
C6	C11	C13''	120.3(4)
C12	C11	C13''	119.8(4)
C11	C12	C13	120.2(4)
C11''	C13	C12	120.0(4)

Primed atoms are related to unprimed ones via the crystallographic inversion center (0, 0, 0).

Double-primed atoms are related to unprimed ones via the inversion center ($1/2, 1/2, 0$).

University of Alberta Department of Chemistry
X-Ray Crystallography Laboratory

Structure Report for Compound 131

XCL Code: RRT0217

Date: 24 June 2002

Compound: 1,4-bis(3,5-bis(6-trimethylsilylhexa-1,3,5-triynyl)phenyl)buta-1,3-diyne, hemi(*n*-hexane) solvate

Formula: C₅₅H₄₉Si₄ (C₅₂H₄₂Si₄•0.5C₆H₁₄)

Supervisor: R. R. Tykwinski

Crystallographer: R.

McDonald

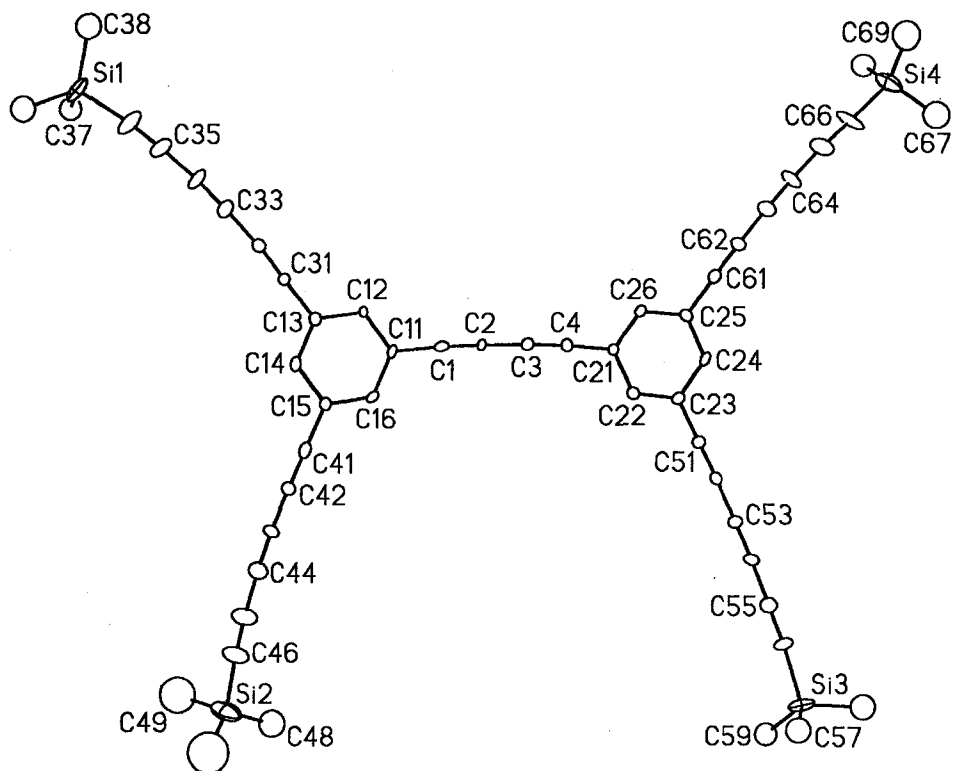


Figure A6. Perspective view of the 1,4-bis(3,5-bis(6-trimethylsilylhexa-1,3,5-triynyl)phenyl)buta-1,3-diyne molecule showing the atom labelling scheme. Non-hydrogen atoms are represented by Gaussian ellipsoids at the 20% probability level. Hydrogen atoms are not shown.

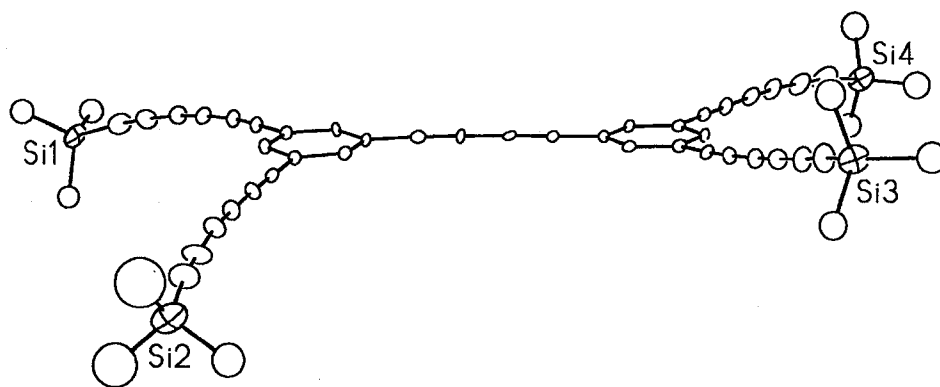


Figure A7. Alternate view of the molecule.

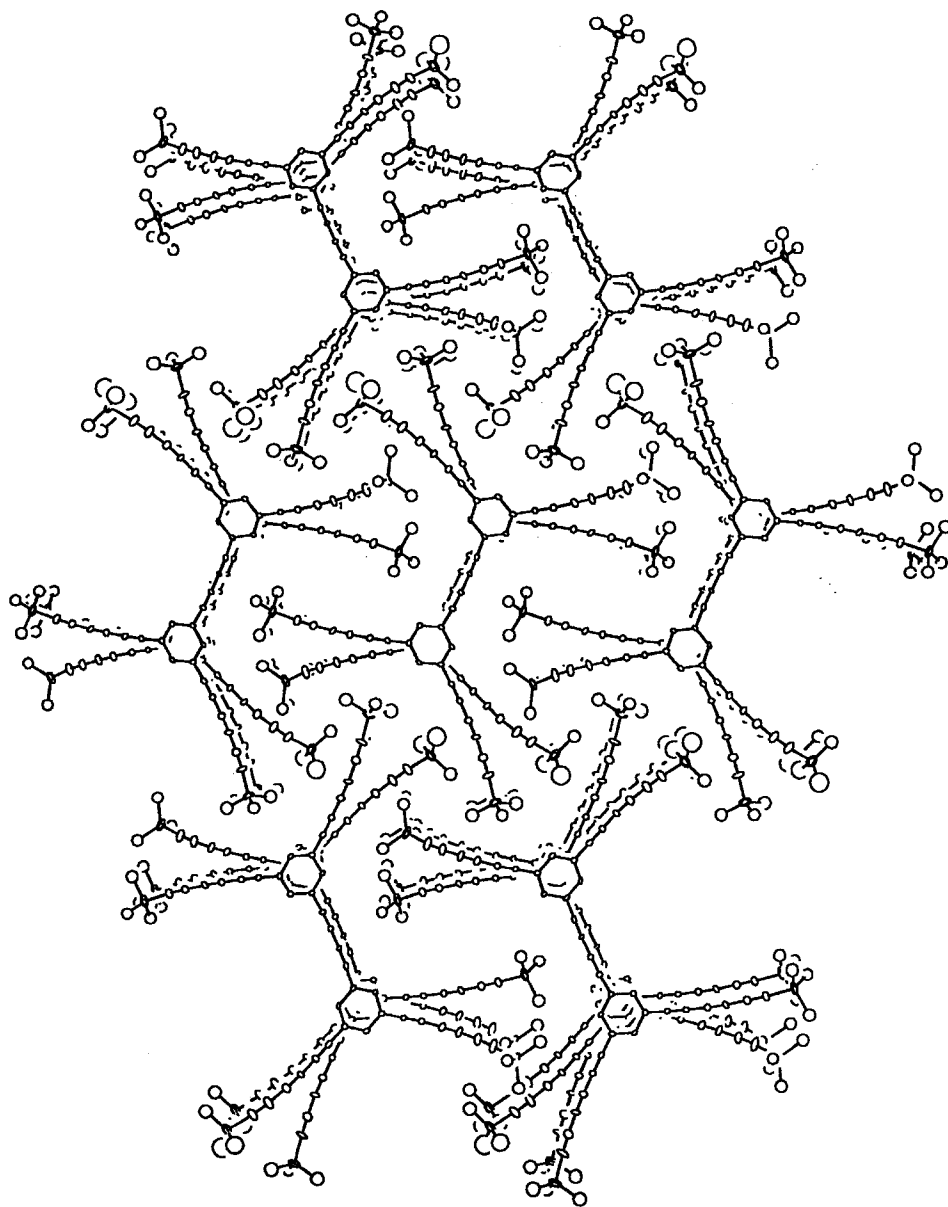


Figure A8. View of crystal packing, with solvent *n*-hexane molecules omitted. View direction is approximately along the crystal *a* axis.

Table A5. Crystallographic Experimental Details**A. Crystal Data**

formula	C ₅₅ H ₄₉ Si ₄
formula weight	822.30
crystal dimensions (mm)	1.00 × 0.10 × 0.03
crystal system	monoclinic
space group	<i>P</i> 2 ₁ / <i>c</i> (No. 14)
unit cell parameters ^a	
<i>a</i> (Å)	7.212 (2)
<i>b</i> (Å)	44.335 (12)
<i>c</i> (Å)	16.183 (4)
β (deg)	93.463 (5)
<i>V</i> (Å ³)	5165 (2)
<i>Z</i>	4
ρ _{calcd} (g cm ⁻³)	1.058
μ (mm ⁻¹)	0.147

B. Data Collection and Refinement Conditions

diffractometer	Bruker PLATFORM/SMART 1000
CCD ^b	
radiation (λ [Å])	graphite-monochromated Mo Kα
(0.71073)	
temperature (°C)	-80
scan type	ω scans (0.2°) (25 s exposures)
data collection 2θ limit (deg)	50.00
total data collected	21024 (-7 ≤ <i>h</i> ≤ 8, -52 ≤ <i>k</i> ≤ 41, -19
≤ <i>l</i> ≤ 18)	
independent reflections	9108 (<i>R</i> _{int} = 0.1952)
number of observed reflections (<i>NO</i>)	2960 [<i>F</i> _o ² ≥ 2σ(<i>F</i> _o ²)]
structure solution method	direct methods (<i>SHELXS-86</i> ^c)
refinement method	full-matrix least-squares on <i>F</i> ²
(<i>SHELXL-93</i> ^d)	
absorption correction method	empirical (<i>SADABS</i>)
range of transmission factors	0.9956–0.8666
data/restraints/parameters	9108 [<i>F</i> _o ² ≥ -3σ(<i>F</i> _o ²)] / 0 / 457
goodness-of-fit (<i>S</i>) ^e	0.990 [<i>F</i> _o ² ≥ -3σ(<i>F</i> _o ²)]
final <i>R</i> indices ^f	
<i>R</i> ₁ [<i>F</i> _o ² ≥ 2σ(<i>F</i> _o ²)]	0.1339
<i>wR</i> ₂ [<i>F</i> _o ² ≥ -3σ(<i>F</i> _o ²)]	0.4207
largest difference peak and hole	1.060 and -0.460 e Å ⁻³

^aObtained from least-squares refinement of 2354 reflections with 4.46° < 2θ <

44.51°.

^bPrograms for diffractometer operation, data collection, data reduction and absorption correction were those supplied by Bruker.

(continued)

Table A5. Crystallographic Experimental Details (continued)

^cSheldrick, G. M. *Acta Crystallogr.* **1990**, *A46*, 467–473.

^dSheldrick, G. M. *SHELXL-93*. Program for crystal structure determination. University of Göttingen, Germany, 1993. Refinement on F_o^2 for all reflections (all of these having $F_o^2 \geq -3\sigma(F_o^2)$). Weighted R -factors wR_2 and all goodnesses of fit S are based on F_o^2 ; conventional R -factors R_1 are based on F_o , with F_o set to zero for negative F_o^2 . The observed criterion of $F_o^2 > 2\sigma(F_o^2)$ is used only for calculating R_1 , and is not relevant to the choice of reflections for refinement. R -factors based on F_o^2 are statistically about twice as large as those based on F_o , and R -factors based on ALL data will be even larger.

^e $S = [\sum w(F_o^2 - F_c^2)^2 / (n - p)]^{1/2}$ (n = number of data; p = number of parameters varied; $w = [\sigma^2(F_o^2) + (0.2000P)^2]^{-1}$ where $P = [\text{Max}(F_o^2, 0) + 2F_c^2] / 3$).

^f $R_1 = \sum |F_o| - |F_c| / \sum |F_o|$; $wR_2 = [\sum w(F_o^2 - F_c^2)^2 / \sum w(F_o^4)]^{1/2}$.

Table A6. Selected Interatomic Distances (Å)*(a) within 1,4-bis(3,5-bis(6-trimethylsilylhexa-1,3,5-triynyl)phenyl)buta-1,3-diyne*

Atom1	Atom2	Distance	Atom1	Atom2	Distance
Si1	C36	1.865(11)	C21	C22	1.399(9)
Si1	C37	1.841(13)	C21	C26	1.386(10)
Si1	C38	1.822(14)	C22	C23	1.380(10)
Si1	C39	1.875(15)	C23	C24	1.395(11)
Si2	C46	1.818(12)	C23	C51	1.426(10)
Si2	C47	1.63(3)	C24	C25	1.406(9)
Si2	C48	1.770(16)	C25	C26	1.401(10)
Si2	C49	1.90(3)	C25	C61	1.442(12)
Si3	C56	1.819(9)	C31	C32	1.187(10)
Si3	C57	1.830(14)	C32	C33	1.404(12)
Si3	C58	1.852(15)	C33	C34	1.177(11)
Si3	C59	1.826(14)	C34	C35	1.384(12)
Si4	C66	1.823(13)	C35	C36	1.174(12)
Si4	C67	1.801(16)	C41	C42	1.205(11)
Si4	C68	1.825(15)	C42	C43	1.335(12)
Si4	C69	1.849(18)	C43	C44	1.192(12)
C1	C2	1.189(10)	C44	C45	1.418(15)
C1	C11	1.460(11)	C45	C46	1.194(13)
C2	C3	1.361(11)	C51	C52	1.190(10)
C3	C4	1.202(10)	C52	C53	1.374(11)
C4	C21	1.424(11)	C53	C54	1.190(10)
C11	C12	1.413(9)	C54	C55	1.407(12)
C11	C16	1.386(10)	C55	C56	1.208(12)
C12	C13	1.402(10)	C61	C62	1.221(12)
C13	C14	1.402(11)	C62	C63	1.379(14)
C13	C31	1.435(10)	C63	C64	1.174(13)
C14	C15	1.397(10)	C64	C65	1.399(16)
C15	C16	1.369(10)	C65	C66	1.203(15)
C15	C41	1.454(12)			

Primed atoms are related to unprimed ones via the crystallographic inversion center ($1/2, 0, 1/2$).

**University of Alberta Department of Chemistry
X-Ray Crystallography Laboratory**

Structure Report for Compound 134

XCL Code: RRT0249

Date: 18 December 2002

Compound: 1,8-Bis(triisopropylsilyl)octa-1,3,5,7-tetrayne

Formula: C₂₆H₄₂Si₂

Supervisor: R. R. Tykwinski **Crystallographer:** R. McDonald

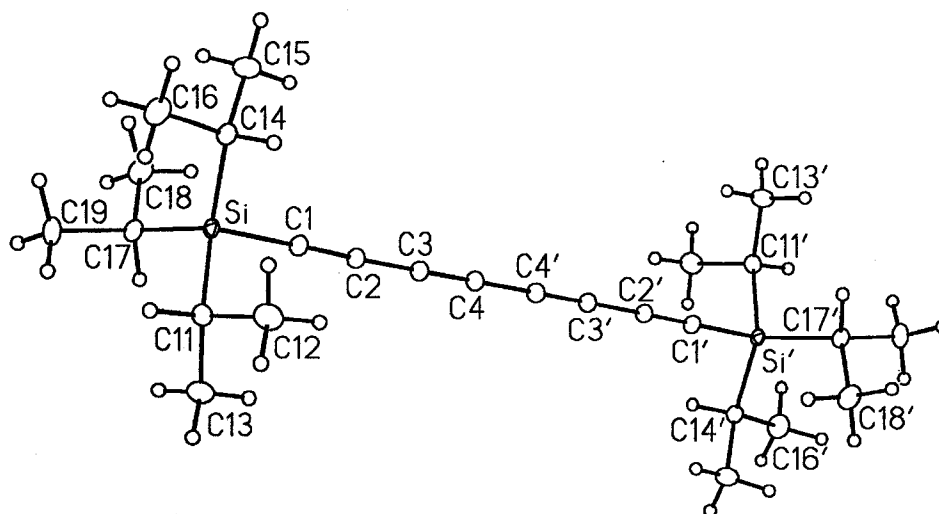


Figure A9. Perspective view of the 1,8-bis(triisopropylsilyl)octa-1,3,5,7-tetrayne molecule showing the atom labelling scheme. Non-hydrogen atoms are represented by Gaussian ellipsoids at the 20% probability level. Hydrogen atoms are shown with arbitrarily small thermal parameters. Primed atoms are related to unprimed ones via the crystallographic inversion center (0, 0, 0) at the midpoint of the C4–C4' bond.

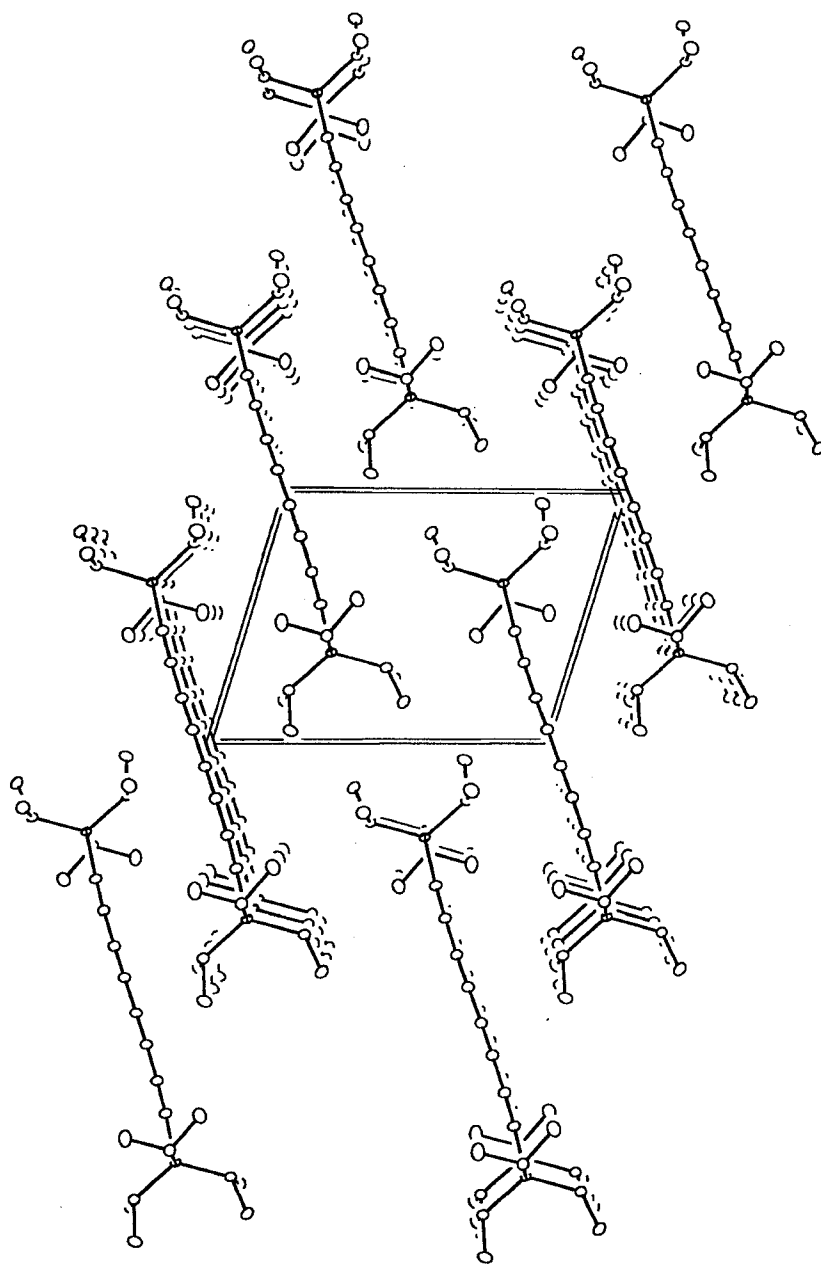


Figure A10. Illustration of crystal packing. View direction is along the unit cell *a* axis.

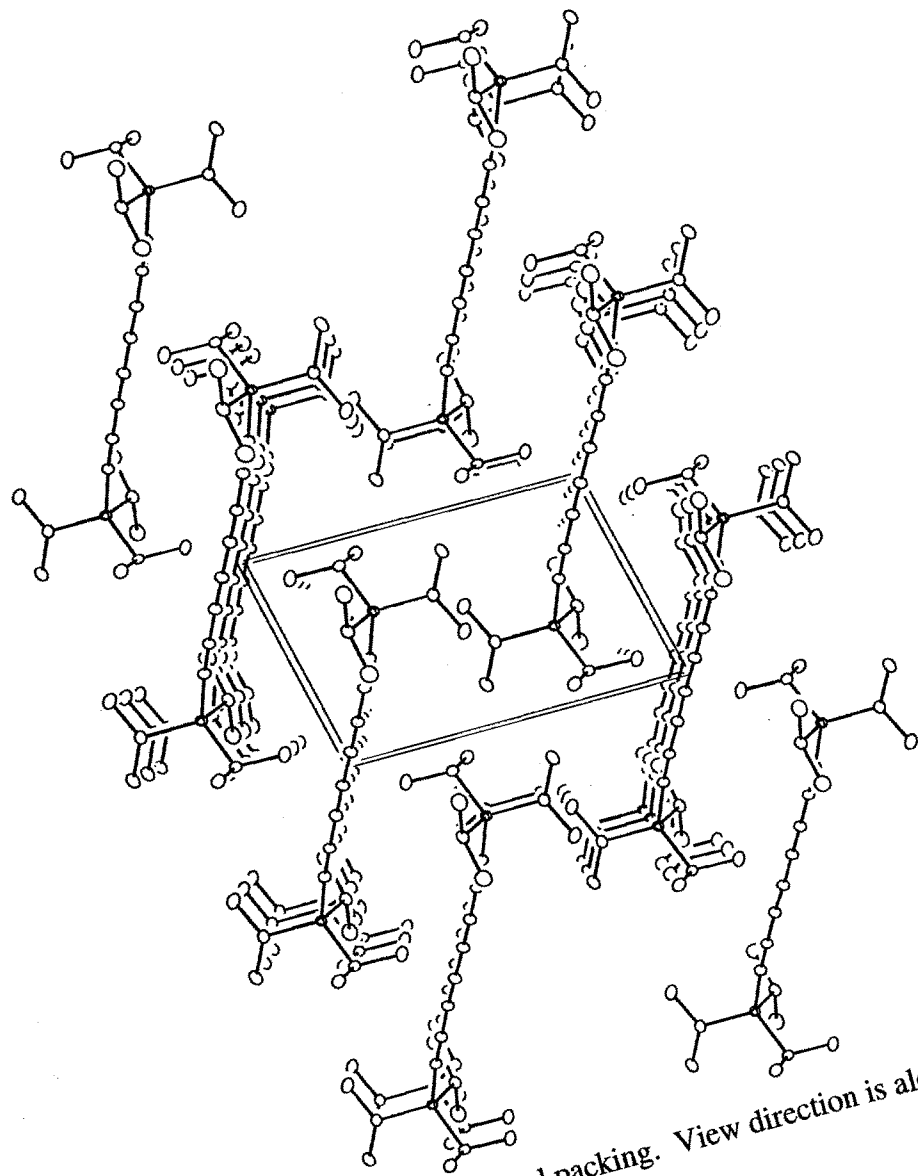


Figure A11. Illustration of crystal packing. View direction is along the unit cell *b* axis.

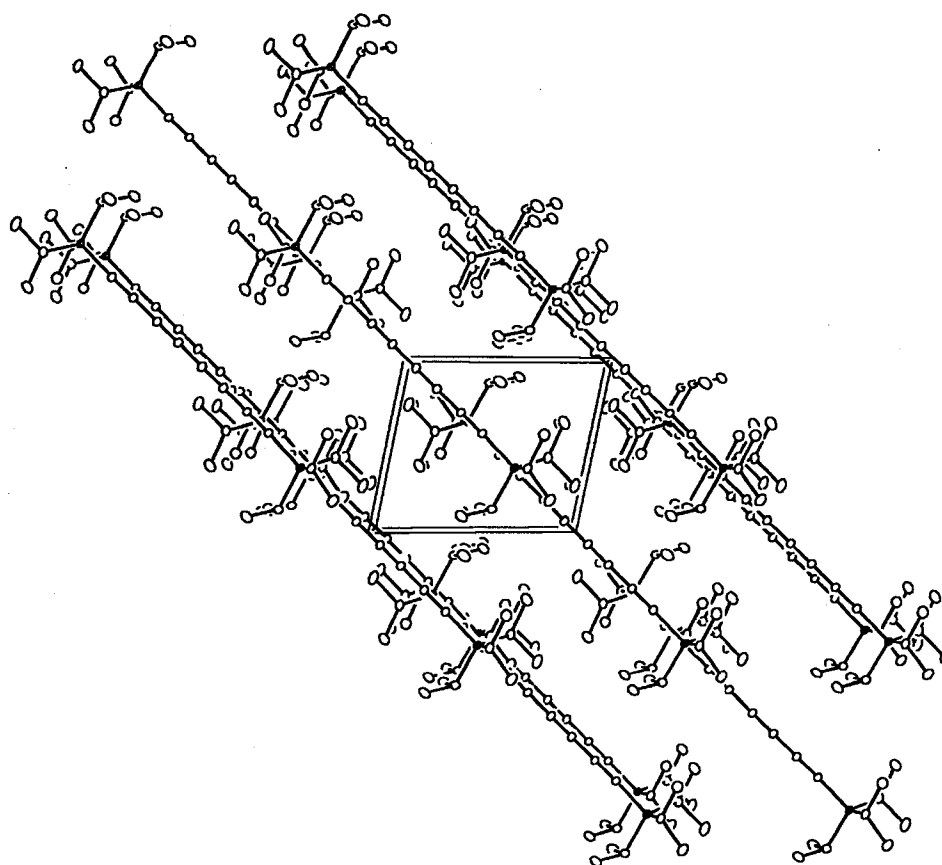


Figure A12. Illustration of crystal packing. View direction is along the unit cell *c* axis.

Table A9. Crystallographic Experimental Details

<i>A. Crystal Data</i>	
formula	C ₂₆ H ₄₂ Si ₂
formula weight	410.78
crystal dimensions (mm)	0.58 × 0.28 × 0.10
crystal system	triclinic
space group	<i>P</i> $\bar{1}$ (No. 2)
unit cell parameters ^a	
<i>a</i> (Å)	7.2615 (6)
<i>b</i> (Å)	8.7028 (7)
<i>c</i> (Å)	11.4850 (9)
α (deg)	104.8780 (13)
β (deg)	100.6479 (15)
γ (deg)	98.4852 (14)
<i>V</i> (Å ³)	674.70 (9)
<i>Z</i>	1
ρ _{calcd} (g cm ⁻³)	1.011
μ (mm ⁻¹)	0.140
<i>B. Data Collection and Refinement Conditions</i>	
diffractometer	Bruker PLATFORM/SMART 1000 CCD ^b
radiation (λ [Å])	graphite-monochromated Mo Kα (0.71073)
temperature (°C)	-80
scan type	ω scans (0.2°) (25 s exposures)
data collection 2θ limit (deg)	52.80
total data collected	3857 (-8 ≤ <i>h</i> ≤ 9, -10 ≤ <i>k</i> ≤ 10, -14 ≤ <i>l</i> ≤ 14)
independent reflections	2717 (<i>R</i> _{int} = 0.0140)
number of observed reflections (<i>NO</i>)	2474 [<i>F</i> _o ² ≥ 2σ(<i>F</i> _o ²)]
structure solution method	direct methods (<i>SHELXS-86</i> ^c)
refinement method	full-matrix least-squares on <i>F</i> ² (<i>SHELXL-93</i> ^d)
absorption correction method	Gaussian integration (face-indexed)
range of transmission factors	0.9861–0.9232
data/restraints/parameters	2717 [<i>F</i> _o ² ≥ -3σ(<i>F</i> _o ²)] / 0 / 127
goodness-of-fit (<i>S</i>) ^e	1.042 [<i>F</i> _o ² ≥ -3σ(<i>F</i> _o ²)]
final <i>R</i> indices ^f	
<i>R</i> ₁ [<i>F</i> _o ² ≥ 2σ(<i>F</i> _o ²)]	0.0379
<i>wR</i> ₂ [<i>F</i> _o ² ≥ -3σ(<i>F</i> _o ²)]	0.1022
largest difference peak and hole	0.444 and -0.146 e Å ⁻³

^aObtained from least-squares refinement of 3607 reflections with 4.95° < 2θ < 52.81°.
(continued)

Table A9. Crystallographic Experimental Details (continued)

^bPrograms for diffractometer operation, data collection, data reduction and absorption correction were those supplied by Bruker.

^cSheldrick, G. M. *Acta Crystallogr.* **1990**, *A46*, 467–473.

^dSheldrick, G. M. *SHELXL-93*. Program for crystal structure determination. University of Göttingen, Germany, 1993. Refinement on F_o^2 for all reflections (all of these having $F_o^2 \geq -3\sigma(F_o^2)$). Weighted R -factors wR_2 and all goodnesses of fit S are based on F_o^2 ; conventional R -factors R_1 are based on F_o , with F_o set to zero for negative F_o^2 . The observed criterion of $F_o^2 > 2\sigma(F_o^2)$ is used only for calculating R_1 , and is not relevant to the choice of reflections for refinement. R -factors based on F_o^2 are statistically about twice as large as those based on F_o , and R -factors based on ALL data will be even larger.

^e $S = [\sum w(F_o^2 - F_c^2)^2 / (n - p)]^{1/2}$ (n = number of data; p = number of parameters varied; $w = [\sigma^2(F_o^2) + (0.0573P)^2 + 0.1686P]^{-1}$ where $P = [\text{Max}(F_o^2, 0) + 2F_c^2]/3$).

$$^fR_1 = \sum |F_o| - |F_c| / \sum |F_o|; wR_2 = [\sum w(F_o^2 - F_c^2)^2 / \sum w(F_o^4)]^{1/2}.$$

Table A10. Selected Interatomic Distances (Å)

Atom1	Atom2	Distance	Atom1	Atom2	Distance
Si	C1	1.8534(14)	C4	C4'	1.363(3)
Si	C11	1.8819(14)	C11	C12	1.529(2)
Si	C14	1.8810(14)	C11	C13	1.528(2)
Si	C17	1.8872(14)	C14	C15	1.531(2)
C1	C2	1.2122(18)	C14	C16	1.535(2)
C2	C3	1.3682(18)	C17	C18	1.529(2)
C3	C4	1.2061(18)	C17	C19	1.5329(19)

Table A11. Selected Interatomic Angles (deg)

Atom1	Atom2	Atom3	Angle
C1	Si	C11	105.35(6)
C1	Si	C14	105.90(6)
C1	Si	C17	106.30(6)
C11	Si	C14	110.55(7)
C11	Si	C17	110.52(6)
C14	Si	C17	117.33(6)
Si	C1	C2	175.85(12)
C1	C2	C3	178.30(15)
C2	C3	C4	178.45(15)
C3	C4	C4'	179.4(2)
Si	C11	C12	111.86(10)
Si	C11	C13	112.07(10)
C12	C11	C13	110.05(12)
Si	C14	C15	115.03(11)
Si	C14	C16	113.02(11)
C15	C14	C16	110.55(13)
Si	C17	C18	114.35(10)
Si	C17	C19	113.43(10)
C18	C17	C19	110.63(12)

**University of Alberta Department of Chemistry
X-Ray Crystallography Laboratory**

Structure Report for Compound 135

XCL Code: RRT0233

Date: 30 September 2002

Compound: 1,10-di(triisopropylsilyl)deca-1,3,5,7,9-pentayne

Formula: C₂₈H₄₂Si₂

Supervisor: R. R. Tykwinski **Crystallographer:** M. J. Ferguson

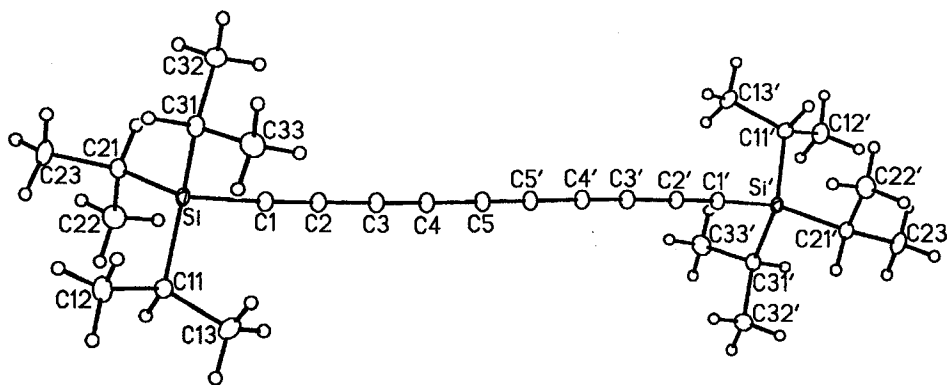


Figure A13. Perspective view of the 1,10-di(triisopropylsilyl)deca-1,3,5,7,9-pentayne molecule showing the atom labelling scheme. Non-hydrogen atoms are represented by Gaussian ellipsoids at the 20% probability level. Hydrogen atoms are shown with arbitrarily small thermal parameters. Primed atoms are related to the unprimed atoms by the crystallographic inversion centre located at $(0, \frac{1}{2}, \frac{1}{2})$.

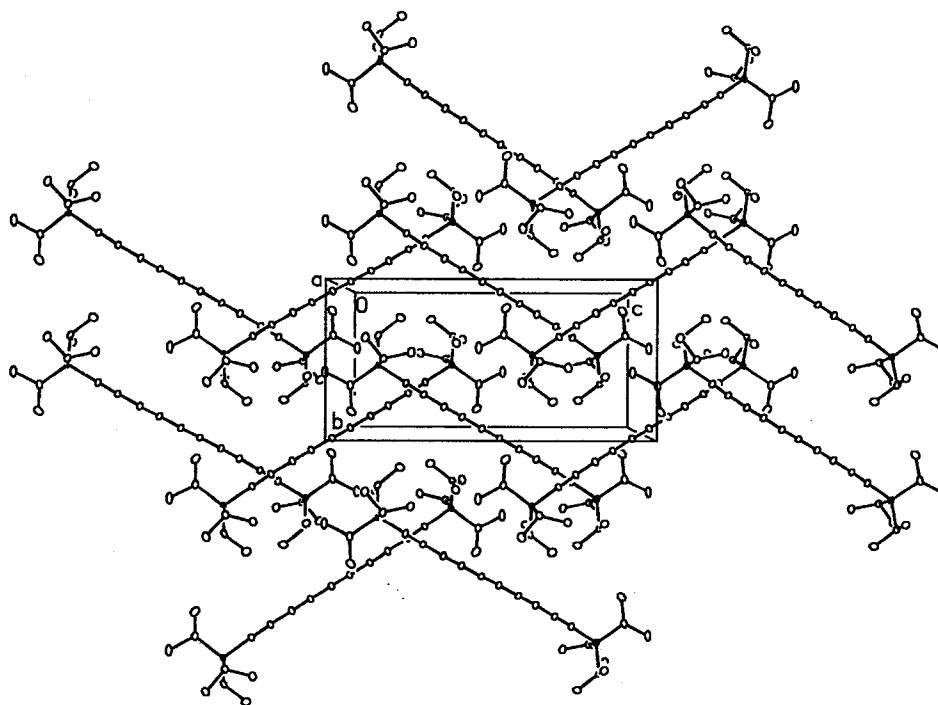


Figure A14. Packing diagram looking down the crystallographic *a* axis. The unit cell is shown.

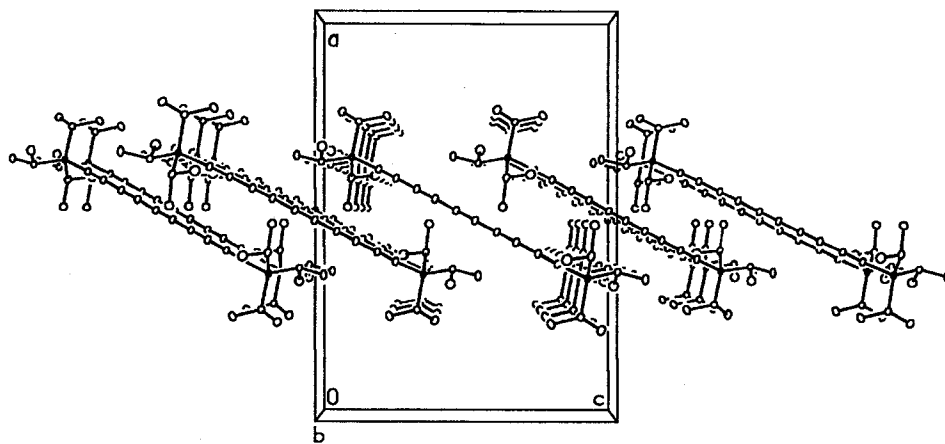


Figure A15. Packing diagram looking down the crystallographic *b* axis. The unit cell is shown.

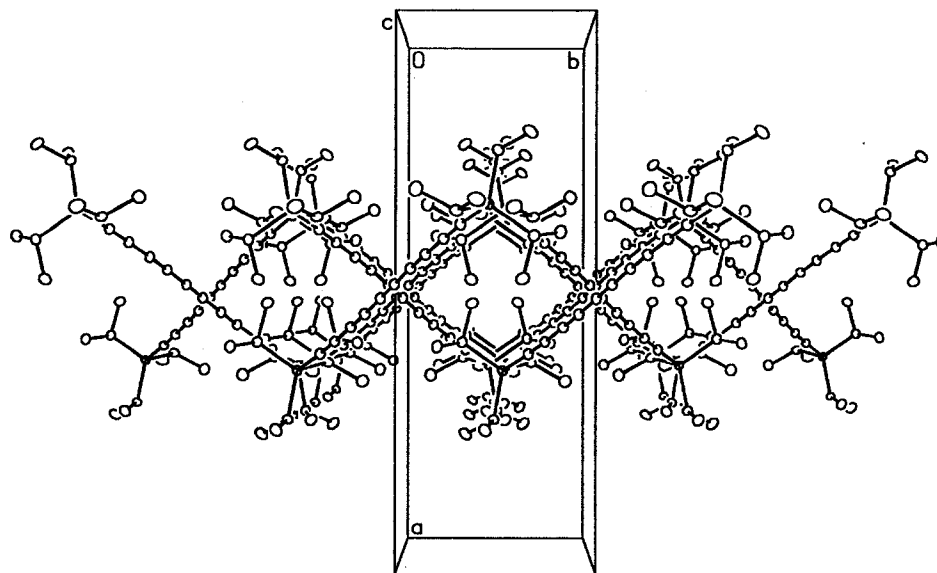


Figure A16. Packing diagram looking down the crystallographic *c* axis. The unit cell is shown.

Table A13. Crystallographic Experimental Details**A. Crystal Data**

formula	C ₂₈ H ₄₂ Si ₂
formula weight	434.80
crystal dimensions (mm)	0.94 × 0.69 × 0.06
crystal system	monoclinic
space group	C2/c (No. 15)
unit cell parameters ^a	
	<i>a</i> (Å) 21.699 (3)
	<i>b</i> (Å) 7.8425 (11)
	<i>c</i> (Å) 16.242 (2)
	β (deg) 90.184 (3)
	<i>V</i> (Å ³) 2764.0 (7)
	<i>Z</i> 4
ρ_{calcd} (g cm ⁻³)	1.045
μ (mm ⁻¹)	0.140

B. Data Collection and Refinement Conditions

diffractometer	Bruker PLATFORM/SMART 1000 CCD ^b
radiation (λ [Å])	graphite-monochromated Mo K α (0.71073)
temperature (°C)	-80
scan type	ω scans (0.2°) (25 s exposures)
data collection 2θ limit (deg)	52.84
total data collected	8681 ($-26 \leq h \leq 27$, $-9 \leq k \leq 9$, $-20 \leq l \leq 20$)
independent reflections	2833 ($R_{\text{int}} = 0.0394$)
number of observed reflections (<i>NO</i>)	2414 [$F_o^2 \geq 2\sigma(F_o^2)$]
structure solution method	direct methods (<i>SIR97</i> ^c)
refinement method	full-matrix least-squares on F^2
(<i>SHELXL-93</i> ^d)	
absorption correction method	empirical (<i>SADABS</i>)
range of transmission factors	0.9916–0.8796
data/restraints/parameters	2833 [$F_o^2 \geq -3\sigma(F_o^2)$] / 0 / 136
goodness-of-fit (<i>S</i>) ^e	1.050 [$F_o^2 \geq -3\sigma(F_o^2)$]
final <i>R</i> indices ^f	
	R_1 [$F_o^2 \geq 2\sigma(F_o^2)$] 0.0420
	wR_2 [$F_o^2 \geq -3\sigma(F_o^2)$] 0.1161
largest difference peak and hole	0.622 and -0.318 e Å ⁻³

^aObtained from least-squares refinement of 5063 reflections with $5.02^\circ < 2\theta < 52.78^\circ$.

^bPrograms for diffractometer operation, data collection, data reduction and

absorption correction were those supplied by Bruker.

Table A13. Crystallographic Experimental Details (continued)

^cAltomare, A.; Burla, M. C.; Camalli, M.; Cascarano, G. L.; Giacovazzo, C.; Guagliardi, A.; Moliterni, A. G. G.; Polidori, G.; Spagna, R. *J. Appl. Cryst.* **1999**, *32*, 115–119.

^dSheldrick, G. M. *SHELXL-93*. Program for crystal structure determination. University of Göttingen, Germany, 1993. Refinement on F_o^2 for all reflections (all of these having $F_o^2 \geq -3\sigma(F_o^2)$). Weighted R -factors wR_2 and all goodnesses of fit S are based on F_o^2 ; conventional R -factors R_1 are based on F_o , with F_o set to zero for negative F_o^2 . The observed criterion of $F_o^2 > 2\sigma(F_o^2)$ is used only for calculating R_1 , and is not relevant to the choice of reflections for refinement. R -factors based on F_o^2 are statistically about twice as large as those based on F_o , and R -factors based on ALL data will be even larger.

^e $S = [\sum w(F_o^2 - F_c^2)^2 / (n - p)]^{1/2}$ (n = number of data; p = number of parameters varied; $w = [\sigma^2(F_o^2) + (0.0717P)^2 + 0.8883P]^{-1}$ where $P = [\text{Max}(F_o^2, 0) + 2F_c^2]/3$).

^f $R_1 = \sum |F_o| - |F_c| / \sum |F_o|$; $wR_2 = [\sum w(F_o^2 - F_c^2)^2 / \sum w(F_o^4)]^{1/2}$.

Table A14. Selected Interatomic Distances (Å)

Atom1	Atom2	Distance
Si	C1	1.8511(15)
Si	C11	1.8847(15)
Si	C21	1.8805(15)
Si	C31	1.8827(16)
C1	C2	1.209(2)
C2	C3	1.3673(19)
C3	C4	1.208(2)
C4	C5	1.357(2)
C5	C5'	1.209(3)†
C11	C12	1.536(2)
C11	C13	1.534(2)
C21	C22	1.531(3)
C21	C23	1.533(2)
C31	C32	1.533(2)
C31	C33	1.533(2)

Table A15. Selected Interatomic Angles (deg)

Atom1	Atom2	Atom3	Angle
C1	Si	C11	107.07(6)
C1	Si	C21	105.69(7)
C1	Si	C31	105.48(7)
C11	Si	C21	112.69(7)
C11	Si	C31	114.62(7)
C21	Si	C31	110.56(7)
Si	C1	C2	177.36(14)
C1	C2	C3	178.89(17)
C2	C3	C4	178.81(17)
C3	C4	C5	178.92(17)
C4	C5	C5'	179.7(2)†
Si	C11	C12	111.70(11)
Si	C11	C13	114.23(11)
C12	C11	C13	110.18(13)
Si	C21	C22	112.59(11)
Si	C21	C23	113.72(12)
C22	C21	C23	110.84(14)
Si	C31	C32	110.51(11)
Si	C31	C33	113.91(11)
C32	C31	C33	109.78(13)

**University of Alberta Department of Chemistry
X-Ray Crystallography Laboratory**

Structure Report for Compound 136

XCL Code: RRT0044

Date: 13 July 2001

Compound: 1,12-Bis(triisopropylsilyl)dodeca-1,3,5,7,9,11-hexayne

Formula: $C_{30}H_{42}Si_2$

Supervisor: R. R. Tykwinski

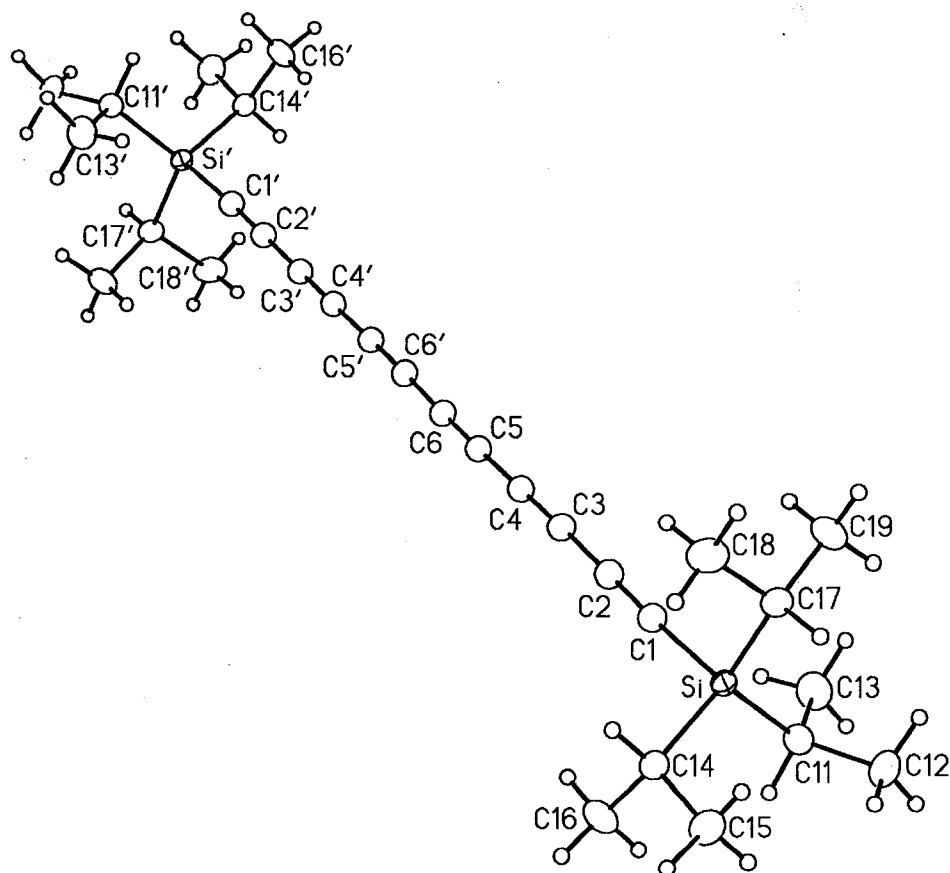


Figure A17. Perspective view of the 1,12-bis(triisopropylsilyl)dodeca-1,3,5,7,9,11-hexayne molecule showing the atom labelling scheme. Non-hydrogen atoms are represented by Gaussian ellipsoids at the 20% probability level. Hydrogen atoms are shown with arbitrarily small thermal parameters. Primed atoms are related to unprimed ones via the crystallographic inversion center ($\frac{1}{2}, 0, \frac{1}{2}$) located at the midpoint of the C6–C6' bond.

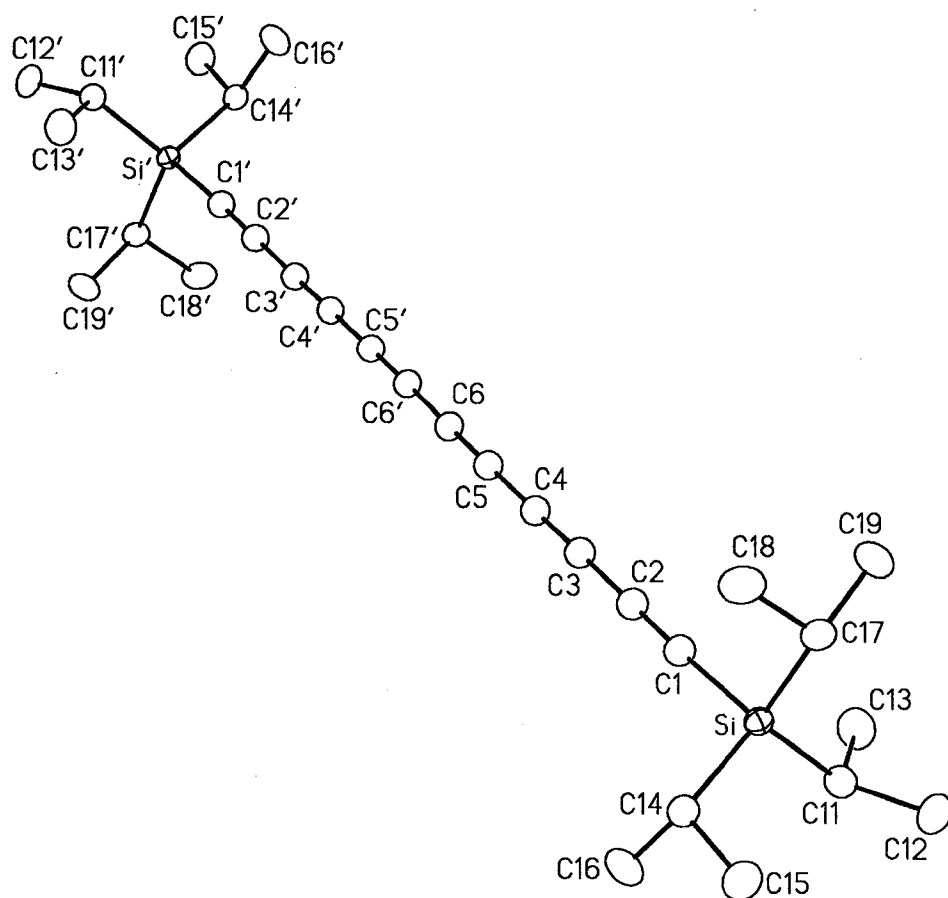


Figure A18. View as in Figure 1, with hydrogen atoms omitted.

Table A17. Crystallographic Experimental Details**A. Crystal Data**

formula	$C_{30}H_{42}Si_2$
formula weight	458.82
crystal dimensions (mm)	0.50 × 0.35 × 0.25
crystal system	monoclinic
space group	$P2_1/c$ (No. 14)
unit cell parameters ^a	
	a (Å) 8.2757 (6)
	b (Å) 13.4444 (11)
	c (Å) 13.9444 (11)
	β (deg) 97.7225 (16)
	V (Å ³) 1537.4 (2)
	Z 2
ρ_{calcd} (g cm ⁻³)	0.991
μ (mm ⁻¹)	0.129

B. Data Collection and Refinement Conditions

diffractometer	Bruker P4/RA/SMART 1000 CCD ^b
radiation (λ [Å])	graphite-monochromated Mo K α (0.71073)
temperature (°C)	-80
scan type	ϕ rotations (0.3°) / ω scans (0.3°) (20 s
exposures)	
data collection 2θ limit (deg)	52.78
total data collected	8904 ($-10 \leq h \leq 9$, $-16 \leq k \leq 16$, $-15 \leq l \leq 17$)
independent reflections	3156
number of observed reflections (NO)	2353 [$F_o^2 \geq 2\sigma(F_o^2)$]
structure solution method	direct methods (<i>SHELXS-86</i> ^c)
refinement method	full-matrix least-squares on F^2
(<i>SHELXL-93</i> ^d)	
absorption correction method	empirical (<i>SADABS</i>)
range of transmission factors	0.9703–0.8350
data/restraints/parameters	3156 [$F_o^2 \geq -3\sigma(F_o^2)$] / 0 / 145
goodness-of-fit (S) ^e	1.029 [$F_o^2 \geq -3\sigma(F_o^2)$]
final R indices ^f	
	R_1 [$F_o^2 \geq 2\sigma(F_o^2)$] 0.0402
	wR_2 [$F_o^2 \geq -3\sigma(F_o^2)$] 0.1067
largest difference peak and hole	0.272 and -0.124 e Å ⁻³

^aObtained from least-squares refinement of 6183 centered reflections.

^bPrograms for diffractometer operation, data collection, data reduction and absorption correction were those supplied by Bruker.

Table A17. Crystallographic Experimental Details (continued)

^cSheldrick, G. M. *Acta Crystallogr.* **1990**, *A46*, 467–473.

^dSheldrick, G. M. *SHELXL-93*. Program for crystal structure determination. University of Göttingen, Germany, 1993. Refinement on F_o^2 for all reflections (all of these having $F_o^2 \geq -3\sigma(F_o^2)$). Weighted R -factors wR_2 and all goodnesses of fit S are based on F_o^2 ; conventional R -factors R_1 are based on F_o , with F_o set to zero for negative F_o^2 . The observed criterion of $F_o^2 > 2\sigma(F_o^2)$ is used only for calculating R_1 , and is not relevant to the choice of reflections for refinement. R -factors based on F_o^2 are statistically about twice as large as those based on F_o , and R -factors based on ALL data will be even larger.

^e $S = [\sum w(F_o^2 - F_c^2)^2 / (n - p)]^{1/2}$ (n = number of data; p = number of parameters varied; $w = [\sigma^2(F_o^2) + (0.0585P)^2 + 0.0187P]^{-1}$ where $P = [\text{Max}(F_o^2, 0) + 2F_c^2]/3$).

^f $R_1 = \sum |F_o| - |F_c| / \sum |F_o|$; $wR_2 = [\sum w(F_o^2 - F_c^2)^2 / \sum w(F_o^4)]^{1/2}$.

Table A18. Selected Interatomic Distances (Å)

Atom1	Atom2	Distance
Si	C1	1.8522(16)
Si	C11	1.8820(16)
Si	C14	1.8811(16)
Si	C17	1.8764(17)
C1	C2	1.206(2)
C2	C3	1.368(2)
C3	C4	1.208(2)
C4	C5	1.356(2)
C5	C6	1.2090(19)
C6	C6'	1.358(3)
C11	C12	1.529(2)
C11	C13	1.526(2)
C14	C15	1.526(2)
C14	C16	1.534(3)
C17	C18	1.531(2)
C17	C19	1.525(2)

Table A19. Selected Interatomic Angles (deg)

Atom1	Atom2	Atom3	Angle
C1	Si	C11	107.37(7)
C1	Si	C14	106.36(7)
C1	Si	C17	104.93(7)
C11	Si	C14	110.91(7)
C11	Si	C17	115.17(8)
C14	Si	C17	111.44(8)
Si	C1	C2	177.88(15)
C1	C2	C3	179.3(2)
C2	C3	C4	178.91(19)
C3	C4	C5	178.50(18)
C4	C5	C6	178.80(18)
C5	C6	C6'	179.3(2)
Si	C11	C12	113.34(12)
Si	C11	C13	114.66(12)
C12	C11	C13	110.32(15)
Si	C14	C15	112.15(12)
Si	C14	C16	111.95(11)
C15	C14	C16	111.22(16)
Si	C17	C18	110.78(12)
Si	C17	C19	112.56(12)
C18	C17	C19	110.06(14)

Primed atoms are related to unprimed ones via the crystallographic inversion center $(\frac{1}{2}, 0, \frac{1}{2})$.

University of Alberta Department of Chemistry
X-Ray Crystallography Laboratory

Structure Report for Compound 137

XCL Code: RRT0137

Date: 25 September 2001

Compound: 1,16-bis(triisopropylsilyl)hexadeca-1,3,5,7,9,11,13,15-octayne

Formula: C₃₄H₄₂Si₂

Supervisor: R. R. Tykwinski **Crystallographer:** R. McDonald

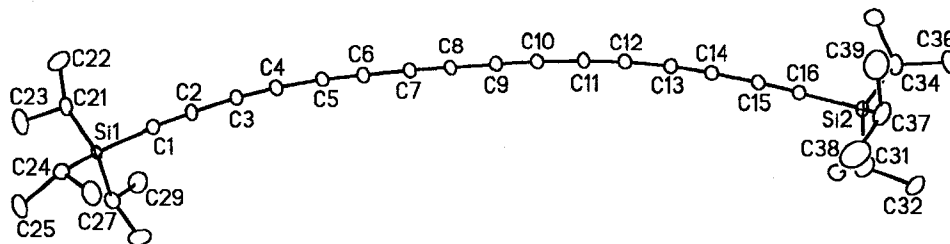


Figure A19 Perspective view of the 1,16-bis(triisopropylsilyl)hexadeca-1,3,5,7,9,11,13,15-octayne molecule showing the atom labelling scheme. Non-hydrogen atoms are represented by Gaussian ellipsoids at the 20% probability level. Hydrogen atoms are not shown.

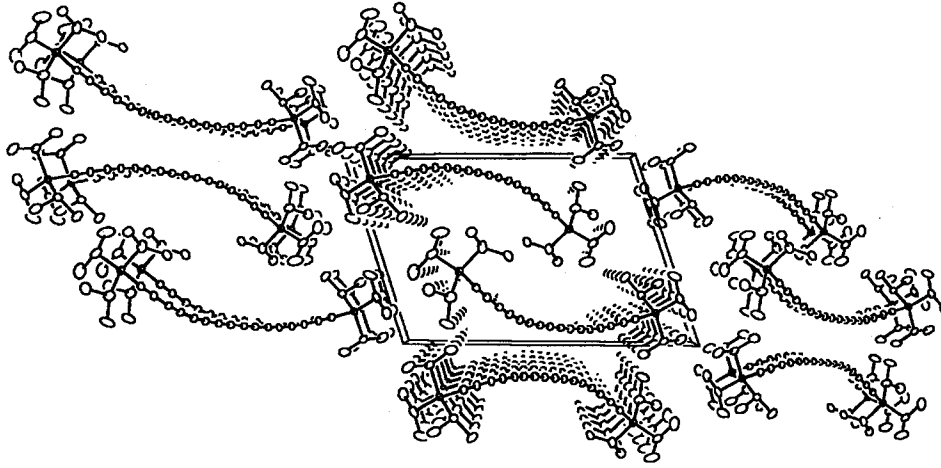


Figure A20. Illustration of crystal packing, with the unit cell boundaries as indicated. The view direction is parallel to the crystallographic a axis.

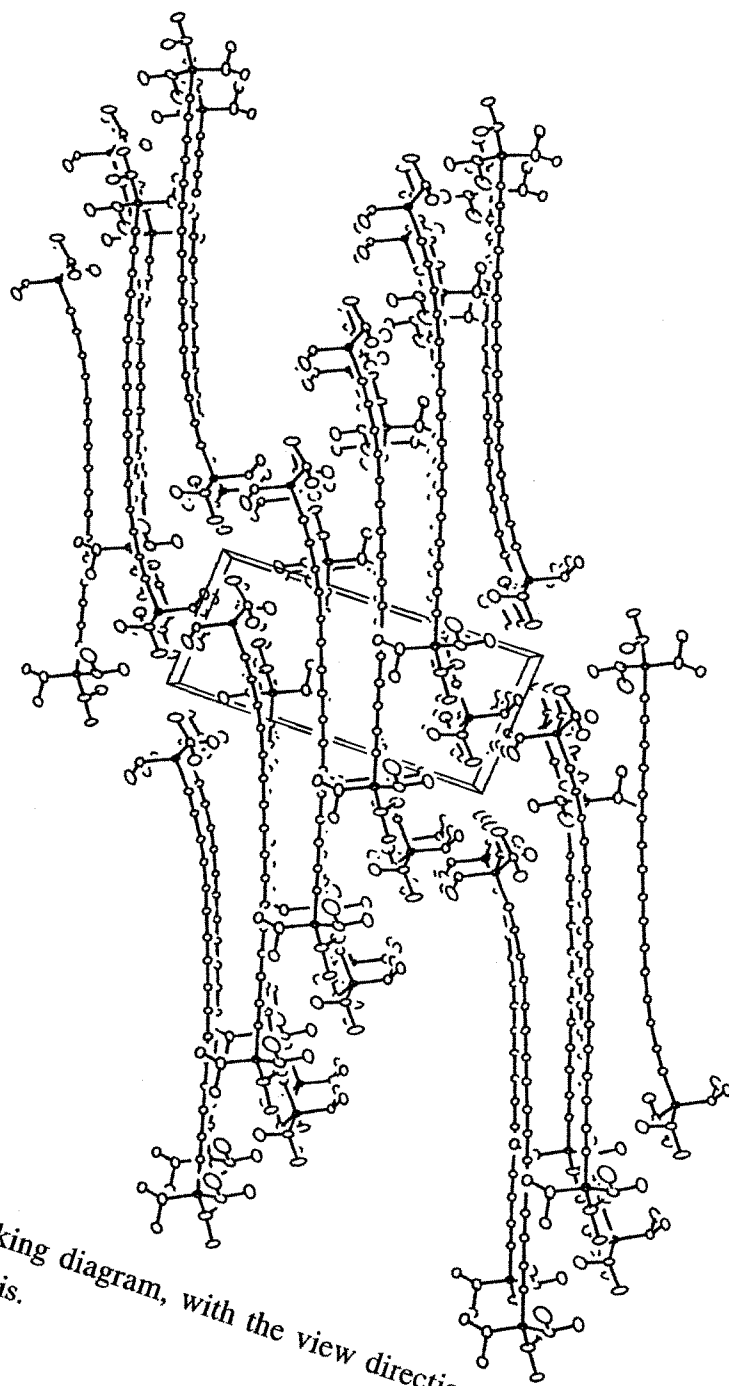


Figure A21. Crystal packing diagram, with the view direction parallel to the crystallographic *b* axis.

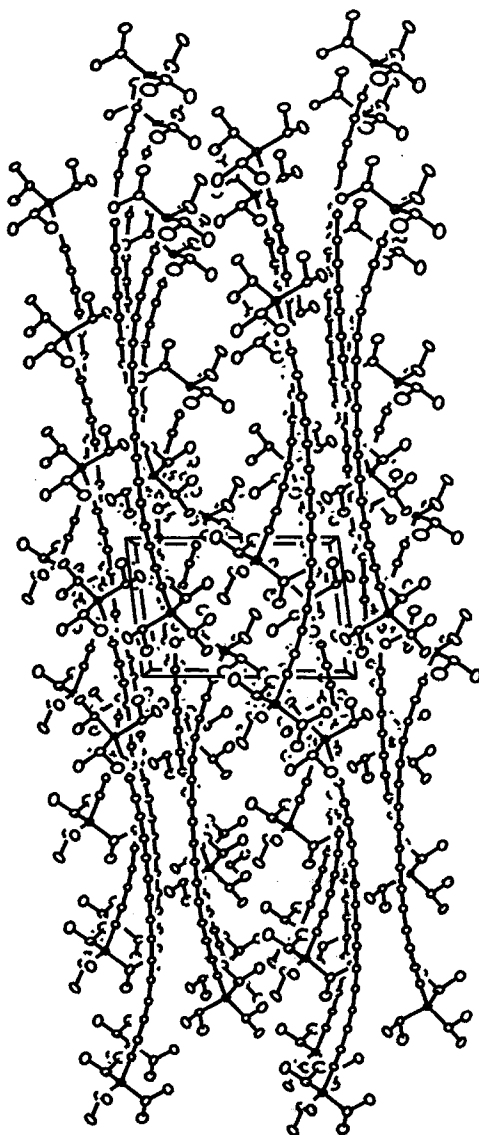


Figure A22. Crystal packing diagram, with the view direction parallel to the crystallographic *c* axis.

Table A21. Crystallographic Experimental Details**A. Crystal Data**

formula	C ₃₄ H ₄₂ Si ₂
formula weight	506.86
crystal dimensions (mm)	0.59 × 0.30 × 0.02
crystal system	triclinic
space group	PI (No. 2)
unit cell parameters ^a	
	<i>a</i> (Å) 7.6441 (14)
	<i>b</i> (Å) 12.485 (2)
	<i>c</i> (Å) 18.300 (3)
	α (deg) 70.701 (4)
	β (deg) 82.758 (4)
	γ (deg) 80.500 (4)
	<i>V</i> (Å ³) 1620.9 (5)
	<i>Z</i> 2
ρ_{calcd} (g cm ⁻³)	1.038
μ (mm ⁻¹)	0.128

B. Data Collection and Refinement Conditions

diffractometer	Bruker PLATFORM/SMART 1000 CCD ^b
radiation (λ [Å])	graphite-monochromated Mo K α (0.71073)
temperature (°C)	-80
scan type	ω scans (0.2°) (30 s exposures)
data collection 2θ limit (deg)	52.74
total data collected	7639 ($-9 \leq h \leq 8, -15 \leq k \leq 15, -21 \leq l \leq 22$)
independent reflections	6146 ($R_{\text{int}} = \text{RINT}$)
number of observed reflections (<i>NO</i>)	0.0748 [$F_o^2 \geq 2\sigma(F_o^2)$]
structure solution method	direct methods (<i>SHELXS-86</i> ^c)
refinement method	full-matrix least-squares on F^2
(<i>SHELXL-93</i> ^d)	
absorption correction method	Gaussian integration (face-indexed)
range of transmission factors	0.9973–0.9585
data/restraints/parameters	6146 [$F_o^2 \geq -3\sigma(F_o^2)$] / 0 / 325
goodness-of-fit (<i>S</i>) ^e	0.877 [$F_o^2 \geq -3\sigma(F_o^2)$]
final <i>R</i> indices ^f	
	R_1 [$F_o^2 \geq 2\sigma(F_o^2)$] 0.0714
	wR_2 [$F_o^2 \geq -3\sigma(F_o^2)$] 0.1673
largest difference peak and hole	0.651 and -0.412 e Å ⁻³

^aObtained from least-squares refinement of 2358 centered reflections.

Table A21. Crystallographic Experimental Details (continued)

^bPrograms for diffractometer operation, data collection, data reduction and absorption correction were those supplied by Bruker.

^cSheldrick, G. M. *Acta Crystallogr.* **1990**, *A46*, 467–473.

^dSheldrick, G. M. *SHELXL-93*. Program for crystal structure determination. University of Göttingen, Germany, 1993. Refinement on F_o^2 for all reflections (all of these having $F_o^2 \geq -3\sigma(F_o^2)$). Weighted R -factors wR_2 and all goodnesses of fit S are based on F_o^2 ; conventional R -factors R_1 are based on F_o , with F_o set to zero for negative F_o^2 . The observed criterion of $F_o^2 > 2\sigma(F_o^2)$ is used only for calculating R_1 , and is not relevant to the choice of reflections for refinement. R -factors based on F_o^2 are statistically about twice as large as those based on F_o , and R -factors based on ALL data will be even larger.

^e $S = [\sum w(F_o^2 - F_c^2)^2 / (n - p)]^{1/2}$ (n = number of data; p = number of parameters varied; $w = [\sigma^2(F_o^2) + (0.0640P)^2]^{-1}$ where $P = [\text{Max}(F_o^2, 0) + 2F_c^2]/3$).

^f $R_1 = \sum |F_o| - |F_c| / \sum |F_o|$; $wR_2 = [\sum w(F_o^2 - F_c^2)^2 / \sum w(F_o^4)]^{1/2}$.

Table A22. Selected Interatomic Distances (Å)

Atom1	Atom2	Distance
Si1	C1	1.849(4)
Si1	C21	1.878(4)
Si1	C24	1.872(4)
Si1	C27	1.862(4)
Si2	C16	1.845(4)
Si2	C31	1.892(5)
Si2	C34	1.853(5)
Si2	C37	1.849(5)
C1	C2	1.199(5)
C2	C3	1.367(5)
C3	C4	1.195(4)
C4	C5	1.373(5)
C5	C6	1.199(4)
C6	C7	1.354(5)
C7	C8	1.197(4)
C8	C9	1.356(5)
C9	C10	1.209(5)
C10	C11	1.352(5)
C11	C12	1.207(4)
C12	C13	1.348(5)
C13	C14	1.199(4)
C14	C15	1.380(5)
C15	C16	1.197(4)
C21	C22	1.519(6)
C21	C23	1.509(5)
C24	C25	1.532(6)
C24	C26	1.512(5)
C27	C28	1.501(6)
C27	C29	1.534(6)
C31	C32	1.521(5)
C31	C33	1.434(6)
C34	C35	1.485(6)
C34	C36	1.520(5)
C37	C38	1.512(7)
C37	C39	1.546(7)

Table A23. Selected Interatomic Angles (deg)

Atom1	Atom2	Atom3	Angle
C1	Si1	C21	106.19(18)
C1	Si1	C24	107.69(17)
C1	Si1	C27	105.89(18)
C21	Si1	C24	112.14(18)
C21	Si1	C27	110.3(2)
C24	Si1	C27	114.1(2)
C16	Si2	C31	105.7(2)
C16	Si2	C34	107.42(19)
C16	Si2	C37	107.41(19)
C31	Si2	C34	110.9(3)
C31	Si2	C37	110.3(3)
C34	Si2	C37	114.7(3)
Si1	C1	C2	173.7(4)
C1	C2	C3	177.6(5)
C2	C3	C4	175.1(4)
C3	C4	C5	176.0(4)
C4	C5	C6	175.8(4)
C5	C6	C7	178.9(4)
C6	C7	C8	178.2(4)
C7	C8	C9	179.3(4)
C8	C9	C10	179.2(5)
C9	C10	C11	177.9(5)
C10	C11	C12	177.6(4)
C11	C12	C13	175.1(4)
C12	C13	C14	174.1(4)
C13	C14	C15	176.2(4)
C14	C15	C16	176.8(4)
Si2	C16	C15	178.6(4)
Si1	C21	C22	112.4(3)
Si1	C21	C23	113.2(3)
C22	C21	C23	110.8(4)
Si1	C24	C25	112.1(3)
Si1	C24	C26	115.3(3)
C25	C24	C26	109.8(4)
Si1	C27	C28	113.6(4)
Si1	C27	C29	111.9(3)
C28	C27	C29	108.7(4)
Si2	C31	C32	112.1(3)
Si2	C31	C33	117.2(4)
C32	C31	C33	115.2(4)

Si2	C34	C35	117.1(3)
Si2	C34	C36	115.1(3)
C35	C34	C36	111.1(4)
Si2	C37	C38	112.9(4)
Si2	C37	C39	113.3(4)
C38	C37	C39	108.9(4)

University of Alberta Department of Chemistry
Structure Determination Laboratory

Structure Report for Compound 233a

SDL Code: RRT9917

Date: 17 June 1999

Compound: *cyclo*-(-C≡C-C{=CMe₂}-C≡C-CH₂-)₂

Formula: C₁₈H₁₆

Supervisor: R. R. Tykwinski

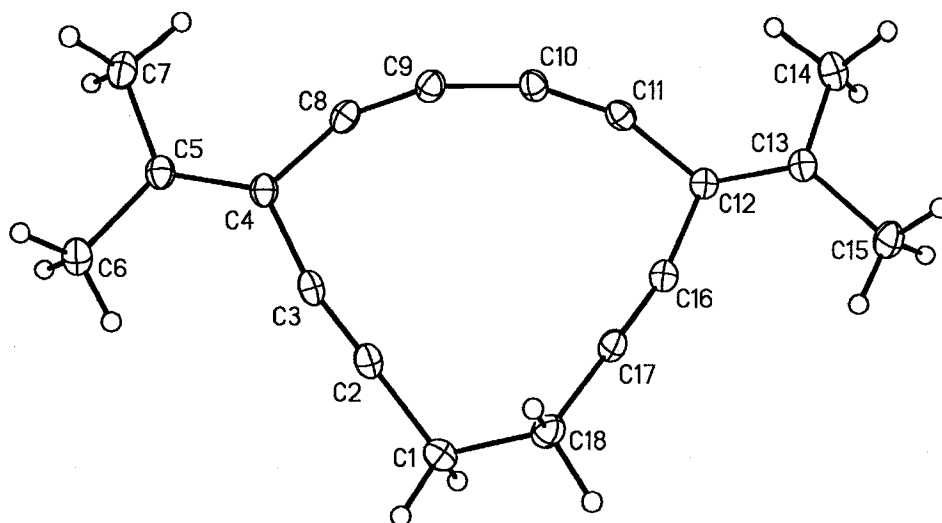


Figure A23. Perspective view of one of the two crystallographically-independent molecules of *cyclo*-(-C≡C-C{=CMe₂}-C≡C-CH₂-)₂ (molecule A) showing the atom labelling scheme. Non-hydrogen atoms are represented by Gaussian ellipsoids at the 20% probability level. Hydrogen atoms are shown with arbitrarily small thermal parameters.

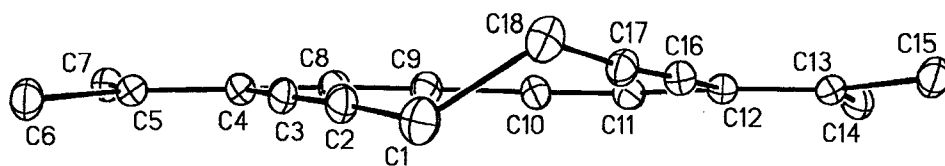


Figure A24. Alternate 'edge-on' view of the molecule with hydrogen atoms omitted, showing the twisting of the cyclododecatetrayne ring.

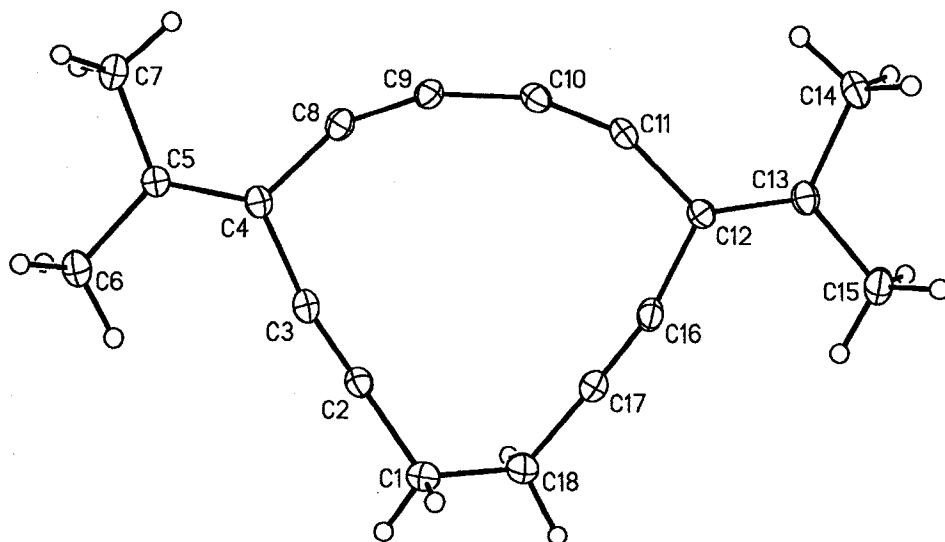


Figure A25. Perspective view of the second crystallographically-independent molecule of *cyclo*-($\text{C}\equiv\text{C}-\text{C}\{\text{=CMe}_2\}-\text{C}\equiv\text{C}-\text{CH}_2$)₂ (molecule B).

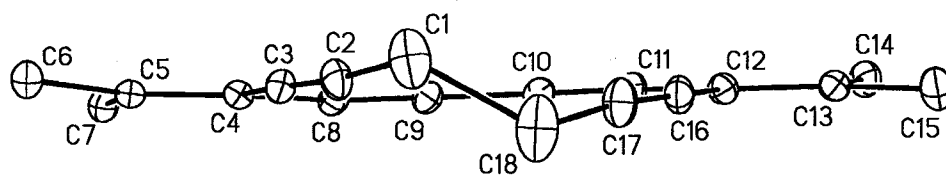


Figure A26. 'Edge-on' view of molecule B with hydrogen atoms omitted.

Table A25. Crystallographic Experimental Details**A. Crystal Data**

formula	C ₁₈ H ₁₆
formula weight	232.31
crystal dimensions (mm)	0.32 × 0.16 × 0.05
crystal system	monoclinic
space group	P2 ₁ /n (a nonstandard setting of P2 ₁ /c [No. 14])
unit cell parameters ^a	
	<i>a</i> (Å) 6.5313 (5)
	<i>b</i> (Å) 26.949 (2)
	<i>c</i> (Å) 15.7798 (14)
	β (deg) 97.878 (2)
	<i>V</i> (Å ³) 2751.2 (4)
	<i>Z</i> 8
ρ_{calcd} (g cm ⁻³)	1.122
μ (mm ⁻¹)	0.063

B. Data Collection and Refinement Conditions

diffractometer	Bruker P4/RA/SMART 1000 CCD ^b
radiation (λ [Å])	graphite-monochromated Mo K α (0.71073)
temperature (°C)	-80
scan type	ϕ rotations (0.3°) / ω scans (0.3°) (30 s
exposures)	
data collection 2 θ limit (deg)	51.40
total data collected	14688 (-7 ≤ <i>h</i> ≤ 7, -31 ≤ <i>k</i> ≤ 32, -19 ≤ <i>l</i> ≤ 19)
independent reflections	5217
number of observations (<i>NO</i>)	2076 [$F_o^2 \geq 2\sigma(F_o^2)$]
structure solution method	direct methods (<i>SHELXS-86</i> ^c)
refinement method	full-matrix least-squares on F^2
(<i>SHELXL-93</i> ^d)	
absorption correction method	<i>SADABS</i>
range of transmission factors	0.9674–0.7507
data/restraints/parameters	5217 [$F_o^2 \geq -3\sigma(F_o^2)$] / 0 / 333
goodness-of-fit (<i>S</i>) ^e	0.818 [$F_o^2 \geq -3\sigma(F_o^2)$]
final <i>R</i> indices ^f	
	R_1 [$F_o^2 \geq 2\sigma(F_o^2)$] 0.0526
	wR_2 [$F_o^2 \geq -3\sigma(F_o^2)$] 0.1229
largest difference peak and hole	0.382 and -0.252 e Å ⁻³

^aObtained from least-squares refinement of 3226 centered reflections.^bPrograms for diffractometer operation, data collection, data reduction and

absorption correction were those supplied by Bruker.

Table 25. Crystallographic Experimental Details (continued)

^cSheldrick, G. M. *Acta Crystallogr.* **1990**, *A46*, 467–473.

^dSheldrick, G. M. *SHELXL-93*. Program for crystal structure determination. University of Göttingen, Germany, 1993. Refinement on F_o^2 for all reflections (all of these having $F_o^2 \geq -3\sigma(F_o^2)$). Weighted R -factors wR_2 and all goodnesses of fit S are based on F_o^2 ; conventional R -factors R_1 are based on F_o , with F_o set to zero for negative F_o^2 . The observed criterion of $F_o^2 > 2\sigma(F_o^2)$ is used only for calculating R_1 , and is not relevant to the choice of reflections for refinement. R -factors based on F_o^2 are statistically about twice as large as those based on F_o , and R -factors based on ALL data will be even larger.

^e $S = [\sum w(F_o^2 - F_c^2)^2 / (n - p)]^{1/2}$ (n = number of data; p = number of parameters varied; $w = [\sigma^2(F_o^2) + (0.0378P)^2]^{-1}$ where $P = [\text{Max}(F_o^2, 0) + 2F_c^2]/3$).

^f $R_1 = \sum |F_o| - |F_c| / \sum |F_o|$; $wR_2 = [\sum w(F_o^2 - F_c^2)^2 / \sum w(F_o^4)]^{1/2}$.

Table A26. Selected Interatomic Distances (Å)*(a) Molecule A*

Atom1	Atom2	Distance
C1	C2	1.477(4)
C1	C18	1.542(3)
C2	C3	1.197(4)
C2	C17	3.075(4)†
C3	C4	1.442(4)
C3	C8	2.349(4)†
C4	C5	1.341(3)
C4	C8	1.448(4)
C5	C6	1.502(3)
C5	C7	1.486(4)
C8	C9	1.195(4)
C9	C10	1.370(4)
C10	C11	1.209(3)
C11	C12	1.442(4)
C11	C16	2.343(4)†
C12	C13	1.339(3)
C12	C16	1.446(4)
C13	C14	1.497(3)
C13	C15	1.485(3)
C16	C17	1.198(4)
C17	C18	1.467(4)

(b) Molecule B

Atom1	Atom2	Distance
C1	C2	1.458(4)
C1	C18	1.489(4)
C2	C3	1.185(3)
C2	C17	3.071(4)†
C3	C4	1.454(4)
C3	C8	2.351(4)†
C4	C5	1.345(3)
C4	C8	1.442(4)
C5	C6	1.495(3)
C5	C7	1.487(3)
C8	C9	1.205(3)
C9	C10	1.381(4)
C10	C11	1.206(3)
C11	C12	1.436(4)
C11	C16	2.348(4)†

C12	C13	1.343(3)
C12	C16	1.449(4)
C13	C14	1.496(3)
C13	C15	1.491(3)
C16	C17	1.188(4)
C17	C18	1.482(4)

†Nonbonded distance.

Table A27. Selected Interatomic Angles (deg)

(a) Molecule A

Atom1	Atom2	Atom3	Angle
C2	C1	C18	114.5(2)
C1	C2	C3	177.1(3)
C2	C3	C4	167.9(3)
C3	C4	C5	126.4(3)
C3	C4	C8	108.7(2)
C5	C4	C8	124.8(3)
C4	C5	C6	121.5(3)
C4	C5	C7	121.8(3)
C6	C5	C7	116.6(2)
C4	C8	C9	157.1(3)
C8	C9	C10	159.8(3)
C9	C10	C11	158.7(3)
C10	C11	C12	156.7(3)
C11	C12	C13	125.7(3)
C11	C12	C16	108.4(2)
C13	C12	C16	125.9(3)
C12	C13	C14	121.8(3)
C12	C13	C15	121.6(3)
C14	C13	C15	116.6(2)
C12	C16	C17	168.5(3)
C16	C17	C18	175.1(3)
C1	C18	C17	115.3(2)

(b) Molecule B

Atom1	Atom2	Atom3	Angle
C2	C1	C18	117.8(3)
C1	C2	C3	175.4(3)
C2	C3	C4	169.1(3)
C3	C4	C5	125.8(3)

C3	C4	C8	108.5(2)
C5	C4	C8	125.7(3)
C4	C5	C6	121.2(3)
C4	C5	C7	122.4(2)
C6	C5	C7	116.4(2)
C4	C8	C9	155.3(3)
C8	C9	C10	159.5(3)
C9	C10	C11	160.1(3)
C10	C11	C12	156.6(3)
C11	C12	C13	126.0(3)
C11	C12	C16	108.9(2)
C13	C12	C16	125.0(3)
C12	C13	C14	122.0(2)
C12	C13	C15	121.7(3)
C14	C13	C15	116.3(2)
C12	C16	C17	168.6(3)
C16	C17	C18	174.0(4)
C1	C18	C17	115.8(3)

University of Alberta Department of Chemistry
X-Ray Crystallography Laboratory

Structure Report for Compound 233b

XCL Code: RRT9932

Date: 29 September 1999

Compound: *cyclo*-(-C=C-C{=CMe₂}-C=C-CH₂)₂CH₂

Formula: C₁₉H₁₈

Supervisor: R. R. Tykwinski

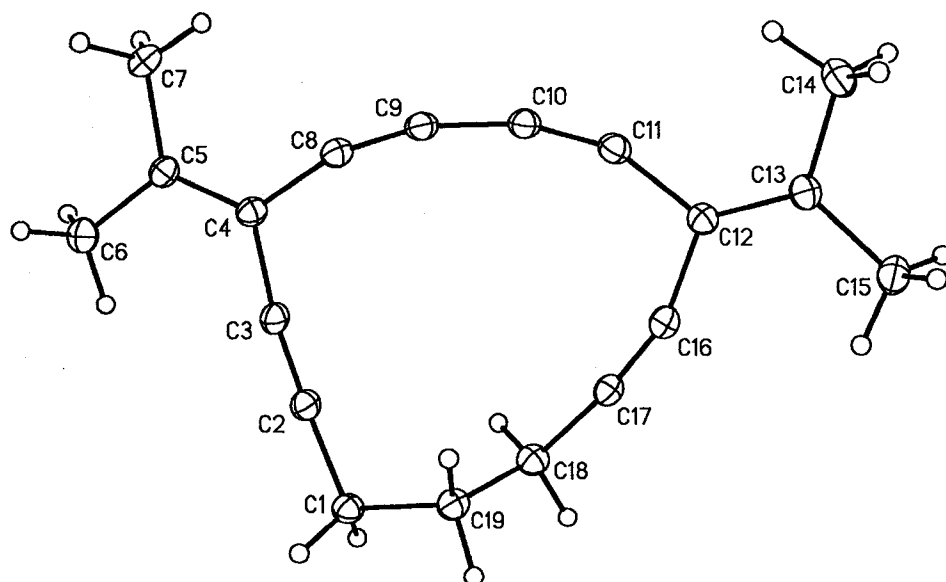


Figure A27. Perspective view of the *cyclo*- $(-C\equiv C-C\{=CMe_2\}-C\equiv C-CH_2)_2CH_2$ molecule showing the atom labelling scheme. Non-hydrogen atoms are represented by Gaussian ellipsoids at the 20% probability level. Hydrogen atoms are shown with arbitrarily small thermal parameters.

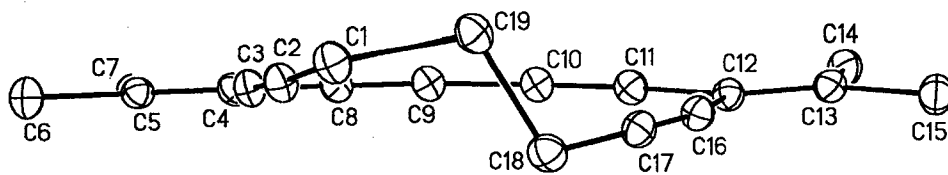


Figure A28. Alternate 'edge-on' view of the molecule with hydrogen atoms omitted, showing the twisting of the cyclotridecatetrayne ring.

Table A29. Crystallographic Experimental Details**A. Crystal Data**

formula	C ₁₉ H ₁₈
formula weight	246.33
crystal dimensions (mm)	0.32 × 0.21 × 0.16
crystal system	triclinic
space group	PI (No. 2)
unit cell parameters ^a	
	<i>a</i> (Å) 8.3222 (13)
	<i>b</i> (Å) 8.3227 (13)
	<i>c</i> (Å) 11.0132 (17)
	α (deg) 97.810 (3)
	β (deg) 96.413 (3)
	γ (deg) 91.112 (3)
	<i>V</i> (Å ³) 750.5 (2)
	<i>Z</i> 2
ρ_{calcd} (g cm ⁻³)	1.090
μ (mm ⁻¹)	0.061

B. Data Collection and Refinement Conditions

diffractometer	Bruker P4/RA/SMART 1000 CCD ^b
radiation (λ [Å])	graphite-monochromated Mo K α (0.71073)
temperature (°C)	-80
scan type	ϕ rotations (0.3°) / ω scans (0.3°) (30 s
exposures)	
data collection 2θ limit (deg)	52.80
total data collected	4005 ($-10 \leq h \leq 10$, $-10 \leq k \leq 10$, $-13 \leq l \leq$
10)	
independent reflections	3058
number of observations (<i>NO</i>)	2111 [$F_o^2 \geq 2\sigma(F_o^2)$]
structure solution method	direct methods (<i>SHELXS-86</i> ^c)
refinement method	full-matrix least-squares on F^2
(<i>SHELXL-93</i> ^d)	
absorption correction method	Gaussian integration (face-indexed)
range of transmission factors	0.9945–0.9774
data/restraints/parameters	3058 [$F_o^2 \geq -3\sigma(F_o^2)$] / 0 / 176
goodness-of-fit (<i>S</i>) ^e	0.969 [$F_o^2 \geq -3\sigma(F_o^2)$]
final <i>R</i> indices ^f	
	R_1 [$F_o^2 \geq 2\sigma(F_o^2)$] 0.0624
	wR_2 [$F_o^2 \geq -3\sigma(F_o^2)$] 0.1760
largest difference peak and hole	0.244 and -0.243 e Å ⁻³

^aObtained from least-squares refinement of 2886 centered reflections.

Table A29. Crystallographic Experimental Details (continued)

^bPrograms for diffractometer operation, data collection, data reduction and absorption correction were those supplied by Bruker.

^cSheldrick, G. M. *Acta Crystallogr.* **1990**, *A46*, 467–473.

^dSheldrick, G. M. *SHELXL-93*. Program for crystal structure determination. University of Göttingen, Germany, 1993. Refinement on F_o^2 for all reflections (all of these having $F_o^2 \geq -3\sigma(F_o^2)$). Weighted R -factors wR_2 and all goodnesses of fit S are based on F_o^2 ; conventional R -factors R_1 are based on F_o , with F_o set to zero for negative F_o^2 . The observed criterion of $F_o^2 > 2\sigma(F_o^2)$ is used only for calculating R_1 , and is not relevant to the choice of reflections for refinement. R -factors based on F_o^2 are statistically about twice as large as those based on F_o , and R -factors based on ALL data will be even larger.

^e $S = [\sum w(F_o^2 - F_c^2)^2 / (n - p)]^{1/2}$ (n = number of data; p = number of parameters varied; $w = [\sigma^2(F_o^2) + (0.1156P)^2]^{-1}$ where $P = [\text{Max}(F_o^2, 0) + 2F_c^2]/3$).

^f $R_1 = \sum |F_o| - |F_c| / \sum |F_o|$; $wR_2 = [\sum w(F_o^2 - F_c^2)^2 / \sum w(F_o^4)]^{1/2}$.

Table A30. Selected Interatomic Distances (Å)

Atom1	Atom2	Distance
C1	C2	1.465(3)
C1	C19	1.539(2)
C2	C3	1.205(3)
C2	C17	4.041(3) [†]
C3	C4	1.440(3)
C3	C8	2.362(3) [†]
C4	C5	1.350(3)
C4	C8	1.435(3)
C5	C6	1.487(3)
C5	C7	1.494(3)
C8	C9	1.208(3)
C9	C10	1.372(3)
C10	C11	1.209(3)
C11	C12	1.438(3)
C11	C16	2.331(3) [†]
C12	C13	1.347(3)
C12	C16	1.454(3)
C13	C14	1.490(3)
C13	C15	1.491(3)
C16	C17	1.192(3)
C17	C18	1.463(3)
C18	C19	1.541(2)

[†]Nonbonded distance.

Table A31. Selected Interatomic Angles (deg)

Atom1	Atom2	Atom3	Angle
C2	C1	C19	110.75(15)
C1	C2	C3	173.07(19)
C2	C3	C4	170.66(19)
C3	C4	C5	125.15(17)
C3	C4	C8	110.49(16)
C5	C4	C8	124.36(18)
C4	C5	C6	121.62(18)
C4	C5	C7	121.73(17)
C6	C5	C7	116.65(17)
C4	C8	C9	163.7(2)
C8	C9	C10	164.6(2)
C9	C10	C11	163.4(2)
C10	C11	C12	156.88(19)

C11	C12	C13	126.12(18)
C11	C12	C16	107.45(16)
C13	C12	C16	126.43(18)
C12	C13	C14	121.53(19)
C12	C13	C15	121.28(18)
C14	C13	C15	117.19(17)
C12	C16	C17	161.6(2)
C16	C17	C18	172.0(2)
C17	C18	C19	114.41(16)
C1	C19	C18	111.92(15)

University of Alberta Department of Chemistry
Structure Determination Laboratory

Structure Report for Compound 233c

SDL Code: RRT9813

Date: 17 December 1998

Compound: *cyclo*-($-\text{C}\equiv\text{C}-\text{C}\{\text{=CMe}_2\}-\text{C}\equiv\text{C}-\text{CH}_2\text{CH}_2-$)₂

Formula: C₂₀H₂₀

Supervisor: R. R. Tykwinski

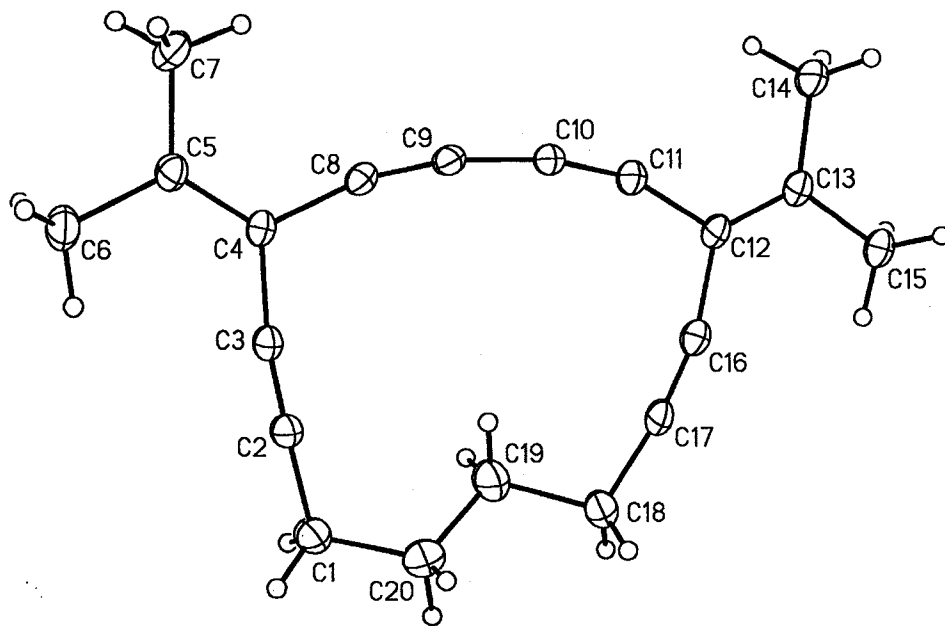


Figure A29. Perspective view of the *cyclo*-($\text{C}\equiv\text{C}-\text{C}\{\text{=CMe}_2\}-\text{C}\equiv\text{C}-\text{CH}_2\text{CH}_2$)₂ molecule showing the atom labelling scheme. Non-hydrogen atoms are represented by Gaussian ellipsoids at the 20% probability level. Hydrogen atoms are shown with arbitrarily small thermal parameters.

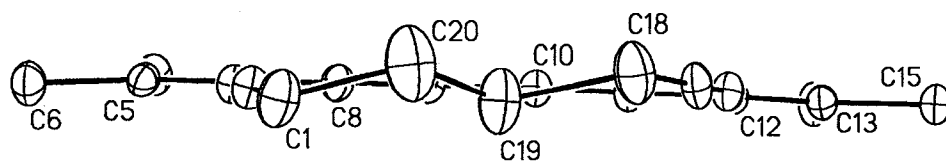


Figure A30. Alternate 'edge-on' view of the molecule with hydrogen atoms omitted, showing the twisting of the cyclotetradecatetrayne ring.

Table A33. Crystallographic Experimental Details**A. Crystal Data**

formula	C ₂₀ H ₂₀
formula weight	260.36
crystal dimensions (mm)	0.60 × 0.30 × 0.23
crystal system	monoclinic
space group	<i>P</i> 2 ₁ / <i>c</i> (No. 14)
unit cell parameters ^a	
	<i>a</i> (Å) 9.2119 (8)
	<i>b</i> (Å) 12.5305 (12)
	<i>c</i> (Å) 14.5747 (10)
	β (deg) 107.744 (7)
	<i>V</i> (Å ³) 1602.3 (2)
	<i>Z</i> 4
ρ_{calcd} (g cm ⁻³)	1.079
μ (mm ⁻¹)	0.061

B. Data Collection and Refinement Conditions

diffractometer	Siemens P4/RA ^b
radiation (λ [Å])	graphite-monochromated Mo K α (0.71073)
temperature (°C)	-60
scan type	θ -2 θ
data collection 2 θ limit (deg)	50.0
total data collected	3000 ($0 \leq h \leq 10, 0 \leq k \leq 14, -17 \leq l \leq 16$)
independent reflections	2814
number of observations (<i>NO</i>)	1399 ($F_o^2 \geq 2\sigma(F_o^2)$)
structure solution method	direct methods (<i>SHELXS-86</i> ^c)
refinement method	full-matrix least-squares on F^2
(<i>SHELXL-93</i> ^d)	
absorption correction method	none ^e
data/restraints/parameters	2814 [$F_o^2 \geq -3\sigma(F_o^2)$] / 0 / 185
goodness-of-fit (<i>S</i>) ^f	1.010 [$F_o^2 \geq -3\sigma(F_o^2)$]
final <i>R</i> indices ^g	
	R_1 [$F_o^2 > 2\sigma(F_o^2)$] 0.0762
	wR_2 [$F_o^2 \geq -3\sigma(F_o^2)$] 0.1977
largest difference peak and hole	0.421 and -0.217 e Å ⁻³

^aObtained from least-squares refinement of 40 reflections with $21.0^\circ < 2\theta < 25.9^\circ$.

^bPrograms for diffractometer operation, data collection, data reduction and absorption correction were those supplied by Siemens.

^cSheldrick, G. M. *Acta Crystallogr.* **1990**, *A46*, 467–473.

Table A33. Crystallographic Experimental Details (continued)

^dSheldrick, G. M. *SHELXL-93*. Program for crystal structure determination. University of Göttingen, Germany, 1993. Refinement on F_o^2 for all reflections (all of these having $F_o^2 \geq -3\sigma(F_o^2)$). Weighted R -factors wR_2 and all goodnesses of fit S are based on F_o^2 ; conventional R -factors R_1 are based on F_o , with F_o set to zero for negative F_o^2 . The observed criterion of $F_o^2 > 2\sigma(F_o^2)$ is used only for calculating R_1 , and is not relevant to the choice of reflections for refinement. R -factors based on F_o^2 are statistically about twice as large as those based on F_o , and R -factors based on ALL data will be even larger.

^eThe very small value of the linear absorption coefficient ($\mu = 0.061 \text{ mm}^{-1}$) suggested that no absorption correction need be employed. When a semiempirical (ψ -scan) correction was attempted, the range of transmission coefficients (0.9929–0.9454) and the final agreement factors ($R_1 [F_o^2 > 2\sigma(F_o^2)] = 0.0766$; $wR_2 [F_o^2 \geq -3\sigma(F_o^2)] = 0.1994$; goodness-of-fit $[F_o^2 \geq -3\sigma(F_o^2)] = 1.011$) suggested that use of the corrected data would yield no improvements to the final model. A face-indexed absorption correction was not attempted due to the irregular shape of the crystal.

^f $S = [\sum w(F_o^2 - F_c^2)^2 / (n - p)]^{1/2}$ (n = number of data; p = number of parameters varied; $w = [\sigma^2(F_o^2) + (0.0764P)^2 + 0.5537P]^{-1}$ where $P = [\text{Max}(F_o^2, 0) + 2F_c^2] / 3$).

^g $R_1 = \sum |F_o| - |F_c| / \sum |F_o|$; $wR_2 = [\sum w(F_o^2 - F_c^2)^2 / \sum w(F_o^4)]^{1/2}$.

Table A34. Selected Interatomic Distances (Å)

Atom1	Atom2	Distance
C1	C2	1.461(5)
C1	C20	1.493(6)
C2	C3	1.180(5)
C2	C17	5.124(5)†
C3	C4	1.455(5)
C3	C8	2.384(5)†
C4	C5	1.336(4)
C4	C8	1.439(5)
C5	C6	1.492(5)
C5	C7	1.497(5)
C8	C9	1.196(4)
C9	C10	1.378(5)
C10	C11	1.207(5)
C11	C12	1.433(5)
C11	C16	2.332(5)†
C12	C13	1.340(5)
C12	C16	1.443(5)
C13	C14	1.497(5)
C13	C15	1.492(5)
C16	C17	1.188(5)
C17	C18	1.466(6)
C18	C19	1.552(6)
C19	C20	1.416(6)

†Nonbonded distance.

Table A35. Selected Interatomic Angles (deg)

Atom1	Atom2	Atom3	Angle
C2	C1	C20	114.3(4)
C1	C2	C3	176.6(4)
C2	C3	C4	171.0(4)
C3	C4	C5	125.2(3)
C3	C4	C8	110.9(3)
C5	C4	C8	123.9(3)
C4	C5	C6	121.8(3)
C4	C5	C7	121.6(3)
C6	C5	C7	116.6(3)
C4	C8	C9	166.5(4)
C8	C9	C10	169.0(4)

C9	C10	C11	168.2(4)
C10	C11	C12	161.7(4)
C11	C12	C13	125.4(4)
C11	C12	C16	108.4(3)
C13	C12	C16	126.2(3)
C12	C13	C14	121.2(3)
C12	C13	C15	121.7(4)
C14	C13	C15	117.1(3)
C12	C16	C17	165.4(4)
C16	C17	C18	170.5(4)
C17	C18	C19	108.8(3)
C18	C19	C20	117.5(4)
C1	C20	C19	119.2(4)

University of Alberta Department of Chemistry
Structure Determination Laboratory

Structure Report for Compound 233d

SDL Code: RRT9905

Date: 1 March 1999

Compound: *cyclo*-($-\text{C}\equiv\text{C}-\text{C}\{\text{=CMe}_2\}-\text{C}\equiv\text{C}-\text{CH}_2\text{CH}_2$)₂CH₂

Formula: C₂₁H₂₂

Supervisor: R. R. Tykwinski

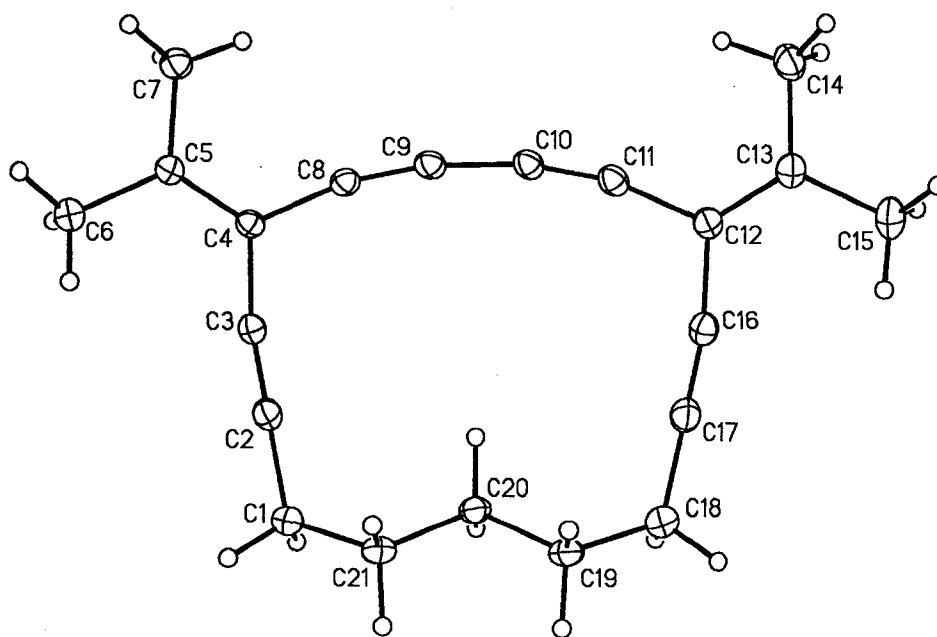


Figure A31. Perspective view of the *cyclo*-($-\text{C}\equiv\text{C}-\text{C}\{\text{=CMe}_2\}-\text{C}\equiv\text{C}-\text{CH}_2\text{CH}_2\text{CH}_2$)₂ molecule showing the atom labelling scheme. Non-hydrogen atoms are represented by Gaussian ellipsoids at the 20% probability level. Hydrogen atoms are shown with arbitrarily small thermal parameters.

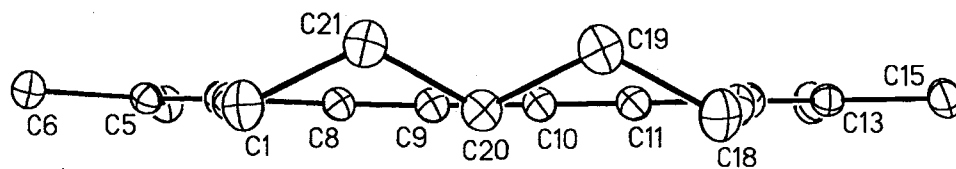


Figure A32. Alternate view of the molecule showing the very nearly planar arrangement of the unsaturated carbons. The dihedral angle between the C3–C4–C5–C8 and C11–C12–C13–C16 planes is $2.82(13)^\circ$ (see Table 6 for least-squares planes calculations).

Table A37. Crystallographic Experimental Details**A. Crystal Data**

formula	C ₂₁ H ₂₂
formula weight	274.39
crystal dimensions (mm)	0.30 × 0.22 × 0.18
crystal system	monoclinic
space group	<i>P</i> 2 ₁ / <i>c</i> (No. 14)
unit cell parameters ^a	

<i>a</i> (Å)	8.4095 (9)
<i>b</i> (Å)	8.3657 (9)
<i>c</i> (Å)	24.095 (3)
β (deg)	92.601 (2)
<i>V</i> (Å ³)	1693.4 (3)
<i>Z</i>	4

ρ_{calcd} (g cm ⁻³)	1.076
μ (mm ⁻¹)	0.060

B. Data Collection and Refinement Conditions

diffractometer	Bruker P4/RA/SMART 1000 CCD ^b
radiation (λ [Å])	graphite-monochromated Mo K α (0.71073)
temperature (°C)	-80
scan type	ϕ rotations (0.3°) / ω scans (0.3°) (20 s
exposures)	
data collection 2θ limit (deg)	51.50
total data collected	8795 (-10 ≤ <i>h</i> ≤ 10, -9 ≤ <i>k</i> ≤ 10, -29 ≤ <i>l</i> ≤ 29)
independent reflections	3225
number of observations (<i>NO</i>)	1478 ($F_o^2 \geq 2\sigma(F_o^2)$)
structure solution method	direct methods (<i>SHELXS-86</i> ^c)
refinement method	full-matrix least-squares on F^2
(<i>SHELXL-93</i> ^d)	
absorption correction method	none ^e
data/restraints/parameters	3225 [$F_o^2 \geq -3\sigma(F_o^2)$] / 0 / 194
goodness-of-fit (<i>S</i>) ^f	0.837 [$F_o^2 \geq -3\sigma(F_o^2)$]
final <i>R</i> indices ^g	
	$R_1 [F_o^2 > 2\sigma(F_o^2)]$ 0.0474
	$wR_2 [F_o^2 \geq -3\sigma(F_o^2)]$ 0.1106
largest difference peak and hole	0.170 and -0.178 e Å ⁻³

^aObtained from least-squares refinement of 2345 centered reflections.

^bPrograms for diffractometer operation, data collection, data reduction and absorption correction were those supplied by Bruker.

^cSheldrick, G. M. *Acta Crystallogr.* **1990**, *A46*, 467–473.

Table A37. Crystallographic Experimental Details (continued)

^dSheldrick, G. M. *SHELXL-93*. Program for crystal structure determination. University of Göttingen, Germany, 1993. Refinement on F_o^2 for all reflections (all of these having $F_o^2 \geq -3\sigma(F_o^2)$). Weighted R -factors wR_2 and all goodnesses of fit S are based on F_o^2 ; conventional R -factors R_1 are based on F_o , with F_o set to zero for negative F_o^2 . The observed criterion of $F_o^2 > 2\sigma(F_o^2)$ is used only for calculating R_1 , and is not relevant to the choice of reflections for refinement. R -factors based on F_o^2 are statistically about twice as large as those based on F_o , and R -factors based on ALL data will be even larger.

^eNo absorption correction was employed due to the small size of the crystal and the low value of the linear absorption coefficient (μ).

^f $S = [\sum w(F_o^2 - F_c^2)^2 / (n - p)]^{1/2}$ (n = number of data; p = number of parameters varied; $w = [\sigma^2(F_o^2) + (0.0374P)^2]^{-1}$ where $P = [\text{Max}(F_o^2, 0) + 2F_c^2] / 3$).

^g $R_1 = \sum |F_o| - |F_c| / \sum |F_o|$; $wR_2 = [\sum w(F_o^2 - F_c^2)^2 / \sum w(F_o^4)]^{1/2}$.

Table A38. Selected Interatomic Distances (Å)

Atom1	Atom2	Distance	Atom1	Atom2	Distance
C1	C2	1.472(3)	C10	C11	1.202(3)
C1	C21	1.526(3)	C11	C12	1.436(3)
C2	C3	1.193(3)	C11	C16	2.373(3) [†]
C2	C17	5.755(3) [†]	C12	C13	1.342(3)
C3	C4	1.443(3)	C12	C16	1.441(3)
C3	C8	2.375(3) [†]	C13	C14	1.497(3)
C4	C5	1.346(3)	C13	C15	1.491(3)
C4	C8	1.431(3)	C16	C17	1.197(3)
C5	C6	1.495(3)	C17	C18	1.469(3)
C5	C7	1.495(3)	C18	C19	1.529(3)
C8	C9	1.198(3)	C19	C20	1.519(3)
C9	C10	1.374(3)	C20	C21	1.515(3)

Table A39. Selected Interatomic Angles (deg)

Atom1	Atom2	Atom3	Angle
C2	C1	C21	113.89(18)
C1	C2	C3	179.5(2)
C2	C3	C4	170.5(2)
C3	C4	C5	124.7(2)
C3	C4	C8	111.47(19)
C5	C4	C8	123.8(2)
C4	C5	C6	122.15(19)
C4	C5	C7	121.1(2)
C6	C5	C7	116.77(18)
C4	C8	C9	168.0(2)
C8	C9	C10	168.8(2)
C9	C10	C11	169.4(2)
C10	C11	C12	166.4(2)
C11	C12	C13	124.2(2)
C11	C12	C16	111.2(2)
C13	C12	C16	124.7(2)
C12	C13	C14	121.4(2)
C12	C13	C15	122.9(2)
C14	C13	C15	115.7(2)
C12	C16	C17	170.4(2)
C16	C17	C18	178.7(3)
C17	C18	C19	114.40(19)
C18	C19	C20	115.65(19)
C19	C20	C21	111.43(18)
C1	C21	C20	115.68(18)

University of Alberta Department of Chemistry
Structure Determination Laboratory

Structure Report for Compound 227

SDL Code: RRT9812

Date: 30 November 1998

Compound: *cyclo*-($-C\equiv C-C\{=CMe_2\}-C\equiv C-CH_2CH_2CH_2$)₂CH₂

Formula: C₂₃H₂₆

Supervisor: R. R. Tykwinski

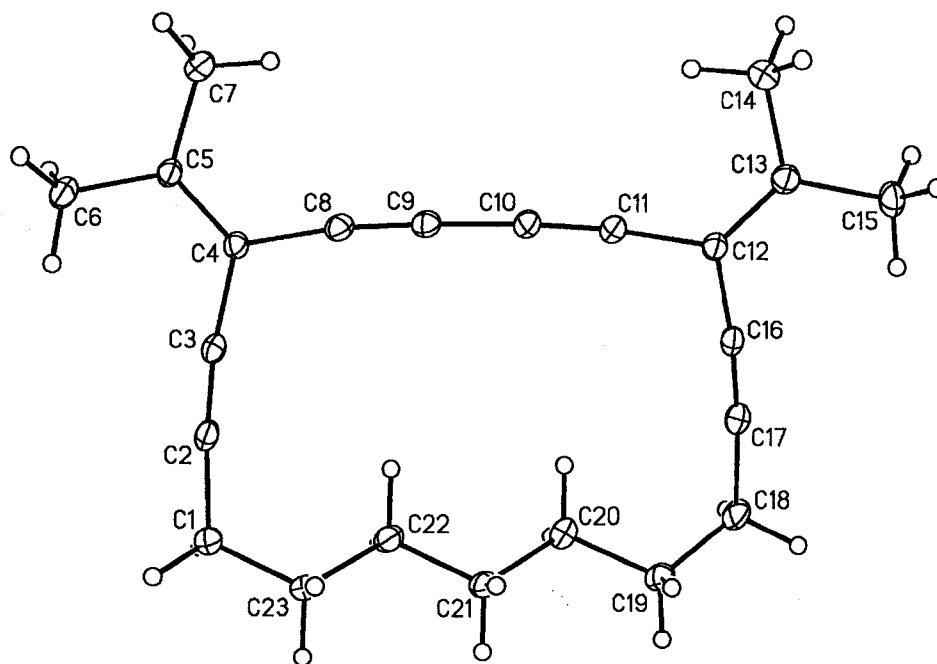


Figure A33. Perspective view of one of the two crystallographically-independent molecules of *cyclo*-($-\text{C}\equiv\text{C}-\text{C}\{\text{=CMe}_2\}-\text{C}\equiv\text{C}-\text{CH}_2\text{CH}_2\text{CH}_2\text{CH}_2\text{CH}_2$)₂CH₂ (molecule A) showing the atom labelling scheme. Non-hydrogen atoms are represented by Gaussian ellipsoids at the 20% probability level. Hydrogen atoms are shown with arbitrarily small thermal parameters.

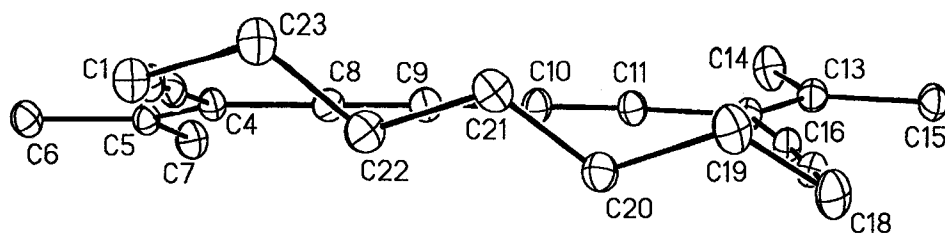


Figure A34. Alternate 'edge-on' view of the molecule with hydrogen atoms omitted, showing the twisting of the cycloheptadecatetrayne ring.

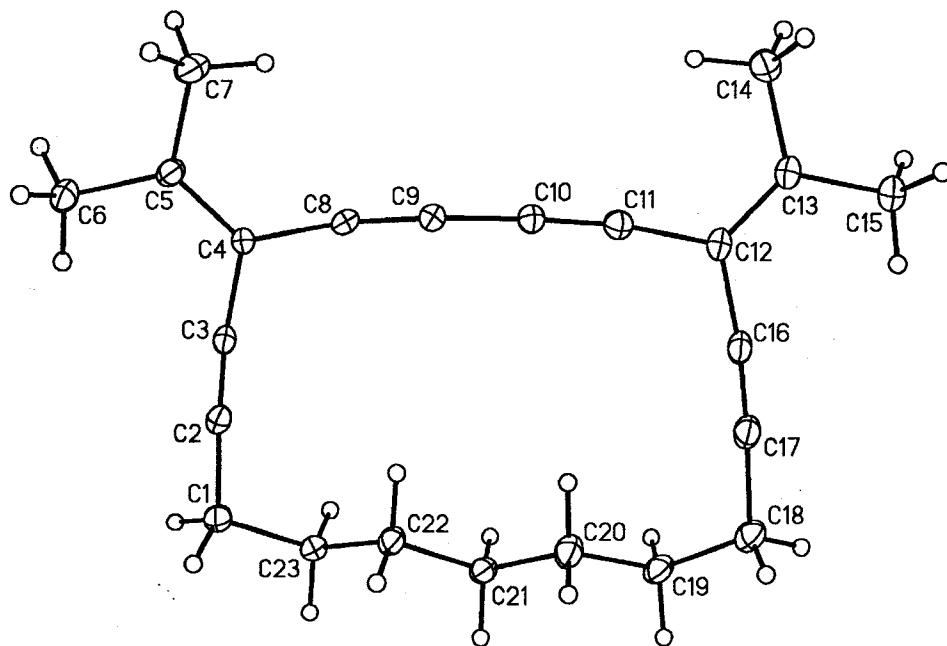


Figure A35. Perspective view of the second crystallographically-independent molecule of *cyclo*-($-\text{C}\equiv\text{C}-\text{C}(\text{=CMe}_2)-\text{C}\equiv\text{C}-\text{CH}_2\text{CH}_2\text{CH}_2$) $_2\text{CH}_2$ (molecule B).

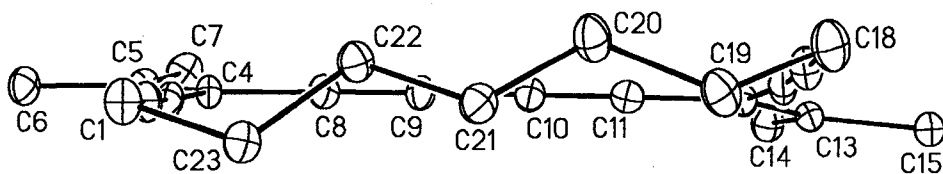


Figure A36. 'Edge-on' view of molecule B with hydrogen atoms omitted.

Table A41. Crystallographic Experimental Details**A. Crystal Data**

formula	C ₂₃ H ₂₆
formula weight	302.44
crystal dimensions (mm)	0.48 × 0.30 × 0.29
crystal system	triclinic
space group	PI (No. 2)
unit cell parameters ^a	
	<i>a</i> (Å) 12.2451 (13)
	<i>b</i> (Å) 12.6784 (11)
	<i>c</i> (Å) 13.5270 (12)
	α (deg) 66.965 (6)
	β (deg) 89.087 (8)
	γ (deg) 80.200 (8)
	<i>V</i> (Å ³) 1901.4 (3)
	<i>Z</i> 4
ρ_{calcd} (g cm ⁻³)	1.056
μ (mm ⁻¹)	0.059

B. Data Collection and Refinement Conditions

diffractometer	Siemens P4/RA ^b
radiation (λ [Å])	graphite-monochromated Mo K α (0.71073)
temperature (°C)	-80
scan type	θ - 2θ
data collection 2θ limit (deg)	50.0
total data collected	6660 ($-14 \leq h \leq 0$, $-13 \leq k \leq 13$, $-16 \leq l \leq 16$)
independent reflections	6334
number of observations (<i>NO</i>)	3139 [$F_o^2 \geq 2\sigma(F_o^2)$]
structure solution method	direct methods (<i>SHELXS-86</i> ^c)
refinement method	full-matrix least-squares on F^2
(<i>SHELXL-93</i> ^d)	
absorption correction method	none ^e
data/restraints/parameters	6334 [$F_o^2 \geq -3\sigma(F_o^2)$] / 0 / 423
goodness-of-fit (<i>S</i>) ⁱ	1.012 [$F_o^2 \geq -3\sigma(F_o^2)$]
final <i>R</i> indices ^j	
	R_1 [$F_o^2 \geq 2\sigma(F_o^2)$] 0.0672
	wR_2 [$F_o^2 \geq -3\sigma(F_o^2)$] 0.1536
largest difference peak and hole	0.202 and -0.179 e Å ⁻³

^aObtained from least-squares refinement of 40 reflections with $22.0^\circ < 2\theta < 25.6^\circ$.

^bPrograms for diffractometer operation, data collection, data reduction and

absorption correction were those supplied by Siemens.

Table A41. Crystallographic Experimental Details (continued)

^cSheldrick, G. M. *Acta Crystallogr.* **1990**, *A46*, 467–473.

^dSheldrick, G. M. *SHELXL-93*. Program for crystal structure determination. University of Göttingen, Germany, 1993. Refinement on F_o^2 for all reflections (all of these having $F_o^2 \geq -3\sigma(F_o^2)$). Weighted R -factors wR_2 and all goodnesses of fit S are based on F_o^2 ; conventional R -factors R_1 are based on F_o , with F_o set to zero for negative F_o^2 . The observed criterion of $F_o^2 > 2\sigma(F_o^2)$ is used only for calculating R_1 , and is not relevant to the choice of reflections for refinement. R -factors based on F_o^2 are statistically about twice as large as those based on F_o , and R -factors based on ALL data will be even larger.

^eThe very small value of the linear absorption coefficient ($\mu = 0.059 \text{ mm}^{-1}$) suggested that no linear absorption coefficient need be employed. When a semi-empirical (ψ -scan) correction was attempted, the range of transmission coefficients (0.9579–0.9449) and the final agreement factors ($R_1 [F_o^2 \geq 2\sigma(F_o^2)] = 0.0673$; $wR_2 [F_o^2 \geq -3\sigma(F_o^2)] = 0.1534$; goodness-of-fit $[F_o^2 \geq -3\sigma(F_o^2)] = 1.023$) suggested that use of the corrected data would yield no significant improvements to the final model. A face-indexed absorption correction was not attempted due to the irregular shape of the crystal.

^f $S = [\sum w(F_o^2 - F_c^2)^2 / (n - p)]^{1/2}$ (n = number of data; p = number of parameters varied; $w = [\sigma^2(F_o^2) + (0.0478P)^2 + 0.1698P]^{-1}$ where $P = [\text{Max}(F_o^2, 0) + 2F_c^2] / 3$).

^g $R_1 = \sum ||F_o| - |F_c|| / \sum |F_o|$; $wR_2 = [\sum w(F_o^2 - F_c^2)^2 / \sum w(F_o^4)]^{1/2}$.

Table A42. Selected Interatomic Distances (Å)

<i>(a) Molecule A</i>			<i>(b) Molecule B</i>		
Atom1	Atom2	Distance	Atom1	Atom2	Distance
C1	C2	1.472(5)	C1	C2	1.476(5)
C1	C23	1.533(4)	C1	C23	1.539(4)
C2	C3	1.193(4)	C2	C3	1.185(4)
C2	C17	7.554(5) [†]	C2	C17	7.482(5) [†]
C3	C4	1.444(5)	C3	C4	1.443(4)
C3	C8	2.397(5) [†]	C3	C8	2.407(5) [†]
C4	C5	1.348(4)	C4	C5	1.351(4)
C4	C8	1.441(4)	C4	C8	1.441(4)
C5	C6	1.488(4)	C5	C6	1.492(4)
C5	C7	1.502(4)	C5	C7	1.490(4)
C8	C9	1.201(4)	C8	C9	1.200(4)
C9	C10	1.382(5)	C9	C10	1.374(5)
C10	C11	1.194(4)	C10	C11	1.198(4)
C11	C12	1.440(4)	C11	C12	1.439(5)
C11	C16	2.404(5) [†]	C11	C16	2.414(5) [†]
C12	C13	1.339(4)	C12	C13	1.350(4)
C12	C16	1.448(5)	C12	C16	1.446(5)
C13	C14	1.498(4)	C13	C14	1.494(4)
C13	C15	1.491(4)	C13	C15	1.497(4)
C16	C17	1.194(4)	C16	C17	1.188(5)
C17	C18	1.461(5)	C17	C18	1.465(5)
C18	C19	1.534(5)	C18	C19	1.517(4)
C19	C20	1.531(4)	C19	C20	1.532(4)
C20	C21	1.514(4)	C20	C21	1.507(4)
C21	C22	1.524(4)	C21	C22	1.525(4)
C22	C23	1.520(4)	C22	C23	1.520(4)

[†]Nonbonded distance.

Table A43. Selected Interatomic Angles (deg)

(a) *Molecule A*

Atom1	Atom2	Atom3	Angle
C2	C1	C23	111.1(3)
C1	C2	C3	174.2(4)
C2	C3	C4	171.9(4)
C3	C4	C5	124.2(3)
C3	C4	C8	112.4(3)
C5	C4	C8	123.4(3)
C4	C5	C6	122.6(3)
C4	C5	C7	121.2(3)
C6	C5	C7	116.1(3)
C4	C8	C9	172.7(4)
C8	C9	C10	177.3(4)
C9	C10	C11	176.6(4)
C10	C11	C12	173.5(4)
C11	C12	C13	123.0(3)
C11	C12	C16	112.7(3)
C13	C12	C16	124.3(3)
C12	C13	C14	122.1(3)
C12	C13	C15	121.9(3)
C14	C13	C15	115.9(3)
C12	C16	C17	174.0(4)
C16	C17	C18	173.7(4)
C17	C18	C19	111.6(3)
C18	C19	C20	112.8(3)
C19	C20	C21	113.5(3)
C20	C21	C22	113.7(3)
C21	C22	C23	112.8(3)
C1	C23	C22	114.0(3)

(b) *Molecule B*

Atom1	Atom2	Atom3	Angle
C2	C1	C23	111.6(3)
C1	C2	C3	176.1(4)
C2	C3	C4	173.0(4)
C3	C4	C5	123.4(3)
C3	C4	C8	113.2(3)
C5	C4	C8	123.4(3)
C4	C5	C6	121.4(3)
C4	C5	C7	121.8(3)
C6	C5	C7	116.7(3)

C4	C8	C9	172.2(4)
C8	C9	C10	176.4(4)
C9	C10	C11	176.8(4)
C10	C11	C12	172.5(4)
C11	C12	C13	122.8(3)
C11	C12	C16	113.6(3)
C13	C12	C16	123.6(3)
C12	C13	C14	122.0(3)
C12	C13	C15	122.1(3)
C14	C13	C15	115.9(3)
C12	C16	C17	173.0(4)
C16	C17	C18	177.0(4)
C17	C18	C19	112.1(3)
C18	C19	C20	115.0(3)
C19	C20	C21	113.1(3)
C20	C21	C22	113.6(3)
C21	C22	C23	112.8(3)
C1	C23	C22	113.9(3)

University of Alberta Department of Chemistry
X-Ray Crystallography Laboratory

Structure Report for 241

XCL Code: RRT9935

Date: 22 November 1999

Compound: $n\text{BuC}\equiv\text{C}-\text{C}(\text{=CMe}_2)-\text{C}\equiv\text{C}-\text{C}\equiv\text{C}-\text{C}(\text{=CMe}_2)-\text{C}\equiv\text{C}n\text{Bu}$

Formula: $\text{C}_{24}\text{H}_{30}$

Supervisor: R. R. Tykwinski

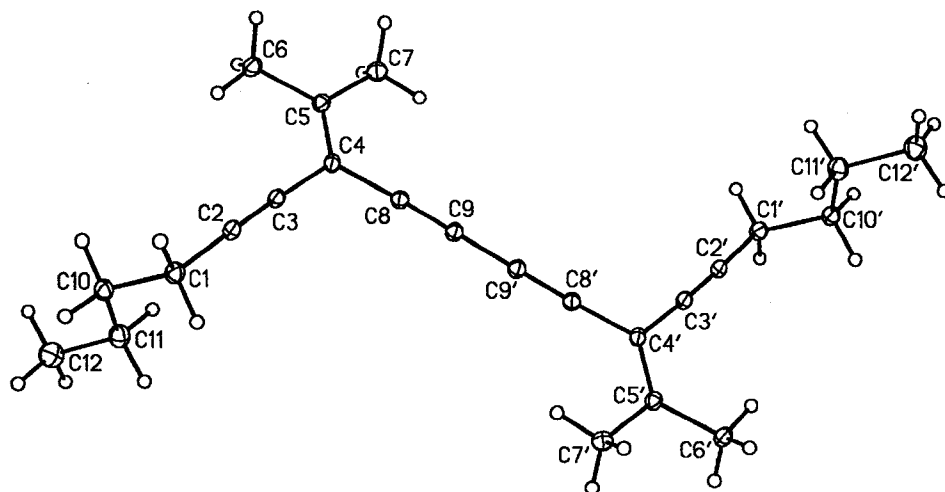


Figure A37. Perspective view of the $n\text{BuC}\equiv\text{C}-\text{C}(=\text{CMe}_2)-\text{C}\equiv\text{C}-\text{C}\equiv\text{C}-\text{C}(=\text{CMe}_2)-\text{C}\equiv\text{C}n\text{Bu}$ molecule showing the atom labelling scheme. Non-hydrogen atoms are represented by Gaussian ellipsoids at the 20% probability level. Hydrogen atoms are shown with arbitrarily small thermal parameters. Primed atoms are related to unprimed ones via the crystallographic inversion center ($1/2, 0, 0$) at the midpoint of the C9–C9' bond.

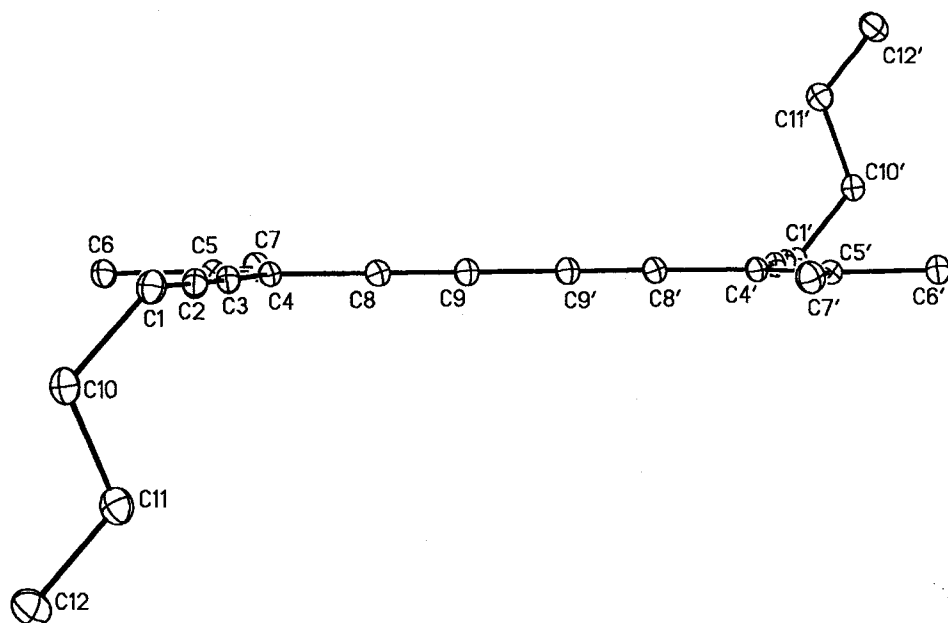


Figure A38. Alternate 'edge-on' view of the molecule. Hydrogen atoms are not shown.

Table A45. Crystallographic Experimental Details**A. Crystal Data**

formula	C ₂₄ H ₃₀
formula weight	318.48
crystal dimensions (mm)	0.40 × 0.27 × 0.08
crystal system	triclinic
space group	PI (No. 2)
unit cell parameters ^a	
	<i>a</i> (Å) 7.2155 (11)
	<i>b</i> (Å) 7.6090 (11)
	<i>c</i> (Å) 10.0757 (15)
	α (deg) 106.604 (3)
	β (deg) 103.335 (3)
	γ (deg) 100.228 (3)
	<i>V</i> (Å ³) 497.93 (13)
	<i>Z</i> 1
ρ_{calcd} (g cm ⁻³)	1.062
μ (mm ⁻¹)	0.059

B. Data Collection and Refinement Conditions

diffractometer	Bruker P4/RA/SMART 1000 CCD ^b
radiation (λ [Å])	graphite-monochromated Mo K α (0.71073)
temperature (°C)	-80
scan type	ϕ rotations (0.3°) / ω scans (0.3°) (30 s
exposures)	
data collection 2θ limit (deg)	52.80
total data collected	2496 ($-9 \leq h \leq 8, -9 \leq k \leq 4, -10 \leq l \leq 12$)
independent reflections	2023
number of observations (<i>NO</i>)	1400 [$F_o^2 \geq 2\sigma(F_o^2)$]
structure solution method	direct methods (<i>SHELXS-86</i> ^c)
refinement method	full-matrix least-squares on F^2
(<i>SHELXL-93</i> ^d)	
absorption correction method	none ^e
data/restraints/parameters	2023 [$F_o^2 \geq -3\sigma(F_o^2)$] / 0 / 111
goodness-of-fit (<i>S</i>) ⁱ	0.985 [$F_o^2 \geq -3\sigma(F_o^2)$]
final <i>R</i> indices ^j	
	R_1 [$F_o^2 \geq 2\sigma(F_o^2)$] 0.0479
	wR_2 [$F_o^2 \geq -3\sigma(F_o^2)$] 0.1325
largest difference peak and hole	0.224 and -0.195 e Å ⁻³

^aObtained from least-squares refinement of 1787 centered reflections.

^bPrograms for diffractometer operation, data collection and data reduction were

those supplied by Bruker.

Table A45. Crystallographic Experimental Details (continued)

^cSheldrick, G. M. *Acta Crystallogr.* **1990**, *A46*, 467–473.

^dSheldrick, G. M. *SHELXL-93*. Program for crystal structure determination. University of Göttingen, Germany, 1993. Refinement on F_o^2 for all reflections (all of these having $F_o^2 \geq -3\sigma(F_o^2)$). Weighted R -factors wR_2 and all goodnesses of fit S are based on F_o^2 ; conventional R -factors R_1 are based on F_o , with F_o set to zero for negative F_o^2 . The observed criterion of $F_o^2 > 2\sigma(F_o^2)$ is used only for calculating R_1 , and is not relevant to the choice of reflections for refinement. R -factors based on F_o^2 are statistically about twice as large as those based on F_o , and R -factors based on ALL data will be even larger.

^eNo absorption correction was applied to the data due to the very low value of the linear absorption coefficient (μ) and the irregular shape of the crystal.

^f $S = [\sum w(F_o^2 - F_c^2)^2 / (n - p)]^{1/2}$ (n = number of data; p = number of parameters varied; $w = [\sigma^2(F_o^2) + (0.0726P)^2]^{-1}$ where $P = [\text{Max}(F_o^2, 0) + 2F_c^2]/3$).

^g $R_1 = \sum |F_o| - |F_c| / \sum |F_o|$; $wR_2 = [\sum w(F_o^2 - F_c^2)^2 / \sum w(F_o^4)]^{1/2}$.

Table A46. Selected Interatomic Distances (Å)

Atom1	Atom2	Distance	Atom1	Atom2	Distance
C1	C2	1.468(2)	C5	C6	1.494(2)
C1	C10	1.532(2)	C5	C7	1.492(2)
C2	C3	1.195(2)	C8	C9	1.2038(18)
C3	C4	1.444(2)	C9	C9'	1.377(3)
C4	C5	1.357(2)	C10	C11	1.515(2)
C4	C8	1.4434(19)	C11	C12	1.518(2)

Table A47. Selected Interatomic Angles (deg)

Atom1	Atom2	Atom3	Angle
C2	C1	C10	114.06(12)
C1	C2	C3	179.19(15)
C2	C3	C4	177.02(15)
C3	C4	C5	123.34(13)
C3	C4	C8	114.77(12)
C5	C4	C8	121.89(13)
C4	C5	C6	121.54(14)
C4	C5	C7	122.26(13)
C6	C5	C7	116.20(13)
C4	C8	C9	177.21(15)
C8	C9	C9'	179.1(2)
C1	C10	C11	113.87(12)
C10	C11	C12	112.92(13)

Appendix B – Selected Spectra

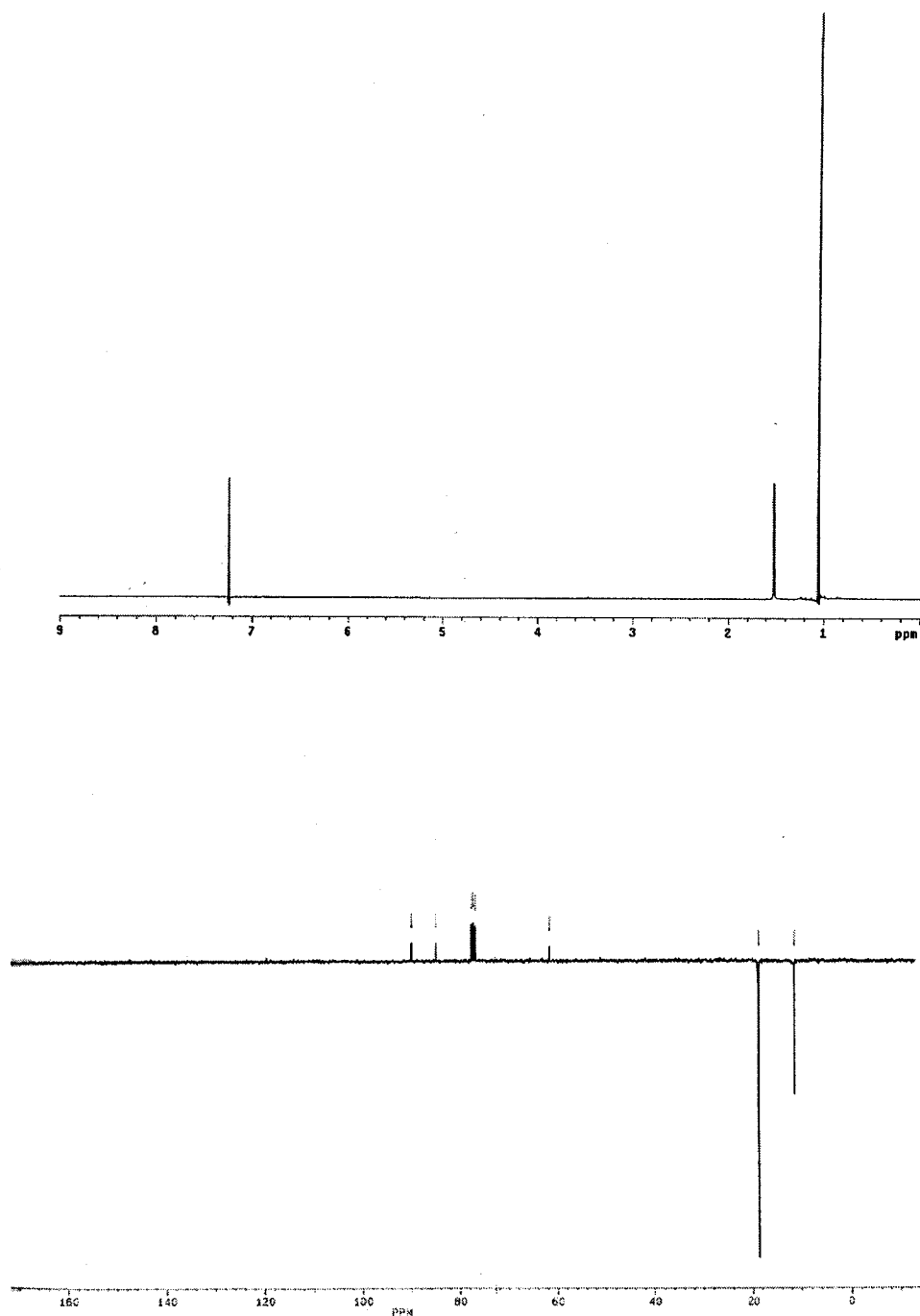


Figure B1 - ^1H NMR and ^{13}C NMR spectra of **93a**

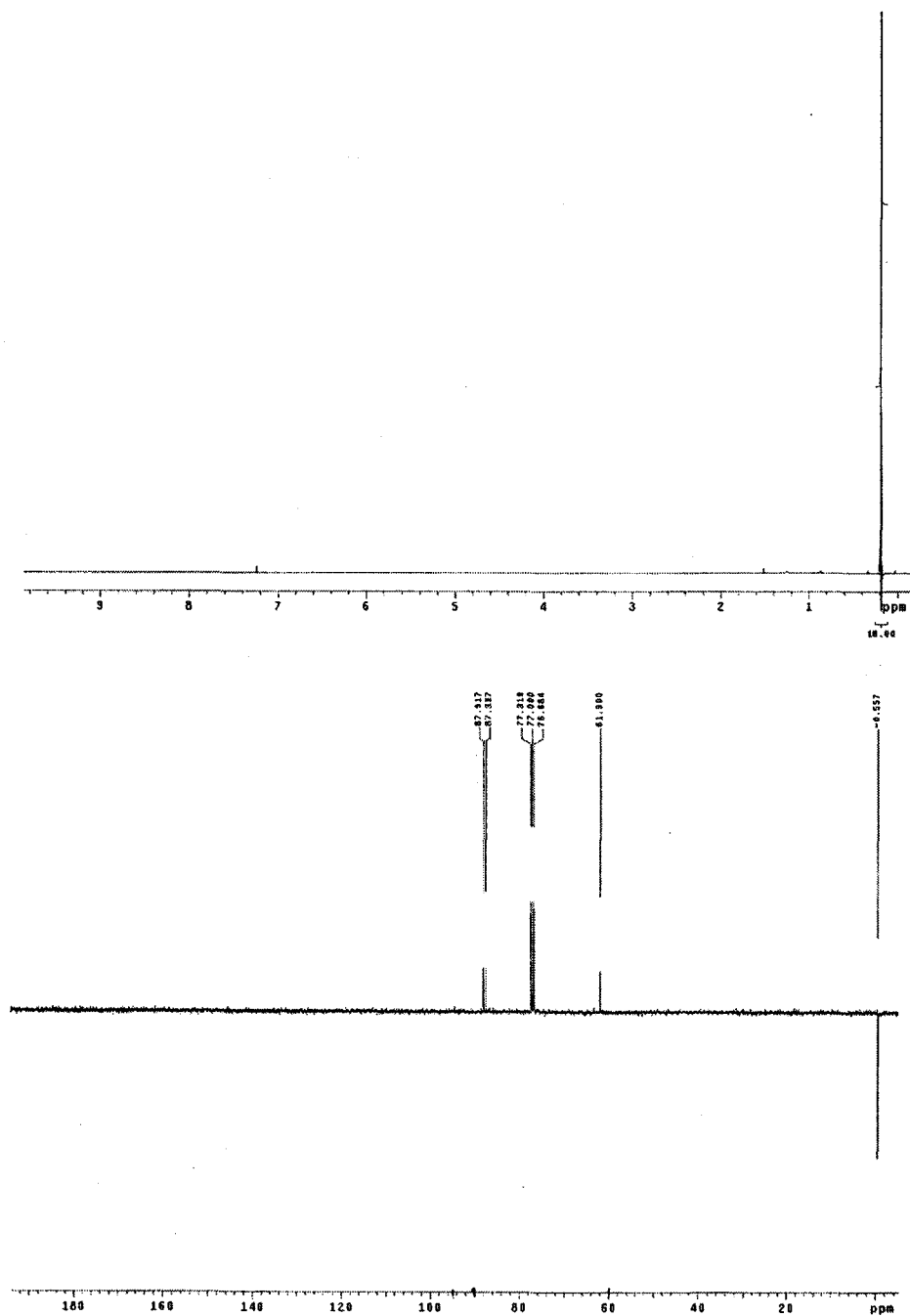


Figure B2 - ^1H NMR and ^{13}C NMR spectra of 93b

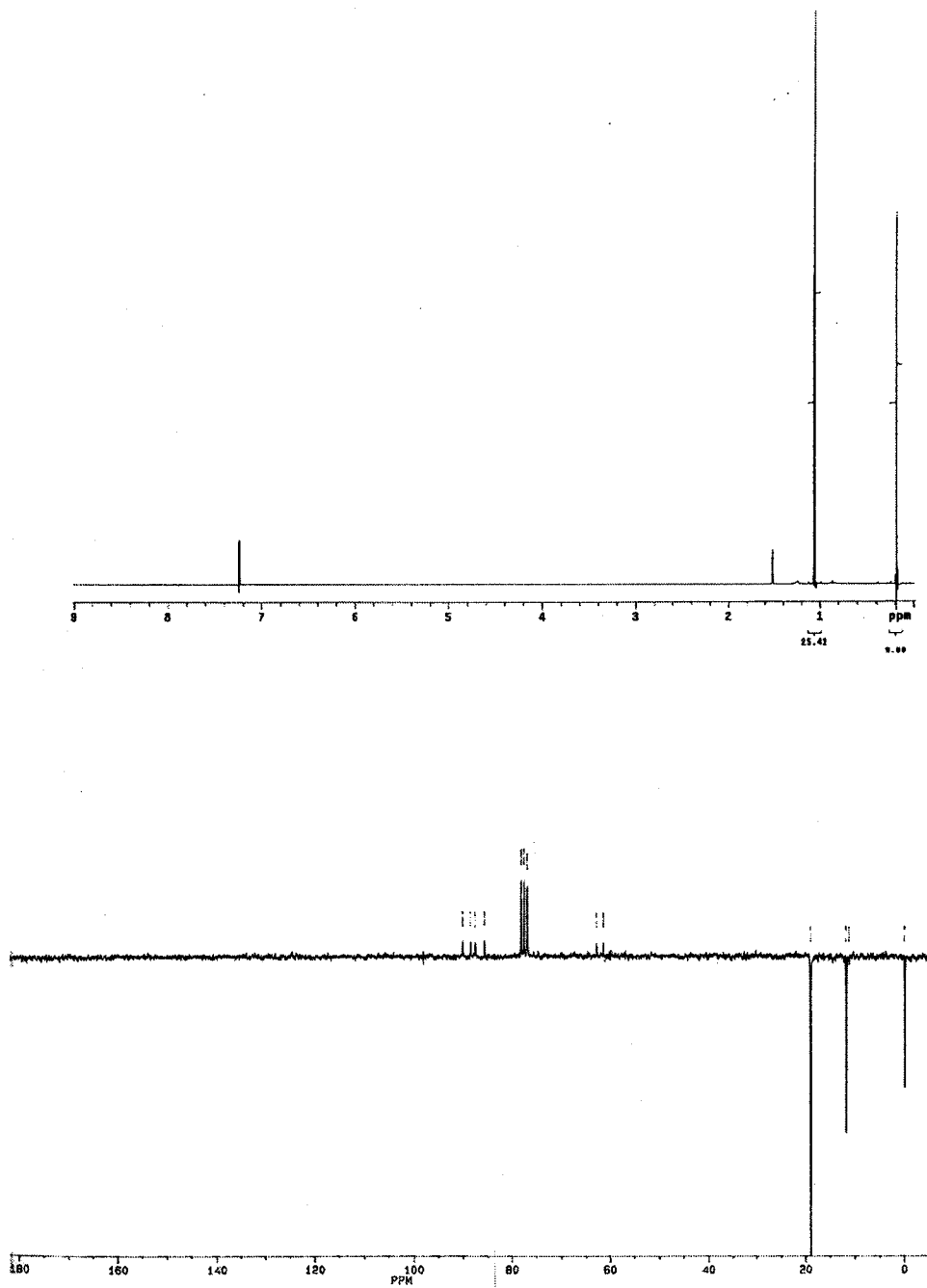


Figure B3 - ^1H NMR and ^{13}C NMR spectra of **93c**

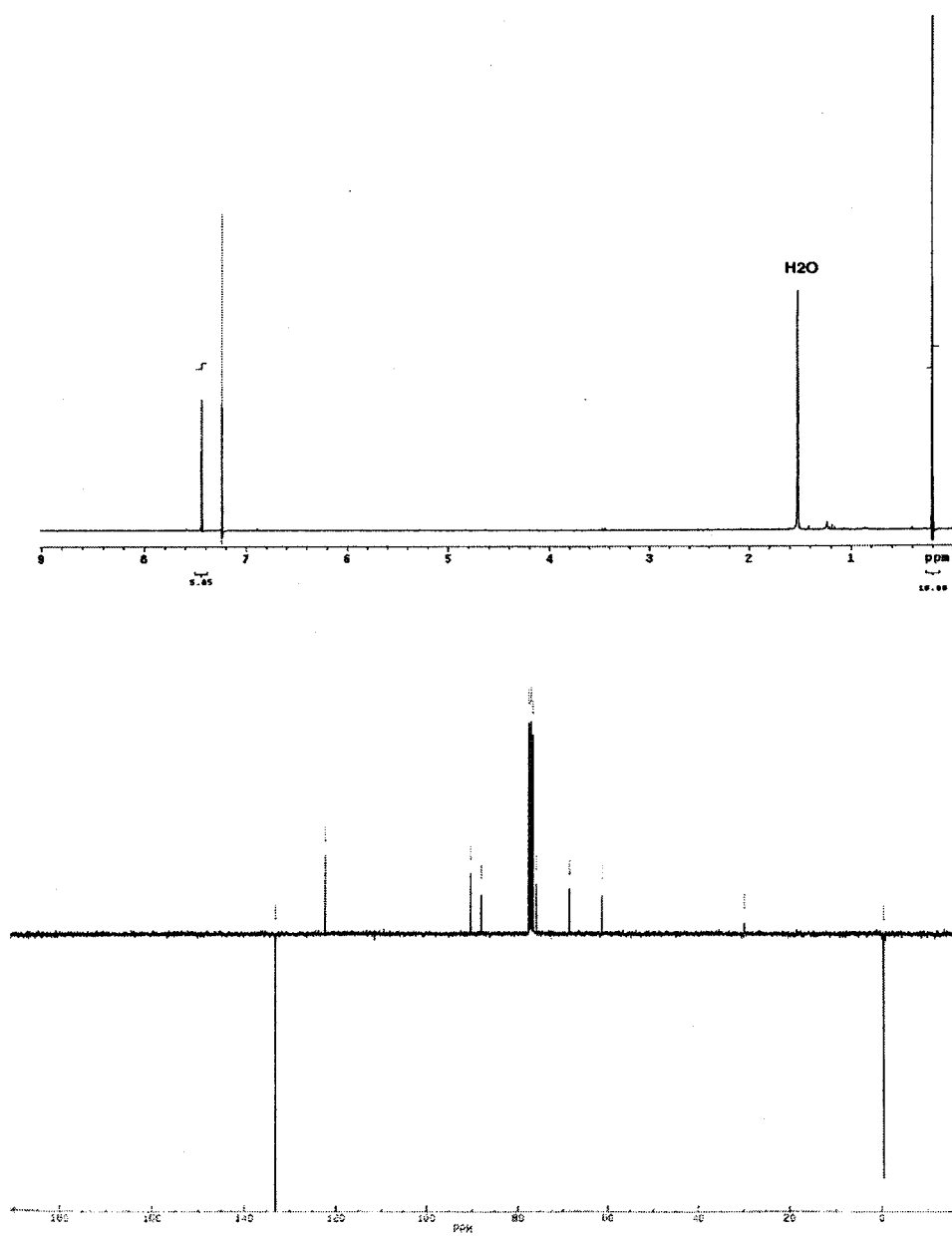


Figure B4 - ^1H NMR and ^{13}C NMR spectra of **121**.

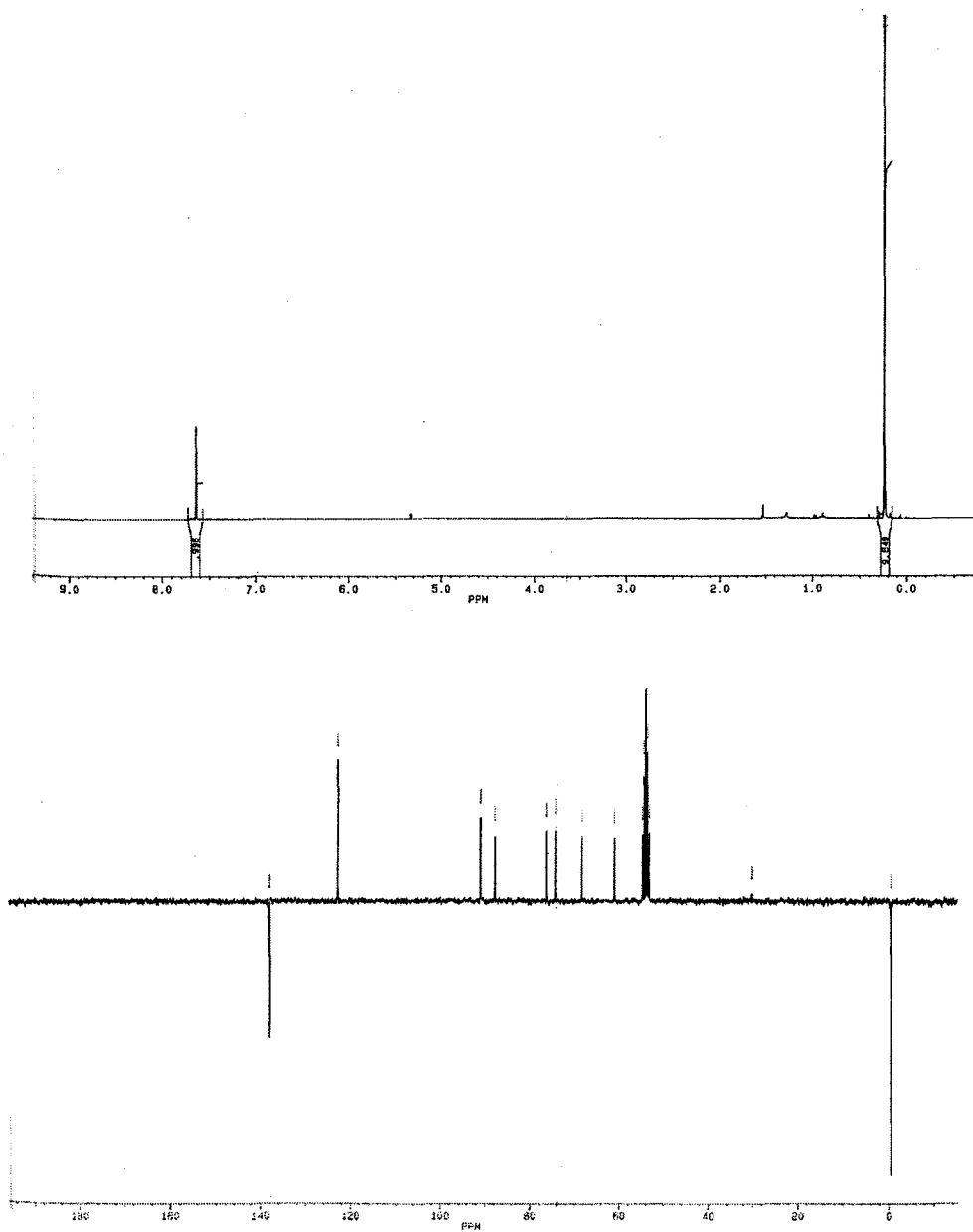


Figure B5 - ^1H NMR and ^{13}C NMR spectra of **126**

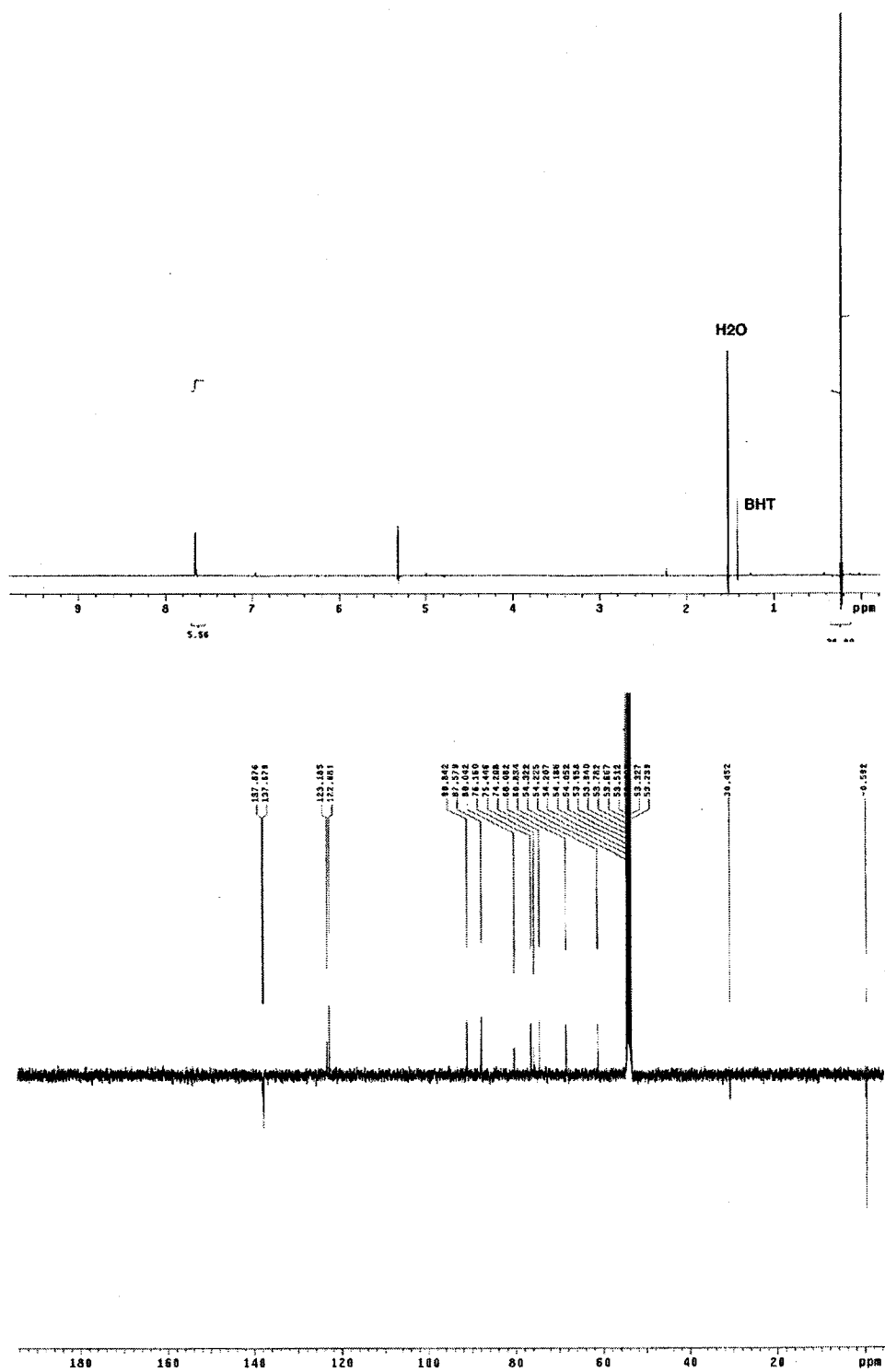


Figure B6 - ^1H NMR and ^{13}C NMR spectra of 131

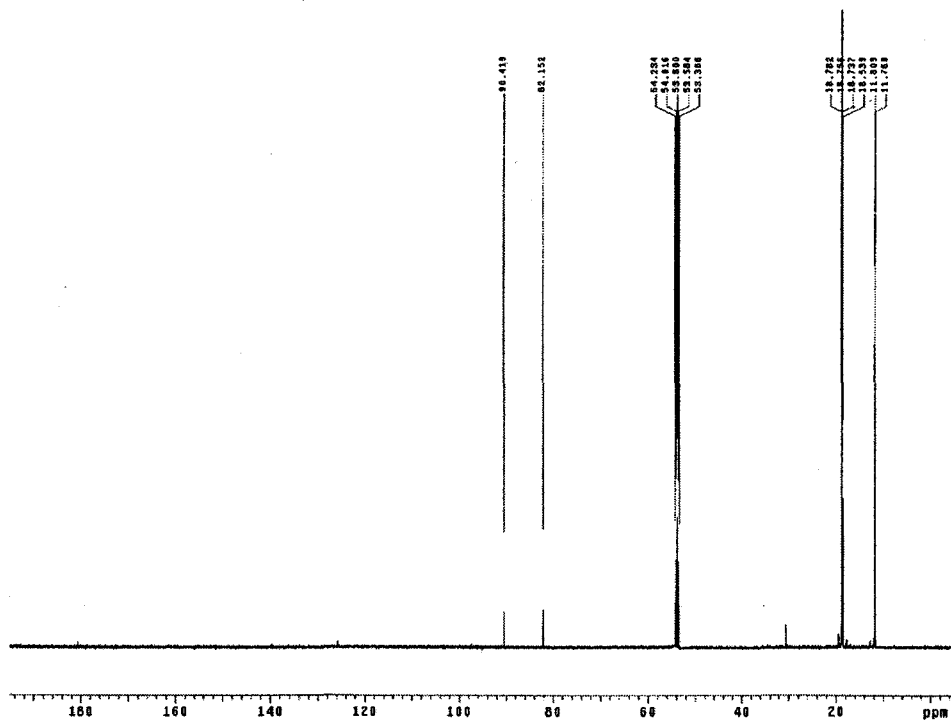


Figure B7 - ¹³C NMR spectra of **132**

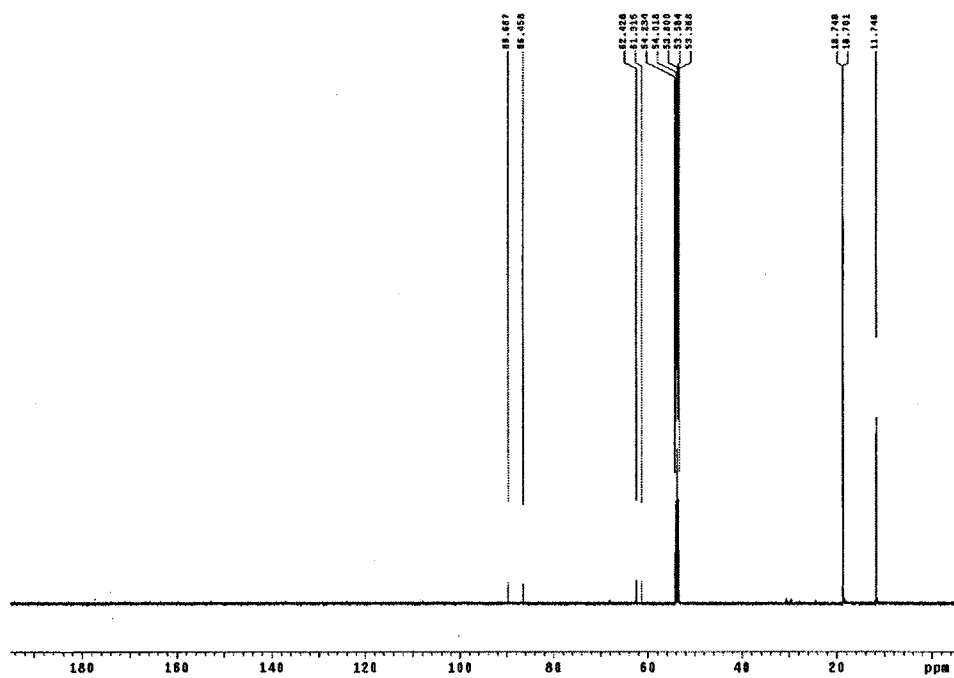


Figure B8 - ^{13}C NMR spectra of **134**

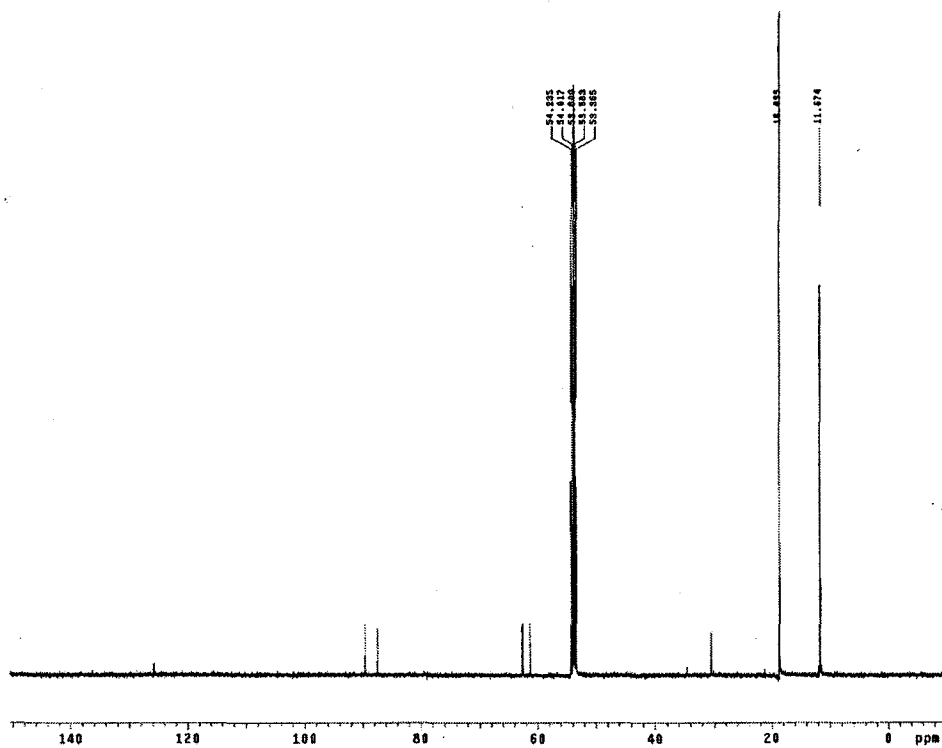


Figure B9 - ^{13}C NMR spectra of **135**

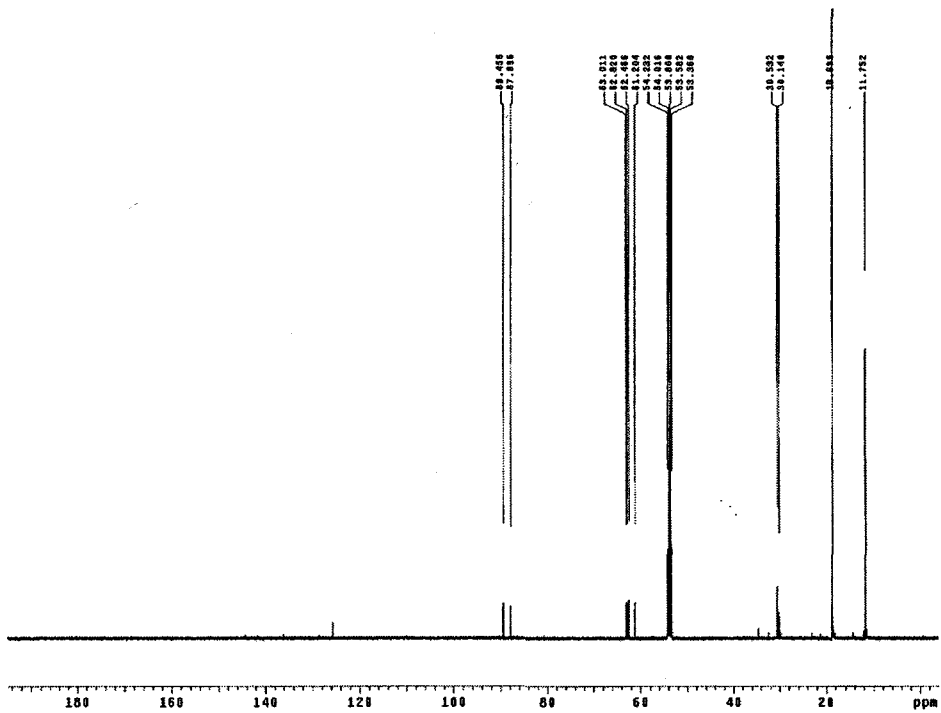


Figure B10 - ^{13}C NMR spectra of **136**

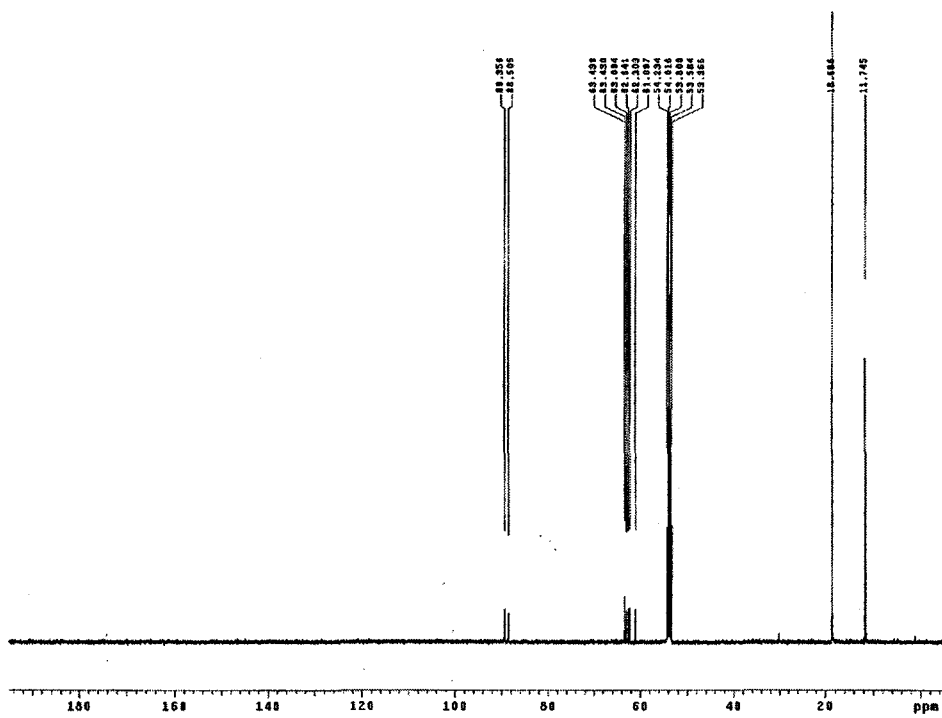


Figure B11 - ^{13}C NMR spectra of **137**

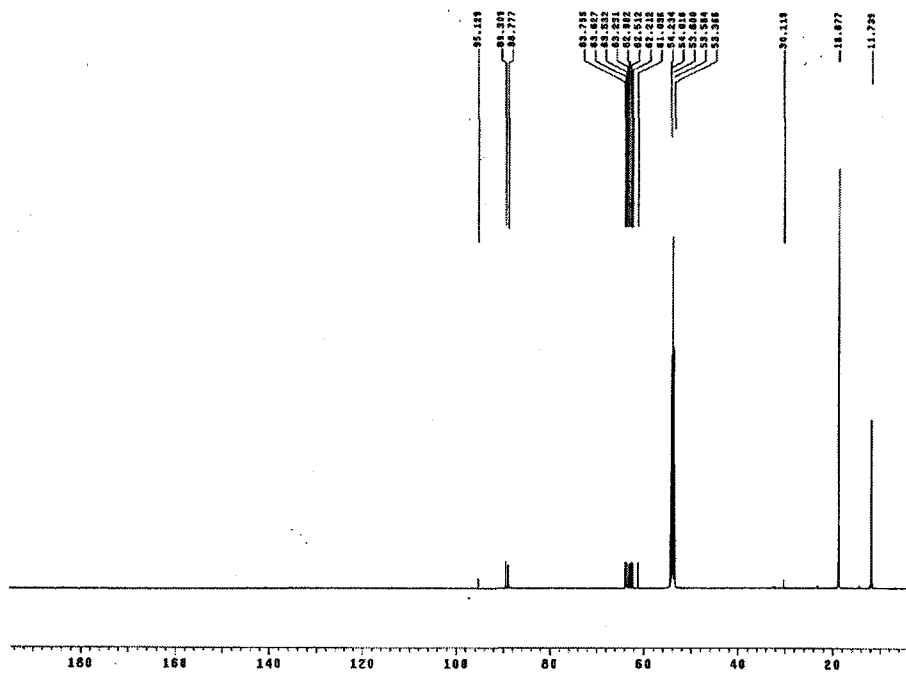


Figure B12 - ^{13}C NMR spectra of **138**

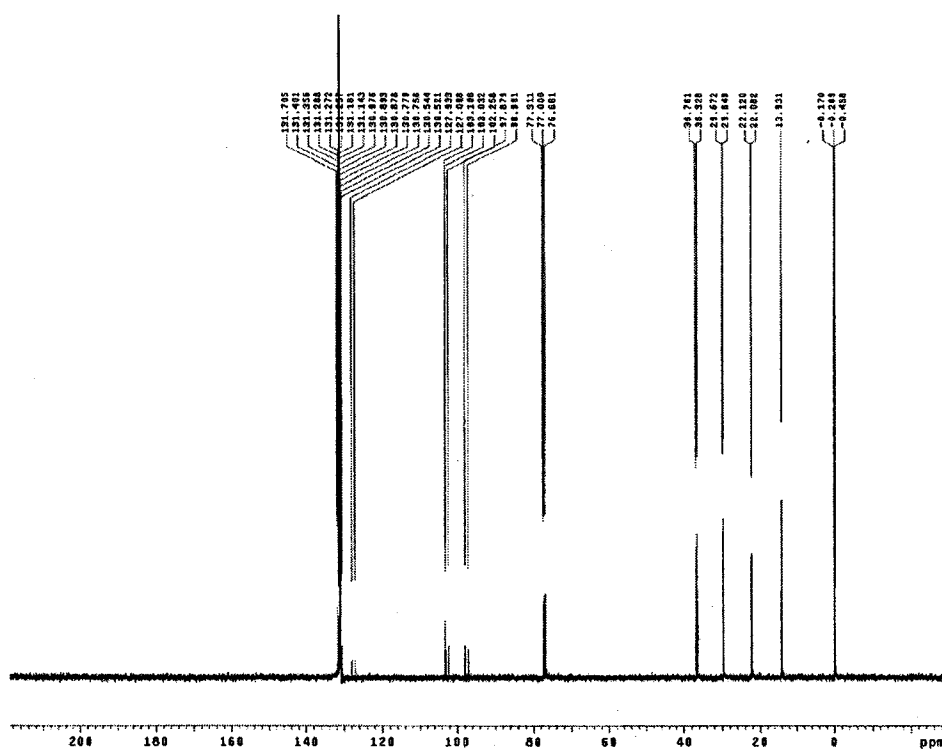
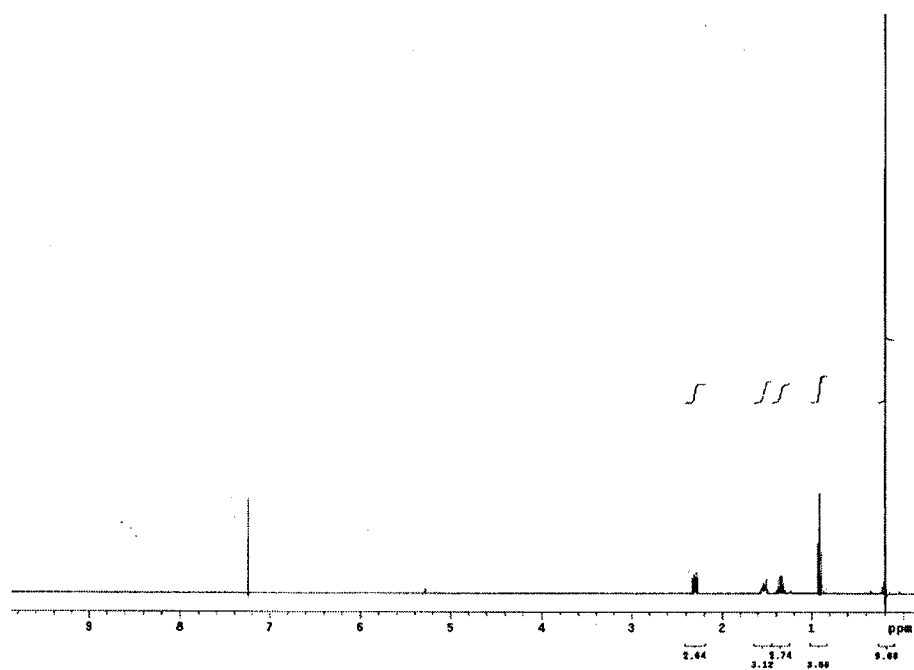


Figure B13 – ^1H NMR and ^{13}C NMR spectra of **170**

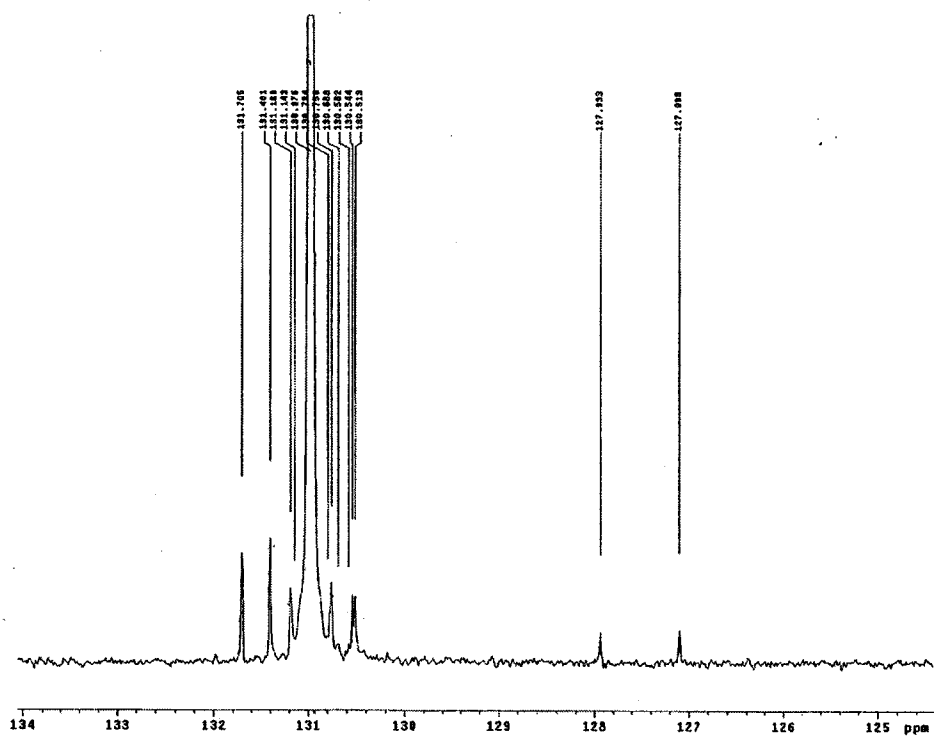


Figure B14 - ^{13}C NMR spectra-expansion of **170**

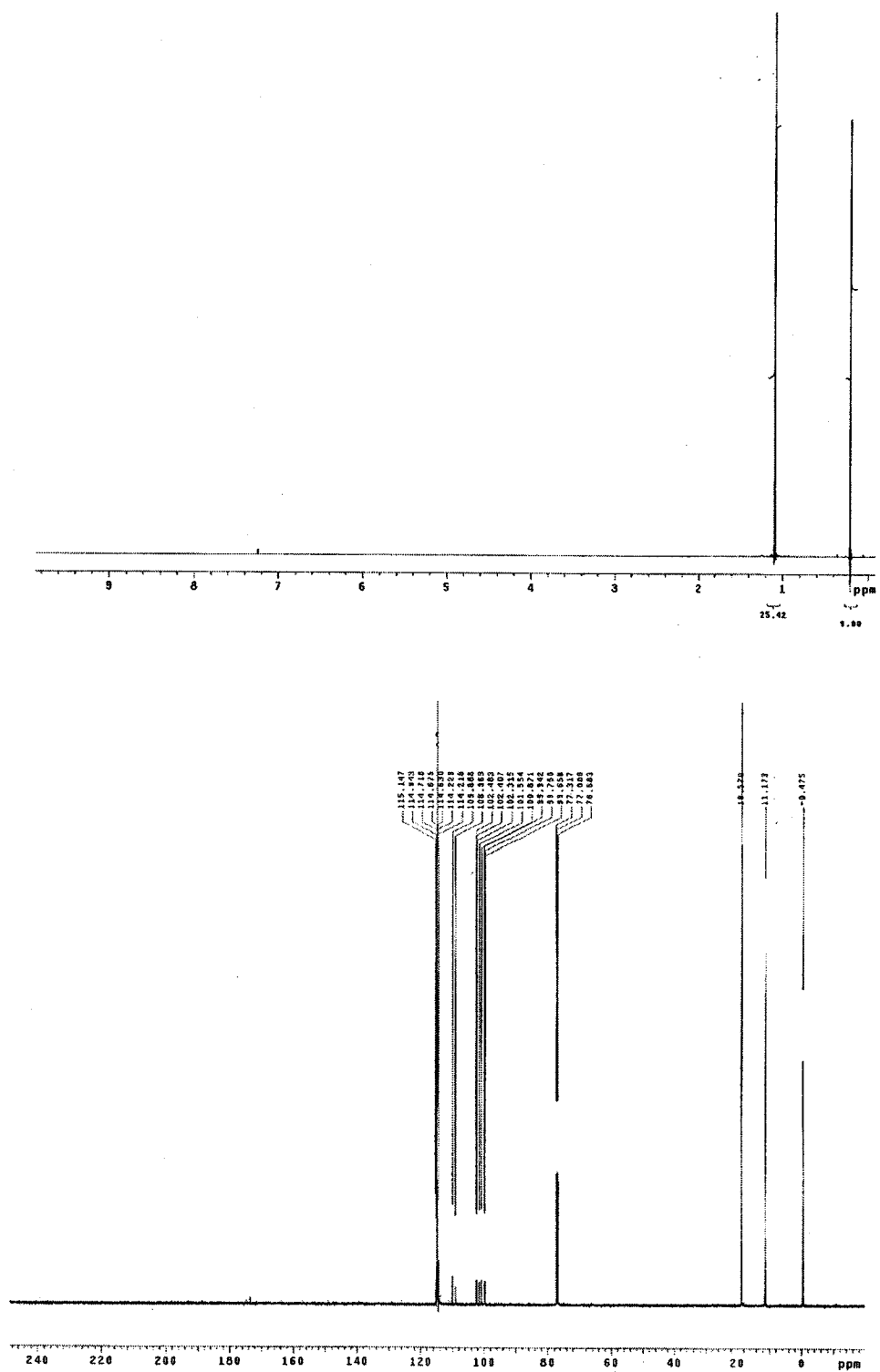


Figure B15 – ^1H NMR and ^{13}C NMR spectra of **174**

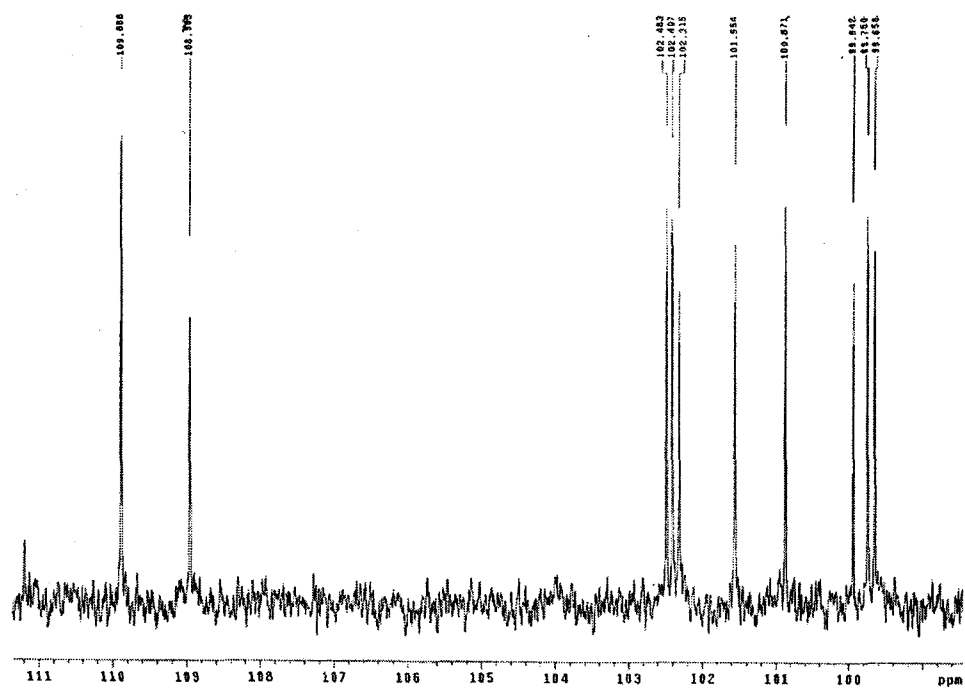


Figure B16 - ^{13}C NMR spectra-expansion of **174**

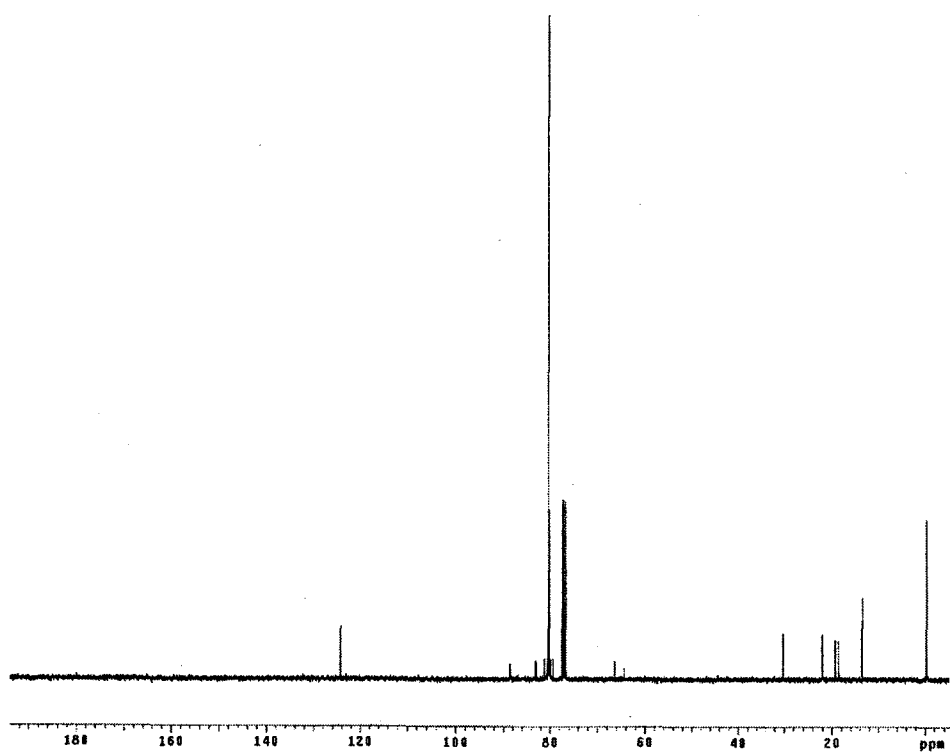
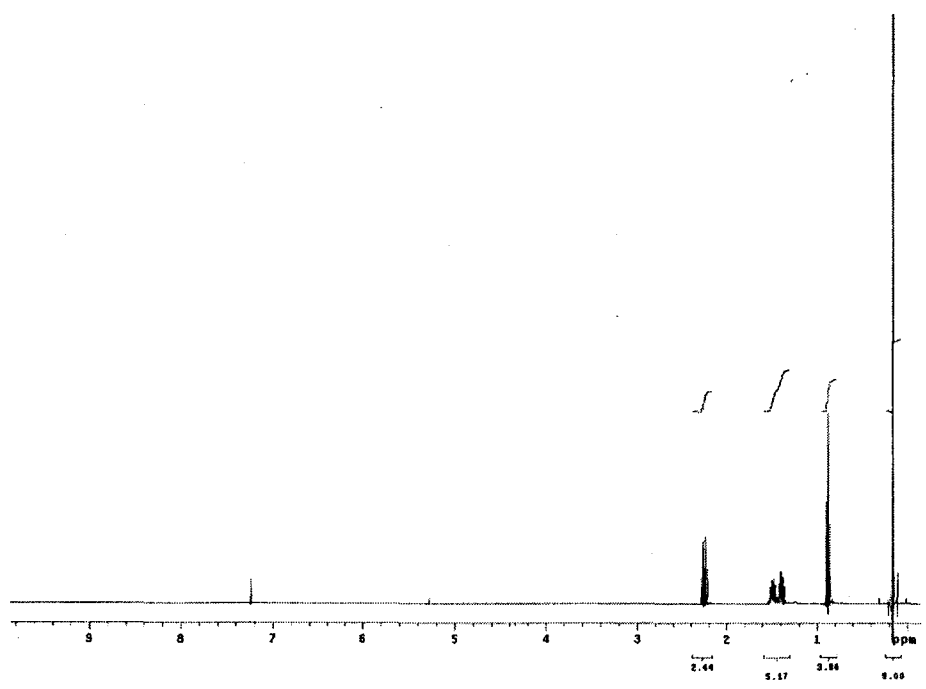


Figure B17 – ^1H NMR and ^{13}C NMR spectra of **175**

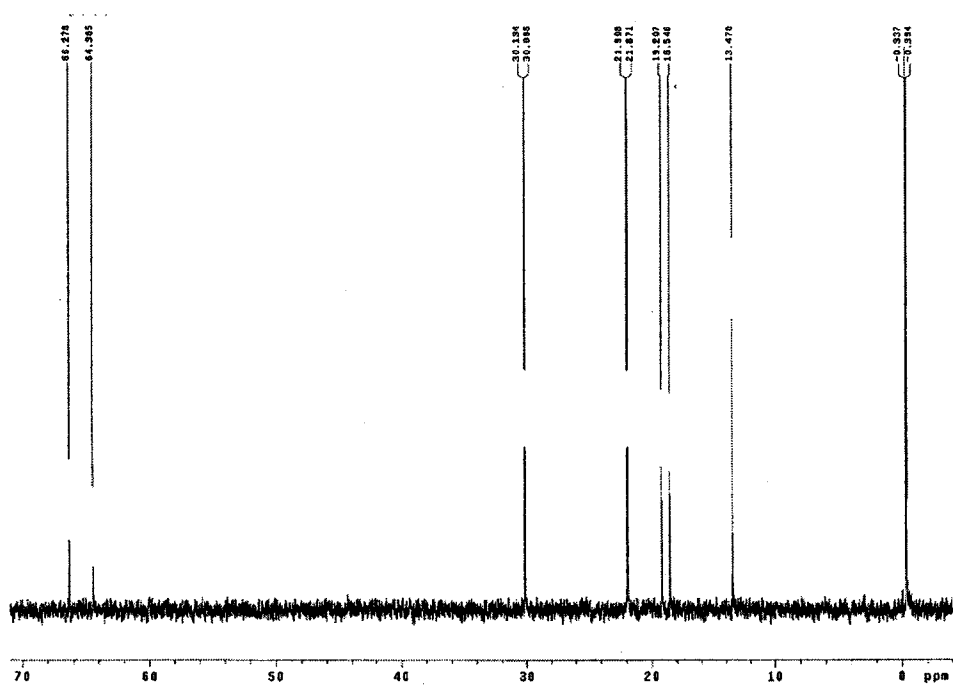
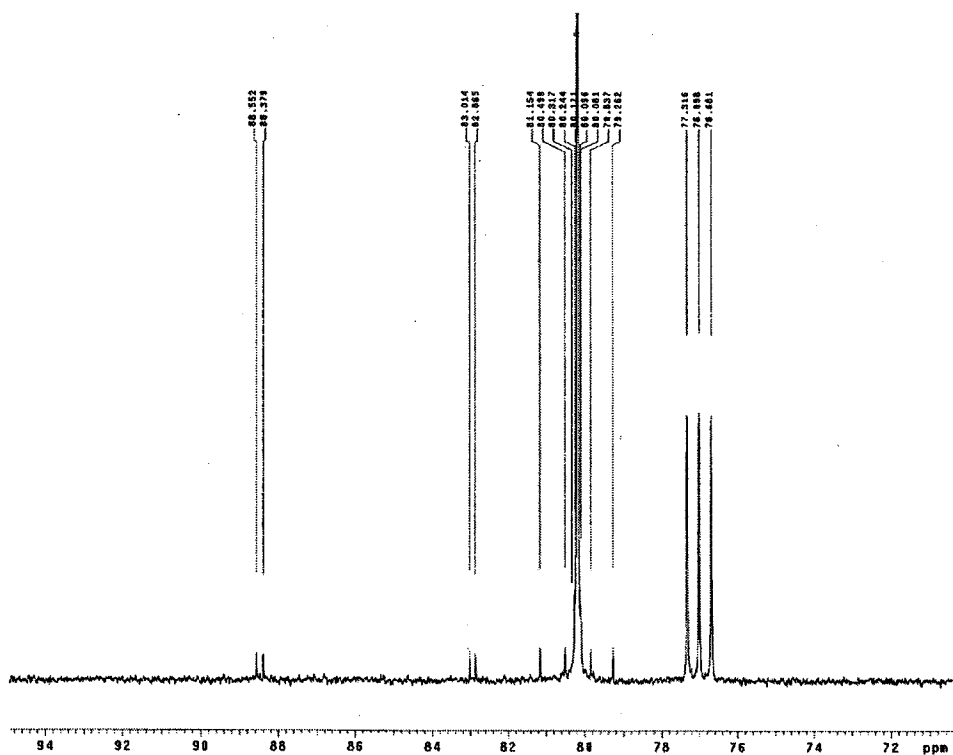


Figure B18 - ¹³C NMR spectra-expansions of **175**

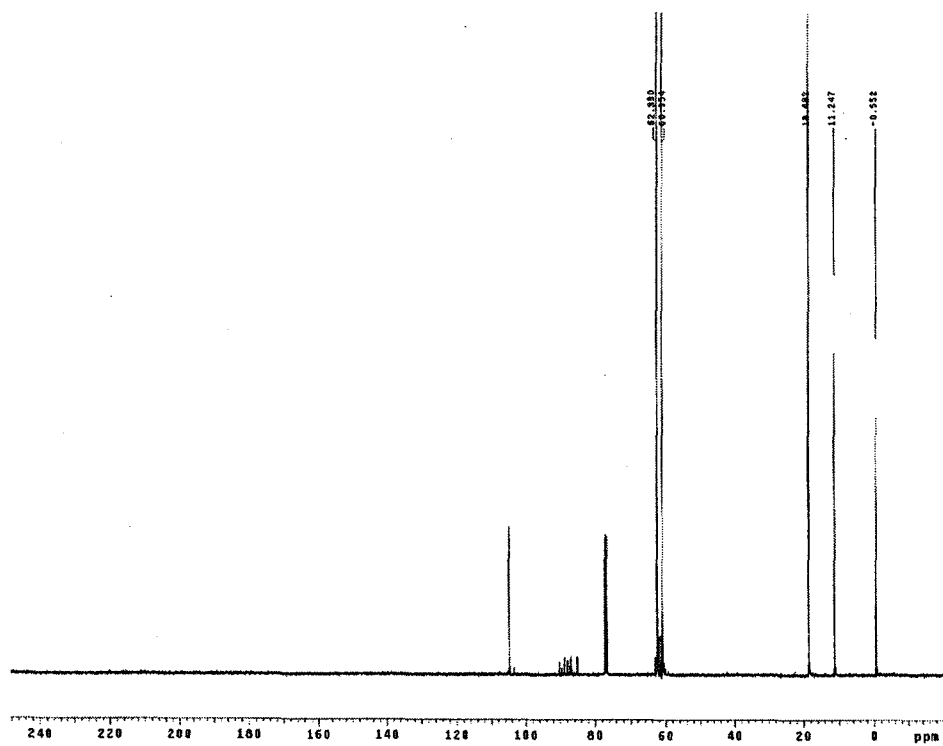
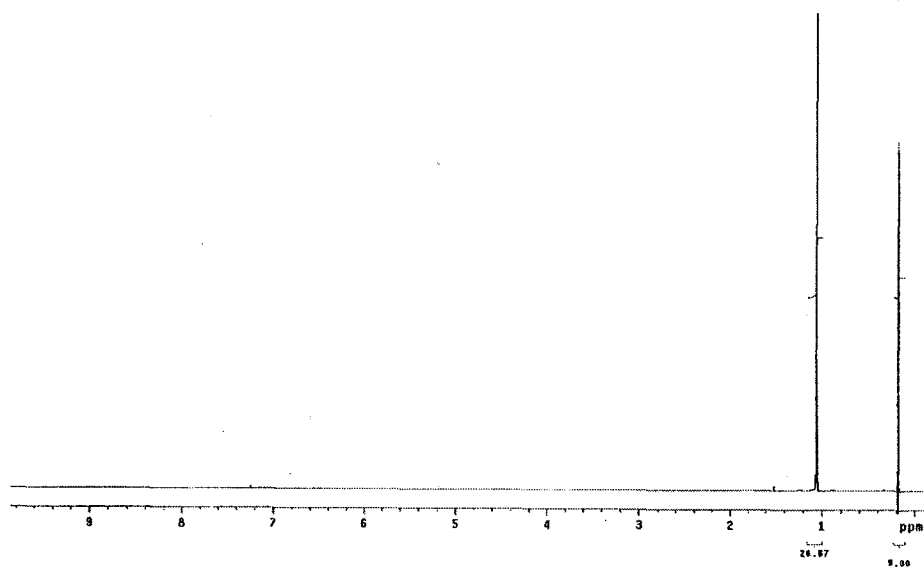


Figure B19 – ^1H NMR and ^{13}C NMR spectra of 177/178

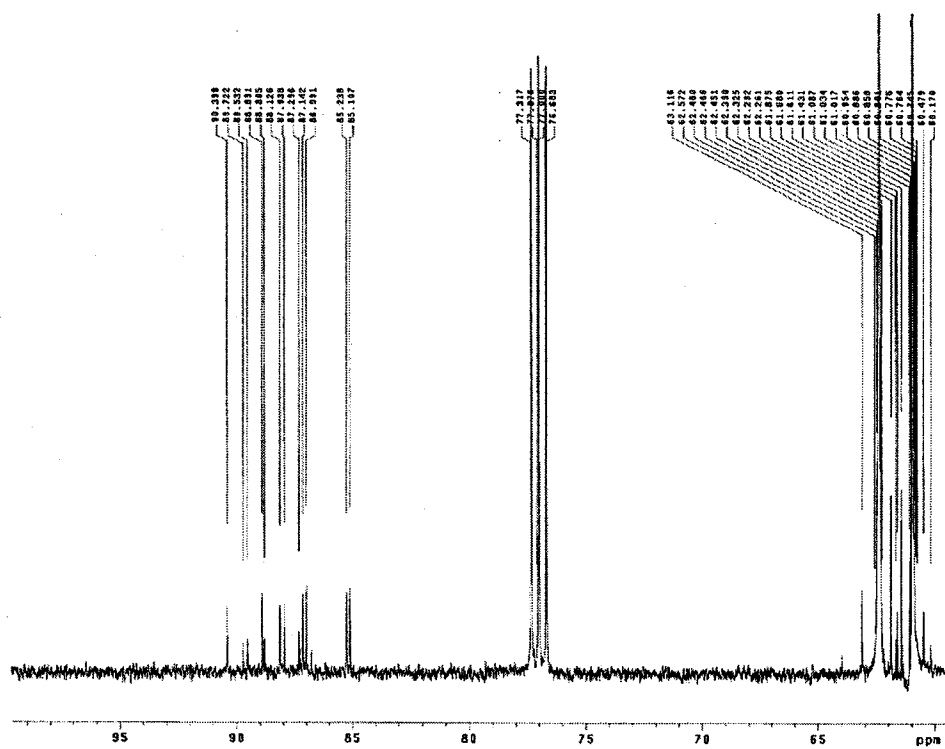


Figure B20 - ^{13}C NMR spectra-expansion of 177/178

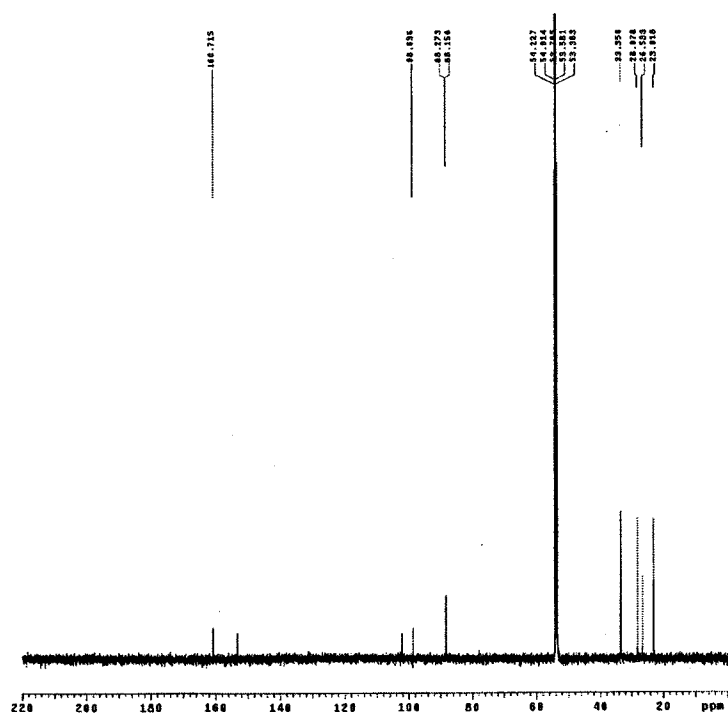
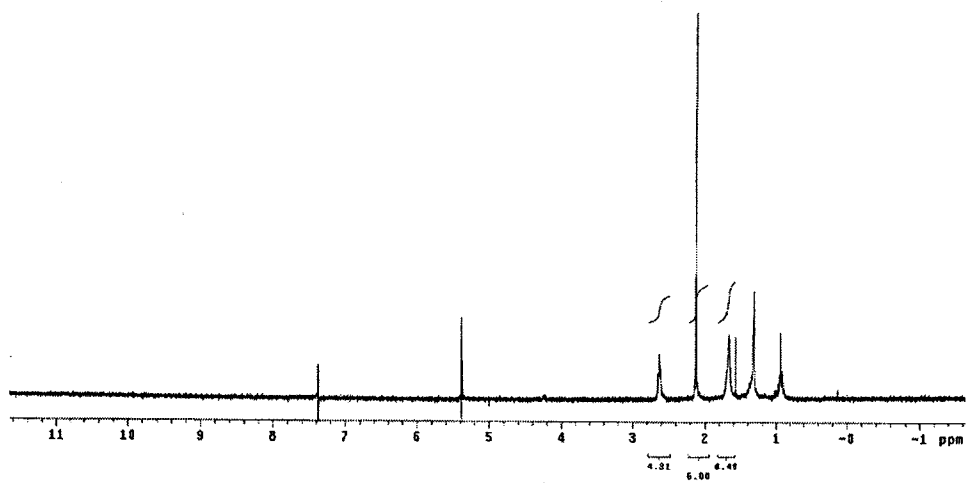


Figure B21 – ^1H NMR and ^{13}C NMR spectra of **219**

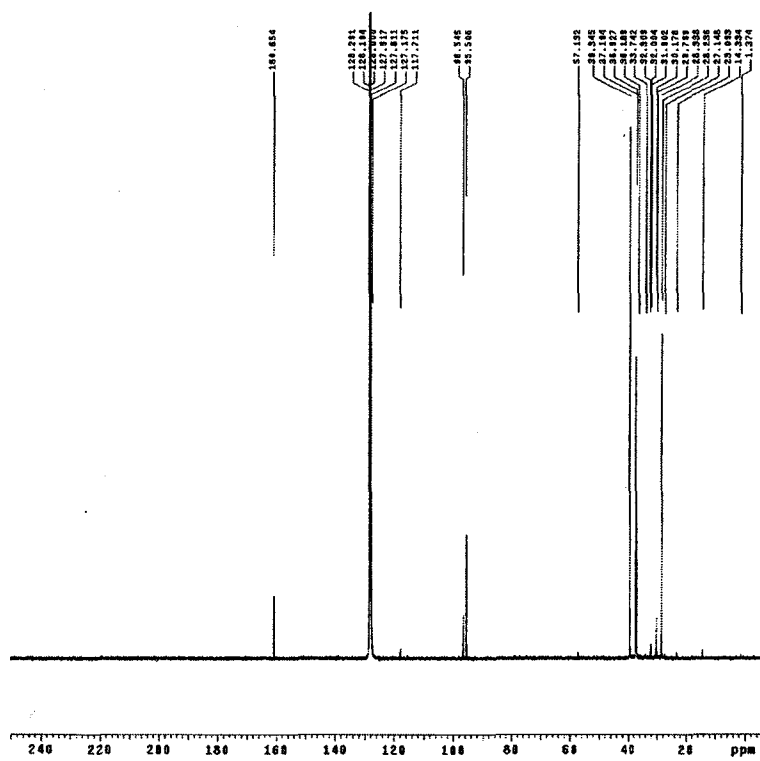
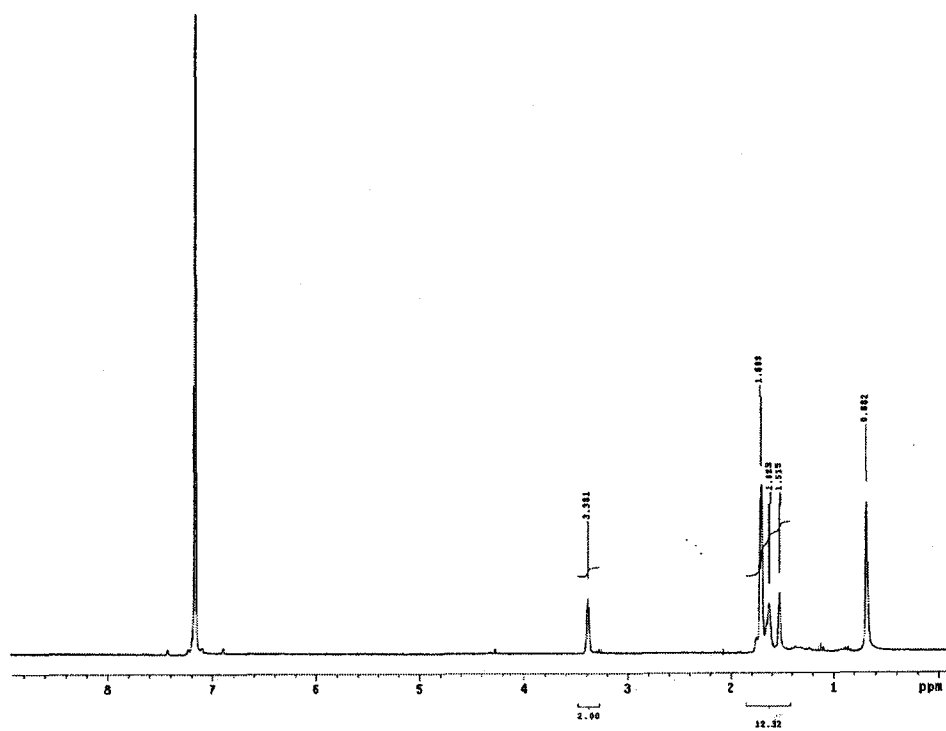


Figure B23 – ¹H NMR and ¹³C NMR spectra of 225

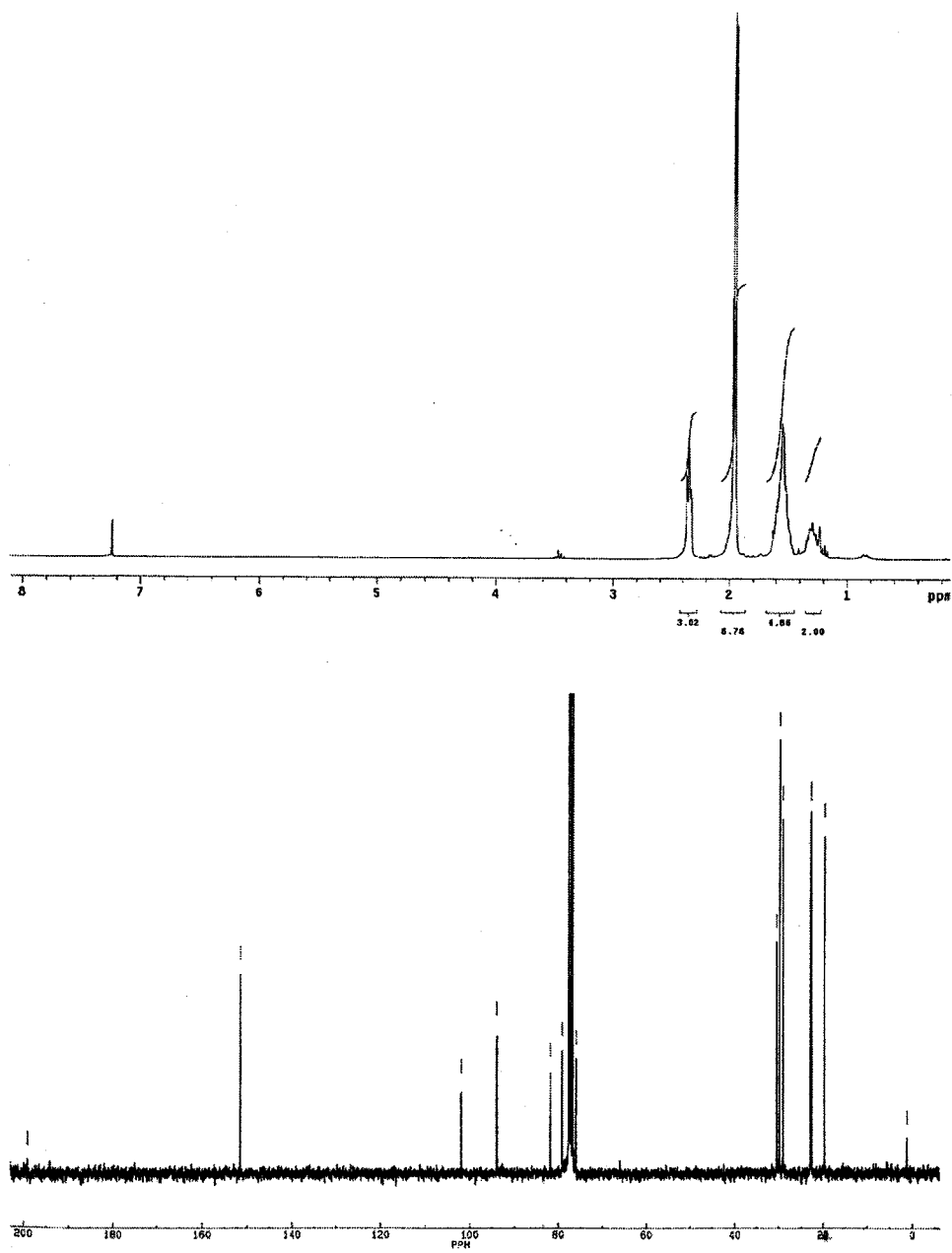


Figure B24 – ^1H NMR and ^{13}C NMR spectra of **227**

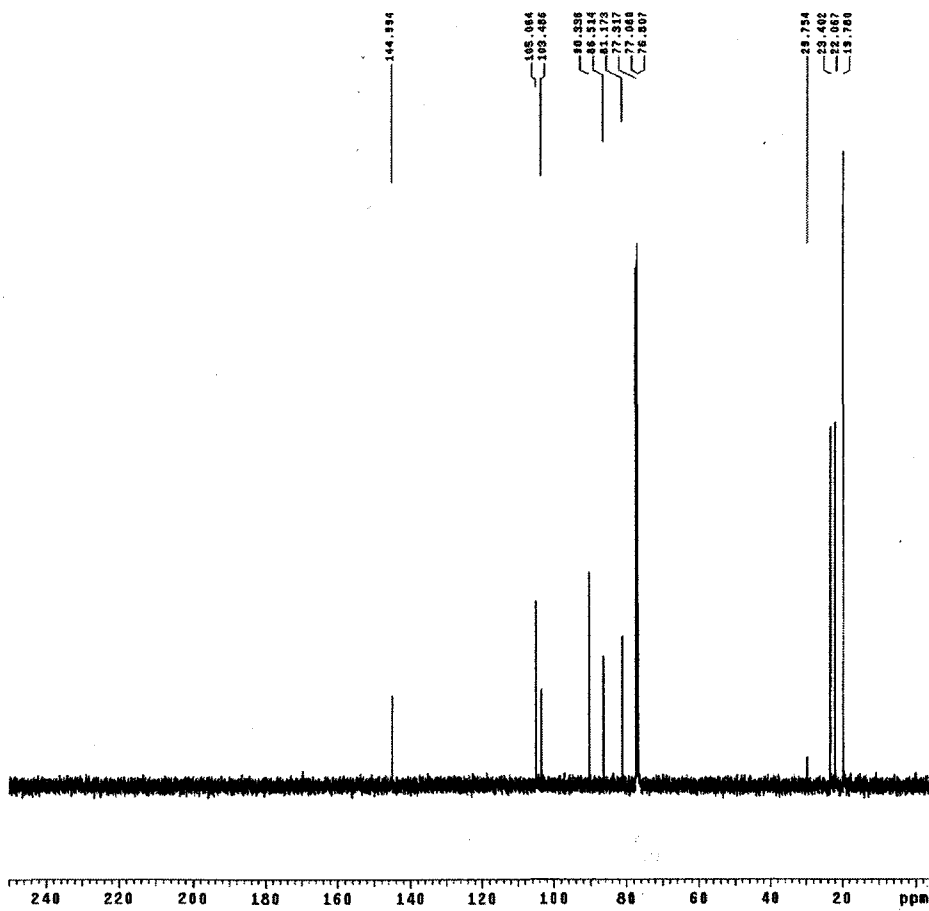
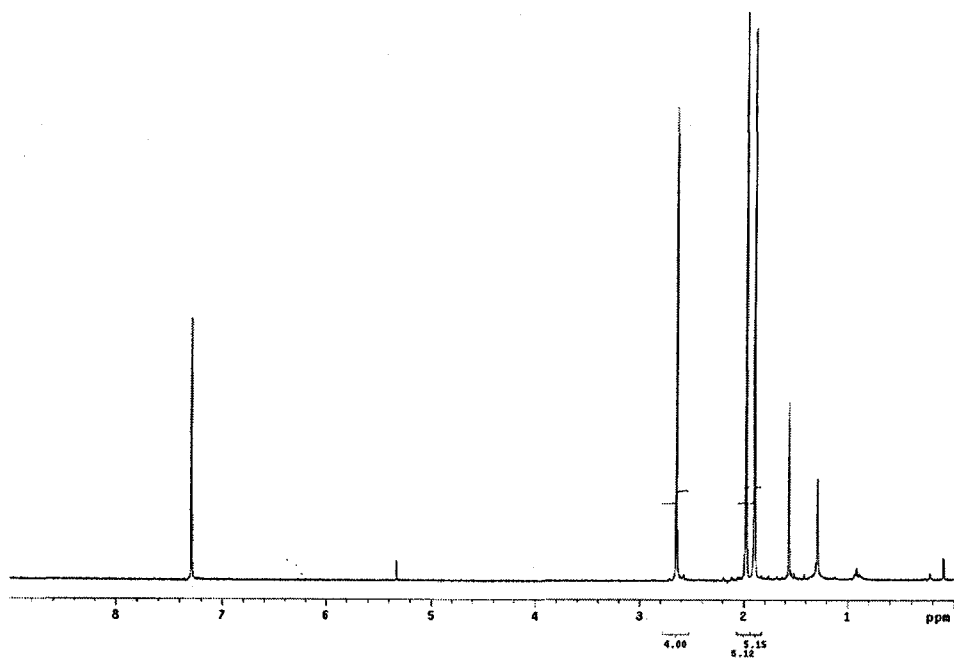


Figure B25 – ^1H NMR and ^{13}C NMR spectra of 233a

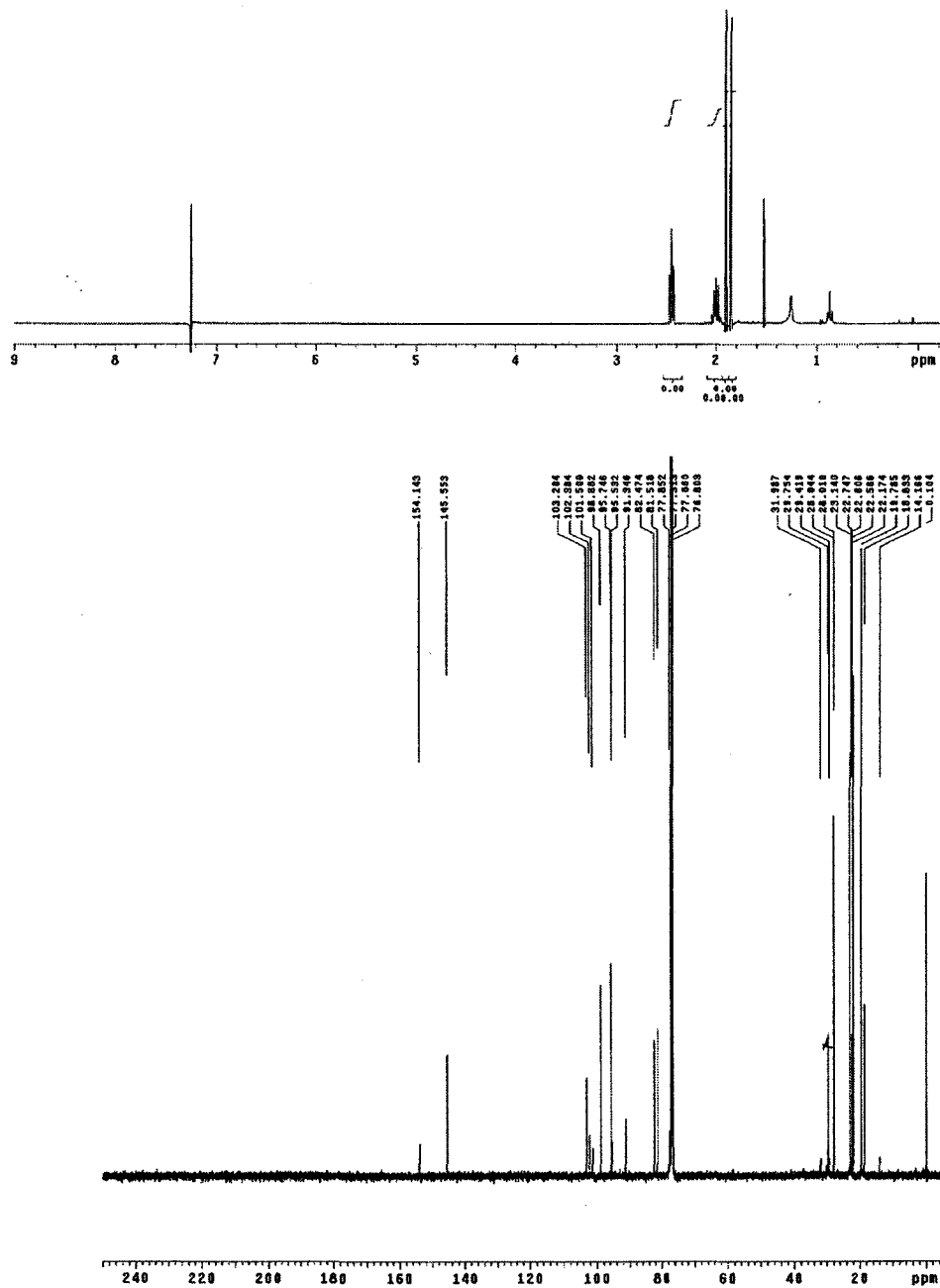


Figure B26 – ^1H NMR and ^{13}C NMR spectra of 233b

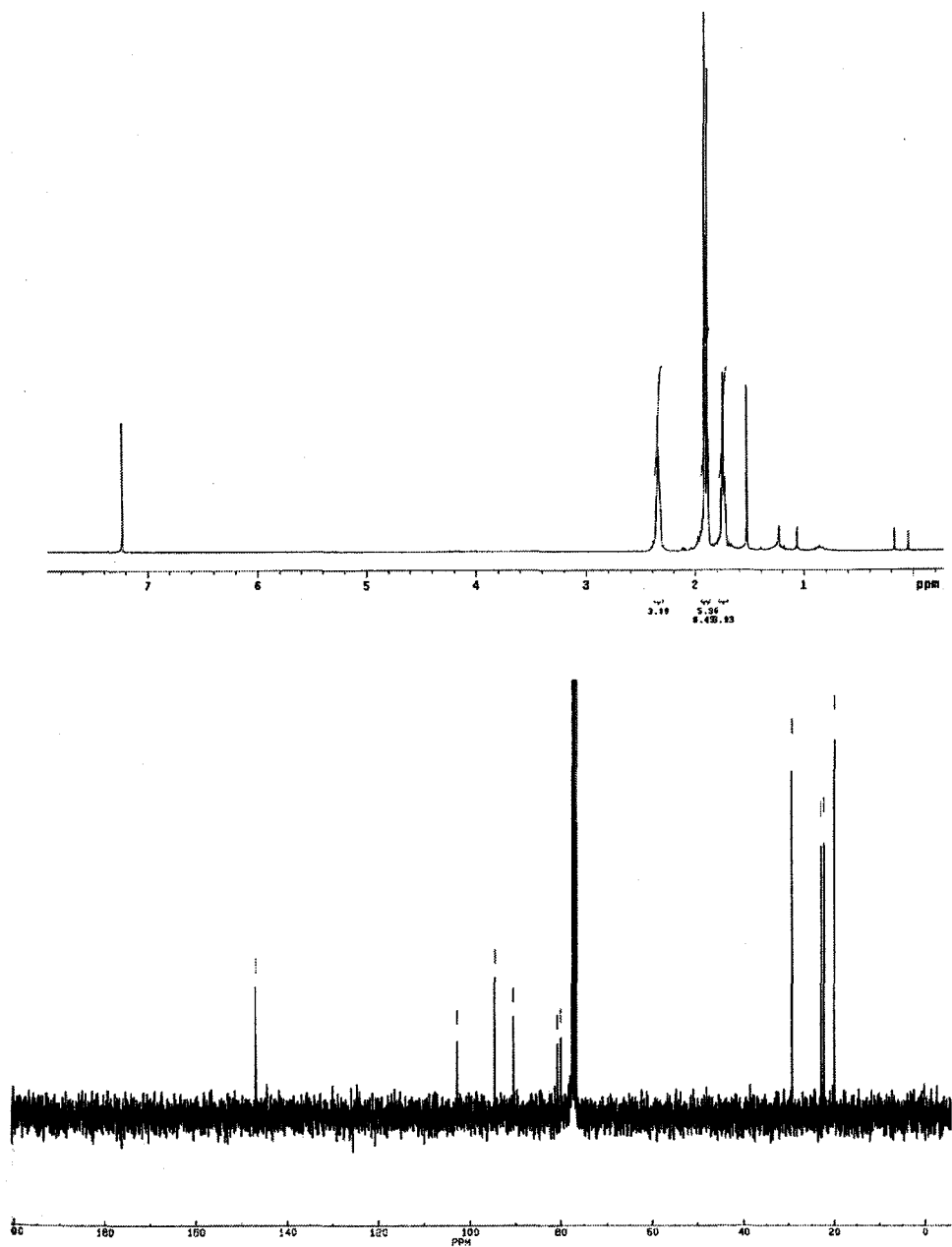


Figure B27 – ^1H NMR and ^{13}C NMR spectra of **233c**

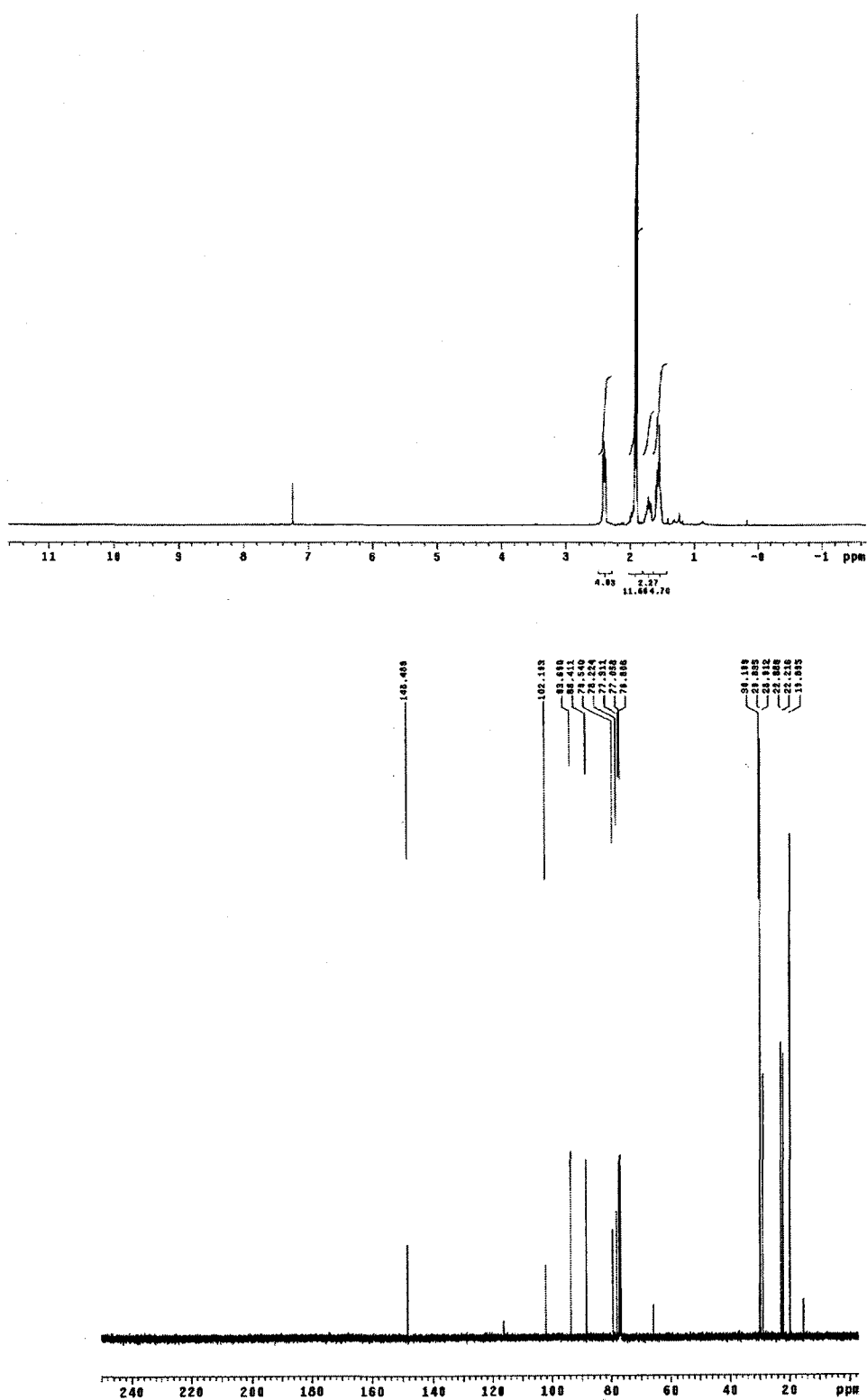


Figure B28 – ^1H NMR and ^{13}C NMR spectra of 233d